HIGHLY SELECTIVE MESOPOROUS SORBENTS FOR MERCURY REMOVAL FROM INDUSTRIAL WASTEWATER

ZIBONENI GOVERNOR GODONGWANA

A thesis submitted in fulfillment
of the requirements for the degree of

Doctor of Philosophy

in the

DEPARTMENT OF CHEMISTRY
UNIVERSITY OF THE WESTERN CAPE

UNIVERSITY of the
WESTERN CAPE

Supervisors: Prof. Emmanuel. I. Iwuoha, University of the Western Cape
Prof. Leslie. F. Petrik, University of the Western Cape

DATE SUBMITTED: MAY 2011

KEYWORDS

"HIGHLY SELECTIVE MESOPOROUS SORBENTS FOR MERCURY REMOVAL FROM INDUSTRIAL WASTEWATER"

ZIBONENI GOVERNOR GODONGWANA

SBA-15

HMS

MCM-41

Template

Mesoporous silica

Carbon Analogue (CA)

Ordered Mesoporous Carbon (OMC)

Modified Ordered Mesoporous Carbon (MOMC)

Liquefied Petroleum Gas (LPG)

Pyrolysis

Etching

Mesoporous carbon

Graphitic carbon

Adsorption

Hg (II)

Capacity

Dosage

Langmuir isotherm

Freundlich isotherm

Desorption

UNIVERSITY of the
WESTERN CAPE

LIST OF ABREVIATIONS

AC	Activated Carbon
ACs	Activated Carbons
ACC	Cloth Activated Carbon
ACF	Fibrous Activated Carbon
AO8	Acid Orange 8
APDC	Ammonium 1-pyrlidine dithio carbonate
BET	Brunauer Emmet Teller
CA	Carbon Analogue
CAC	Commercial Activated Carbon
CMK –1	mesoporous carbon molecular sieve synthesized from MCM-48 template.
CNT	Carbon Nano Tubes
CTEAB	(cetyltrietthylammonium bromide)
CTMAB	(cetyltrimethylammonium bromide)
CV-AAS	Cold Vapour Atomic Absorption Spectrometry
CV-AFS	Cold Vapour Atomic Fluorescence Spectrometry
CVD	Chemical Vapour Deposition
EDS	Energy Dispersive Spectroscopy
EELS	Electro Energy Loss Spectroscopy
EPA	Environmental Protection Agency
FTIR	Fourier Transform Infra Red Spectroscopy
GAC	Granular Activated Carbon
GC	Gas Chromatography

UNIVERSITY of the
WESTERN CAPE

Hg(II)	Mercury (2+) ion
HMS	Hexagonal Mesoporous Silica
HPLC	High performance liquid chromatography
HRTEM	High Resolution Transmission Electron Microscopy
ICP\MS	Inductively Coupled Plasma Mass Spectrometry
LPG	Liquefied Petroleum Gas
MB	Methylene Blue
MCM	Mobil Composition of Matter
MCNT	Mesoporous Carbon Nano Tubes
MOMC	Modified Ordered Mesoporous Carbon
MPTES	3- Mercaptopropyltriethoxysilane
MSM	Mesoporous Silica Material
ODS	Octadecylsilane
OMC	Ordered Mesoporous Carbon
PAC	Powder Activated Carbon
RB	Rhodamine B
SAED	Selected Area Electro Diffraction
SBA-15	Santa Barbara Amorphous type material
SEM	Scanning Electron Microscopy
SIACs	Sulphur Impregnated Activated Carbons
TGA	Thermo Gravimetric Analysis
WHO	World Health Organization
WMA	West and Marico Adsorption
XRD	X-ray Diffraction

UNIVERSITY of the
WESTERN CAPE

ABSTRACT

"HIGHLY SELECTIVE MESOPOROUS SORBENTS FOR MERCURY REMOVAL FROM INDUSTRIAL WASTEWATER"

Z. G. GODONGWANA

The development of scientific approaches, for preparation of novel materials for the effective separation of mercury from South African industrial waste water using novel synthetic adsorbents is the main focus of this study. Based on the concept of industrial ecology, this study investigated the removal efficiency between ordered mesoporous carbons modified with organic sulphur containing ligands and carbonaceous surfaces (unmodified ordered mesoporous carbons and activated carbon), and the application of these material for mercury control in water. Hydrothermal treatment of the carbon materials in the reflux condenser was applied as a modification technique.

All materials were characterized by High Resolution Transmission Electron Microscopy (HR-TEM), X-ray diffraction (XRD), Selected Area Electron Diffraction (SAED), Nitrogen Sorption (BET), Raman spectroscopy, Energy Dispersive Spectroscopy (EDS), Thermo Gravimetric Analysis (TGA) and UV-Vis Spectrometry.

Ordered mesoporous carbon (OMC) analogues were prepared by use of HMS, SBA-15 and MCM-41 as sacrificial templates. In this study the XRD

UNIVERSITY of the WESTERN CAPE

spectra as well as the TEM micrographs indicate a high degree of mesostructural ordering in the HMS, SBA-15 and MCM-41 prepared for use as sacrificial silica templates. The nitrogen sorption data confirmed that all the silica templates possessed high porosity and mesostructural ordering, therefore, were suitable for use as solid templates for ordered mesoporous carbon synthesis.

The application of Liquefied Petroleum Gas (LPG) as carbon precursors at different times of LPG pyrolysis deposition for preparation of ordered mesoporous carbons was successfully achieved to prepare the carbon analogue that resulted in a mesoporous material exhibiting both well-ordered mesoporosity and high levels of graphitic character. The unique architecture of the HMS, SBA-15 and MCM-41 silica sacrificial templates, which explain large textural porosity, was achieved in the parent Si materials and reproduced in the templated ordered mesoporous carbons.

UNIVERSITY of the
WESTERN CAPE

The ordered mesoporous carbons prepared by use of the HMS, SBA-15 and MCM-41 as sacrificial templates were found to be highly porous and graphitic, with a large surface area exceeding that of the parent silica sacrificial template. However, the OMC prepared by using SBA-15 template had the highest surface area compared to OMCs prepared from HMS and MCM-41. The results obtained depict that a carbon mesoporous analogue of the SiO_2 based SBA-15, HMS and MCM-41 were successfully achieved. The formation of graphitic structures in the pores takes place during the chemical vapor deposition step of SBA-15, HMS and MCM-41 at high temperatures. The

dissolution of the SiO_2 framework of the mesoporous SBA-15, HMS and MCM-41 used as template were achieved by use of NaOH. Etching of the SiO_2 framework created the mesopores in the carbon that were observed by N_2BET and Raman spectroscopy. The regular mesostructure of the new carbon materials was demonstrated by the appearance of the peaks at 12.64 ^{0} 2 θ in XRD spectra that indicated that there is a regular mesostructured carbon framework at 11.6 Å and 6.8 Å d spaced distances. This is a novel for carbon analogues of SBA-15 and MCM-41 finding and has not been previously reported.

The results of this study show that novel mesoporous carbons were obtained as inverse replica of SBA-15, HMS and MCM-41 silica templates, with a large pore diameter (2-4 nm), a BET surface area of 1867, 874 and 910 m^2g^{-1} respectively for CA_SBA-15_LPG_105, CA_HMS_LPG_80 and CA_MCM-41_LPG_80 with bimodal pore size distribution (PSD) in the mesopores range. The results obtained show that mesoporous carbon with graphitic structures can be synthesized via the LPG route.

Unmodified OMC and activated carbon (AC) were subsequently utilized as adsorbents for the adsorption capability of acid dyes, Acidic Orange 8 (AO8) and basic dyes Methylene Blue (MB) and Rhodamine B. The equilibrium data fitted well the Langmuir and Freundlich isotherms for AO8 and MB but fitted only Langmuir isotherm for RB showing monolayer coverage of RB dye molecules at the surface of OMC and AC adsorbent. The R_L values for AO8,

UNIVERSITY of the
WESTERN CAPE

MB and RB were found to be between 0 and 1 indicating that adsorption was favorable for the OMC and AC adsorbents.

The carbon analogue with the highest surface area i.e. CA_SBA-15_LPG_105 was initially modified with HNO_3 and thereafter with a sulphur containing ligand (3- Mercaptopropyltriethoxysilane) and later used as an adsorbent for Hg(II) removal from water. The efficiency for mercury removal capacity for the modified ordered mesoporous carbon (MOMC) was compared to unmodified OMC and activated carbon (AC). Unmodified OMC had a higher removal efficiency compared to AC, whereas removal capacity was the highest by MOMC.

UNIVERSITY of the
WESTERN CAPE

It was shown in this study that removal of Hg (II) from water by MOMC, OMC and AC is influenced by effect of contact time, adsorbent dosage, pH and sulphur containing ligands. The optimum conditions for the removal of Hg (II) were at pH 5.5 and adsorbent dosage of 10 mg/50 mL. Adsorption of Hg (II) by MOMC, OMC and AC fitted to the Freundlich model. However, adsorption by MOMC fitted to both Freundlich and Langmuir models. In this study it is shown that OMC is effective and economic for treatment of water contaminated with Hg (II).

DECLARATION

I declare that

"HIGHLY SELECTIVE MESOPOROUS SORBENTS FOR MERCURY REMOVAL FROM INDUSTRIAL WASTE WATER"

is my own work, that it has not been submitted for any degree or examination in any other university and that all the resources I have used or quoted have been indicated and acknowledged by means of complete references.

UNIVERSITY of the
WESTERN CAPE

Ziboneni G. Godongwana

Signed:

Date:

ACKNOWLEDGEMENTS

I thank my Heavenly Father, God almighty, for the grace of education and for making me reach this far in my Chemistry career. I thank my wife Vuyokazi Pandorah Godongwana, for her encouragement concerning this hard work.

I thank my supervisor Prof. Emmanuel Iwuoha for his dedication and support in relation to all aspects of this PhD study.

I would like to express my sincere gratitude to my supervisor Prof. Leslie Petrik, for accepting me in her research group, intellectual input and for her providence with all the resources that I needed to complete my research.

UNIVERSITY of the
WESTERN CAPE

I thank postdoctoral fellow Dr. Nuran Boke for assistance, advice with many of the aspects related to the research topic, intellectual input, support and encouragement.

I thank Dr. Alexander Nechaev for his intellectual, assistance and advice with many of the aspects related to the research topic.

A big thank you to Prof. Basil Julies, Dr. Frich Koch and Mr. Adrian B. Josephs for their help with the HR-TEM, EELS, SEM and EDS analysis, Physics department UWC and for their benevolence of going an extra mile to assist with any difficulties encountered.

A big thank you to Dr. Neil P. Young, Research Fellow, Electron Microscopy and Microanalysis Group, Department of Materials, University of Oxford for assistance pertaining Electron Diffraction analysis.

A big thank you to Dr. Remy Bucher and Dr. Tshepo Ntsoane for their assistance with the XRD facility at Ithemba Laboratories.

A big thank you to Dr. Gerald Malgas for his commitment and wise advice pertaining to thesis structure.

A big thank you to Rudolph Erasmus for his help with Raman Spectroscopy analysis, Physics Department Wits University.

A big thank you to Timothy Lesch for his assistance with UV-Vis Spectroscopy analysis, UWC Chemistry Department.

I extend my gratitude to all my fellow postgraduate students especially to Rallston Richards and Jeremy Johnson for assistance with adsorption studies and encouragement.

The financial assistance of *Coaltech*, *Mintek* and the *National Research Foundation (NRF)* towards this research is hereby acknowledged. Opinions expressed and conclusions arrived at are those of the author and are not necessarily to be attributed to Coaltech, Mintek or the NRF.

UNIVERSITY of the
WESTERN CAPE

In loving memories of my late mother (Mrs. Nobantu Marthable Nowinile Godongwana) and father (Mr. Mxokozeli Tylden Godongwana).

UNIVERSITY of the
WESTERN CAPE

CONTENTS

UNIVERSITY of the
WESTERN CAPE

UNIVERSITY of the
WESTERN CAPE

UNIVERSITY of the
WESTERN CAPE

UNIVERSITY of the
WESTERN CAPE

UNIVERSITY of the
WESTERN CAPE

UNIVERSITY of the
WESTERN CAPE

UNIVERSITY of the
WESTERN CAPE

UNIVERSITY of the
WESTERN CAPE

LIST OF FIGURES AND TABLES

UNIVERSITY of the
WESTERN CAPE

UNIVERSITY of the
WESTERN CAPE

UNIVERSITY of the
WESTERN CAPE

UNIVERSITY of the
WESTERN CAPE

UNIVERSITY of the
WESTERN CAPE

UNIVERSITY of the
WESTERN CAPE

UNIVERSITY of the
WESTERN CAPE

UNIVERSITY of the
WESTERN CAPE

UNIVERSITY of the
WESTERN CAPE

UNIVERSITY of the
WESTERN CAPE

CHAPTER 1

1.1. INTRODUCTION

Nanoporous sorbent materials with high performance for heavy metal removal from wastewater could be designed and developed. These novel materials are created from a combination of synthetic mesoporous ceramic templates that have specifically tailored pore sizes (2 to 10 nm) and very high surface areas (~ 1000 m^2/g) with self - assembled monolayers of well - ordered functional groups that have high affinity and specificity for specific types of free or complex cations or anions.

In this study ordered mesoporous carbon (OMC) has been synthesized and modified with sulphur containing ligands (3-mercaptopropyltriethoxysilane) after prior modification with nitric acid (HNO_3) for effective adsorption of mercury from water.

UNIVERSITY of the WESTERN CAPE

1.2. BACKGROUND TO THE STUDY

The industrial revolution of the early 20^{th} century led to extraordinary economic growth in South Africa. However, it also brought significant environmental pollution. The economic benefits of increased industrial production outweighed consideration of the emerging environmental problems. Much of the environmental damage has continued and became

more in the last two decades in South Africa. Contrary to other parts of the world, for instance United States of America and the United Kingdom, in South Africa there has not been an explosion of research in the application of nanotechnology for environmental remediation. However, in South Africa some nano research has started as far as the design and synthesis of nano-structured materials, but it has been slow. These nano-structured materials contain specific, predictable nanostructures whose chemical composition or interfacial structures enable them to perform a specific job. The ability to design, synthesize and manipulate specific nanostructured materials lies at the very heart of the future of nanotechnology. Nanomaterials may have unique physical and chemical properties compared to their bulk counter parts, such as large surface area to volume ratios or high interfacial reactivity. Such properties give hope for new chemical capabilities arising from exciting new classes of nanomaterials. Nanomaterials have been developed for specific applications that involve interfacial reactions or molecular transport processes.

UNIVERSITY of the
WESTERN CAPE

1.3. MOTIVATION OF THE STUDY

Mercury is considered one of the most toxic metals in the environment because of its bio accumulative property and consequent toxic effects on human health. It is included on the list of priority pollutants by U.S. EPA and has a permitted discharge limit of 10 mg/L in wastewater and a maximum concentration level of 2 mg/L for drinking water. In addition to natural mercury

emissions to the atmosphere, both inorganic and organic mercury species are produced from industrial sources (paper industry, agriculture, pharmaceutical uses, etc.), which contribute to contaminate our environment. Among them, methyl mercury is the most dangerous because of its neurotoxicity by, e.g. blocking the active sites of enzymes, interfering in protein synthesis, or preventing thymidine incorporation into DNA. This hazardous contaminant, however, can be produced by biologically induced conversion of inorganic mercury (e.g. by algae or bacteria), making the ubiquitous inorganic mercury species thus potentially toxic for living organisms. Both organic and inorganic mercury tends to interact strongly with sedimentary minerals and organic matter.

The health hazards due to the toxic effect of mercury at Minamata, Japan and Iraq are very well known. The toxicological effects of mercury depend upon the type of mercury compound, the amount ingested and the mode of entry into the body. It is carcinogenic, mutagenic, teratogenic and promotes tyrosinemia. It also causes blindness, mental and emotional deterioration, involuntary mobilization and loss of consciousness.

UNIVERSITY of the WESTERN CAPE

To meet the permitted limits, a variety of treatment methods have been proposed for mercury removal from aqueous solutions, including precipitation, coagulation, membrane separation, ion exchange, and adsorption. Much work has been done to remove contaminants from aqueous solutions by adsorption processes because they are easy to operate and cost effective. A range of sorbents (such as carbon), both raw and modified materials with sulphur containing functional groups, have been extensively studied for mercury

removal. However, nano porous materials have not been extensively evaluated. Though it is desirable to have zero mercury levels in effluents, it is practically impossible to accomplish this.

Among the popular modification methods, grafting sulphur-containing groups to the raw material has attracted much attention due to their high affinity toward mercury compared with other ligands.

Elemental sulphur-impregnated activated carbons (SIACs) have been extensively studied for mercury removal. Sulphur impregnation can greatly improve the performance of carbon adsorbents for mercury removal.

UNIVERSITY of the
WESTERN CAPE

1.4. PROBLEM STATEMENT

Mercury is one of the most toxic metals in the environment as previously stated. Mercury is particularly dangerous once it gets into aquatic systems, because under certain conditions it is converted into methyl mercury - a more toxic form. It is readily taken up by phytoplankton and then accumulates up the food chain, with the result that people eating methyl mercury-contaminated fish on a regular basis soon experience the symptoms of mercury poisoning. Once it enters the food chain, accumulation of mercury compounds takes place in humans and animals. Mercury attacks the central nervous system, so dementia, memory loss and speech and gait problems are

typical symptoms of mercury poisoning. The term as 'mad as a hatter' was coined because, in the old days, mercury was used in the manufacture of felt hats, so mercury poisoning was somewhat of an occupational hazard.

Coal-fired power stations are the primary source of mercury emissions globally, and given that most of South Africa's power stations are located in Mpumalanga - where 80% of the country's coal are produced especially the Olifants Water Management Area (WMA). Another major mercury emitter is the cement industry, which uses coal as a kiln fuel. Although the cement industry is more evenly distributed throughout South Africa, there is a concentration of facilities in the Crocodile (West) and Marico WMA.

UNIVERSITY of the
WESTERN CAPE

Adsorption on activated carbon is one of the cost effective and conventional methods for removal of Hg (II) from wastewater. Activated carbons (ACs) are utilized worldwide in many industries as adsorbents for waste water treatment. ACs have highly developed internal surface area and porosity. The development of micro and mesopores allows activated carbon to adsorb molecules of different sizes. The complexity of the carbon structure prevents the conventional activation process from preparing carbon materials with strictly controlled or uniform pore structure, although voluminous research has been done and a great effort has been made towards the control of pore size and its distribution.

To discover chemically interesting phenomena specific to a particular pore size, ordered porous materials are needed which have a defined pore size

and a well developed porous structure. The recent development of industrial technology requires that carbon should have desired pore structure for new application fields. For adsorption the carbon material should have mesoporosity and a high surface area. Mesoporous carbons with accessible pore sizes > 2 nm can be obtained as inverse replicas of mesoporous silica materials used as templates. However, the framework of these carbons contains some amorphous character.

The research problem is that, it is not possible to modify OMC with nitric acid and later graft sulphur containing ligands on the OMC surface.

UNIVERSITY of the
WESTERN CAPE

1.5. OBJECTIVES OF THE STUDY

The objective of this study is to:

- Develop novel adsorbents for effective removal of mercury from water.
- Utilize ordered mesoporous silica (OMSi) material as sacrificial templates to attain ordered mesoporous carbon (OMC) material. The goal was to obtain a negative replica of the initial OMSi as well as ensure a high level of mesoporosity in the desired OMC product.
- Probe the OMC product with acidic, neutral and basic dyes; in order to ascertain the surface properties of the novel OMC materials.

1.6. RESEARCH QUESTIONS

- Is it possible to form mesoporous carbons using SBA-15, HMS and MCM-41 mesoporous silica substrates as templates?
- What is the optimum condition to achieve this? (Method development)
- Is this methodology reproducible? (Method validation)
- Is it possible to determine surface properties of an ordered mesoporous carbon (OMC) by probing the OMC with Acidic and basic dyes?
- Is it possible to modify the mesoporous carbon surface for mercury removal?
- What is the optimum condition to achieve this? (Method development)
- Do the unmodified ordered mesoporous carbon (OMC) and modified ordered mesoporous carbon (MOMC) adsorb mercury from water? Is MOMC a better Hg (II) adsorbent compared to OMC?
- What are the optimum conditions for adsorption of Hg (II) by OMC and MOMC? (Method development)
- Is it possible to achieve graphitization of the MOMC structure?

UNIVERSITY of the
WESTERN CAPE

1.7. RESEARCH APPROACH

In this work, a novel and facile route to prepare ordered mesoporous carbon (OMC) from ordered mesoporous silica (SiO_2) based sacrificial templates is described by making use of hydrocarbon vapours. These ordered

mesoporous carbon (OMC) nanostructured materials were synthesized via a pyrolysis method using ordered mesoporous silica (OMSi) materials as solid templates **[1-4].** Chemical vapor deposition (CVD) with the use of liquefied petroleum gas (LPG) as the carbon precursor was applied for the preparation of graphitic ordered mesoporous carbon analogues. The method developed is based on the use of ordered mesoporous silica materials SBA-15, HMS and MCM-41 as templates. Liquefied Petroleum Gas (LPG) that was used as carbon precursor is normally composed of 90 % propane (C_3H_8), 2.5 % butane (C_4H_{10}) and higher hydrocarbons, and the balance ethane and propylene **[1]**. The transformation process of silica templates to OMC was achieved through use of LPG as a carbon precursor by being infiltrated in the porous silica framework and then the precursor was carbonized at high temperatures. The pores were filled up to create a negative replica of the template's structural order in the desired carbon product. Infiltration of carbon into the silica pores and carbonization was followed by the dissolution of the SBA-15, HMS and MCM-41 silica framework by chemical etching with NaOH. Etching was performed to remove the silica skeleton / framework from the silica-carbon composite; so that the remaining framework is mostly made up of carbon. Thus a negative carbon replica or carbon analogue of the parent silica material was formed, often referred to as ordered mesoporous carbon or OMC.

UNIVERSITY of the
WESTERN CAPE

In order to ascertain the character of surface interactions or surface properties of ordered mesoporous carbons (OMCs), OMCs were probed with Acid orange 8 (AO8), an acidic dye containing one sulfo group, Methylene

Blue (MB), a cationic basic dye containing two alkyl amino groups and Rhodamine B (RB), a non polar basic dye **[284].**

In order establish if it was possible to improve the uptake capacity of mercury adsorption in aqueous media, OMC was modified with HNO_3 and 3-mercaptopropyltriethoxysilane.

Finally, the modified ordered mesoporous carbon (MOMC) and unmodified ordered mesoporous carbon (OMC) were applied as adsorbents for mercury (II) removal in aqueous media.

UNIVERSITY of the
WESTERN CAPE

1.8. SCOPE

In this study ordered mesoporous carbons were synthesized from ordered mesoporous silica templates and were modified with sulphur containing ligands (3- mercaptopropyltriethoxysilane) and were designated as modified ordered mesoporous carbon (MOMC). The MOMC was eventually utilized as an adsorbent for mercury (II) removal from water. The mercury (II) removal efficiency of the unmodified OMC as well as MOMC was compared to that of commercialized activated carbon.

1.9. DELIMITATIONS

The study will not address the speciation of mercury. According to the official definition by IUPAC speciation analysis is the process leading to the identification and determination of the different chemical and physical forms of an element existing in a sample. The analytical activity involved in identifying and measuring species is hence defined as 'speciation analysis. The determination of the concentration of specific chemical forms, such as organic mercury rather than elemental mercury is highly essential for the interpretation of their biochemical behavior or assessment of the potential danger to humans and organisms. Speciation of mercury was not addressed in this study because of time constraints and analytical limitations due to equipment unavailability. UV-Vis spectrophotometry was used as an analytical technique for mercury detection. Due to the simplicity of this technique and its replicability as well as time, cost and availability constraints there was limited use of other techniques for mercury detection.

The study will only encompass SBA-15, HMS and MCM-41 material as templates in the preparation of mesoporous carbon materials. The use of other silica molecular sieves was not investigated

The study only used one modification method to functionalize ordered mesoporous carbon. Chemical ligating groups such as 3-

mercaptopropyltriethoxysilane were engrafted on ordered mesoporous carbon surface to trap Hg (II) ions. Modification was only performed on the carbon analogue of SBA-15 and was limited to 3- mercaptopropyltriethoxysilane as the grafting agent. Time constraints limited modification on the carbon analogues of HMS and MCM-41 as well as use of other chemical ligating groups for mercury entrapment was not investigated.

Due to the cost and the lack of availability of certain instrumentation, e.g. Boehm technique for evaluation of surface functional groups of adsorbents or X-ray photoelectron spectroscopy (XPS), the characterization study was limited to the use of HR-TEM, EELS, FTIR, SAED, EDS, SEM, XRD, BET, Raman spectroscopy and TGA as characterization techniques.

UNIVERSITY of the
WESTERN CAPE

1.10. HYPOTHESIS

The adsorption of Hg (II) from wastewater is possible by employing modified and unmodified ordered mesoporous carbon synthesized from ordered mesoporous silica. The achievement of high surface area, thermally stable ordered mesoporous carbon material will enhance the efficiency of mercury removal from waste water. Modification of ordered mesoporous carbon using nitric acid and chemical ligating groups such as 3-mercaptopropyltriethoxysilane will improve mercury adsorption capacity.

1.11. THESIS OUTLINE

This thesis will be presented according to the following outline.

Chapter 1: Introduction

Chapter 1 gives a brief introduction and background, motivation of the study, problem statement, and main objectives of this research study. It also states the research questions and approaches thereafter used to answer the questions. The scope and delimitations to the study are also covered in this chapter as well as hypothesis and investigation outline.

UNIVERSITY of the
WESTERN CAPE

Chapter 2: Literature Review

The literature review focuses on discussion of the general problems related to wastewater, focusing on mercury as a global water pollutant. This is followed by a discussion on modern technologies used in water treatment. Adsorption as a technique for wastewater treatment as well as kinetics of adsorption are extensively discussed in this chapter. Low cost adsorbents and synthetic adsorbents are compared and discussed. Template synthesis of mesoporous carbons are reviewed as well as their chemical surface modification. This is followed by the discussion of different physico-chemical characterization methods for ordered mesoporous silica, ordered mesoporous carbon and

modified mesoporous carbon. The chapter is concluded by a detailed review of analytical methods for mercury determination.

Chapter 3: Methodology

Chapter 3 is dedicated to the materials and methodology of the experimental approaches applied for the preparation and characterization of mesoporous silica, mesoporous carbons and modified mesoporous carbon. All aspects of the preparation of samples or materials, characterization, and treatment of data are discussed. The chapter is initiated with an introduction to the detailed methodologies for the preparation of mesoporous silica, mesoporous carbons and modified mesoporous carbon, followed by an elaborative review and validation of characterization techniques used in the study, and the experimental parameters used in their operation.

UNIVERSITY of the
WESTERN CAPE

Chapter 4: Production of mesoporous carbon materials using SBA-15, HMS and MCM-41 mesoporous silica templates

Chapter 4 gives methodology of preparation and characterization results for ordered mesoporous silica templates (SBA-15, HMS and MCM-41) as well as ordered mesoporous carbon (CA_SBA-15_LPG_105, CA_HMS_LPG_80 and CA_MCM-41_LPG_80) material. Characterization results for activated carbon (AC) as well as modified ordered mesoporous carbon (OMC) were also discussed in this chapter.

Chapter 5: Dye Adsorption

The adsorption methodology applied and results of the adsorption characteristics of ordered mesoporous carbon (CA_SBA-15_LPG_105) and activated carbon (AC) are presented. The results and graphs that describe the adsorption, dosage, pH, and equilibrium isotherms of Acid Orange 8, Rhodamine B and Methylene Blue dye adsorption processes for both mesoporous carbon (CA_SBA-15_LPG_105) and activated carbon (AC) are presented and extensively discussed here.

Chapter 6: Mercury Adsorption

UNIVERSITY of the
WESTERN CAPE

The adsorption characteristics of ordered mesoporous carbon (CA_SBA-15_LPG_105), modified ordered mesoporous carbon (MOMC) and activated carbon (AC) for mercury are presented. The results and graphs that describe the adsorption, dosage, pH and equilibrium isotherms of the Hg (II) adsorption process for mesoporous carbon (CA_SBA-15_LPG_105), modified ordered mesoporous carbon (MOMC) and activated carbon (AC) are presented and extensively discussed here.

Chapter 7: Conclusions and recommendations

The study is concluded with designation of surface properties for ordered mesoporous carbon (CA_SBA-15_LPG_105), the removal capacity for dyes (Acid Orange 8, Rhodamine B, Methylene Blue) and Hg (II) of the CA_SBA-

15_LPG_105 (and MOMC in the case of Hg (II) adsorption) as an adsorbent are discussed. Recommendations are made, anomalies noted, and the larger relevance and implications of the study are discussed. Directions for future work and industrial applications of the study are suggested.

UNIVERSITY of the
WESTERN CAPE

CHAPTER 2

LITERATURE REVIEW

2.1. WATER SCARCITY

Water scarcity has emerged as one of the most pressing problems in the 21st century. Most countries around the world, including South Africa, are faced with the growing challenge of access to clean, safe drinking water. It is estimated worldwide that 2.7 billion people will face water scarcity by 2025 **[5].** Recent statistics indicate that more people are dying annually from unsafe water than from all forms of violence combined including war. In South Africa, an estimated 5.7 million lack access to basic water services and about 18 million people lack basic sanitation services. These figures are likely to increase due to industrial expansion, rising population and climate change, which is set to affect sub-Saharan Africa. The gradual deterioration of the water quality is a factor, which must be managed efficiently in order to treat and sustain water resources in the long run **[6].** Water scarcity causes enormous problems for the vulnerable populations and societies **[7].** As a result all industries must be prepared to become involved in the preservation of natural water resources.

UNIVERSITY of the
WESTERN CAPE

The mining industry in particular is under enormous pressure to recycle and re-use water in order to minimize the intake of fresh water from rivers and from water utility companies and eliminate the continuous decantation of polluted mine water into the environment and local river systems **[7].** The practice in the mining community over the past decades has been the continuous pump-out of the rising underground mine water into the river systems **[8].** This has resulted in the pollution of surface and ground water bodies, the soil and the vegetation surrounding the mining areas, and the catchment areas. A rise in pollution and salinity of the water makes the surface water supply unfit for drinking, agriculture or environmental purposes.

UNIVERSITY of the
WESTERN CAPE

In South Africa, water is recognised as a crucial element in the battle against poverty, the cornerstone of prosperity, and a limiting factor to growth **[9].** South Africa is a semi-arid country, where water is scarce compared to most other countries. Wise utilisation of water resources in a sustainable manner is, therefore, essential for the future of the country. Already the freshwater resources of the country are under stress. For instance, most of the country's major rivers have been dammed to provide water for the increasing population; in some areas over 50 % of the wetlands have been converted for other land-use purposes **[10].** South Africa's water pollution mainly comes from mining industries, which effluents contain potentially toxic elements including heavy metals such as mercury, arsenic, cadmium, chromium, copper, lead and zinc that mix with ground water. Agricultural runoff from phosphorus fertilizers, synthetic organic compounds from textile industries

and sewage from municipal waste add to the problem. Therefore, in South Africa there is a need to solve the present water pollution problem, where conventional water treatment technologies are not sufficient. One of the approaches being explored in South Africa and in many countries is the application of Nanotechnology.

2.1.1. What is nanotechnology?

Nanotechnology is the manipulation of materials at a very tiny scale – essentially at the atomic and molecular scales. At the nanoscale, the normal rules of physics and chemistry often do not apply, and as a result many materials display unique properties that make them well suited for treating water **[12].** Hence, nanotechnology provides an opportunity to refine and optimize current techniques and also new and novel methods for treating industrial, mining and domestic wastewater. In fact, nanotechnology can offer solutions that are tailor – made to remove a specific contaminant from wastewater by making use of different nano-based techniques. This is ideal for water purification because water contains different forms of contaminants at different locations, such as heavy metals (e.g. mercury, arsenic), biological toxins including water borne disease causing pathogens (e.g. cholera, typhoid), as well as organic and inorganic solutes **[12].**

2.1.2. Nanotechnology in South Africa

In South Africa the National Nanotechnology Strategy (NNS) was launched in 2006, although nanotechnology has been embedded in national strategy and

policy since the publication of the White Paper on Science and Technology in 1996. Water is one of the six focus areas highlighted in the NNS where nanotechnology can offer the most significant benefits for South Africa. To date the government has invested through the Department of Science and Technology over R 170 million in different aspects of nanotechnology research and development (R&D) **[11].**

2.1.3. Benefits of nanotechnology

Nanotechnology offers a number of benefits to the water sector by enabling more effective removal of contaminants at lower concentrations due to increased specificity and filtration tailored for specific uses. Novel reactions at the nanoscale due to increased numbers of surface atoms may also enable the removal of contaminants that were previously very difficult to treat. The number of treatment steps, the quantity of materials, as well as the cost and energy required to purify water could be radically reduced using nanotechnology **[11].**

UNIVERSITY of the WESTERN CAPE

2.2. MERCURY AS A GLOBAL WATER POLLUTANT

Water pollution by the disposal of effluents containing heavy metals has become a worldwide concern over the past few decades. It is well known that some heavy metals are harmful and cause toxic effects to human beings and disturb sound ecological environments. Mercury is one of the first metals

known and its compounds have been under use throughout human history. Mercury and its compounds with unusual chemical and physical properties are global pollutants. Even at very low concentration, mercury causes potential hazards due to its accumulation in the food chain. The maximum concentrations of arsenic and mercury recommended by the World Health Organization are 10 ppb and 1 ppb, respectively **[12].**

The major sources of mercury pollution are effluents from chloro alkali, pulp paper, oil refining, electrical, rubber processing and fertilizer industries **[13].** Other major sources of mercury emission into the atmosphere is from flue gases emitted by coal combustors used in electricity generation **[14].** More than half of the mercury released into the environment today is from anthropogenic sources. Acute exposure to elemental mercury may cause chest pain, laboured breathing, vomiting, diarrhea, fever, metallic taste in the mouth, and a skin rash. Chronic exposure may lead to tremors, limb weakness, loss of appetite, excessive shyness, irritability, headache and memory loss. Mercury also has adverse effects on the central nervous system, pulmonary and kidney functions and the chromosomes **[15].** It is reported that mercury exposure is more harmful for developing foetuses and children under the age of four because it interferes with normal brain development. This necessitates the removal of mercury from wastewater before its recycle, transport and discharge into the environment. Commercial activated carbon is a well-known adsorbent for the removal of heavy metals from natural water and wastewater. But its high cost limits its use as an adsorbent. Hence, there is a growing need to develop low cost activated

UNIVERSITY of the
WESTERN CAPE

carbon adsorbent materials from cheaper and locally available agricultural waste materials. Numerous researchers **[16 -19]** have studied the removal of mercury from water and wastewater using low cost activated carbon adsorbents prepared from different agricultural materials.

Mercury levels in the environment have increased in the last 10–15 years due to human activities **[20–22]**. Mercury is a naturally occurring element that exists in several forms. The three most important chemical forms of mercury known to be present in the environment are: elemental mercury (Hg^0), which has a high vapour pressure and relatively low solubility in water, mercurous (Hg_2^{2+}) and mercuric (Hg^{2+}) inorganic cations which are far more soluble in water and which have a strong affinity for many inorganic and organic ligands especially those containing sulphur. Table 2.1 shows the major mercury species in the environment and biological samples **[20, 23 - 25]**.

UNIVERSITY of the
WESTERN CAPE

Table 2. 1: Major Mercury species in the environment

Elemental mercury		Hg^0
Inorganic mercury	Mercurous ion Mercuric ion	Hg_2^{2+} Hg^{2+}
Organic mercury	Methyl mercury	CH_3Hg^+
	Ethyl mercury	$CH_3CH_2Hg^+$
	Phenyl mercury	$C_6H_5Hg^+$
	Dimethyl mercury	$(CH_3)_2Hg^+$

South Africa is regarded as the country with the second highest Hg emissions in the world. This assumption is based on the estimates of total Hg emissions derived from gold mining and coal combustion. These estimates are approximate, since most countries, including South Africa, lack formal Hg inventories. Because of the health risk associated with Hg, it is important to clarify the many uncertainties regarding the transport, fate and consequences of Hg pollution from fossil fuel burning **[24, 25]**. Cases such as the Minamata incident (1950s) and the THOR Chemicals incident (1987) focused attention on the importance of Hg speciation and the toxicity of mercury **[26, 27]**.

2.2.1. Overview of mercury

UNIVERSITY of the WESTERN CAPE

Metallic mercury is a shiny, silver white metal that is a liquid at room temperature. Mercury is the familiar liquid metal used in thermometers and some electrical switches. At room temperature some of the metallic mercury will evaporate and form mercury vapours **[20, 24]**. Mercury is mined as cinnabar (HgS) ore. The metallic form is refined from mercuric sulfide ore by heating the ore to temperatures above 600ºC. This vaporizes the mercury in the ore, and the vapours are then captured and cooled to form the liquid metal mercury. Most inorganic mercury compounds are white powders or crystals except HgS which is a red salt that turns red after exposure to light **[25]**.

When mercury combines with carbon the compounds formed are called organic mercury compounds or organo-mercurials. There are a large number of organic mercury compounds, but by far the most common organic mercury compounds found in the environment are methyl mercury and phenyl mercury.

In the past a number of these organic mercury compounds were used in pesticides and as biocides in some paints, pharmaceuticals and cosmetics **[26]**. While many of the uses of mercury have decreased in the recent years, some parts of the world are still using these toxic compounds. Some examples are the use of seed dressing with mercury compounds in some countries **[20]**, use of dimethyl mercury **[26]** in small amounts as a reference standard for some chemicals tests and thimerosal (which contains ethyl mercury) used as a preservative in some vaccines and other medical and cosmetic products **[21]**.

Mercury levels in the environment need to be monitored more strictly due to the fact that all mercury species can interchange in the environment **[24]**. The most common organic mercury form that micro organisms and natural processes generate is methyl mercury. Methyl mercury is of particular concern because it can build up in many edible freshwater and saltwater fish and marine life to levels that are many times greater than levels in surrounding water. Methyl mercury can be formed in both chemical processes (abiotic) and by micro organisms (biotic) in the environment. It is believed that its formation in nature is predominantly due to the latter. Being an element, mercury cannot be broken down or degraded into harmless substances **[21].** Mercury may change between different states and forms in its cycle (Figure 2.1).

UNIVERSITY of the
WESTERN CAPE

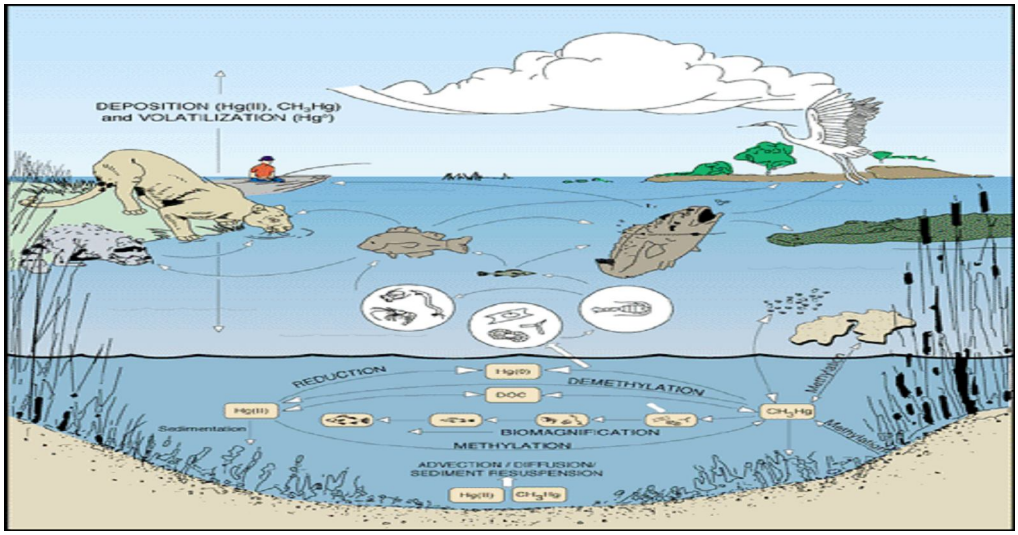

Figure 2. 1: Mercury cycle in the environment **[21]**

UNIVERSITY of the
WESTERN CAPE

2.2.2. Mercury species in soil

In soil the formation of inorganic mercury compounds are preferred. Compounds such as $HgCl_2$, Hg $(OH)_2$ and inorganic Hg^{2+} are found in soil, and can form complexes with organic anions. This complexing ability limits the mobility of mercury in soil. Much of mercury in soil is bound to bulk organic matter. For this reason mercury has a long retention time in soil and as a result, the mercury accumulated in soil may continue to be released to surface waters and other media for long periods of time **[21, 22]**.

2.2.3. Toxicology

Bio-inorganic co-factor cobaltamin has been referred to as the nature's most beautiful co-factor, but it may be one of nature's most deadly. It is responsible for methyl transfer reactions, including the methylation of inorganic Hg^{2+}. Methylcobalamin (a structural analogue of vitamin B12 figure.2.2), contains a cobalt atom in an octahedral geometry with and axial methyl group. In sulphate reducing bacteria such as *Desulfovibrio desulfricans* the methylation of mercury by methylcobalmin is enzymatically catalyzed **[25, 26, and 28].** The mechanism of this reaction is not fully understood, although it is believed to be a one step process. The methylated product is stable in water due to the more covalent nature of the mercury carbon bond. It is also soluble in lipid membranes common to living organisms. Although all forms of mercury are toxic, the methylated form of mercury is considered to be by far the most toxic.

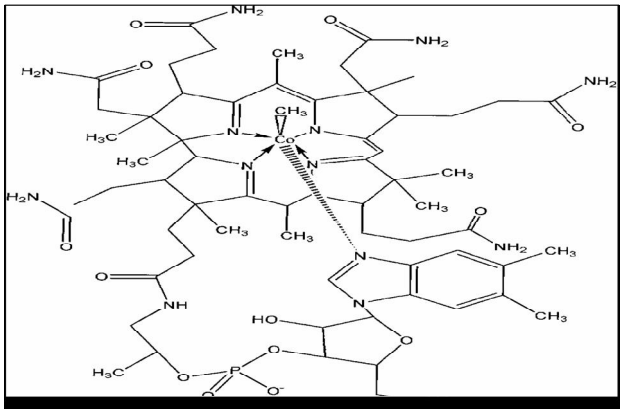

Figure 2. 2: Structure of Methylcobalmin **[21].**

$$Hg^{2+} + CH_3B_{12} \rightarrow CH_3Hg^{+} + CH_3B_{12} \rightarrow (CH_3)_2Hg^{+}$$

(2.1)

The liver reabsorbs rather than excretes methyl mercury due to a process known as enterohepatic recirculation **[25].** This is why methyl mercury tends to bio-accumulating in living organisms; once it is consumed, it is almost never excreted. Methyl mercury also crosses the blood –brain barrier and tends to accumulate in the brain of mammals. Methyl mercury is a well known neurotoxicant. Once inside the human methyl mercury attacks the nervous system by binding to key biological sulphur containing compounds. The result is a loss of feeling in the hands and feet, constriction in vision, tremors, loss of hearing and eventually death. History records several major cases of methyl mercury poisoning **[24].** When methyl mercury was first synthesized and reported in the early 1850s, two of the chemist working on the project died and a third was debilitated. In 1956 residents of the Minamata Bay, Japan area, suffered from a strange nervous disorder due to polluted waste water containing mercury. This was eventually diagnosed as mercury poisoning due to waste dumped by the Chisso Minamata Acetaldehyde Plant and the Minamata Chemical Industrial Plant. The pollution affected the people in the form of methyl mercury poisoning known as “Minamata disease”. People eating large quantities of contaminated fish and shellfish from the Bay were all affected. Many people lost their lives or suffered from physical deformities **[24, 26, 29, 30].**

UNIVERSITY of the WESTERN CAPE

In September 1971 due to fears of famine Iraq imported large amounts of seed wheat which had been treated with methyl mercury fungicides. Imported mercury treated seed grains arrived after the planting season and were subsequently used as grain to make into flour that was baked into bread. Unlike the long term exposure in Japan, the methyl mercury poisoning incident in Iraq was much shorter, but the magnitude of the exposure was high. The number of people admitted to the hospital with symptoms of poisoning has been estimated to be approximately 6500, with 459 fatalities reported. Currently a new epidemic of Minamata disease is building in the Amazon River region, where gold mining has resulted in widespread mercury release into the river. There the mercury is methylated and is now bioaccumulation in fish. No deaths have yet been reported but many people seem to suffer from mild cases of Minamata disease **[20 - 26, 29, 30].**

UNIVERSITY of the
WESTERN CAPE

2.2.4. Impact of mercury on the environment

An important factor in the impacts of mercury to the environment is its ability to build up in the organism and along the food chain. The term bio-accumulation refers to the net accumulation over time of metals within an organism from both biotic (other organisms) and abiotic (soil, air and water) sources. Biomagnifications refers to the progressive build up of some heavy metals by successive trophic levels-meaning this relates to the concentration ratio in a tissue of predator organisms as compared to that in its prey. Although all forms of mercury can accumulate to some degree, methyl mercury accumulates to a greater extent than other forms of mercury.

Inorganic mercury can also be absorbed, but is taken up at a much slower rate with lower efficiency than methyl mercury **[22-24].**

2.2.5. Sources of mercury

The emissions of mercury to the biosphere can be grouped in the following categories:

- Emissions due to natural mobilisation
- Anthropogenic sources
- Re-emissions of previous anthropogenic releases
- Product and process releases of mercury

UNIVERSITY of the
WESTERN CAPE

2.2.6. Natural sources of mercury

Natural sources of mercury include volcanoes, evaporation from soil and water surfaces, degradation of minerals, forest fires etc. Mercury can be found in all geological media in relatively small concentrations. Elemental and some oxidized mercury are permanently coming into the atmosphere due to their volatility. High temperature in the earth mantle results in high mercury mobility and mercury continuously diffuses to the surface. Today's emissions of mercury from soil and water are however not only from natural sources but are also influenced by previous deposition of mercury from other sources. This makes it very difficult to determine the actual natural mercury emissions. A number of attempts have been made to estimate the global natural

emissions of mercury. It is however difficult to do so with any precision and research is still done in this field by different research groups **[20-26].**

2.2.7. Anthropogenic sources of mercury

Mercury is naturally present in coal and other fossil fuels as well as in minerals like lime used for making cement. Coal fired power production has been shown to be the single largest global source of atmospheric mercury emissions. This is due to the increasing global power consumption worldwide **[31].** Mining and other metallurgic activities involving the extraction and processing of recycled minerals like iron, steel, gold and zinc also contributes to mercury releases as an anthropogenic source **[25].**

UNIVERSITY of the
WESTERN CAPE

2.2.8. Industrial uses of mercury

Mercury has found a number of uses throughout history. Prehistoric cave man appears to have used cinnabar (HgS) as a red pigment **[25].** Mercury amalgams were also used to extract precious metals from ores. Until recently mercury was the preferred thermometric medium for thermometers because of its uniform thermal expansion. It has also been widely used in barometers and manometers for pressure measurements, leading to mercury contamination. Another important use of mercury is in the lighting industry. Most fluorescent lamp utilizes mercury vapour, along with an inert gas such as argon to convert an electrical discharge to useful light. The tube shaped bulbs contain this mercury gas mix. The mercury is excited by a flow of electrons

and radiates light in the UV region. Mercury in electrolytic cells used in the chloro-alkali industry is also a major use. Chloro-alkali plants produce sodium hydroxide and chlorine gas via the electrolysis of brine. The mercury serves as an anode converting the sodium cations to sodium metal, amalgamating the sodium and carrying it into a second reaction where it reacts with water to form sodium hydroxide. This process is a major source of mercury pollution. Because of this, mercury cells are being replaced by diaphragm cells. Mercury cell batteries were also used widely for applications such as hearing aids. The standard mercury cell battery contains a mercury/zinc amalgam as the anode and a mercuric oxide/graphite cathode. Mercury is also found in zinc-silver cell batteries and traces of mercuric chloride are found in zinc-carbon batteries **[24-26].**

UNIVERSITY of the
WESTERN CAPE

2.2.9. Environmental regulations

Federal state and local governments can issue fish consumption advisories about which fish are unsafe to eat or which bodies of water are unsafe to fish. Laws and regulations are used as major tools to protect the environment from mercury released through emissions from manufacturing use, or disposal activities. These regulations are often enforced by agencies such as the Environmental Protection Agency (EPA). The EPA provides specific rules and details for how to put the law into practice. The World Health Organization (WHO) has published a maximum daily human consumption limit of 0.48 µg total mercury per kg body weight **[31, 32].** EPA has also published methods

used by industrial and municipal facilities to analyze the components of wastewater, drinking water, sediment and other environmental samples.

The following table includes a list of the more prominent methods used by the environmental community **[20, 26]** to establish mercury content.

Table 2. 2: Analytical methods for mercury detection **[26]**

Method Number	Description
EPA 200.8	Metals in water using ICP\MS
EPA 245.1	Mercury in water using CV-AAS
EPA 1631E	Mercury in water using CV-AFS
EPA 7471A	Mercury in solids using CV-AAS
EPA 101A	Gaseous mercury using CV-AAS
ASTM D-6350	Mercury sampling in natural gas CV-AFS

UNIVERSITY of the
WESTERN CAPE

2.3. MORDERN TECHNOLOGIES IN WATER TREATMENT

There are several ways of separating heavy metals and organic compounds from waste water; these include chemical precipitation, membrane filtration, electro chemical treatment, ion exchange carbon adsorption and co-precipitation or adsorption. All these methods, with the exception of adsorption

are not economically viable, have low output and are incapable of removing trace levels of heavy metal ions from wastewater **[33].** Sorption techniques involve the use of ion exchange and affinity chromatography. Adsorption is a removal process where certain elements or ions are bound to an adsorbent particle surface by either chemical or physical adsorption.

Adsorbents are widely used for water and wastewater treatment due to their higher output and lower costs. Among current adsorbents, activated carbons are used in different industries as water purifiers. This is due to their highly developed internal surface area and porosity. Especially the development of micro and mesopores is of great importance because it allows the carbon to adsorb atoms or molecules of different sizes **[33, 34].** According to the IUPAC compendium, a mesopore is the name given to the pores with width between those of micropores (pore size < 2 nm) and macropores (pore size > 50 nm). The difference in size does not simply lead to various molecular sieving effects, but also to a wide range of characteristic chemical phenomena occurring within the pores **[35, 36].**

UNIVERSITY of the
WESTERN CAPE

To discover chemically interesting phenomena specific to a particular pore size, ordered porous materials are needed, which have a defined pore size and a well developed porous structure **[35].** Activated carbons have wide pore size distribution from micropores to mesopores; the micropores usually contribute a significant fraction of the total pore volume. This pattern of pore size distribution is not suitable for solid materials to be used in solution. Considerable effort has been devoted to diminishing the number of small

micropores in order to increase the uptake capacitance of activated carbons **[34].** The reason is that, activated carbon is made by heating organic material, such as wood or bone, until all that is left is carbon riddled with tiny holes that trap pollutants **[34].** The high surface area and porosity of activated carbons are the result of the activation process; physical or chemical activation. During activation process, carbonaceous char with little internal surface is oxidized in an atmosphere of air, carbon dioxide, or steam at a temperature of 800 to 900 ^{0}C. This results in the oxidation of some of the regions within the char in preference to others so that a preferential etching takes place, as the combustion proceeds, causing an increase in surface area **[34].**

The complexity of the carbon structure prevents the conventional activation process from preparing carbon materials with strictly controlled or uniform pore structure, although extensive research has been done and great effort has been made toward the control of pore size and its distribution. The recent development of industrial technology requires that carbon should have the desired pore structure for new application fields **[34, 35].**

The more important parameters that determine the adsorptive removal of adsorbates from water are the nature and molecular dimension of an adsorbate, the porous structure and chemical nature of the carbon surface, and pH of the solution. For adsorption on a solid surface carbon as an adsorbent for water treatment, the carbon material should have a mesoporous structure. Activated carbons have specific surface areas often exceeding 2000 m^2/g however they have wide pore size distribution from micropores to

macropores. The micropores usually contribute a significant fraction of the pore volume and the BET surface area. This pattern of pore size distribution is not suitable for the carbon materials to be used in solution. Hence, considerable effort has been devoted to diminishing the number of small micropores to mesopores in order to increase the uptake capacity of the carbon materials **[35].** Therefore, high surface area and narrow pore size distribution of mesopores play a major role in increasing adsorption capacity.

Until recently, there have been numerous studies conducted on the environmental applications of ordered mesoporous silica (OMSi) materials as adsorbents for water treatment. However, these materials have several defects in spite of their advantages for adsorption of toxic substances from water. One of the major disadvantages of ordered mesoporous silica (OMSi) is the instability of the silica mesoporous structure under hydrothermal conditions, such as boiling water **[35].** The fragility in water provokes a doubt about its durability in practical application.

UNIVERSITY of the WESTERN CAPE

Hence, the major focus of the existing study is to develop highly stable, ordered mesoporous carbon (OMC) materials for effective removal of organic compounds (e.g. Organic Dyes) and Inorganic Mercury (Hg^{2+}) from water. The determination of surface properties of ordered mesoporous carbon (OMC) materials using acidic and basic organic dyes may give special insight about the OMC **[35].**

2.4. ADSORPTION ON A SOLID SURFACE

Activated carbons or porous carbons are unique and versatile adsorbents. Their adsorbent properties are attributed to their large interparticulate surface area, uniform adsorption effect, high adsorption capacity, a high degree of surface reactivity and a favorable pore size which make the internal surface available and enhances the adsorption rate. The most widely used activated carbons or porous carbons have a surface area of about 800 to 1500 m^2/g. In activated carbons, this surface area is contained predominantly within micropores which have effective diameter less than 2 nm. The pore size distribution in a given carbon depends on the type of the raw material, the method and conditions under which the carbon has been prepared **[35].**

UNIVERSITY of the

Forces that hold a solid material together tend to produce a field of force around each ion, atom, or molecule. At the surface of the molecule these forces cannot suddenly disappear and thus reach out in space beyond the surface of the solid. Due to these unsaturated and unbalanced forces, the solid has a tendency to attract and retain on its surface molecules and ions of other substances with which it comes into contact. Thus, when a solid surface comes in contact with a gas or liquid, the concentration of the gas or liquid is always greater on the surface of the solid than in the bulk gas or liquid phase. The balance of the forces is partially restored by the adsorption of the gas or liquid on the surface of the solid. The substance attached to the surface is

called the *adsorbate*, and the substance to which it is attached is called the *adsorbent* **[34, 37-39].**

Adsorption of a gas or liquid on a solid surface is a spontaneous process. It is, therefore, accompanied by a decrease in the free energy of the system. Furthermore, the gaseous or liquid molecules in the adsorbed state have fewer degrees of freedom than in the gaseous or liquid state. This results in a decrease in entropy during adsorption. Using the thermodynamic relationship

$$\Delta G = \Delta H - T\Delta S \qquad (2.2)$$

It follows that the term ΔH, which is the heat of adsorption, must be negative indicating that adsorption is an exothermic process. However, a few adsorption cases have been reported to be endothermic. For example the adsorption of hydrogen on glass, adsorption of oxygen on silver, and adsorption of hydrogen on iron are endothermic. The endothermicity of these adsorption processes is attributed to an increase in the entropy of the adsorbate due to the dissociation of the molecules during the adsorption process or increase in the entropy of the adsorbent **[37-39].**

Depending on the nature of the forces that are at hand; adsorption is of two types; physical or Van der Waals adsorption, and chemisorption or chemical adsorption. In the case of physical adsorption, the adsorbate is bound to the surface by weak Van der Waals forces identical with molecular forces of cohesion that are involved in the condensation of vapours into liquids. Chemisorption, on the other hand involves exchange or sharing of electrons

UNIVERSITY of the WESTERN CAPE

between adsorbate molecules and the surface of the adsorbent, resulting in chemical reaction. The bond formed between the adsorbate and the adsorbent is a chemical bond and is much stronger than in physical adsorption **[37, 39].**

Because the nature of the forces involved in the two types of adsorption are different, the two differ in several ways. The most common difference between the two kinds of adsorption is in the magnitudes of the heat of adsorption. In the case of physical adsorption, the heat of adsorption is of the same order as the heat of condensation and does not usually exceed 10 to 20 KJ per mole, whereas in chemisorption the heat of adsorption is usually 40 to 400 KJ per mole. However, in some cases the heat of chemisorption does not differ substantially from the heat of physical adsorption. Physisorption does not require any activation energy so that the rate of adsorption is very high, even at low temperatures. The chemisorption, on the other hand, requires activation energy; the rate of adsorption is low and depends on the temperature of adsorption. However, when the surface of the adsorbent is very reactive, as in the case of ultra clean carbon surfaces, the rate of chemisorption can be very high, even at low temperatures **[34, 37-39].**

UNIVERSITY of the
WESTERN CAPE

Similarly, physisorption in microporous adsorbents may be very much retarded by the slow diffusion of the adsorbate into the fine pores and may require activation energy. Physical adsorption is non specific and may occur between any adsorbate – adsorbent system, while chemisorption is specific. For example, carbon dioxide is not chemisorbed by an iron catalyst at 450 ^{0}C,

whereas nitrogen can be chemisorbed with surface coverage of about 50 %. The thickness of the adsorbed phase is another point of difference between chemisorption and physisorption. In physisorption, the thickness is multimolecular, whereas, with chemisorption, the thickness is monomolecular **[38].**

The type of adsorption that takes place in an adsorbate-adsorbent system depends upon the reactivity of the surface, the nature of the adsorbate, the nature of the adsorbent, and the temperature of adsorption. For example, the adsorption of oxygen on active carbon is physical and adsorption takes place to a large extent at temperatures below -100 ^{0}C. When it is not certain that the process of adsorption is either physisorption or chemisorption, or when both are occurring in appreciable proportions, it is preferential to use a less committal term: *sorption* **[34, 37-39].**

UNIVERSITY of the
WESTERN CAPE

2.5. ADSORPTION EQUILIBRIUM

When a solid surface is exposed to a gas or liquid, the molecules of the gas or liquid strike the surface of the solid. Some of the striking molecules stick to the solid surface and become adsorbed while the others rebound. Initially the rate of adsorption is large as the whole surface is bare but as more and more of the surface becomes covered by the molecules of the gas or liquid, the available bare surface decreases and so does the rate of adsorption.

However, the rate of desorption, which is the rate at which adsorbed molecules rebound from the surface, increases because desorption takes place from the covered surface. As time passes, the rate of adsorption continues to decrease until equilibrium is reached between the rate of adsorption and the rate of desorption. At this stage the solid is in adsorption equilibrium with the gas or liquid, and the rate of adsorption is equal to the rate of desorption **[34].** It is a dynamic equilibrium because the number of molecules sticking to the surface is equal to the number of molecules rebounding from the surface.

For a given adsorbate-adsorbent system, where the adsorbate is a gas; the equilibrium amount adsorbed x/m is a function of pressure and temperature; i.e.

UNIVERSITY of the
WESTERN CAPE

$$\frac{x}{m} = f(p,T) \qquad (2.3)$$

where x/m is the amount adsorbed per unit mass of the adsorbent at the equilibrium pressure p, and T is the temperature of adsorption **[39].**

2.6. ADSORPTION ISOTHERM EQUATIONS

The adsorption isotherm is the most extensively employed for representing the equilibrium state of an adsorption system. It can give useful information regarding adsorbates, the adsorbent, and the adsorption process. It helps in the determination of the surface area of the adsorbent, the volume of the pores, and their size distribution, the heat of adsorption, and the relative adsorbability of a gas or vapor on a given adsorbent. Several adsorption isotherm equations have been derived. The more important adsorption isotherms are the Langmuir, the Freundlich, the Temkin, the Brunauer-Emmett-Teller (BET), and the Dubinin equations. The first three isotherm equations are very important for chemisorption, although the Langmuir and Freundlich isotherms are equally important for physisorption. The BET equation and the Dubinin equations are more important for analysis of the physical adsorption of gases and vapors on porous carbons **[34].**

UNIVERSITY of the
WESTERN CAPE

There are three possible theoretical approaches for deriving the adsorption isotherms:

- The kinetic approach
- The statistical approach
- The thermodynamic approach

In the kinetic approach, the condition of the equilibrium is that the rate of adsorption is equal to the rate of desorption at equilibrium. In the statistical approach, the equilibrium constant is represented by a ratio of partition functions of vacant sites, adsorbed molecules and gas phase molecules. The isotherm equation can be obtained by equating this ratio to the corresponding ratio of the concentrations; this approach has the advantage that it gives a numerical value to the constants that cannot be evaluated by the kinetic approach. The equilibrium can also be approached thermodynamically, using either the conditions that the work done in transferring an infinitesimal amount of gas from the gas phase to the surface at constant temperature is zero, or alternatively the Gibbs adsorption equation **[34, 37-39].**

UNIVERSITY of the
WESTERN CAPE

2.7. LANGMUIR ISOTHERM EQUATION

The Langmuir equation is the first theoretically developed adsorption isotherm. Many of the equations proposed later and which fit the experimental results over a wide range are either based on this equation, or these equations have been developed using the Langmuir concept. Thus, the Langmuir equation still retains an important position in physisorption as well as chemisorption theories. The equation has also been derived using thermodynamic and statistical approaches but the commonly used kinetic approach will be used for its derivation **[39].**

The American scientist, I. Langmuir, derived this equation based on certain assumptions. The more important of these assumptions are

● The adsorbed entities (atoms or molecules or ions) are attached to the surface at different localized sites.

● Each site accommodates one and only one adsorbed entity.

● The energy state of each adsorbed entity is the same at all sites on the surface independent of the presence or absence of other adsorbed entities at neighboring sites. Thus, the Langmuir model (also called localized model) assumes that the surface is perfectly smooth and homogeneous and that the lateral interactions between the adsorbed entities are negligible **[38].**

In the original kinetic approach, the equilibrium is assumed to be dynamic in that the rate at which the molecules from the gas phase strike the surface and condense on the bare sites is equal to the rate at which the molecules evaporate from the occupied sites **[42-44].** In other words, the rate of adsorption is equal to the rate of desorption.

UNIVERSITY of the
WESTERN CAPE

If at any pressure *p* of the gas the fraction of the sites occupied is θ_0 (so that $\theta + \theta_0 = 1$) then the rate of condensation (adsorption) is

$$rads = r_{ads} = akp\theta_0 \qquad (2.4)$$

where *p* is the pressure and *k* is a constant given by the kinetic theory of gases k = $N/(2\pi kmT)^{1/2}$; a is the condensation coefficient that is the fraction of the striking molecules that actually condense on the surface **[41- 43].**

The evaporation (desorption) of an adsorbed molecule from the surface is essentially an activated process in which the energy of activation, E, for desorption may be identified with – ΔH, the differential (isosteric) heat of desorption. The rate of evaporation r_{des} can be written as

$$rdes = Z_m \theta v e^{-E/RT} \qquad (2.5)$$

where Z_m is the number of molecules adsorbed (occupied sites) per unit area of the surface so that Z_m represents the corresponding number of adsorbed molecules, and *v* is the frequency of oscillation of the molecules perpendicular to the surface and closely related to the frequency of vibration of the atoms or molecules of the adsorbent. Thus, at equilibrium,

$$r_{ads} = r_{des} \qquad (2.6)$$

$$akp\theta_0 = Z_m \theta_1 v e^{-E/RT} \qquad (2.7)$$

$$akp(1-\theta) = Z_m \theta v e^{-E/RT} \qquad (2.8)$$

so that

$$\frac{\theta}{1-\theta} = \frac{akp}{Z_m ve^{-E/RT}} = bp \qquad (2.9)$$

where

$$b = \frac{ak}{Z_m ve^{-E/RT}} = bp \qquad (2.10)$$

or

$$\theta = \frac{bp}{1+bp} \qquad (2.11)$$

The fraction θ of the surface covered can also be written as the ratio of volume v of the gas or vapour adsorbed at pressure p and V_m, the volume of the adsorbate required to form a monomolecular layer. Thus, Equation 2.11 can also be written as

UNIVERSITY of the
WESTERN CAPE

$$\frac{V}{V_m} = \frac{bp}{1+bp} \qquad (2.12)$$

$$V = \frac{V_m bp}{1+bp} \qquad (2.13)$$

This relationship shows that V tends asymptotically to V_m as p tends to infinity. Equation 2.11 is a well known Langmuir isotherm equation. θ can also be written as

$$n/n_m = \frac{bp}{1+bp} \qquad (2.14)$$

where

n is the number of moles adsorbed per gram of the adsorbent and n_m is the monolayer capacity in moles.

Similarly, θ can also be expressed in terms of the amount adsorbed in grams as $\frac{x}{m}$ so that

$$\frac{x}{m} = \frac{bp}{1+bp} \qquad (2.15)$$

UNIVERSITY of the
WESTERN CAPE

where x in grams is the amount adsorbed per gram of the adsorbent, and x_m is the monolayer capacity in grams.

Depending upon the pressure, Equation 2.13 reduces to two limiting expressions. At low pressure the value of bp is less than unity; i.e., at the beginning of the adsorption process it reduces to the approximate form

$$V = V_m bp \qquad (2.16)$$

which indicates proportionality between the amount adsorbed and the equilibrium pressure?

At high pressure $K_p >> 1$ (i.e. for advanced stage adsorption), equation 2.13 is reduced to

$$V = V_m \qquad (2.17)$$

This indicates that at higher pressure, adsorption is independent of pressure because it has attained the highest value equal to V_m, the volume required to cover a surface by a monolayer.

Rearrangement of equation 2.13 gives the linear form of the equation

$$p/V = \frac{1}{V_m b} + \frac{p}{V_m} \qquad (2.18)$$

UNIVERSITY of the
WESTERN CAPE

The slope of the linear plot gives the value of V_m, while the value of b can be obtained from the intercept. The value of V_m can be used to calculate the surface area of the adsorbent **[38-40].**

The linear Langmuir isotherm does not necessarily mean that the adsorption process meets the requirements of the idealized localized monolayer model even when reasonable values of V_m and b are obtained. This is due to the fact that perfectly energetically homogeneous surfaces are rare and difficult to obtain. In some cases the effect of non-homogeneity of the surface may be compensated by adsorbate – adsorbent interactions and thus give rise to linear Langmuir plots. Bansal and Goyal **[34]** suggested that along with

Langmuir adsorption different heats of adsorption should also be measured which, according to the Langmuir concept, should be independent of the degree of surface coverage.

2.8. APPLICABILITY OF LANGMUIR ISOTHERM EQUATION

The Langmuir equation

$$\theta = \frac{V}{V_m} = \frac{bp}{1+bp} \tag{2.19}$$

can be transformed into the following three linear forms:

UNIVERSITY of the
WESTERN CAPE

$$\frac{p}{V} = \frac{1}{bV_m} + \frac{p}{V_m} \tag{2.20}$$

$$\frac{V}{V_m P} = b - \frac{bV}{V_m} \tag{2.21}$$

$$\frac{V_m}{V} = 1 + \frac{1}{bp} \tag{2.22}$$

Thus, it is apparent that plots of $\frac{P}{V}$ against p, $\frac{V}{P}$ against $-V$, and $\frac{1}{V}$ against $\frac{1}{P}$ should yield straight lines from which the values of V_m and b can be calculated.

The last linear plot i.e. $\frac{1}{V}$ against $\frac{1}{P}$ should be avoided because it lays too much emphasis on the low pressure region of the isotherm and adsorption is rarely representative of the whole surface **[44].**

The applicability of the Langmuir isotherm equation to the experimental data was carried out by a number of workers, but deviations were often noticed. According to the Langmuir isotherm equation, the plot of p/v against p should be linear from $\theta = 0$ to $\theta = \infty$, and it should give a reasonable value of V_m; furthermore V_m should be temperature independent. When the experimental data was subjected to these criteria, only few data conformed to Langmuir model. Titoff **[43]** observed that the value of V_m fell from 231 cm^3 (NTP) g^{-1} at 195.6 K to 113 cm^3 at 303 K. Furthermore, the Langmuir theory requires the heat of adsorption to be independent of the surface coverage while direct determinations of heat of adsorption are found to decrease invariably with increasing surface coverage. Thus, although the Langmuir isotherm equation is of limited significance for interpretation of the adsorption data because of its idealized character, the equation remains of basic importance for expressing dynamic adsorption equilibrium. Furthermore, it has provided a good derivation of other more complex models. The assumption that the adsorption sites on solid surface are energetically homogeneous and that there are no lateral interactions between the adsorbed molecules are the weak points of the Langmuir model **[44-45].**

UNIVERSITY of the
WESTERN CAPE

2.9. FREUNDLICH ADSORPTION ISOTHERM

The Freundlich isotherm is a limited form of the Langmuir isotherm, and is applicable only in the middle ranges of vapour pressure. The general form of the Langmuir isotherm is written as follows

$$V = \frac{V_m bp}{1 + bp} \qquad (2.23)$$

At low pressure, bp is much smaller than unity and, therefore, can be neglected in the denominator so that the equation becomes

$$V = V_m bp \qquad (2.24)$$

UNIVERSITY of the

indicating that the amount adsorbed is proportional to the first power of the pressure. At high pressures, equation (2.24) becomes $V = V_m$ so that the amount adsorbed becomes independent of the pressure. It is thus apparent that in the middle ranges of pressure, the amount adsorbed can be represented by a fractional exponent $\frac{1}{n}$, which will tend to vary between zero and unity, depending upon whether the pressure increases or decreases. This can be expressed by a general form of the adsorption equation.

$$\frac{V}{V_m} = bp^{1/n} \qquad (2.25)$$

This is known as the *Freundlich equation*, which is followed only at medium pressures. The equation is of greater significance for chemisorptions although

some physical adsorption have also been explained using this equation. For adsorption from solution phase, the equation can be written as

$$\frac{V}{V_m} = \frac{x}{m} = Kc^{1/n} \qquad (2.26)$$

where c is the equilibrium concentration and x/m is the amount adsorbed per unit mass of the adsorbent **[32].** The constant n is the Freundlich equation constant that represents the parameter characterizing quasi Gausian energetic heterogeneity of the adsorption surface. The equation can be written in linear form as

$$\ln \frac{x}{m} = \ln k + \frac{1}{n} \ln c \qquad (2.27)$$

UNIVERSITY of the
WESTERN CAPE

so that a plot of $\ln(x/m)$ against $\ln c$ gives a straight line with an intercept on the ordinate axis. The value of n and K can be obtained from the slope and the intercept of the linear plot. The value of n is always greater that unity **[34].**

2.10. EQUILIBRIUM MODELING OF ADSORPTION IN A LIQUID PHASE.

Equilibrium data, commonly known as adsorption isotherms, are basic requirements for the design of adsorption systems used for the removal of organic dyes or/and mercury (II) from aqueous media. The Langmuir, Freundlich are the most frequently used two-parameter models in the

literature describing the non-linear equilibrium between the adsorbed pollutant (adsorbate) on the adsorbent (q_{eq}) in solution (C_{eq}) at a constant temperature.

2.10.1. The Langmuir Model

The Langmuir equation which is valid for monolayer sorption onto a surface with a finite number of identical sites is given by equation (2.28).

$$q_{eq} = \frac{Q_o b C_{eq}}{1 + bC_{eq}} \qquad (2.28)$$

where q_{eq} is the amount adsorbed (mg/g), C_{eq} is the equilibrium concentration of the adsorbate (mg/L), and parameters Q_o and b are Langmuir constants related to maximum adsorption capacity (mg/g) (monolayer capacity) and bonding energy of adsorption (L/mg), respectively, which are functions of the characteristics of the system as well as time **[44].**

UNIVERSITY of the
WESTERN CAPE

Plots were obtained from $\left[\frac{1}{q_{eq}} = \frac{1}{Q_o} + \frac{1}{bQ_o C_{eq}} \right]$ which was the linearized form of the Langmuir equation, for $1/q_{eq}$ versus $1/C_{eq}$, for the adsorption of pesticides showing the applicability of the equation. The values of monolayer capacity (Q_0) and Langmuir constant (b) have been evaluated from the intercept and the slope of these plots.

The adsorption capacity can be correlated with the variation of surface area and porosity of the adsorbent. Higher surface area and pore volume will

result in higher adsorption capacity. The Langmuir equation is used for homogeneous surfaces.

2.10.2. The Freundlich Model

The Freundlich model assumes neither homogeneous site energies nor limited levels of sorption. The Freundlich equation has the general form:

$$q_{eq} = K_F C_{eq}^{1/n} \qquad (2.29)$$

where q_{eq} is the amount adsorbed (mg/g), C_{eq} is the equilibrium concentration of the adsorbate (mg/L), K_F ((mg/g)*(mg/L)^n) and n are the Freundlich constants related to adsorption capacity and adsorption intensity, respectively **[45].** Equation (2.29) can be linearized in logarithmic form.

UNIVERSITY of the WESTERN CAPE

Plots were obtained from $\left[\ln q_{eq} = \ln K_F + \frac{1}{n}\ln C_{eq}\right]$ which was the linearized form of Freundlich equation. ln q_{eq} versus ln C_{eq} linear plots would give the value of $\frac{1}{n}$ as slope and K_F as intercept. The value of K_F can be used as alternative measure of adsorption capacity, while 1/n determines the adsorption intensity.

2.11. LOW COST ADSORBENTS

Sorption of metals depends heavily on experimental conditions such as pH, metal concentration, ligand concentration, competing ions, and particle size

[33]. Heavy metal contamination exists in aqueous waste streams of many industries, such as metal plating facilities, mining operations, and tanneries. The soils surrounding many military bases are also contaminated and pose a risk of groundwater and surface water contamination. Some metals associated with these activities are cadmium (Cd), chromium (Cr), lead (Pb), and mercury (Hg). Heavy metals are not biodegradable and tend to accumulate in living organisms, causing various diseases and disorders. Treatment processes for metals contaminated waste streams include chemical precipitation, membrane filtration, ion exchange, carbon adsorption, and coprecipitation/adsorption. Cost effective alternative technologies or sorbents for treatment of metals contaminated waste streams are needed. Natural materials that are available in large quantities, or certain waste products from industrial or agricultural operations, may have potential as inexpensive sorbents. Due to their low cost, after these materials have been expended, they can be disposed of without expensive regeneration **[46, 47].**

UNIVERSITY of the
WESTERN CAPE

A sorbent can be assumed as “low cost” if it requires little processing, is abundant in nature, or is a by-product or waste material from another industry. Improved sorption capacity may compensate the cost of additional processing. Scattered research has already been conducted on a wide variety of sorbents. Some of the reported low-cost sorbents include: bark/tannin-rich materials, lignin, chitin/chitosan, dead biomass, seaweed/algae/alginate, xanthate, zeolite, clay, fly ash, peat moss, bone gelatin beads, leaf mould, moss, iron-oxide-coated sand, modified wool, and modified cotton **[33].**

2.11.1. Zeolites

Zeolites, such as clinoptilolite are generally known to demonstrate strong affinity for Pb and other heavy metals **[46].** Zeolites are naturally occurring silicate minerals, which can also be produced synthetically. Clinoptilolite is probably the most abundant of more than 40 natural zeolite species **[49].** Deposits of this mineral occur in abundance throughout the western United States and in South Africa, making it readily available and inexpensive. The adsorption properties of zeolites result from their ion-exchange capabilities. The three dimensional structure of zeolite possesses 4 angstron (zeolite A) **[68]** channels containing negatively charged sites resulting from Al^{3+} replacement of Si^{4+} in the tetrahedra. Sodium, calcium, potassium and other positively charged exchangeable ions occupy the channels within the structure, and can be replaced with heavy metals **[48 - 50].**

UNIVERSITY of the
WESTERN CAPE

2.11.2. Fly ash

Grover and Narayanaswamy **[50]** observed that fly ash, a waste product from thermal power plants, has some adsorption capabilities for Cr (VI). Fly ash consists of carbon and oxides of silica, alumina and iron. An adsorption capacity of 4.250 mg Cr (VI)/g was observed at pH 2.0. Kapoor and Viraraghavan **[51]** noted that the properties of fly ash are extremely variable and the adsorption capacity varies with the lime content. Banerjee et al **[52]** reported on the adsorption kinetics of organic compounds and deduced that

capacity increases with carbon content. The surface area of flyash is reported as 1± 6 m^2/g. A potential advantage of fly ash is that it could easily be solidified after the metals are adsorbed because it contains pozzolanic particles that react with lime in the presence of water, forming cementitious calcium-silicate hydrates. It is important to note that fly ash may contain heavy metals and trace amounts of radioactive elements. The possibility of competitive displacement or leaching should also be considered and evaluated **[50 - 52].**

2.11.3. Lignin

UNIVERSITY of the WESTERN CAPE

Srivastava et al **[53]** studied adsorption of lead (Pb) and zinc (Zn) onto lignin. The lignin was extracted from black liquor, a waste product of the paper industry. The adsorption capacity for lignin at 30 ^{0}C was found to be 1587 mg/g for Pb and 73 mg/g for Zn, which increased to 1865 and 95 mg/g, respectively at 40 ^{0}C. The high adsorption capacity of lignin is due in part to polyhydric phenols and other functional groups on the surface. Ion exchange may also play a role in the adsorption of metals by lignin. Masri et al **[54]** treated lignin with sulphuric acid and found uptake capacity of Hg to be 150 mg/g.

2.11.4 Chitosan and seafood processing wastes

Another material shown to adsorb metals is chitin. Chitin is second only to cellulose in terms of abundance in nature and is found in the exoskeletons of crabs and other arthropods and in the cell walls of some fungi **[55].** Chitin is also a waste product of the crab meat canning industry. It is estimated that more than 40,000 tons of chitin is available from the fisheries industry of crustaceans annually. However, more important than chitin is its deacetylated derivative, glucosamine, or chitosan. Chitosan can be produced chemically from chitin and is found naturally in some fungal cell walls. This is done by processing chitin in a basic solution at an elevated temperature **[56].** This deacetylation step requires much more concentrated solutions than those needed for protein removal **[57].** As a result, this step also provides a potential hazard to workers and the environment.

UNIVERSITY of the
WESTERN CAPE

Not only is chitosan inexpensive and abundant, it is highly adsorbent for heavy metals. Yang and Zall **[58]** reported that chitosan chelates five to six times greater amounts of metals than chitin due to the free amino groups exposed during deacetylation. Besides being soluble in acidic solution, another limitation of chitosan is that it is nonporous. Hsien and Rorrer **[59]** suggested N-acylation as a means of increasing porosity. They N-acylated chitosan, cast it into beads, then crosslinked the beads with glutaric dialdehyde in order to overcome solubility. Analysis of the internal surface area showed the beads had higher surface area (223.6 m^2/g) than

uncrosslinked N-acylated beads (192.4 m^2/g) and nonacylated crosslinked beads (42.6 m^2/g) **[59].**

However, comparisons of the low cost adsorbents are difficult because of inconsistencies in data presentation. Although much has been accomplished in the area of low-cost sorbents, more work is necessary to better understand low-cost adsorption processes and to demonstrate the technology **[33].** Due to the above mentioned problem associated with low cost adsorbents, i.e. inconsistencies in data presentation, synthetic adsorbents or high capacity adsorbents offer a possible solution and hence form the main focus of this study.

UNIVERSITY of the WESTERN CAPE

2.12 SYNTHETIC ADSORBENTS/HIGH CAPACITY ADSORBENTS

Examples of high capacity adsorbents, to mention a few are activated carbon, ordered mesoporous silica and ordered mesoporous carbon.

2.12.1. Activated carbon

Based on its size and shape activated carbon is classified into four types: powder (PAC), granular (GAC), fibrous activate carbon (ACF), and cloth (ACC). Due to the different sources of raw materials, the extent of chemical activation, and physicochemical characteristics; each type of activated carbon

has its specific application as well as inherent advantages and disadvantages in wastewater treatment **[60].** Commercial activated carbon (CAC) is still being used intensively today in wastewater treatment. A large number of researchers are still studying the use of activated carbon for removing heavy metals such as mercury, copper, lead, chromium, cadmium, Ni, zinc, and lithium. Various types of CAC for heavy metal removal have been reported. The removal efficiency of mercury using different brands of PAC was evaluated. It was reported that about 99-100 % of total 0.2 mM Hg(II) removal was attained at pH 4.0 - 5.0 **[60].**

The major problem associated with synthetic adsorbents is their cost. Synthetic adsorbents have a disadvantage of adsorbing more than one element hence are not specific for one metal in solution. Therefore, a possible solution to this problem is to modify the surface.

UNIVERSITY of the
WESTERN CAPE

2.12.1.1 Variety of pores in Activated carbon

In general, the structure of activated carbon is tridisperse, containing micropores, mesopores and macropores. The description of adsorption in micropores is not related to the physical image of the interphase but also give information to the adsorbate-adsorbent interactions. For different activated carbons, the volume of micropores usually lies within the range of 0.05 to 0.6 cm^3/g as demonstrated by Figure 2.3 and their specific surface area approximately amounts at least 90 percent of the total surface area **[61].**

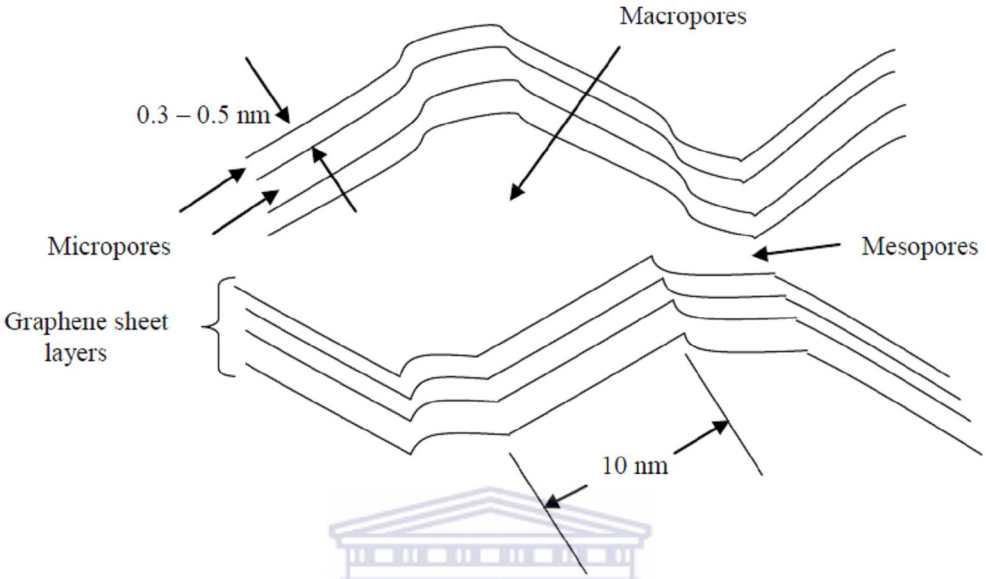

Figure 2. 3: A sketch diagram of AC structure (Straight line segments refer to graphene sheets) **[61].**

UNIVERSITY of the
WESTERN CAPE

The adsorbent properties of activated carbons are essentially due to their surface area, universal adsorption effect, highly microporous structure, and high degree of surface reactivity. The availability of favourable pore sizes makes the internal surface accessible and enhances the adsorption rate. The most widely used activated carbons have surface area of 800 to 1500 m^2/g. This surface area is contained predominantly within micropores that have effective diameters smaller than 2 nm **[61].**

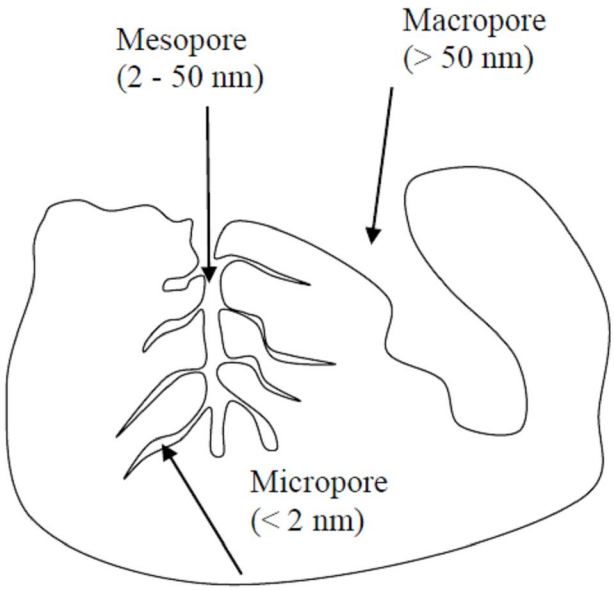

Figure 2. 4: Schematics of a pore structure observed in AC **[61].**

UNIVERSITY of the
WESTERN CAPE

Adsorption in mesopores amounts to the formation of successive adsorption layers on the pore surface and is completed by their filling according to the capillary condensation mechanism. The phenomenon of capillary condensation of vapours and gases in mesopores of activated carbons is characterised by a clearly defined region of hysteresis due to the non – coincidence of the sorption and desorption branches on the adsorption isotherm. The irreversibility of the adsorption – desorption process is due to the emptying of the mesopores proceeding differently from their filling. In general activated carbons serving for adsorption of gases and vapours usually do not posses developed mesoporosity, and the specific surface areas in such carbons do not exceed 50 m^2/g. However, active carbons with developed mesoporosity may attain considerable surface area values ranging from 200 to 450 m^2/g. Active carbons of this type are usually used for decolouring

solutions by removing colouring impurities with large molecules or particles with colloidal degree of dispersity **[62].** The function of the microporous structure of activated carbons is inaccessible for such impurities, and hence their adsorption occurs mainly on the surface of mesopores. The adsorption - adsorption function of mesopores in gaseous phase is twofold. First, in adsorption under sufficient high pressures, adsorbate vapours are entrapped in them by the mechanism of capillary condensation. The second function of these pores is that they serve as passage for the adsorbate molecules to the micropores. Pores with radii larger than 50 nm are classified as macropores. The macropores do not contribute significantly towards the overall surface area of AC but act as conduits as for the passage of the adsorbate into the interior mesopores and micropore surface where most of the adsorption takes place. These pores cannot be filled by capillary condensation for number of reasons, some of which are of kinetic nature. Experiments on forcing mercury into these pores enables one to get an idea on the volume distribution of macropores and their specific surface area. The specific surface area of macropores lie in the range of 1.0 to 4 m^2/g which indicate that macropores do not play an appreciable role in the adsorption values. The significance of macropres is mainly that they act as transport arteries and enable the molecules of the adsorbate to pass rapidly to smaller pores situated deeper within the particle of activated carbon**.** The pores of large size are important as the places of deposition during the adsorption process.

UNIVERSITY of the
WESTERN CAPE

Some special carbons have been prepared that are highly microporous and have a large surface area but still do not adsorb appreciable amounts of

molecules larger than a particular size. Such carbons are called molecular sieve carbons (MSC).These carbons may be viewed as a form of activated carbons, distinct from peat, coconut-based, and other conventional activated carbons. The microporous structure of such carbons is unique, because the slit like apertures or constrictions of their micropores are of a size similar to the molecular dimensions of the adsorbing species. In separation of adsorbate molecules that are smaller than the size of the adsorbent micropore constriction rapidly diffuse through them into the associated micropore volume. On the other hand large adsorbate molecules are denied access to the volume behind the constriction. In this study the molecular sieving properties of activated carbon (AC), ordered mesoporous carbon (OMC) and modified ordered mesoporous carbon (MOMC) were used as adsorbents for removal of dyes and mercury from water. The dyes chosen were of different molecular sizes and were used as adsorbate materials in this study. Although the adsorption capacity of activated carbons is determined by their physical or porous structure it is strongly influenced by the chemical structure of their surface.

UNIVERSITY of the
WESTERN CAPE

2.12.1.2 Chemical Composition of Activated carbon

The adsorption properties of activated carbon are not only determined by its porous structure but also by its chemical composition. In graphite, for example, which have a highly ordered crystalline structure, the adsorption capacity is determined by the dispersion component of London forces. In the

case of activated carbons, however, the random ordering of the aromatic sheets causes a variation in the arrangement of electron clouds in the carbon skeleton, which results in the creation of unpaired electrons and incompletely saturated valences that would undoubtedly influence the adsorption behavior. In addition, active carbons are generally associated with oxygen and hydrogen, which are present in the form of carbon-oxygen and carbon-hydrogen surface groups. These surface groups are bonded at the edges of the aromatic sheets. Because these edges constitute the main adsorption surface, these surface groups profoundly influence the adsorption behavior of activated carbons. Besides, the activated carbon surface has active sites in the form of edges, dislocations and discontinuities that determine the chemical reactions and the catalytic properties of activated carbons.

UNIVERSITY of the
WESTERN CAPE

The presence of hetero atoms and surface complexes affect the adsorption and electronic properties of the carbon **[62].** Of the gaseous substances chemisorbed on activated carbon, oxygen and hydrogen are of special importance. Oxygen can interact with the surface of the active carbon in one of two different ways which depend on the temperature of adsorption. At low temperature, a substantial portion of oxygen is adsorbed physically and with the rise of temperature, the chemisorption of oxygen increases. According to Dubinin **[63]**, reactions of gaseous oxygen within the surfaces of activated carbon at temperatures somewhat below 100 ^{0}C produce complexes which on hydration form hydroxyl (or other) groups which act as ion exchangers **[64].** In general, surface oxides formed from 300 ^{0}C to 500 ^{0}C have acidic character that are also capable of ion exchange **[65, 66].** The respective amount of

acidic and basic oxygen complexes of carbon can be determined by their neutralization with alkali or acid respectively. Juza et al **[67]** have studied the ratio of physically and chemically adsorbed oxygen by a magnetic method employing the paramagnetism of physically absorbed oxygen and very weak diamagnetic behavior of chemically bonded oxygen. They found out that at 200 ^{0}C the ratio of physically to chemically adsorbed oxygen depends on the temperature of preliminary degassing of the surface. At high degassing temperature, the amount of chemically bonded oxygen become more because the physically adsorbed oxygen become bound by chemical forces to the most active sites on the activated carbon surface. At 200 ^{0}C and higher temperature, high oxygen containing carbons are obtained with simultaneous formation of carbon dioxide and carbon monoxide **[68].**

UNIVERSITY of the
WESTERN CAPE

Surface oxygen complexes on carbonaceous surfaces are also formed by the action of water vapours **[69]** nitrogen dioxide **[70]** carbon dioxide **[71].** These surface oxygen complexes can also be formed by oxidation in aqueous medium at elevated temperatures by oxidizing agents at room temperature **[72].** In general, the rate of formation of oxygen complexes decreases with increasing particle size, ash contents, degree of graphitization and decreasing surface area. Chemical and physico-chemical methods of analysis provide information about the total amount of oxygen bonded with carbonaceous substances and to a certain extent also on the functional groups formed by oxygen. Infrared spectroscopy shows that the principle functional groups which are formed on the surface of carbon are <C=O, —OH, and —COOH with some evidence for a number of ester groups **[73-76].** The presence of

these groups, as well as aromatic rings and C—H bonds are also shown by NMR studies **[77- 78].** Studies show that the acidic groups on the surface are primarily lactones and only to a small extent phenolic and there appears to be no evidence for alcoholic hydroxyl groups on carbon surface **[79].** The presence of the oxygen containing functional groups, and their ratio, depends on the nature of the starting material and also on the methods of carbonization and activation. In general, the presence of chemisorbed oxygen on the surface of carbonaceous substances have no appreciable effect on the physical adsorption of non polar gases but these complexes do affect the adsorption of polar or polarisable gases. The adsorption of water, methanol, ammonia, carbon dioxide and sulphur dioxide is greatly increased due to oxygen surface complexes; therefore these gases are unreliable for surface area measurements **[80, 81].** However, these gases may be useful for characterizing the polar sites on a carbon surface. Ammonia and methyl ammonia are adsorbed so abnormally that it has been suggested that probably they dissolve in the surface oxide to form a salt. Similarly, sulphur dioxide on the chars in the presence of oxygen complexes, forms such a stable complex that cannot be desorbed up to 220 ^{0}C. The structure of activated carbon and properties depending on it, are similar to the structure and properties of graphite. Hence, in this study activated carbon was used as a base line material in the determination of surface properties of novel nanostructured materials as well as Mercury (II) adsorption from water.

UNIVERSITY of the
WESTERN CAPE

2.12.1.3. Activated carbon adsorption of Mercury

Activated carbons have been found to be potential adsorbents for the removal of trace metal cations from municipal wastewater; hence a considerable amount of work has been carried out on the activated carbon adsorption of mercury and its compounds. The adsorption of Hg(II) from aqueous solutions using activated carbons was found to be influenced by the pH of the solutions **[82-84].** The adsorption increased as the pH of the solution was decreased, the acidic pH range being most favourable. When the pH of the solution was brought from 9 to the acidic range, the adsorption of mercury was almost doubled. Yoshida et al **[58, 95]** studied the adsorptive removal of Hg(II) using several activated charcoals and observed that the removal of carbon depended on the nature of carbon and the nature of activation treatment, which is received during its preparation. The activated carbon prepared from wood, coconut shell and coal; and activation in steam were found to have a higher adsorption capacity for Hg(II) from solution with pH below 5. The ability decreased with increase in the pH of the solution above 5. The wood charcoal prepared by chemical activation with zinc chloride was found to have a higher adsorption capacity of Hg(II) ions, even at pH higher than 5. These workers, though, did not appreciate the differences in the chemical structures of the carbon surface prepared from different source raw materials and by different activation treatments, they did suggest that the mechanism of adsorption of Hg(II) ions was different in acidic (HCl) and alkaline (NaOH) medium. The Hg(II) was adsorbed as $HgCl_4^{2-}$ complex in the HCl medium, and the adsorption was reversible both in the case of steam-activated and chemically

UNIVERSITY of the WESTERN CAPE

activated carbons but in alkaline medium (pH>7), the steam activated carbons showed irreversible adsorption of Hg(II) as Hg(OH) accompanied by its reduction to Hg on the surface of the carbon.

Homerick and Schoor **[179]** evaluated the influence of process variables such as pH, chelate type, and activated carbon dose on the adsorption of Hg(II) from mercuric chloride solutions by activated carbon. The presence of chelating or ligating compounds such as Ammonium 1-pyrlidine dithio carbonate (APDC) and triethylene tetramine significantly enhanced the uptake of Hg(II) ions. The increase in adsorption of mercury was 40% for a 50 g/L of triethylene tetramine chelate but the same amount of APDC removed virtually all the Hg(II) present in the solution. The adsorption of Hg(II) was also considerably enhanced when activated carbon was used after presoaking in CS_2 and drying. It was postulated that during the CS_2 treatment, sulfide and other sulphur compounds are formed on the carbon surface, which then reacted with the Hg(II) ion.

UNIVERSITY of the
WESTERN CAPE

At lower pH (pH = 4) the removal of mercury involves physical adsorption or reduction of Hg(II) in addition to the above chemisorption process. The pH of the aqueous solution was also found to have a profound influence on the amount of Hg(II) adsorption by an activated carbon. The adsorption was several times more at a lower pH value of the solution (pH = 4) than at higher pH Value (pH = 10). It has been suggested that at lower pH value the carbon - surface charge due to the presence of surface oxides is neutralized by hydrated protons, and this facilitates the pore diffusion of mercury chloride

complexes, while at higher pH value the basic surface charge of the carbon may have repelled the mercury complexes.

Thiem et al **[83]** evaluated the adsorptive removal of Hg(II) from aqueous solution and deduced that the amount removed depends on pH of the solution and amount of carbon.

About twice as much of mercury was removed at pH 7 as at pH 9. Increasing the hydroxyl ion concentration evidently decreased the adsorption of mercury by the carbon. The addition of chelating or ligating agents such as tannic acid, EDTA, or citric acid enhanced the adsorption. The addition of as small 0.02 mg/L of the chelating agent enhanced the adsorption of Hg (II) from 10 to 30% depending upon the pH of the solution and the amount of carbon used.

UNIVERSITY of the WESTERN CAPE

Lopez-Gonzalez et al **[85]** studied the adsorption of $HgCl_2$ from aqueous solutions on active carbons associated with carbon-oxygen and carbon-sulphur surface complexes. The adsorption of Hg(II) decreased on oxidation of the as received carbon with hydrogen peroxide. However, when the oxidized carbon was degassed on heat treatment in helium at 873 K, the adsorption capacity of the original carbon was restored. The adsorption of as received or oxidised carbon was also enhanced on sulphurisation of the carbon by saturation with CS_2 at 288 K followed by heat treatment at 773 K. These workers are of the view that oxidation of the activated carbon with H_2O_2 results in the loss of phenolic and hydroquinonic groups by conversion into carboxylic groups. They proposed that the adsorption of Hg(II) on activated carbons takes place as molecular $HgCl_2$ by the reduction of Hg(II) into Hg(I)

on phenolic and hydroquinonic sites. The adsorption decreases on oxidation as these sites are lost and the adsorption is restored when these sites become available after heat treatment of Hg(II) in helium.

$$> C - OH + Hg_2 \rightarrow > C = O + HgCl_2 + HCl \qquad (2.30)$$

In the case of sulfurised carbon samples also the reduction of Hg(II) into Hg(I) enhances the adsorption of Hg(II) ions. The observations of the postulations made by Lopez-Gonzalez et al **[85]** in respect of the decrease in adsorption of Hg(II) ions on oxidation with H_2O_2 and the increase in adsorption of Hg(II) ions at higher pH values, appear to be contrary to the general behaviour of oxidised carbon that show adsorption of metal cations due to the formation of negatively-charged site on the active carbon surface. Adams **[86]** while examining a carbon surface contacted with $HgCl_2$ solution by an electron microscope, also observed the presence of mercury, confirming the reduction of $HgCl_2$. Similar results were obtained by Huang and Blankenship **[87]** while studying the adsorption of Hg(II) ions on the two L-type and H-type activated carbons. These workers observed that the removal of Hg(II) ions involved both adsorption and a reduction process. The acidic carbons showed a better removal capacity of Hg(II) ions over a pH range between 3 and 11, due to its larger reduction capacity.

Jason et al **[85]** studied the adsorption of Hg(II) ions from aqueous solutions of mercury acetate on activated carbon cloth using shaking and flow through techniques in the pH range of 2.6 and 5.5. The adsorption of Hg(II) could not be studied at pH higher than 5.5 because of the precipitation of mercury as

Hg(II) oxide. The adsorption capacity of the activated carbon cloth increased as the pH of the solution increased from 3 to 5.5. The iso-electric point for the carbon cloth was at pH 2.7 **[85]** so that any increase in pH beyond 2.7 increased the negative character of the carbon surface. This resulted in an increase in the attractive electrostatic interactions between the positively-charged Hg(II) ions and the negatively-charged activated carbon surface.

Namasivayam and Periasmi **[89]** examined the effect of several experimental conditions such as agitation time, metal ion concentration, adsorbent dose, and pH of the solution on the adsorption of Hg(II) on activated carbons obtained from coir pith and bicarbonate-treated peanut hulls and a commercial activated carbon. In their earlier work on commercial and peanut hull carbons, they found that the adsorption decreased at pH < 4 in both the carbons but showed a different trend at pH > 4. The decrease in adsorption at pH < 4 was attributed to the formation of $HgCl_2$ because the trend above pH 4 was not clearly elucidated. In later publications using coir pith carbon, they observed that the adsorption of Hg(II) increased with pH from 2 to 5 and remained almost constant at higher pH values up to 11.

UNIVERSITY of the WESTERN CAPE

2.12.2. Ordered Mesoporous Silica Templates

Of the synthetic adsorbents, examples that stand out and specifically those that will be the focus to the research topic are Ordered Mesoporous Silica (OMSi) e.g. hexagonal mesoporous silica (HMS) **[90]**, Santa Barbara molecular Assembly (SBA-15) **[91]**, Mobil Composition of Matter (MCM-41) **[61]**, Activated Carbon (AC) and Ordered Mesoporous Carbon (OMC). OMCs

are negative replicas synthesized from Ordered Mesoporous Silica (OMSi) as templates **[92-96].**

2.12.1.1 Hexagonal Mesoporous Silica (HMS).

Hexagonal mesoporous siliceous material (HMS) has a wormhole framework structure which can be accomplished through a positively charged organic surfactant, S^+ and a negatively charged inorganic species I^- , (S^+I^-) assembly synthetic mechanism using quaternary ammonium ions as the surfactant and silicate anions which serve as the inorganic precursors. Related mesoporous structures of HMS silicas, have been obtained through a neutral organic surfactant, S^0 and an uncharged inorganic species I^0 by hydrogen bonding (S°I°) or assembly, where S° is an alkylamine and I° is a silicon alkoxide **[97].** In general, surfactant removal from the neutral frameworks of HMS silica can be achieved by simple solvent extraction, whereas the displacement of the electrostatically bound surfactants from the anionic framework of S^+I^- assemblages requires proton exchange or destruction of the surfactant by combustion. HMS silicas show one or, at most, two broad X-ray peaks as a consequence of a small crystallite domain size and/or a much lower degree of channel packing order **[91].**

HMS molecular sieves exhibit a sharp step in their nitrogen adsorption isotherms, corresponding to the presence of a regular mesoporous framework. Owing to the very small elementary particle size of many HMS derivatives, they can exhibit complementary textural mesopores, in addition to

UNIVERSITY of the WESTERN CAPE

framework pores. The textural pore volumes for HMS can be up to 1.5 or more times as large as the framework pore volumes. The textural mesopores are important because they greatly facilitate mass transport to the framework mesopores **[89].**

2.12.1.2 Mobil Composition of Matter (MCM-41).

Unlike HMS, MCM-41 has hexagonal or honeycomb packing of uniform mesopore channels **[91].** The pores are aligned and exhibit a 1D channel system. The most common way to structurally characterize the material is x-ray diffraction (XRD). This technique allows the recording of information on the long range ordering of pores. MCM-41 derivatives typically exhibit three or more X-ray diffraction lines indicative of long-range hexagonal channel packing. However, XRD interpretation is hampered by the large unit cell, because of diffraction peaks in the small-angle region. A broadening of the peaks, induced by the small crystal size, further reduces the accuracy, especially when several phases are present. High-resolution transmission electron microscopy (HRTEM) combined with electron diffraction (ED) is therefore a more powerful technique to determine the structure of mesoporous materials on a local scale. Analogous to HMS, MCM-41 molecular sieves also exhibit a sharp step in their nitrogen adsorption isotherms, corresponding to the presence of a regular mesoporous framework **[91].**

UNIVERSITY of the WESTERN CAPE

2.12.2.3 Santa Barbara molecular Assembly (SBA-15).

SBA-15 posseses a hexagonically ordered cylindrical channel structure with the mesopores that are most probably interconnected through the walls via micropores. Since the discovery of MCM-41, several types of mesoporous silica have been developed. SBA-15 {(Santa Barbara molecular Assembly), 15 signifies the batch number} has recently been synthesized in an acidic medium with poly(alkylene oxide) triblock copolymers, such as poly(ethylene oxide)–poly(propylene oxide)–poly(ethylene oxide) (PEO–PPO–PEO) and found to have uniform and large tubular channels up to 30 nm in diameter. Since SBA-15 also possesses thick pore walls, the hydrothermal stability is much higher than MCM-41 **[60, 90].**

UNIVERSITY of the
WESTERN CAPE

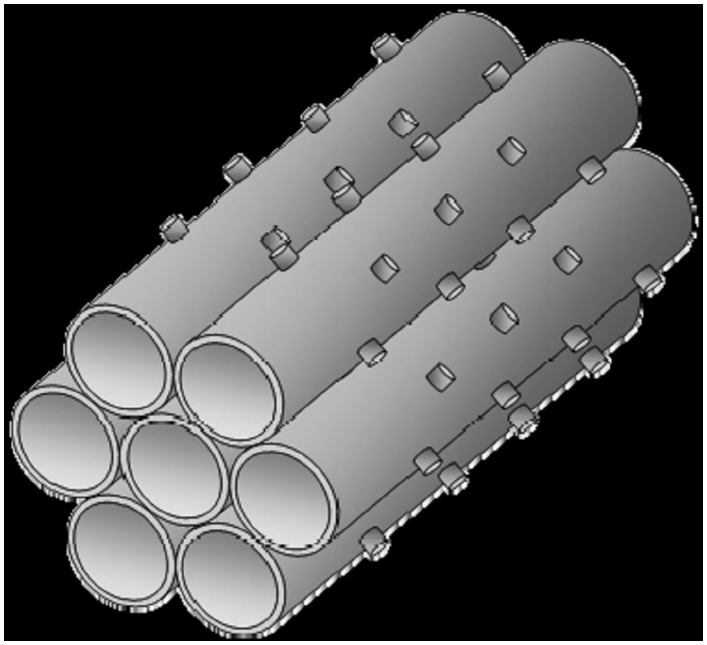

Figure 2. 5: Schematic diagram of SBA-15 **[137].**

2.13. CHARACTERISTICS OF MESOPOROUS MATERIALS

The pores in solid are classified into three categories. According to the IUPAC compendium, a mesopore is the name given to the pores with widths between those of micropores (pore size < 2 nm) and macropores (pore size > 50 nm) **[33, 34].** The difference in size does not simply lead to various molecular sieving effects, but also to a wide range of characteristic chemical phenomena occurring within the pores. To discover chemically interesting phenomena specific to a particular pore size, ordered porous materials, which have a defined pore size and a well-developed porous structure are a necessity **[33].** Mesoporous silica with periodic structure was first reported in the early 1990s. Attention has been drawn to this material because of the unique way in which the structure is formed, the narrow pore size distribution on the meso-scale and the periodicity of mesostructure.

UNIVERSITY of the
WESTERN CAPE

Various kinds of surfactant micelles have been used as templates for directing the structure of mesoporous silicas, in which the size of the pores is almost the same as the micelle and the arrangement of the pore channels traces self organized pattern of the micelle **[98-100].**

The procedure for synthesis of mesoporous silica is as follows; a silica precursor (e.g. tetraethyl orthosilicate, TEOS) and a surfactant are mixed in a basic or acidic solution. The mixture is maintained at 273 to 373 K for several days during which extensive hydrolysis occurs giving rise to the formation of

siloxane (Si-O-Si) bonds. This polymerization leads to precipitation and the solid is filtered out, washed and collected. Finally the product is calcined at 600 to 900 K or washed with a suitable solvent, such as hydrochloric acid or ethanol, to remove the surfactant. The space occupied by the surfactant micelle is converted into mesopores at lattice points in a certain space group. The structural characteristics of mesoporous silica, therefore, arise from micelle structure. The pore size is distributed according to the micelle structure and the framework is usually amorphous **[33].**

A considerable number of studies deal with the functionalisation of the mesopore with reactive organic compounds, such as organic silanes. The adsorption of environmentally toxic cations and anions on such functionalized mesoporous silicas have been intensively investigated **[33].**

The application of this type of silica has been explored in most of the fields concerned with interfacial phenomenon, such as molecular sieving, catalysis, sensor, etc.

UNIVERSITY of the
WESTERN CAPE

From time to time, this synthesis is called “inverse replication”. This is much different to the structure of crystalline zeolite prepared with a molecular ion template, which gives a much narrower pore size distribution than surfactant micelle. The choice of a surfactant is quite important in obtaining particular mesostructures. CTMAB (cetyltrimethylammonium bromide) CTEAB (cetyltrietthylammonium bromide) and Pluronic P123 are typically used for the synthesis of MCM-41 (and MCM-48 too), SBA-1 and SBA-15, respectively **[33].**

Mesoporous silicas have frequently been employed as platforms for the synthesis of functionalized solids in the development of remediation tools. This is due to the fact that large surface areas are often required in the application of solid materials. This surface should be accessible to the molecules and ions in the particular application, while the value determined by the BET surface area measurement, using nitrogen adsorption, does not always characterize the surface properly. Thus, when a certain environmental application of a solid is conceived or planned, the physical and chemical properties of the surface should be considered; for instance, whether it is hydrophilic or hydrophobic, porous or nonporous, the pore size distribution, etc **[31].**

UNIVERSITY of the
WESTERN CAPE

Since the surface energy increases with the specific surface area, fine particles tend to coagulate, resulting in a decrease in surface area and the deterioration in performance while they function. The porous structure is an important factor in extending the surface area while at the same time preventing such coagulation. This explains why the attention of researchers concerned with applications requiring large surface areas has been drawn towards porous solids **[31].**

The uniform pore size is considered to be one of the characteristics of practical importance. Among porous solids, zeolites and carbon have been most frequently studied. Well known microporous materials are zeolites **[103]** and aluminophosphate molecular sieves **[104]** which are inorganic minerals having a crystalline three-dimensional framework comprised of tetrahedral

atoms such as aluminium, silicon, phosphorous etc, bridged by oxygen atoms. These materials possess uniform channels, pores or cavities circumscribed by rings of a definite number of tetrahedral atoms. The exploitation of the architectural features of zeolites resulting in different acid sites and acid strengths, exchangeable ions, shape and size selective channels and pores has been well established by now. In zeolites, which are found naturally or synthesized artificially, the pore size is at most 1.3 nm or less. This is not large enough for aqueous ions to diffuse rapidly into the pores. Moreover, the chemical nature of the zeolites is not always favorable for aqueous ions because of the following reasons. The pore surface of pure silica is hydrophobic rather than hydrophilic due to its crystalline nature. Hydrophobicity in zeolites is sometimes a disadvantage for the adsorption of toxic materials in an aqueous environment **[101, 102].** Higher hydrophilicity is obtained by choosing zeolites containing Al, which gives rise to defects containing acidity.

UNIVERSITY of the
WESTERN CAPE

Modification of the zeolite framework and extra- framework composition makes these materials useful for catalyzing heterogeneous reactions. Prior to Brecker **[103]** heterogeneous catalysis presented using zeolites was restricted to the use of materials with pore sizes less than 2 nm and consequently the reactant molecules trapped and transformed inside them were also small. The usefulness of the microporous molecular sieves in processing high molecular weight reactants of increasing importance was limited by their pore size (~ 0.7 nm). Hence there has been an ever-growing interest in expanding the pore sizes of the zeotype materials from the micropore region to the mesopore

region. The requirement of adsorbing larger molecules at the catalytic sites has led to the development of molecular sieves with pore diameters larger than those of the traditional zeolites. Moreover, the inorganic framework of these mesoporous materials is not crystalline as in the case of zeolitic structures.

In order to preserve the remarkable catalytic properties of zeolites while expanding their use to process bulkier molecules, new synthesis routes have been undertaken to increase their pore diameters. This approach has led to the synthesis of ultra large pore molecular sieves. In 1982 Wilson and co-workers **[105]** synthesized a novel crystalline, microporous aluminophosphate ($AlPO_4$) material with a pore diameter of about 0.8 nm. Later, in 1988, Davis et al **[106]** reported the synthesis of VPI-5, an $AlPO_4$ molecular sieve with 18 tetrahedral atoms that could sorb molecules about 1.2 nm in size. Since then, microporous materials with pore openings containing 20 tetrahedral atoms have been synthesized. These large pore openings overcome the configurational diffusion limitations of zeolitic systems.

UNIVERSITY of the
WESTERN CAPE

However, these materials lack the required thermal stability and catalytic activity because their frameworks are electrically neutral. Researchers have made significant efforts to synthesize mesoporous materials such as silica **[107]**, transitional alumina **[108]** or pillared clays and silicates **[109, 110]**, which are electrically charged. However, the pores in these materials are generally irregularly spaced and broadly distributed in size. Synthesis of amorphous silica-alumina with a narrow pore size distribution in the presence

of tetraalkylammonium cations **[111]** has been reported, where the average pore diameter was related to the size of the tetraalkylammonium cations. Although these materials were found to be active for acid catalyzed organic reactions, they were not thermally stable at high temperatures.

In 1992 researchers at Mobil Research and Development Corporation reported the synthesis of a new family of silicate/aluminosilicate mesoporous molecular sieves (M41S) with exceptionally large uniform pore structures **[112-118].** These materials possess well-defined mesopores whose diameters can be tailored in the range of 1.5-10 nm. The understanding about the synthesis of these materials and the corresponding mechanism has opened up a new era of molecular engineering. The most outstanding feature of the preparation of these materials is the role of the templating agents. The template molecules used are not single solvated organic cations as used in zeolite synthesis, but a self assembled surfactant molecular array around which the main structure is built up (Figure 2.6). Surfactants are large organic molecules having a long hydrophobic tail of variable length (e.g. alkyltrimethylammonium cations with formula $C_nH_{2n+1}(CH_3)_3N^+$, where n > 8) and a hydrophilic head.

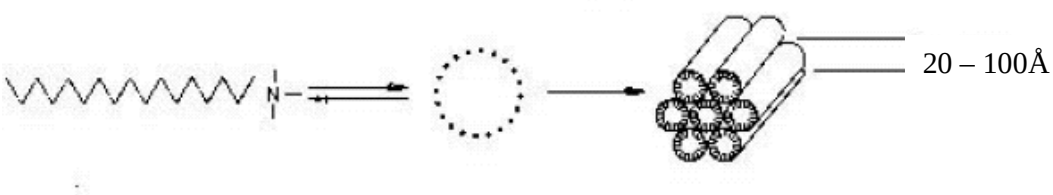

Figure 2. 6: The formation of mesoporous molecular sieves using long chain alkyl quaternary cations **[119].**

2.14. SYNTHESIS OF MESOPOROUS MOLECULAR SIEVES

Similar to zeolite and molecular sieves syntheses, mesoporous molecular sieves are hydrothermally synthesized by mixing organic molecules (surfactants), silica or a silica alumina source to form a gel, which is then crystallized at a temperature between 70-150 ° C for a selected period of time. Surfactant molecules function as templates forming an ordered organic-inorganic composite material **[120].** The product obtained after crystallization is filtered, washed with water and dried at ambient temperature. Surfactant molecules are removed by calcination leaving porous silicate/aluminosilicate network. The structure of mesoporous materials can be altered by varying the surfactant/SiO_2 ratio **[121].** It has been found that as the surfactant/silica molar ratio increased **[122],** the siliceous products obtained could be classified into four groups as presented in Table 2.3.

UNIVERSITY of the
WESTERN CAPE

Table 2. 3: Classification of mesoporous molecular sieves **[25]**

Surfactant/silica	Phase
< 1.0	Hexagonal (MCM-41)
1.0-1.5	Hexagonal (MCM-48), HMS
1.2-2.0	Thermally unstable materials
2.0	Cubic octamer $[(CTMA)SiO_{2.5}]_8$

One of the most unique and useful features of M41S family of materials is the ability to tailor the pore diameter (15–100Å). This can be achieved in three different ways; (i) by varying the chain length of alkyl groups (from 8 to 22 atoms) in surfactant molecules **[112, 117]**, (ii) by adding auxiliary chemicals such as 1,3,5 trimethylbenzene **[112, 117, 120, 123, 124]** which dissolve in the hydrophobic region of the micelles, thus increasing their size, or (iii) by aging a sample prepared at a lower temperature in its mother liquor at a higher temperature for different periods of time **[125].**

Besides, the pore diameter synthesis of mesoporous molecular sieves also depends on other factors such as temperature, pH and crystallization time **[110, 126].** Ever since the first report on the synthesis of mesoporous molecular sieves in alkaline medium appeared **[112-118],** a large number of publications on synthesis of mesoporous materials, mainly MCM-41 has been reported **[127-130].** The synthesis of mesoporous materials has also been done in acidic and neutral medium. Huo et al **[128, 132]** reported the synthesis of mesoporous silica under acidic conditions, while Tanev and Pinnavaia **[121]** proposed a neutral templating synthesis mechanism based on hydrogen bonding between primary amines and neutral inorganic species (Table 2.4). Such mesoporous molecular sieves are named HMS (hexagonal mesoporous silica). These HMS molecular sieves were used as templates for supporting metals or as precursors for mesoporous carbons synthesis in this study.

UNIVERSITY of the WESTERN CAPE

Mesoporous silica materials (MSM) are used as templates for hosting metals or for the synthesis of mesoporous carbons, which are negative replicas of the MSM. There are different varieties of MSM that are applicable to the functions mentioned above, however, Mobil Composition of Matter - MCM-41 and MCM-48 (number represents a batch number) as well as Hexagonal Mesoporous Silica (HMS) are mostly mentioned in literature **[140].** On the other hand, HMS has several advantages compared to MCM-48 from a synthetic point of view:

1) The use of cheap alkyl amines as the structure directing agent
2) A higher silica recovery yield (>95 %) than MCM-48 (~50%)
3) A shorter synthetic time (18 h for HMS and 4 days for MCM-48) and
4) No hydrothermal reaction **[141].**

UNIVERSITY of the
WESTERN CAPE

The pore connectivity of mesoporous materials is important in catalytic and electrochemical applications. However, the pore structure and the pore connectivity of HMS have not yet been elucidated. Table 2.4 depicts routes for synthesis of mesoporous molecular sieves, with specific types of starting surfactant and pH, there is a different type of resulting OMSi template phase.

Table 2. 4: Routes for synthesis of mesoporous molecular sieves

Surfactant	**Example**	**pH**	**Resulting Phase**	**Reference**
S^+I^-	Cetyltrimethyl ammonium ions + silicate species	10-13	Hexagonal, cubic and lamellar	**[112]**
$S^+X^-I^-$	Cetyltrimethyl ammonium ions + silicate species	< 2	Hexagonal	**[113]**
S^0I^0	$C_{12}H_{25}NH_2$ + $(C_2H_5O)_4Si$	< 7	Hexagonal	**[120, 121]**

UNIVERSITY of the WESTERN CAPE

2.15. MESOPOROUS CARBON MOLECULAR SIEVES AND CARBON STRUCTURES

Following the discovery of well-ordered silica based mesoporous materials; the supramolecular assembly approach to mesostructured material has rapidly expanded to include the synthesis of nonsiliceous materials. Among nonsiliceous mesoporous materials, mesoporous carbon material are of particular interest because of their extraordinary properties, such as high specific surface area, large pore volume, good mechanical stability and chemical inertness. Mesoporous carbon materials are potentially useful for a wide range of applications including gas storage, water and air purification, and catalytic supports in fuel cells or components of electrodes **[135].**

UNIVERSITY of the
WESTERN CAPE

Mesoporous carbons with a large BET surface area, a high pore volume and a porosity made up of accessible pores with sizes > 2nm that facilitates mass transport of molecules or ions and a good electronic conductivity for rapid charge transfer can be obtained as inverse replicas of mesoporous silica materials which are used as templates **[107].** These mesoporous carbons are of great interest for high performance applications such as electrocatalytic supports in fuel cells, water electrolysis, new type of hosts for quantum particles and wires in nanotechnology **[136, 137].** However, the framework of these mesoporous carbons is made up of amorphous material and so they have a poor electrical conductivity.

To improve the conductivity of mesoporous carbon supports the carbon framework must contain structures with some degree of graphitization. Till now, mesoporous carbon with completely graphitized structure remains an interesting topic for researchers and facile synthetic routes for these materials are still much the focus of research. Interest in these structures comes from the inherent structural strength due to the covalent in-plane carbon bonds in graphite, which is considered to be one of the strongest in nature. Graphite is extremely light (hence high strength/density ratio, 1–2 orders of magnitude greater than steel), highly electrically and thermally conducting and corrosion resistant. One example of these graphite carbon structures is the carbon nanotubes observed by Iijima (1991) while studying the surface of carbon electrodes used in an electric arc-discharge apparatus, which had been used to make fullerenes.

UNIVERSITY of the
WESTERN CAPE

Carbon in its sp^2 hybridized bonding state, with two-dimensional layered graphite being the most stable form, has shown great promise for conversion into structures having one- and zero-dimensional topologies **[138].**

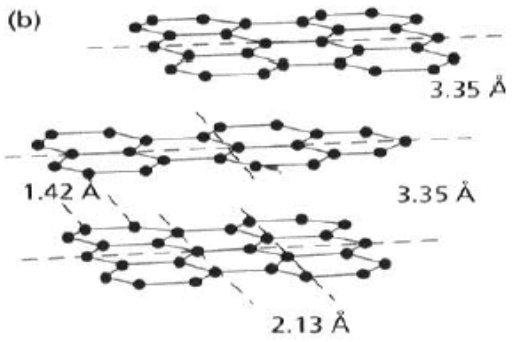

Figure 2. 7: Structural diagram of porous graphitic carbon, a two dimensional graphite **[138].**

UNIVERSITY of the
WESTERN CAPE

According to Prabhuram et al **[139]** the discovery of fullerenes has added an important milestone in carbon research. More importantly, research in this field has proved that various possibilities exist for producing a whole new range of carbon structures of various sizes, shapes and dimensions. For example, carbon nanotubes are perfectly straight nanometre-sized tubules with properties close to that of the ideal graphite fiber.

Most existing mesoporous carbon structures are grown in the temperature range between 800 and 1500 ^{0}C and are made either by extruding polymer structures followed by heat treatment or by catalysing hydrocarbon gases using transition metal catalysts. The goal is to make porous carbons that are straight and stiff having the hexagons in the graphite honeycomb lattice perfectly oriented along the porous carbon axis. The resulting structure will be nearly singly crystalline along the axial direction providing the theoretical strength of the covalent carbon bonds as in a single plane of graphite **[144].**

A number of studies have appeared recently, which describe the preparation of porous carbon with a crystalline framework. Ryoo et al **[145]** reported the synthesis of mesoporous carbon molecular sieves exhibiting a highly ordered X-ray powder diffraction (XRD) pattern.

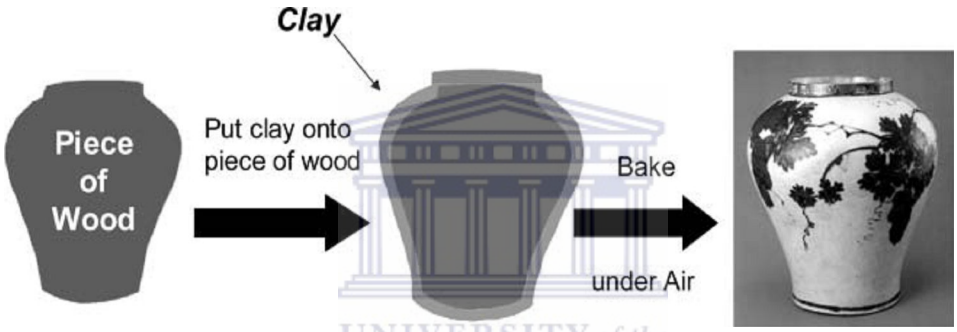

UNIVERSITY of the WESTERN CAPE

Figure 2. 8: Schematic outline of the template synthesis procedure **[143].**

General principles for the synthesis of mesoporous carbons by using hard templating method are illustrated in Figure 2.8 and Figure 2.9. The synthesis starts with filling porous silica (used as a hard template) with a carbon precursor, which often is a polymerising organic compound (e.g., furfuryl alcohol or divinylbenzene) **[145, 147].** The precursor is introduced to the template pores in the form of monomer, which can be easily polymerised under controllable conditions. Also, other carbon precursors can be employed such as petroleum pitch or mesophase pitch that are high-molecular-weight polyaromatic compounds **[144].** All these precursors are infiltrated into template pores in a liquid form by dissolving in a solvent or by introducing

carbon precursor melt at elevated temperature. A driving force for the migration of carbon-containing molecules into pores is capillary effect, which can occur only when a proper attractive interaction exists between hydroxyl-groups present on the surface of silica pore walls and the aforementioned molecules. Hence, the selection of suitable carbon precursor is extremely important to successfully produce mesoporous carbons by using nanoporous silicas as hard template. Various kinds of carbon precursors are effective, and their selection depends on the desired properties of the resulting product. Carbonisation of carbon precursor inside template pores is usually conducted at temperature higher than 800 °C in an atmosphere of neutral gas such as argon or nitrogen. The carbonaceous product being the inverse replica of the starting porous silica template is obtained by dissolution of silica. The hard templating synthesis ensures that the pores and walls of the template become, respectively, the walls and pores in the resulting carbon. Thus, this method allows one to control the pore size in the resulting carbon by varying the pore wall thickness of the silica template used **[144].**

UNIVERSITY of the
WESTERN CAPE

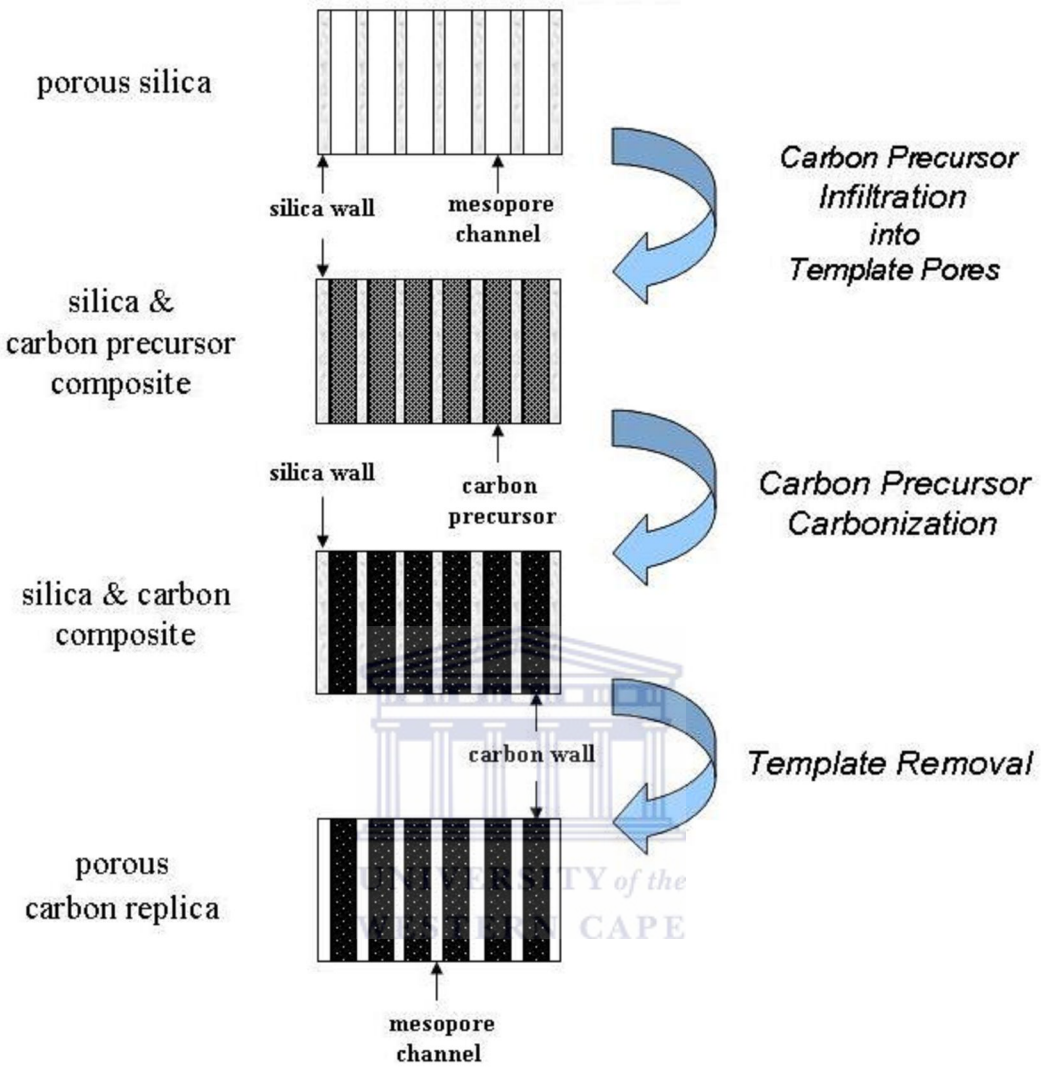

Figure 2. 9: Illustration of the synthesis of mesoporous carbons via hard templating method (The ordered structure of porous silica is used here as the example) **[144].**

Lee and coworkers **[142]** synthesised mesoporous carbon molecular sieves using sucrose as the carbon precursor inside the cubic mesoporous silica molecular sieves MCM-48 that were used as the template. The sulfuric acid

was added as the carbonization catalyst. After the carbonisation step was complete the silica framework was removed using NaOH or HF.

As illustrated in Figure 2.10 MCM-48 silica consists of the pair of separate (disconnected) pore systems that were filled by carbon. After removal of the silica template from the carbon-silica composite, the carbon structures that occupied the separate pore channels of the template, underwent displacement, which joined them. The obtained structure exhibited tetragonal $I4_1/a$ symmetry (or lower) **[144].** The result of this structural transformation was a double enlargement of the size of pores and walls in the carbon with respect to the corresponding walls and pores of the silica. Thus, the diameter of uniform pores in the CMK-1 carbon reached the value of about 3 nm instead of 1.3 nm, where the latter is the wall thickness of the MCM-48 silica used.

UNIVERSITY of the
WESTERN CAPE

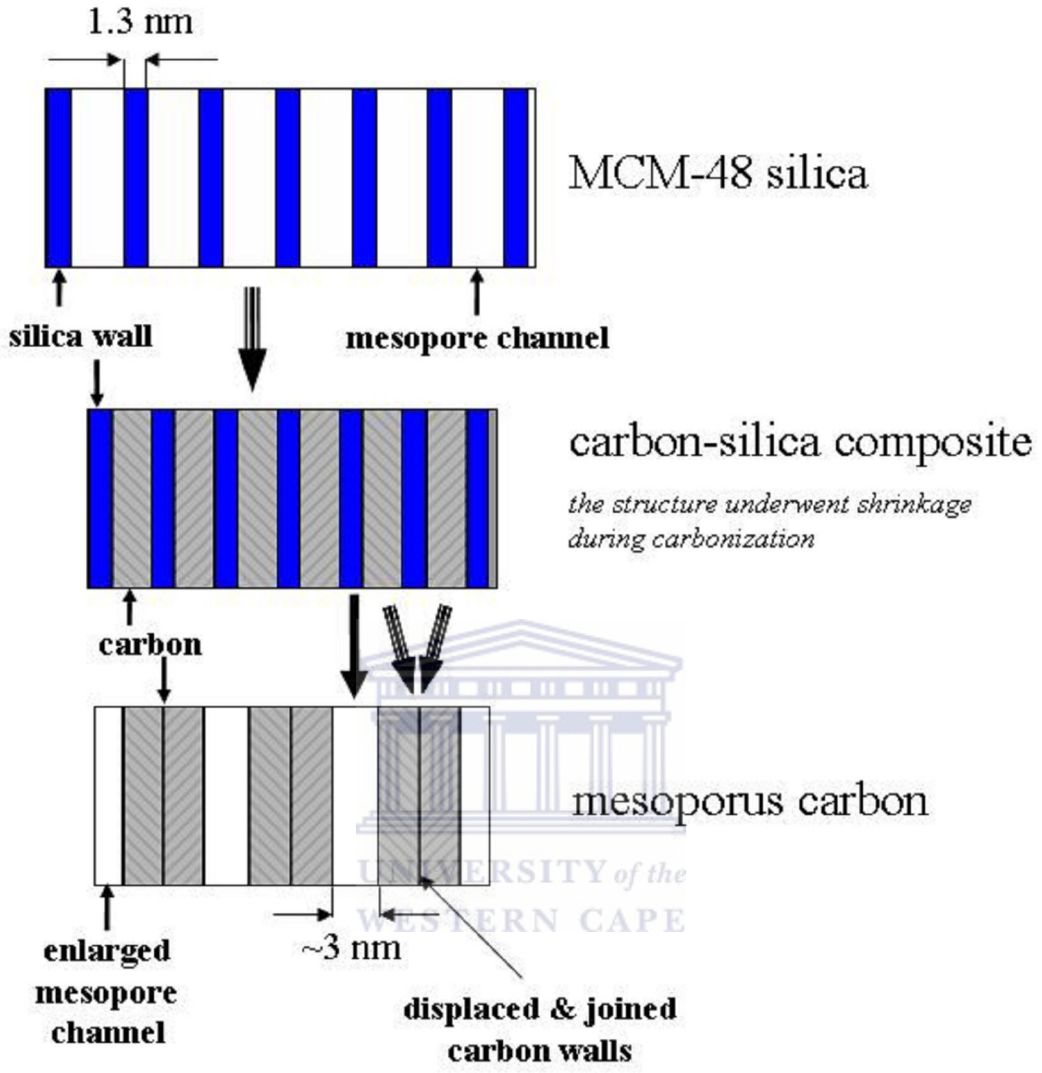

Figure 2. 10: Synthesis of the CMK-1 mesoporous carbon templated by MCM-48 silica (The shape of mesopores in MCM-48 shown in this figure is simplified and does not reflect the real structure of this OMSi) **[144].**

However, the carbon framework that resulted from the above procedure showed no Bragg lines in the region 2 θ greater than 10 ^{0} on analysis by XRD, indicating that the carbon framework was atomically disordered and no degree

of graphitisation was produced. Nonetheless, the mesoporous carbon that was formed had a high specific surface area (BET area 1380 $m^2 g^{-1}$).

2.16. TEMPLATE SYNTHESIS TECHNIQUE FOR MESOPOROUS CARBON

The preparation of mesoporous carbons using mesostructured silica materials as templates was first reported by Ryoo et al **[146-147].** By means of this technique it is possible to obtain porous carbons, with a large surface area, a high porosity and controlled narrow pore size distributions (PSDs) in the mesopore range.

UNIVERSITY of the
WESTERN CAPE

The preparation of these porous carbons consists of:

(a) the infiltration of the porous structure of an inorganic material (template) by the carbon precursor (generally a polymer or prepolymer),

(b) the polymerisation of infiltrated substance,

(c) the carbonisation of the nanocomposites formed and

(d) the elimination of the template.

This procedure is very useful for synthesising mesoporous carbons with controlled porous characteristics. Thus, depending on the type of mesostructured silica that is used as template, carbons with different structures and pore sizes are prepared.

First, Ryoo et al **[146]** used a MCM-48 silica as template to synthesise an ordered mesoporous carbon (CMK-1) with a cubic structure (Pore size: 3 nm, SBET: 1380 m^2 g^{-1}). Later, the same authors **[147]** used a SBA-15 mesostructured silica to prepare a carbon (CMK-3) with a 2-D hexagonal structure (Pore size: 4.5 nm, SBET: 1520 m^2 g^{-1}), which was a faithful inverse replica of the silica framework. Parmentier et al **[148]** also synthesized mesoporous carbon materials with different pore diameters using HMS and SBA-15 materials synthesized at different temperatures. These materials have been utilized for the immobilization of biomolecules from aqueous solutions.

Kim and Pinnavaia **[149]** described the preparation of a mesoporous carbon with a hexagonal structure (pore size: 3.9 nm; SBET: 1230 m^2 g^{-1}) from a MSU-H silica template. Lee et al **[150]** demonstrated that the pore size of an ordered mesoporous carbon can be accurately modified between 2.2 and 3.3 nm by changing the composition of the surfactant used in the synthesis of the mesostructured silica. All of these carbons are inverse replicas of the mesostructured silica frameworks, their porosity being a replica of the silica skeleton. Thus, hexagonally ordered carbons such as CMK- 3 can be visualised as a network of hexagonally ordered carbon nanorods which are interconnected by means of carbon spacers. Given that the pores in carbons obtained from mesostructured silica templates are derived from the silica framework, they are limited by the thickness of the silica walls. For this reason, most of the mesoporous carbons prepared in this way have mesopores with sizes limited to the narrow 2–4 nm range **[147-151].** For some of the potential uses of mesoporous carbons, such as those related to

UNIVERSITY of the WESTERN CAPE

catalysis, adsorption or double-layer electrical capacitors, the diffusion rate needs to be enhanced. In this case materials with a 3-D pore arrangement are more appropriate than materials containing well ordered 2-D pore structures **[151].** Apart from the pores derived from the silica framework, the presence of larger pores (complementary mesoporosity), would contribute to enhancing diffusivity in the pore network for the applications mentioned above. Recently, some authors reported on the preparation of mesoporous carbons containing two pore networks: (i) pores related with the silica framework and (ii) pores derived from the incomplete filling of silica porosity. Thus, Lee et al **[153]** used a mesocellular silica foam to prepare a porous carbon, which exhibits a bimodal PSD with spherical cells of 27 nm interconnected by small mesopores of around 3.6 nm. Joo et al **[154]** used an SBA-15 template to prepare a porous carbon whose structure was formed by interconnected carbon nanopipes. This porous carbon shows two pore sizes, 5.9 nm (internal diameter of carbon cylinders) and 4.2 nm (pores between adjacent cylinders).

UNIVERSITY of the WESTERN CAPE

The main purpose of this work is to investigate the preparation of mesoporous carbons with a 3-D pore structure, which combine two pore systems in the mesopore range, pores derived from silica skeleton and larger pores obtained from the partial filling of silica porosity. In addition, new methods to enable the carbon precursor to infiltrate into silica pores are being investigated. A mesoporous silica with a disordered mesostructure was used as template. Depending on the method used to introduce the carbon precursor into the silica nanopores, carbons with different mesostructures could be obtained **[145].**

Li and co-workers **[153]** prepared hollow graphitic carbon nanoparticles and carbon nanocoils by carbonising resorcinol–formaldehyde gels doped with cobalt and nickel salts. These metals act as catalysts for graphitisation and they facilitate the formation of graphite crystallites at relatively low temperatures (900 ^{0}C). The XRD patterns of these carbons show that a certain degree of graphitisation was attained (d002 _ 0.34 nm).

In the template synthesis approach, the pore network of the carbon is an inverse replica of the skeletal of the inorganic material used as template. This aproach, which permits a precise control of the carbon porosity has been widely used to fabricate non-graphitisable mesoporous carbon using different types of mesoporous silica materials (MSM) as templates The structural characteristics (i.e. surface area, pore volume, pore size, particle size, morphology, etc.) of carbons synthesised in this way can be modulated by selecting an appropriate template. With this technique porous carbons with a graphitic framework can be obtained if the porosity of the template is infiltrated by a graphitisable carbon precursor. Kim et al **[152]** analysed this method and prepared ordered graphitic carbons by infiltrating the porosity of mesostructured silica materials (i.e. MCM-48, SBA-1 and SBA-15) with acetanaphthene. The infiltrated material is treated at 750 ^{0}C under pressure in an autoclave and then heated at 900 ^{0}C under vacuum. The resulting carbon showed a turbostratic structure with a d002 spacing of 0.36 nm. The textural properties (SBET, pore volume, pore size, etc.) of such carbons were not reported, so their porous characteristics cannot be evaluated.

UNIVERSITY of the
WESTERN CAPE

Fuertes et al **[143]** reported a novel route, based on the template approach, for the fabrication of porous carbons with a graphitic framework and a large surface area with an accessible porosity made up of mesopores. The synthesis of these materials was carried out by simply infiltrating, under ambient conditions (temperature and pressure), the porosity of a mesostructured silica with a solution containing a polymer, which was converted into a graphitisable carbon after the carbonisation step. Heat treatment of the graphitisable carbon at high temperature (2300 ^{0}C) gives rise to a porous carbon with a well-developed graphitic order. The polymeric material chosen to be infiltrated was a poly(vinyl chloride (PVC). As templates, two different MSM were used, i.e. a well-ordered silica (SBA-15) and a silica with a wormhole pore structure (MSU-1).

UNIVERSITY of the
WESTERN CAPE

Recently, Ndungu and co-workers **[155]**, synthesized mesoporous carbon material with a graphitic nature using chemical vapour deposition (CVD). Liquified petroleum gas was applied as the carbon source in the successful pyrolytic synthesis of nanostructured carbon materials. Both ordered mesoporous carbon and carbon nano tubes were prepared via this route. The use of a silica based mesoporous template HMS in the CVD system resulted in the successful penetration of the precursor LPG into the HMS template. Thermal decomposition of the precursor produced a graphitic, structurally stable and well ordered mesoporous carbon in a single step. An additional advantage to this method is that the ordered mesoporous carbon produced

was mainly graphitic, thus there is no need for any additional graphitisation steps.

2.17. CHEMICAL SURFACE MODIFICATION OF SORBENTS

In addition to high capacity adsorbents, chemical modification of mesoporous carbon adsorbent surfaces will be one of the important properties that will be explored relating to the adsorption of mercury (II) from aqueous solution onto mesoporous carbon. Hence, this innovative approach will be of prime importance to this research study in introducing novelty.

UNIVERSITY of the
WESTERN CAPE

2.17.1. Modification of silica surfaces

Modification of oxides (silica and alumina), surfaces relates to all the processes that lead to changes in chemical composition of the surface. Surface can be modified either by physical treatment (thermal or hydrothermal) that leads to change in ratio of silanol and siloxane concentration of the silica surface or by chemical treatment that leads to changes in the chemical characteristics of silica surface. By modification, the adsorption properties are significantly affected. Chemisorption of chelating molecules on silica surface provides immobility, mechanical stability and water insolubility, thereby increases the efficiency, sensitivity and selectivity of the analytical application **[156, 157].** Silica gel surfaces can be modified by two

distinct processes: organofunctionalisation, where the modifying agent is an organic group, and inorganofunctionalisation, in which the group anchored on the surface can be an organometallic composite or a metallic oxide.

The possibilities of target directed variation of the chemical and analytical properties of the sorbent by modifying them is almost limitless. Chemical modification of silica surfaces by an organic chelating group acts as an ion-exchanger, which provides greater selectivity for the analyte than that offered by traditional ion-exchangers. The most convenient way to develop a chemically modified surface is achieved by simple immobilization (or fixing) of the group on the surface by adsorption or electrostatic interaction or hydrogen bond formation or other type of interaction **[157].** Simple impregnation of the solution of modifiers or covalent binding, so called, covalent grafting of the chelating molecule to the silica matrix is the common practice of developing a functionalised silica surface.

UNIVERSITY of the
WESTERN CAPE

2.17.2. Modification of carbon surfaces

Porous carbons had been widely used as adsorbents material due to its higher surface area, larger pore volume and surface chemical functional groups. The surface chemical functional groups are mainly derived from activation process, precursor, heat treatment and post chemical treatment of porous carbon. So, many researchers focused on how to modify as well as to characterise the surface functional groups of carbon materials in order to improve or extend their practical applications **[159-161].** Radovic et al **[162]**

reviewed the carbon materials as adsorbents in aqueous solution and pointed out that the control of chemical and physical conditions might be harnessed to produce carbon surfaces suitable for particular adsorption applications**.** Radovic et al **[162]** compared the surface chemistry of the carbon which has a great influence on both electrostatic and non-electrostatic interactions, and could be considered the main factor in the adsorption mechanism from dilute aqueous solutions. Modification of the surface chemistry of porous carbons might be a viable attractive route toward novel applications of these materials. A modified activated carbon containing different functional groups could be used for technological applications such as extracting metallic cations from aqueous and nonaqueous solutions, in catalysis, for treatment of waste and toxic effluents produced by a variety of chemical processes **[162].**

UNIVERSITY of the
WESTERN CAPE

The heteroatoms on the surface of activated carbon takes on a significant role during its application. The heteroatoms of porous carbon surface mainly contain oxygen, nitrogen, hydrogen, halogen, etc, which bonded to the edges of the carbon layers and governed the surface chemistry of activated carbon **[163].** Among these heteroatoms, the oxygen-containing functional groups (also denoted as surface oxides) were the most widely recognized and the most common species formed on the surface of carbons, which significantly influenced their performance in sensors **[164]** energy storage and conversion systems **[165]**, catalytic reactions **[166],** and adsorptions **[167].**

The nitrogen-containing groups generally provide basic property, which could enhance the interaction between porous carbon and acid molecules, such as,

dipole - dipole, H-bonding, covalent bonding, and so on. The nitrogen groups were introduced by amine treatment and nitric acid treatment.

2.18. METHODS FOR MODIFICATION OF CARBON SURFACES

The nature and concentration of surface functional groups might be modified by suitable thermal or chemical post-treatments. Oxidation in the gas or liquid phase could be used to increase the concentration of surface oxygen groups; while heating under inert atmosphere might be used to selectively remove some of these functions. It was shown that gas phase oxidation of the carbon mainly increased the concentration of hydroxyl and carbonyl surface groups, while oxidations in the liquid phase increased especially the concentration of carboxylic acids **[168].** While, the ammonization could introduce the basic groups, such as, C-H, C=N groups, amino, cyclic amides, nitrile groups, pyrrole-like structure **[169,170].** In addition halogen-containing groups could be produced through porous carbon reacted with halogen at moderate temperature, this modified porous carbon showed potential application in electrochemistry or batteries **[171].**

UNIVERSITY of the WESTERN CAPE

2.18.1. Acid treatment

Acid treatment can be generally used to oxidise the porous carbon surface; it enhanced the acidic property, removed the mineral elements and improved the hydrophilicity of surface. The acid used in this case should be oxidizing in

nature; the nitric acid and sulphuric acid are most often used. Liu et al **[172]** reported that coconut-based activated carbon was modified by nitric acid and sodium hydroxide; it showed excellent adsorption performance for Cr (VI). Pereira et al **[173]** reported that a commercial activated carbon was selectively modified, without significantly changing its textural properties, by means of chemical treatments, using HNO_3 for adsorption of dyes.

2.18.2. Sorption of Hg(II) ions on SiO_2 based materials

Most works dealing with mercury uptake by organic–inorganic hybrids have been performed with thiol-functionalized silicas, and they were essentially directed to increase the binding efficiency (high capacity, quantitative uptake by all ligands, low levels of remaining mercury in solution) and to improve the selectivity of the binding process with respect to other metal cations. Fewer efforts, however, have been devoted to the selective uptake of mercury as a function of its speciation in solution, although many analytical strategies have been proposed for determining mercury speciation in environmentally related samples **[174].**

UNIVERSITY of the
WESTERN CAPE

Previous research by Walcarius et al **[175]**, indicated the possible mercury binding to both amine- and thiol-functionalized silicas, but the effect of speciation on the uptake processes was not discussed**.** Walcarius et al **[175]** provided a thorough analytical investigation of silica gels grafted with organic ligands applied to remove inorganic mercury species from aqueous media, selectively as a function of their main chemical forms. Materials containing

either amino or mercapto ligands were chosen to distinguish between some of the most common species of Hg(II) that could be found in water in wide pH and chloride concentration ranges, i.e. $Hg(OH)_2$, $HgCl_2$, $HgCl_3^-$, and $HgCl_4^{2-}$; the speciation corresponds especially to aquatic systems that are highly contaminated with mercury from industrial sources **[176].** These ligands were selected for their complexation behavior towards mercuric species and for the acid–base properties of amine groups that could be turned positively charged in acidic medium. These researchers also investigated Hg(II) uptake by amorphous silica gels grafted with aminopropyl and mercaptopropyl groups using batch experiments performed at various pH values and chloride concentrations.

UNIVERSITY of the
WESTERN CAPE

2.18.3. Sorption of Hg(II) ions on carbon based materials

The surface chemical modification of activated carbon (AC) has been recognised as an effect approach for enhancing metal removal from aqueous media **[177].** For example modification of AC by organosilane has been reported by Elwing et al **[178]** using APTES molecule containing active-NH_2 Terminal groups**.** These researchers reported that APTES strongly interact with hydroxyl group and hydrolised head groups. Homerick and Schoor **[179]** evaluated the influence of chelate type on the adsorption of mercury (II) from mercuric chloride solution by AC (Filtrasorb-300). The presence of chelating compounds such as ammonium 1-pyrolidine dithio carbonate (APDC) and triethylene tetramine significantly enhanced the uptake of Hg(II) ions. The increase in the same amount of APDC removed virtually all the Hg(II) present

in the solution. AC (Filtrasorb-300) was used after pre-soaking in CS_2 and drying. It was postulated that during the CS_2 treatment, sulphide and other sulphur compounds are formed on the carbon surface, which then reacted with Hg(II) ion.

In this study novel ordered mesoporous carbon (OMC) will be functionalized using a two stage reaction process. The first step involves acid treatment with HNO_3 and the second step involves modification using organosilane chelating group, 3-mercapropyltriethoxysilane.

UNIVERSITY of the
WESTERN CAPE

2.19. PHYSICO-CHEMICAL CHARACTERIZATION

A number of techniques are used to characterize mesoporous molecular sieves. Among these, x-ray powder diffraction (XRD), transmission electron microscopy (TEM) and adsorption measurements are considered the essential techniques to identify the structure of the mesoporous molecular sieves. Thermal Gravimetric Analysis (TGA) and Raman spectroscopy have been applied to obtain additional structural information about molecular sieves. The Braunauer-Emmett-Teller (BET) nitrogen adsorption technique is used for surface area determination and pore size distribution. Selected-area electron diffraction (SAED) is used in the qualitative measure of crystallinity and symmetry of materials. Scanning electron microscopy (SEM) has been used for producing images with great depth of field and high magnification. Energy dispersive spectroscopy (EDS) has also been used for sample elemental composition or percentage weight, refer to chapter 2 for experimental work, sample preparations and set up conditions pertaining to the use of these physico-chemical techniques.

UNIVERSITY of the
WESTERN CAPE

2.19.1. X-ray diffraction (XRD)

X-ray diffraction was used to identify the crystallinity, crystal size and elemental composition in the samples. A diffractometer with a Cu tube was used with a wavelength λ = 1.5 nm. The diffractometer operates in the (θ -2θ) geometry. The detector rotates at twice the rate of the sample and is at an

angle of 2θ with respect to the incoming x-ray beam. The x-rays reflected from the different planes in the crystal undergo interference with each other as illustrated in Figure 3.7.

The basis for x-ray diffraction is described by the Bragg's law, equation 2.31, which describes the condition of constructive interference of x-rays, scattered from atomic planes of a crystal:

$$n\lambda = 2d\sin\theta \qquad (2.31)$$

where n is an integer, λ is the wavelength of the radiation, d is the spacing between atomic planes and θ the angle between the radiation and atomic planes, known as the Bragg angle **[180].** This relation demonstrates that interference effects are observable only when radiation interacts with physical dimensions that are approximately the same size as the wavelength of the radiation. During the first order reflection constructive and destructive interference takes place. Constructive interference occurs if the rays that are scattered by all atoms in all the planes are in phase and reinforce one another to form a diffracted beam. While in destructive interference all the scattered beams are out of phase and cancel one another leading to no scattering. For the first order diffraction, n =1, the Bragg's law can be written as:

$$\lambda = 2dSin\,\theta \qquad (2.32)$$

Figure 2.11 show the Interference of radiation between atomic planes in a crystal. Two parallel planes of atoms A–A' and B–B' which have the same h, k, and l Miller indices separated by the interplanar spacing d_{hkl} are shown in Figure 2.11 If we assume that a parallel, monochromatic, and coherent (in-phase) beam of x-rays of wavelength λ is incident on these two planes at an angle θ. Two rays in this beam, labelled 1 and 2, are scattered by atoms P and Q. Constructive interference of the scattered rays 1' and 2' occurs also at an angle θ to the planes, if the path length difference between 1–P–1' and 2–Q–2' is equal to a whole number, n, of wavelengths. That is the condition for Bragg's law.

UNIVERSITY of the
WESTERN CAPE

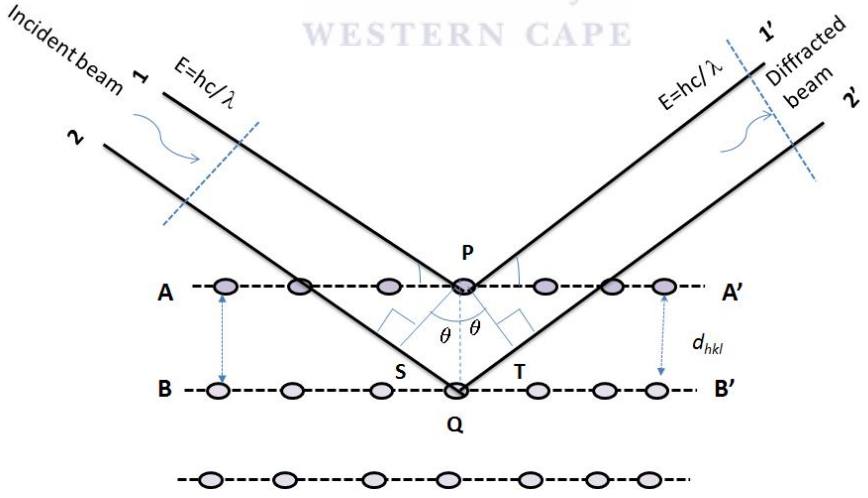

Figure 2. 11: Interference of radiation between atomic planes in a crystal **[180,181].**

2.19.2.1. Instrumental set up of an X-ray diffractometer.

When the incident beam strikes a powder sample, diffraction occurs in every possible orientation of 2θ, this is shown in the schematic diagram of XRD (Figure 2.12). The diffracted beam may be detected by using a moveable detector which is connected to a chart recorder. In normal use, the counter is set to scan over a range of 2θ values at a constant angular velocity.

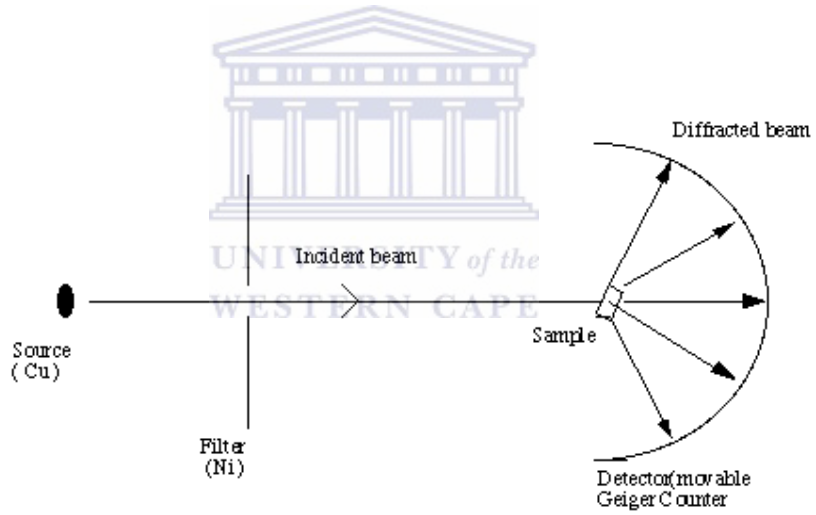

Figure 2.12: Schematic representation of a typical X-ray diffraction Instrument **[180,181].**

There are two limiting angles $2\theta_1$ and $2\theta_2$ on both sides of the diffraction peak beyond which the diffracted intensity must drop to zero. It follows that the diffracted intensity at angles near $2\theta_B$ **(**$2\theta_2 \leq \theta \leq 2\theta_1$**)** is not zero but intermediate between zero and the maximum intensity of the beam diffracted

at an angle $2\theta_B$**.** The curve of the diffraction intensity versus 2θ will have the form of Figure 2.12 in contrast to Figure 2.13, which illustrate the hypothetical case of diffraction occurring at the exact Bragg angle.

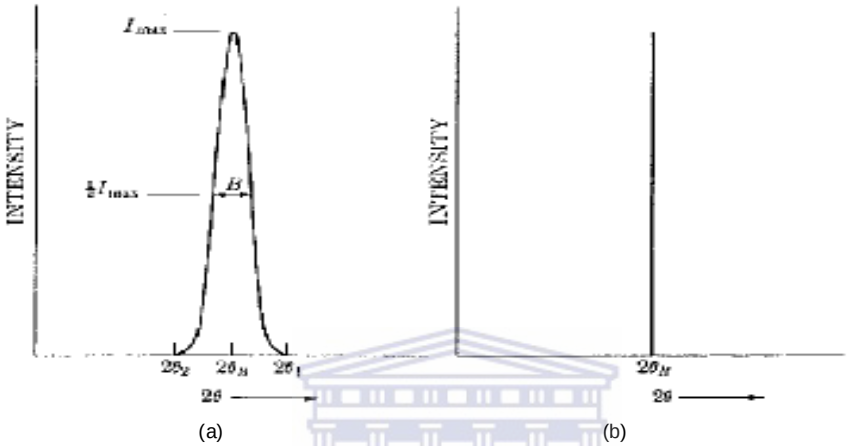

Figure 2. 13: The effect of fine particle size on diffraction curves **[180,181].**

UNIVERSITY of the
WESTERN CAPE

Powder x-ray diffraction can be used to identify the structure, phase purity, degree of crystallinity, unit cell parameters and crystallite size of a material. It is also applied in the study of the kinetics of crystallization of molecular sieves. As the powder pattern is the identifying spectrum of the molecular sieve structure, phase purity and percent crystallinity of the synthesized molecular sieve can be ascertained by comparison with the standard published pattern for the molecular sieve under investigation. XRD patterns of mesoporous phases exhibit peaks in the low angle region; the most intense peak being the (100) reflection. In the case of MCM-41 the wall thickness of hexagonal channels is usually calculated by subtraction of the inside pore diameters

obtained by nitrogen gas adsorption from the unit cell dimensions determined by XRD.

The process of X-ray diffraction by a crystal can be thought of as one of reflection of the X-rays off planes of atoms within the crystal. In a diffraction pattern from a crystal lattice, a number of reflections are generated, each one being associated with a lattice plane (identified by the Miller indices *h, k,l*) and occurring at an angular position (2θ) depending on the related interplanar spacing (*d(hkl)*) and on the X-ray wavelength (λ), as defined by the well-known Bragg's law **[180].**

UNIVERSITY of the
WESTERN CAPE

$$\lambda = 2dSin2\,\theta \qquad (2.33)$$

λ- the wavelength of the X rays

d - the spacing of the planes in the crystal

2θ - the angle of diffraction

Determination of particle size from XRD may be calculated using the Scherrer equation. The XRD line broadening versus crystallite size effect can be exploited to determine the average size of metal crystallites on various supports, e.g. Pt crystallite sizes in reforming catalysts. The Scherrer equation

may be used to determine the average crystallite size of the Pt particles. The full-width at half maximum (FWHM), B, is related to the mean dimension of crystallites perpendicular to the hkl planeo, t, by Scherrer's equation,

$$D = \frac{0.9\lambda}{\beta \cos\theta} \qquad (2.34)$$

where D is the particle diameter (nm) measured at its half maximum intensity, λ is the wavelength of the X-ray radiation, β is the FWHM (radians) and θ is the angle of reflection. The FWHM is strongly affected by crystal defects and distortions, which cause line broadening. Here, the variation in the FWHM (β) is used as a rough indication of the changes in crystal size as a function of radiation dose **[182].** The Scherrer's equation is mainly specific to perfectly spherical particles. As a result there may be discrepancies in particle size determination for non-spherical particles. In this study XRD is used to determine structure, degree of crystallinity, unit cell parameters and crystallite size of materials.

UNIVERSITY of the WESTERN CAPE

2.19.2. Determination of surface area and pore size distribution

Molecular sieves have the ability to adsorb probe molecules of different sizes. Sorption capacities for probe molecules such as n-hexane, water, benzene, nitrogen and so on, yield information about the hydrophilicity/hydrophobicity, pore dimensions and pore volume of the molecular sieves. The Braunauer-

Emmett-Teller (BET) volumetric gas adsorption technique using gases such as nitrogen or argon is a standard method for the determination of the surface areas and pore size distribution of finely divided porous samples **[183].** The relation between the mass of gas adsorbed and the equilibrium pressure of the gas at constant temperature is defined by the adsorption isotherm. This relation is represented by the BET equation i.e.

$$\frac{1}{W[(P_0/P)-1} = \frac{1}{W_m C} + \frac{(C-1)P}{W_m C P_0} \qquad (2.35)$$

Where, W = weight of N_2 adsorbed at a given relative pressure (P/P_0)

W_m = weight of N_2 producing monolayer coverage (θ =1.00 ml).

UNIVERSITY of the
WESTERN CAPE

N_2-adsorption-desorption isotherms of MCM-41, MCM-48 and HMS are of the type IV isotherm. This means increase in N_2 adsorption (within the P/P_0 range between 0.2 to 0.4) corresponds to capillary condensation within uniform pores. The sharpness and the height of this step reflect the uniformity of the pore size and the pore volume respectively. In this study BET was used to determine pore size distribution and specific surface area of materials.

2.19.2.1. Classification of Gas Adsorption Isotherms

Experimental gas adsorption isotherms usually fall into six categories out of which five (Types I-V according to the IUPAC classification see Figure 2.14) are relevant to this study **[184].**

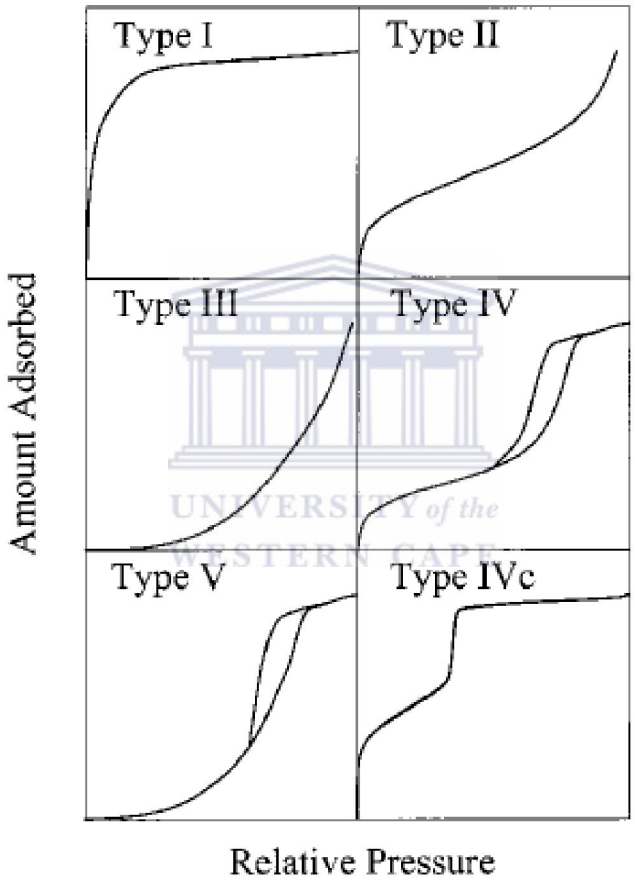

Figure 2. 14: Classification of gas adsorption isotherms **[184, 185].**

In figure 2.14, Type I isotherms exhibit prominent adsorption at low relative pressures (the relative pressure is defined as the equilibrium vapor pressure divided by the saturation vapor pressure) and then level off. Type I isotherm is

usually considered to be indicative of adsorption in micropores or monolayer adsorption due to strong adsorbent adsorbate interactions (which may be the case for chemisorption, which involves chemical bonding between the adsorbate and the adsorbent surface) **[184, 185].** It should be noted that pores are classified herein on the basis of their diameter (or width) as micropores (below 2 nm), mesopores (between 2 and 50 nm), and macropores (above 50 nm) **[184].** In the case of nonpolar gases commonly used for characterization of porous solids (nitrogen, argon) **[184, 185]** chemisorption is unlikely and therefore a classical interpretation would associate Type I with microporosity. However, Type I isotherms may also be observed for mesoporous materials with pore sizes close to the micropore range **[186].**

In particular, in the case of adsorption of N2 at 77 K or Ar at both 77 and 87 K in cylindrical pores, a Type I isotherm would have to level off below the relative pressure of about 0.1 for the material to be exclusively microporous, as inferred from the results of recent studies of siliceous ordered mesoporous materials (OMMs) **[184, 185].** Consequently, when a Type I isotherm does not level off below the relative pressure of 0.1, the sample is likely to exhibit an appreciable amount of mesopores or even be exclusively mesoporous. However, such Type I behavior may be indicative of some degree of broadening of the mesopore size distribution. This is because materials with highly uniform cylindrical pores may exhibit discernible steps on adsorption isotherms (and therefore these isotherms are classified as Type IV) at relative pressures down to 0.1 or perhaps even lower (for N2 at 77 K and Ar at 77 and 87 K) **[184, 185].** Type I isotherms are quite common for OMMs with organic

UNIVERSITY of the WESTERN CAPE

groups bonded to a silica framework, both prepared via chemical bonding **[184]** and co-condensation **[185].** Adsorption on many macroporous solids proceeds via multilayer formation in such a manner that the amount adsorbed increases gradually as the relative pressure increases, although the multilayer buildup close to the saturation vapor pressure may be quite abrupt. This unrestricted multilayer formation process gives rise to Type II and III isotherms. In this case, the adsorption and desorption branches of the isotherm coincide; that is, there is no adsorption-desorption hysteresis. Depending on the surface properties of a given solid, there may be a pronounced stage of the monolayer formation (Type II) or the adsorption isotherm may be convex in the whole pressure range (Type III). The latter behavior can be observed when lateral interactions between adsorbed molecules are strong in comparison to interactions between the adsorbent surface and adsorbate. N2 adsorption isotherms similar to Type II were reported for several as-synthesized (surfactant-containing) OMMs. Type III adsorption isotherms were reported for water adsorption on certain OOINs with hydrophobic surfaces **[184, 185].**

UNIVERSITY of the WESTERN CAPE

Adsorption on mesoporous solids proceeds via multilayer adsorption followed by capillary condensation (Type IV and V isotherms). Therefore, the adsorption process is initially similar to that on macroporous solids, but at higher pressures the amount adsorbed rises very steeply due to the capillary condensation in mesopores. After these pores are filled, the adsorption isotherm levels off. Capillary condensation and capillary evaporation often do not take place at the same pressure, which leads to the appearance of

hysteresis loops. However, it was suggested long ago **[184]** and unequivocally confirmed after the discovery of OMMs **[185]** that the capillary condensation-evaporation in mesopores may also be reversible (this behavior will be denoted herein as Type IVc) **[184, 186].** Type IV in general and IVc in particular is typical for many ordered organic – inorganic nanocomposites (OOINs) with accessible mesopores, although when the size of the pores is close to the micropore range or pore size distribution (PSD) is broad, Type I isotherms can be observed. The family of ordered organic-inorganic nanocomposites (OOINs) currently includes OMMs with silica-based frameworks and surfaces functionalized with chemically bonded organic groups, OMMs with organosilica frameworks. The distinction between Types IV and V is analogous to that between Types II and III. Finally, it should be noted that some OOINs may exhibit adsorption isotherms that can be regarded as a combination of the aforementioned five types of isotherms as a result of the presence of several different types of pores in the structure **[186].**

UNIVERSITY of the
WESTERN CAPE

2.19.2.2 Classification of Adsorption – Desorption Hysteresis Loops

The adsorption process on mesoporous solids is often accompanied by adsorption-desorption hysteresis. This phenomenon was a subject of numerous studies [**184]** but its origin is still not fully understood. The hysteresis is usually attributed to the thermodynamic or network effects or the combination of these two effects **[185].** The thermodynamic effects are related

to the metastability of adsorption or desorption (or both) branches of the adsorption isotherm.

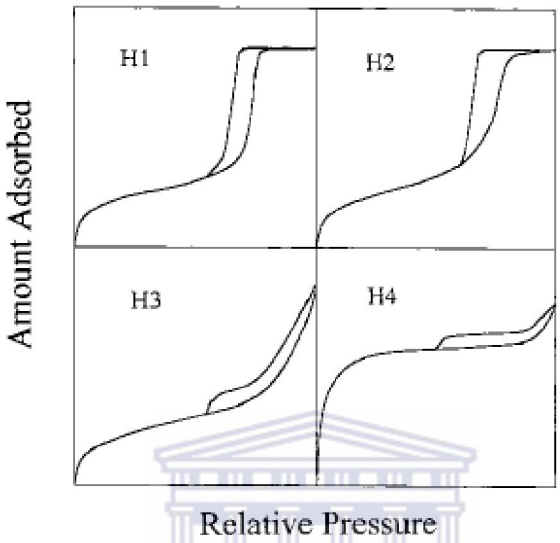

Figure 2. 15: Classification of adsorption-desorption hysteresis loops **[184].**

UNIVERSITY of the
WESTERN CAPE

Namely, the capillary condensation or evaporation may be delayed and take place at higher or lower pressures, respectively, in comparison to the pressure of co-existence between the gaslike and liquidlike phases in the pore. In addition, the hysteresis may also be caused by pore connectivity (network) effects, which are expected to play an important role in desorption processes. Namely, if larger pores have access to the surrounding only through narrower pores, the former cannot be emptied at the relative pressure corresponding to their capillary evaporation since the latter are still filled with the condensed adsorbate **[184].**

The larger pores may be emptied at the relative pressure corresponding to the capillary evaporation in the smaller connecting pores (or at the relative pressure corresponding to the lower limit of adsorption-desorption hysteresis). Hysteresis loops observed experimentally most likely arise from some combination of thermodynamic and network effects, although the latter are often particularly prominent. Adsorption isotherms for certain porous solids may also exhibit low-pressure hysteresis loops (loops that do not close, even at low relative pressures). Low-pressure hysteresis may arise from swelling of the adsorbent during the adsorption process or when physical adsorption is accompanied to some extent by chemisorption processes **[185].** According to the IUPAC recommendations hysteresis loops are classified into four types. The Type H1 loop exhibits parallel and nearly vertical branches (see Figure 2.15). This kind of hysteresis loop was often reported for materials that consisted of agglomerates (assemblages of rigidly joint particles) or compacts of approximately spherical particles arranged in a fairly uniform way **[185].** H1 hysteresis loops are also characteristic of materials with cylindrical pore geometry and a high degree of pore size uniformity **[184 - 186].** Hence, the appearance of the H1 hysteresis loop on the adsorption isotherm for a porous solid generally indicates its relatively high pore size uniformity and facile pore connectivity. The Type H2 hysteresis loop has a triangular shape and a steep desorption branch. Such behavior was observed for many porous inorganic oxides and was attributed to the pore connectivity effects **[185]** which were often considered to be a result of the presence of pores with narrow mouths (ink-bottle pores), but the latter identification may be grossly oversimplified. Indeed, H2 hysteresis loops were observed for materials with relatively

UNIVERSITY of the WESTERN CAPE

uniform channel-like pores, when the desorption branch happened to be located at relative pressures in the proximity of a lower pressure limit of adsorption desorption hysteresis **[186].** This lower limit is characteristic of a given adsorbate at a given temperature (a relative pressure of about 0.4 for N2 at 77 K; 0.34 and 0.26 for Ar at 87 and 77 K, respectively). It should be noted that, in certain relatively rare cases, hysteresis extends below this limit; that is, low-pressure hysteresis is observed. Thus, the appearance of a H2 hysteresis loop in the proximity of the lower pressure limit of adsorption-desorption hysteresis should not be regarded as evidence of poor pore connectivity or ink-bottle pore shape. Novel materials having uniform cagelike pores (and thus suitable as model solids with ink-bottle pores) exhibited adsorption isotherms with broad hysteresis loops but without any dramatic differences in steepness of adsorption and desorption branches **[184 - 186].** These hysteresis loops seemed to be intermediate between Types H2 and H1, rather than being Type H2, as could be expected from the aforementioned simplistic interpretation. Isotherms with Type H3 loops that do not level off at relative pressures close to the saturation vapor pressure were reported for materials comprised of aggregates (loose assemblages) of platelike particles forming slitlike pores **[186].**

UNIVERSITY of the
WESTERN CAPE

Type H4 loops feature parallel and almost horizontal branches and their occurrence has been attributed to adsorption-desorption in narrow slitlike pores. However, recent experimental data for well defined systems question this interpretation. Namely, the Type H4 loop was reported for MCM-41 that exhibited particles with internal voids of irregular shape and broad size distribution (between 5 and 30 nm) **[184].** Hollow spheres with walls

composed of ordered mesoporous silica also exhibited hysteresis behavior of the H4 type **[184].** This would suggest that H4 hysteresis loops may merely arise from the presence of large mesopores embedded in a matrix with pores of much smaller size. Because Type H3 loops are quite similar to Type H4 loops, one can also expect that the former are not attributable solely to platelike materials with slitlike pores. It should be noted that an appearance of a hysteresis loop similar to Type H4 but of triangular shape with an almost horizontal desorption branch that falls steeply close to the lower limit of adsorption desorption hysteresis may be indicative of the presence of disordered domains resulting from collapse of lamellar structures **[186].**

2.19.3. High resolution transmission electron microscopy

UNIVERSITY of the WESTERN CAPE

High resolution transmission electron microscopy (HRTEM) is used to elucidate the pore structure of mesoporous molecular sieves **[187-191].** It provides topographic information of materials at near atomic resolution. However, the exact analysis of pore sizes and thickness of the pore walls is not possible without additional simulations because of the resolution problem. More than one model with a hexagonal array of large cylindrical pores with thin walls gives a similar XRD pattern, but HRTEM gives a direct, precise and simultaneous image of the pore. HRTEM can be successfully used to examine the microstructural feature of mesoporous molecular sieves. In addition to structural characterization, it can also be used to detect the location of metal clusters and heavy cations in the framework. In this study HRTEM was used to determine the pore structure of materials.

2.19.3.1. Selected-area electron diffraction

Selected-area electron diffraction (SAED) can be used in the qualitative measure of crystallinity and symmetry of materials. In SAED, the electrons are scattered by electric fields associated with atoms in thin sample films. Diffraction patterns produced give single-crystal diffractive contributions from multitudes of crystallographic arrangements. In addition, highly polycrystalline materials may constitute concentric Debye-Scherrer rings in the pattern. The appearance of the diffraction pattern is dependent on the crystallinity of the sample material and may become more complex as the degree of polycrystallinity increases. Also, amorphous materials result in patterns that are diffused or blurry **[112].** In this study, SAED is limited to a rapid qualitative measure of the crystallinity and symmetry of nanoparticles.

UNIVERSITY of the
WESTERN CAPE

2.19.3.2. Electron Energy Loss Spectroscopy (EELS)

Electron energy loss spectroscopy (EELS) measure the changes in the energy distribution of an electron beam transmitted through a thin specimen. Each type of interaction between the electron beam and the specimen produces a characteristic change in the energy and angular distribution of scattered electrons. The energy loss process is the *primary* interaction event. All other sources of analytical information (i.e. X-rays, Auger electrons, etc.) are *secondary* products of the initial inelastic event. Thus, EELS has the highest potential yield of information/inelastic event.

Fast electrons travelling through a specimen medium will undergo a mixture of elastic and inelastic scattering events **[192].**

Elastic scattering arising from interactions of Coulombic nuclear potential, provide the most important contribution to the contrast in TEM images and may be loosely defined as scattering events that suffer negligible energy loss. However, inelastic scattered electrons loose energy as a result of Coulombic interactions with the atomic electrons of the medium, and are concentrated within smaller scattering angles. The most important energy – loss mechanisms for EELS studies are plasmon and core loss excitations, and the resultant energy loss spectrum reveals a wealth of chemical and electronic state information regarding the medium under analysis.

UNIVERSITY of the
WESTERN CAPE

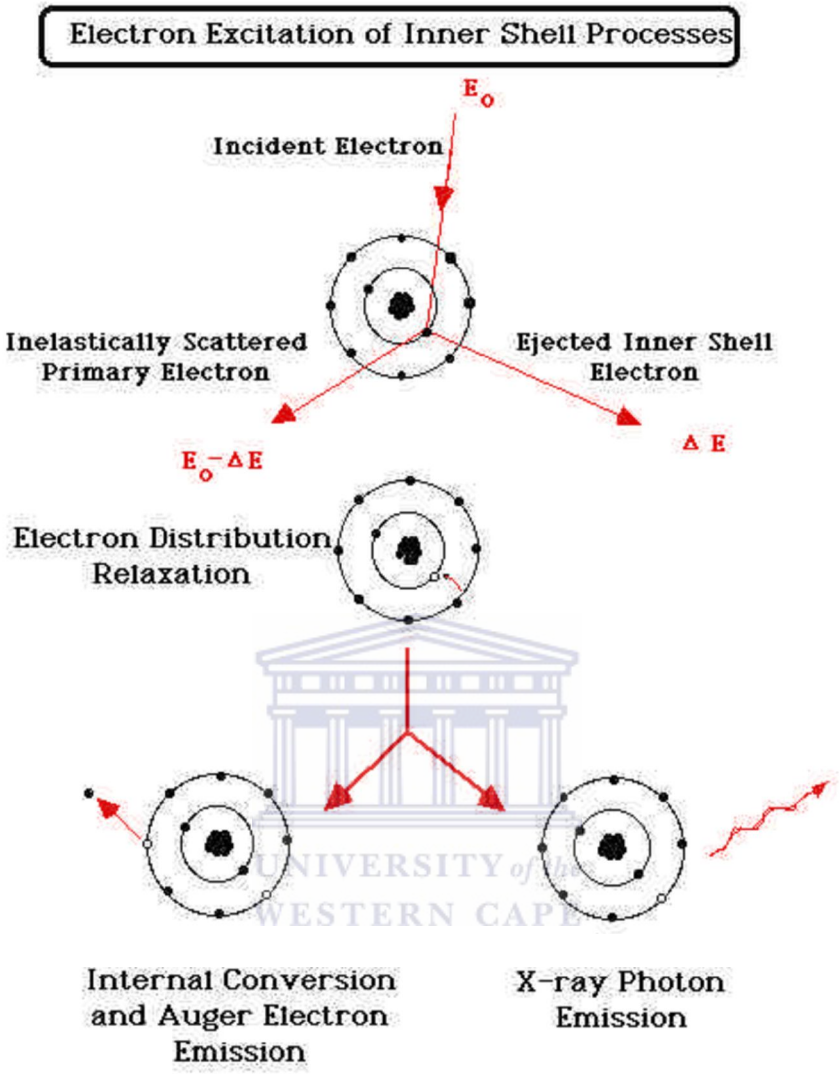

Figure 2. 16: Electron excitation of inner shell processes **[196].**

Elastic scattering arises primarily because of the interaction between the incident electron and the nucleus. Consider a typical electron-atom interaction: electrons are attracted by the positive nuclear charge and pass the atom on a hyperbolic trajectory, with scattering angle q which increases as a function of decreasing impact parameter *b* (Figure 2.16). Energy-loss via

kinetic-energy transfer is negligible for typical TEM collection angles and acceleration potentials, since the target atom is far more massive than the scattered electron. Hence elastic scattering conserves both kinetic energy and momentum to a very good approximation. By analogy with the scattering of alpha particles, elastic scattering from a single atom is often referred to as *Rutherford* scattering.

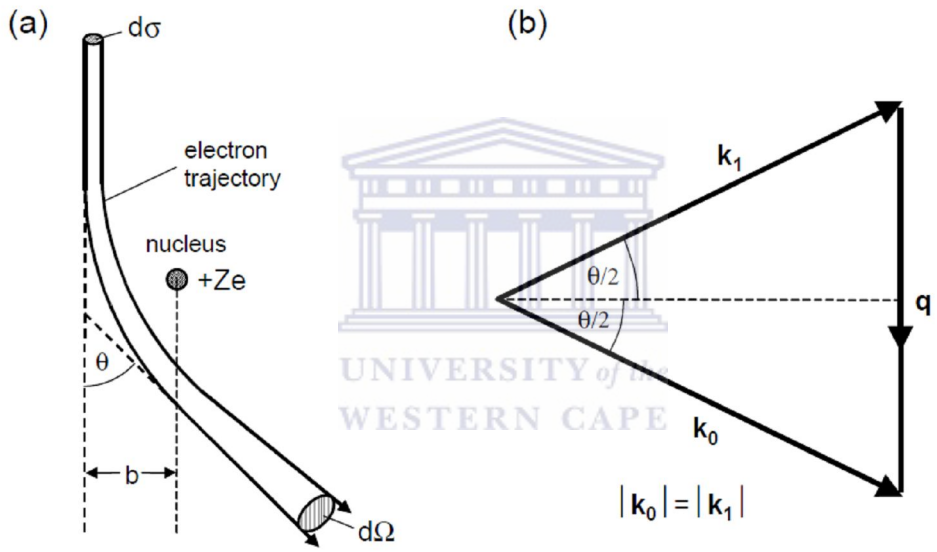

Figure 2. 17: Schematic diagram illustrating the elastic scattering of a fast electron **[194].**

Despite being the most important interaction for obtaining contrast and high-resolution information in the TEM, the elastic signal contains little information of direct use in EELS analysis **[193].** However, the elastic or *zero-loss* signal (Figure 2.17) is indirectly of interest as it provides information regarding the

modification of the angular distribution of electrons undergoing mixed elastic-inelastic, or multiple, scattering. Such mixed scattering results in diffraction effects within the inelastic signal, which may be normalised using the appropriate zero-loss signal. Further, the ratio of elastic to inelastic intensity is useful in EELS investigations for both thickness calculations and quantitative determination of chemical composition.

All features within the electron energy-loss spectrum, excluding the zero-loss peak, result from inelastic scattering of the incoming electron beam. An example of an EEL spectrum, acquired from a stainless steel sample, is shown in Figure 2.18. Inelastic scattering results from the excitation of inner shell, valence or conduction electrons. Thermal diffuse, or *phonon*, scattering events are also strictly inelastic in nature. However, the small energy losses involved, typically 20 meV-1 eV, cannot be resolved in EELS in the TEM due to the energy spread of electron source. Various types of inelastic scattering may occur depending on whether the atomic electrons are
excited singly (in the case of inner-shell electrons), or collectively (valence or conduction electrons). As a consequence of the different energies involved in inner and outer-shell scattering, these losses occupy different parts of the electron energy loss spectrum. The collective excitation of the loosely bound outer-shell electrons results in low energy losses, such as surface and bulk mode *plasmon oscillations*.

UNIVERSITY of the
WESTERN CAPE

These excitations dominate the so-called *low-loss spectrum*, defined loosely as the loss region up to 50 eV. In general these excitations have a broad

distribution with no well-defined activation energy, since a range of possible initial energy-states exists within the valence or conduction band. Conversely, the more tightly bound inner shell electrons suffer larger energy losses, giving rise to the *core-loss region* from approximately 50 eV loss and above. As the initial states have a sharply defined energy, transitions are more discrete, resulting in a well-defined critical ionization energy. This threshold energy represents the minimum energy transfer required for ionisation and the resulting energy-loss spectrum shows a sharp increase in energy above the ionisation energy.

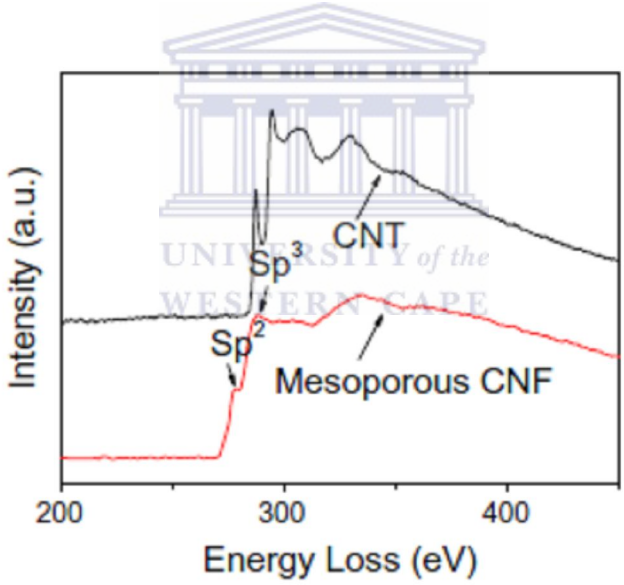

Figure 2. 18: EELS spectra taken on CNT and MCNF **[192].**

2.19.4. Scanning electron microscopy

The schematic diagram of a SEM instrument is shown in Figure 2.19 with all the important components labeled. All SEM instruments are built around an electron column, which produces a stable electron beam, controls beam current, beam size and beam shape.

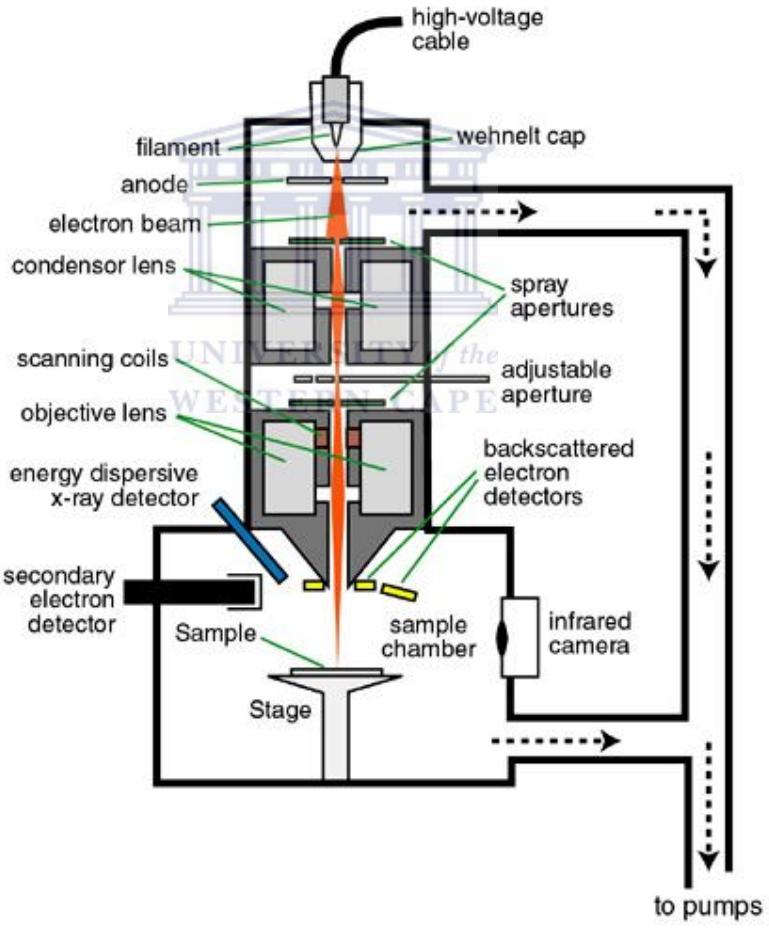

Figure 2. 19: Schematic diagram of a typical SEM instrument **[195].**

2.19.4.1. Resolution

The degree to which a specimen can be magnified is not the only consideration in microscopy. A far more important factor to consider is its resolution. The limit of resolution is the smallest separation at which two points can be seen as distinct entities. As the resolution improves, the images of the objects tend to separate until they can be independently visualized. This ability of the instrument to resolve fine structure is limited by the diameter of the probe, and the number of electrons contained within the beam. The image is effectively made up of lines of image points, each point being the size of the beam probe. If a structure is smaller than the probe, it is not resolved. If however, the probe is too small in relation to the area being imaged, it misses out on several smaller regions on the specimen thereby forming a poor quality image. There is a finite relationship between magnification and the optimum probe size to obtain the derived signal level, and it varies from specimen to specimen. Typical resolution levels in modern scanning electron microscopes are around 4 nm. The relationship between resolution and wavelength is given by Abbe's equation (Equation 2.36) **[195].**

UNIVERSITY of the
WESTERN CAPE

$$d = 0.612\lambda / n\sin\theta \qquad (2.36)$$

where d is the resolution, λ the wavelength of the energy source, n the refractive index of the medium through which the energy source travels, and θ the aperture angle. Abbe's equation signifies the mathematical limit of

resolution for an optical system. When the high energy electron beam interacts with the specimen, a variety of signals may be detected in the scanning electron microscope (Figure 2.20). These signals include secondary electrons, backscattered electrons, transmitted electrons, X-rays (EDX), Cathodoluminescence and Auger electron. The first three types of electronic signals provide visual information about the specimen, while information regarding specimen composition can be determined using characteristic X-rays, Cathodoluminescence and Auger electron signals.

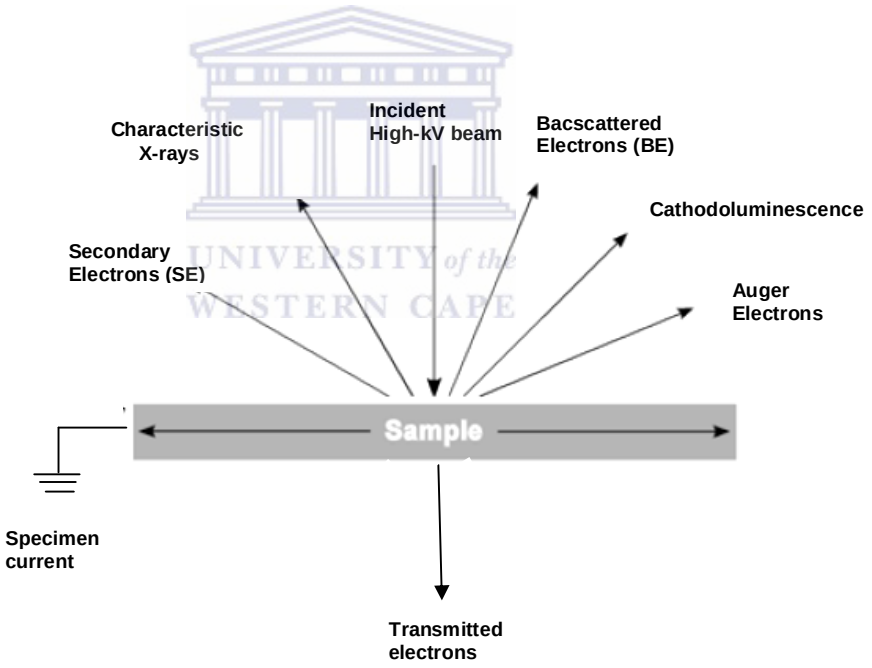

Figure 2. 20: Illustration of possible signals generated when a high beam interacts with a thin specimen **[196].**

Scanning electron microscopy (SEM) utilizes a focused beam of high-energy electrons that systematically scans across the surface of a specimen. The interaction of the beam with the specimen produces a large number of signals (radiations) at or near the specimen surface **[197, 198].** In this study SEM is used to produce images with great depth field and high magnification.

2.19.6. Energy dispersive spectroscopy

Many SEMs are equipped with an energy dispersive spectrometer (EDS) detection system, which is able to detect and display most of the spectrum of elements making up the sample elemental composition or percentage weight. In the EDS, X-ray energy analysis may be accomplished by energy dispersion, which is the segregation of x-rays according to their energy. The method currently preferred for energy dispersion is with a semiconductor detector normally a Si(Li) crystal. A bias of – 500 to – 1500 volts is applied to the Si(Li) crystal (through positive and negative contacts) **[198].** EDS is used to determine the elemental composition of particles. This composition is normally recorded as a percentage ratio, however there are qualitative problems associated with quantitative analysis in scanning electron microscopy. In this study EDS is used to determine sample elemental composition and semi quantitative weight percentage of materials.

UNIVERSITY of the WESTERN CAPE

2.19.5. Thermal analysis

Data obtained from Thermal Gravimetric Analysis (TGA) and Differential Scanning Calorimetry (DSC) analysis are useful in evaluating the thermal properties of molecular sieves **[143].** Thermal analysis is widely used to study the structural stability of as-synthesized forms of molecular sieves such as zeolites and mesoporous materials. It provides information about the temperature required for the removal of adsorbed water, decomposition of the occluded organic cations in the pores and channels of molecular sieves and dehydroxylation at higher temperatures to produce Lewis acid sites and may give indications of temperature induced structural collapse.

UNIVERSITY of the

After the loss of water molecules the shape and splitting of the endotherms (low temperature) helps to identify the location of water molecules and also helps in studying the kinetics of dehydration. The temperature at which an exotherm appears in the TGA, gives helpful information about the temperature required to remove the template molecules from the pores of the molecular sieves during calcination. Phase transformations (if any) can also be understood from the exotherms obtained at higher temperatures. In this study TGA is used to determine the structural stability of as-synthesized forms of molecular sieves.

2.19.6. Raman spectroscopy

Raman spectroscopy is a very useful technique for material identification. This molecular spectroscopic technique is used for both quantitative and mainly, qualitative analysis because of its ease-of-use (e.g. minimal sample preparation) and its non-destructive character. Raman spectroscopy is based on inelastic scattering of monochromatic light, usually from a laser source and it involves illuminating a sample with monochromatic light and using a spectrometer to examine light scattered by the sample. Inelastic scattering means that the frequency of photons in monochromatic light changes upon interaction with a sample. Photons of the laser light are absorbed by the sample and then re-emitted. Frequency of the re-emitted photons is shifted up or down in comparison with original monochromatic frequency, which is called the Raman Effect **[199].**

UNIVERSITY of the
WESTERN CAPE

This shift provides information about vibrational, rotational and other low frequency transitions in molecules. The laser beam can be considered as an oscillating electromagnetic wave with electrical vector. Upon interaction with the sample it induces electric dipole moment which deforms molecules. Raman scattering occurs when the system exchanges energy with the photon and the system subsequently decays to vibrational energy levels above or below that of the initial state. The frequency shift corresponding to the energy difference between the incident and scattered photon is termed the Raman shift. Depending on whether the system has lost or gained vibrational energy,

the Raman shift occurs either as an up- or down-shift of the scattered photon frequency relative to that of the incident photon **[199].**

Because of periodical deformation, molecules start vibrating with characteristic frequency ν. Such oscillating dipoles emit light of three different frequencies shown in Figure 2.21. When a molecule with no Raman-active modes absorbs a photon with the frequency v, the excited molecule returns back to the same basic vibrational state and emits light with the same frequency v as an excitation source. This type if interaction is called an elastic Rayleigh scattering **[199].**

A photon with frequency ν is absorbed by Raman-active molecule which at the time of interaction is in the basic vibrational state. Part of the photon's energy is transferred to the Raman-active mode with frequency v1 and the resulting frequency of scattered light is reduced to $\nu - \nu_1$. This Raman frequency is called Stokes frequency or just "Stokes" as shown in Figure 2.21(b). When a photon with frequency ν is absorbed by a Raman-active molecule, which, at the time of interaction is already in the excited vibrational state, excessive energy of the excited Raman active mode is released, molecule returns to the basic vibrational state and the resulting frequency of scattered light goes up to $\nu + \nu_1$. This Raman frequency is called Anti-Stokes frequency, or just "Anti-Stokes" (Figure 2.21(c)).

Most of all the incident photons in spontaneous Raman undergo elastic Rayleigh scattering and only about 0.001% of the incident light produces inelastic Raman signal with frequencies $\nu \pm \nu_1$. Spontaneous Raman

scattering is very weak and special measures should be taken to distinguish it from the predominant Rayleigh scattering (Figure 2.21).

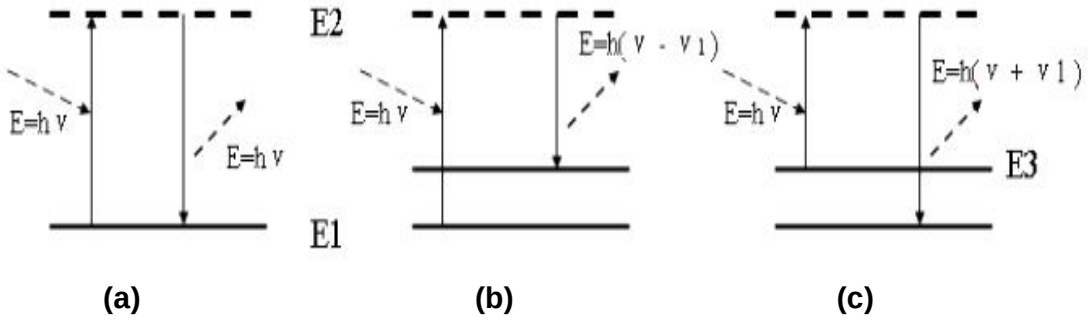

Figure 2. 21: Three different possible scattering scenarios are shown here (E1 is the lowest vibrational energy level while E3 is a excited higher energy level. E2 is a metastable state) **[199].**

UNIVERSITY of the
WESTERN CAPE

2.19.6.1 Schematics of Raman spectroscopy

A schematic diagram of a typical Raman Spectrometer is shown in Figure 2.22. Lasers are used as a photon source due to their highly monochromatic nature, and high beam fluxes because Stokes lines are very weak (~105 times weaker than Rayleigh scattered component). In the system used in this study, a laser is passed into the spectrometer and directed into the microscope by a series of mirrors. The laser is then focused onto the surface of the sample. Light reflects off the sample. This Rayleigh radiation is filtered out at the holographic notch filter. The light then passes through a lens and a slit to filter the light **[199].** The light is than passed through another lens, onto

a mirror and then onto a grating. The resulting beam of light is then captured on a charge - coupled device (CCD) detector. A computer then interprets the CCD information and displays a spectrum. The laser Raman spectrometer used in this study was a Dilor XY-multi-channel Raman spectrometer, with a 514.5 nm Ar ion excitation laser. In order to reduce heating effects and degradation of the samples the laser power was set at 100 mW, thereby only probing at about 100nm depth of the sample surface **[199].**

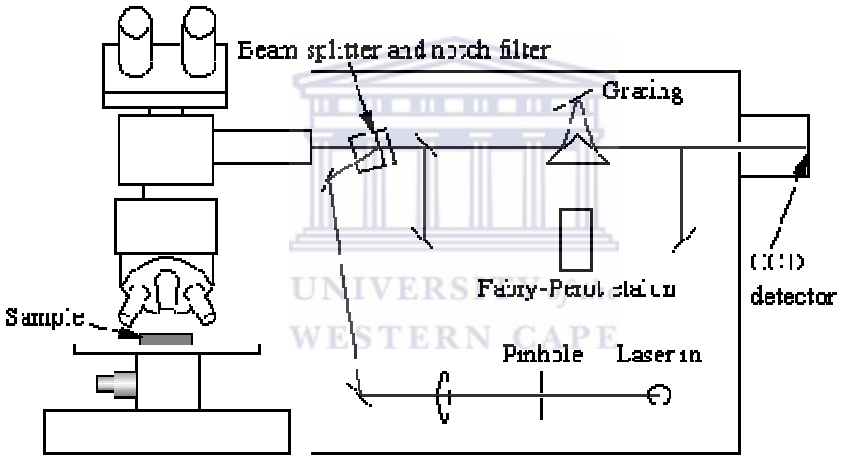

Figure 2. 22: Schematic diagram of a Raman spectrometer **[199].**

Raman spectroscopy is an ideal tool for the investigation of carbon compounds, since Raman spectra can resolve changes in the microscopic structure of the crystals. Most Raman spectrometers are built in with a prism and an aperture to select the 514.6 nm nanometer line of a Coherent Ar ion laser, which is focused to a 100-µm spot on the sample. The laser beam intersect the plane of the filter at a certain angle, normally 75^{0} on which the

sample is suspended. The maximum laser power is normally limited to about 300 mW, although most spectra are taken at less than 100mW to prevent sample heating, and where possible lower powers down to 10 mW could be used **[199].**

Raman spectra can be used to characterize the extent of graphitisation of prepared carbon samples; the well known D and G peaks of graphite are the main feature observed. The D and G peaks have varying degrees of intensity and width, in the 1350 and 1575 cm^{-1} regions respectively. The G peak corresponds to the only allowed Raman transition in this region of the spectrum of large graphite crystals. The D peak is used as an indication of disordered, amorphous structure in the carbon framework **[199].** In this study Raman spectroscopy is used to determine the extent of graphitisation of already prepared mesoporous carbon materials.

UNIVERSITY of the
WESTERN CAPE

2.19.7. Fourier Transform Infra Red Spectroscopy (FTIR).

In Fourier Transform Infra Red spectroscopy, IR radiation is passed through a sample. Some of the infrared radiation is absorbed by the sample and some of it is transmitted. The resulting spectrum represents the molecular absorption and transmission, creating a molecular fingerprint of the sample. Like a fingerprint no two unique molecular structures produce the same infrared spectrum. This makes infrared spectroscopy useful for several types of analysis. Infrared spectroscopy can result in a positive identification (qualitative analysis) of every different kind of material **[200].**

The Sample Analysis Process

The normal instrumental process is as follows:

1. The Source: Infrared energy is emitted from a glowing black-body source. This beam passes through an aperture which controls the amount of energy presented to the sample (and, ultimately,to the detector).

2. The Interferometer: The beam enters the interferometer where the "spectral encoding" takes place. The resulting interferogram signal then exits the interferometer.

3. The Sample: The beam enters the sample compartment where it is transmitted through or reflected off of the surface of the sample, depending on the type of analysis being accomplished. This is where specific frequencies of energy, which are uniquely characteristic of the sample, are absorbed.

UNIVERSITY of the
WESTERN CAPE

4. The Detector: The beam finally passes to the detector for final measurement. The detectors used are specially designed to measure the special interferogram signal.

5. The Computer: The measured signal is digitized and sent to the computer where the Fourier transformation takes place. The final infrared spectrum is then presented to the user for interpretation and any further manipulation **[200].**

.

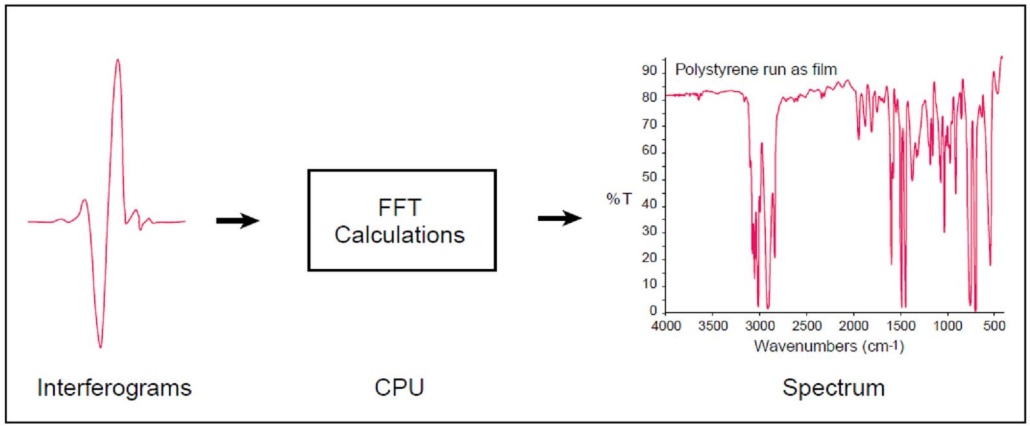

Figure 2. 23: Schematic representation of FTIR **[201].**

FTIR transmission spectra of OMC materials are shown in Table 2.5. The FTIR spectrum of OMC-600 shows bands at 765, 833 and 890 cm^{-1} (Figure 2.23 and Table 2.5) which are attributable to C–H vibrations **[201].** The higher intensity of the band at 1621 cm^{-1} is attributable to C-C vibrations in terminal olefinic C=C bonds **[201].** The band at 1718 cm^{-1} is ascribable to C=O vibrations in carbonyl groups. The bands at 1384 and 1465 cm^{-1} appear due to vibrations of –CH2 and –CH3 groups **[201].** The characteristic bands due to C–O stretching vibrations are observed in the range of 100–1300 cm^{-1}. It is difficult to assign the bands in this region because the bands of functional groups are overlapped. The bands at 1172 and 1268 cm^{-1} can be assigned to C–O–C stretching vibrations of alcoholic, phenolic and carboxylic groups **[201].** The band at 1103 cm^{-1} may be due to O– H.

UNIVERSITY of the WESTERN CAPE

Table 2.5: Carbon Groups in relation to assigned vibrational frequency bands **[201].**

Group or functionality	Assignment regions (cm^{-1})	Group or functionality	Assignment regions (cm^{-1})
C-O in ethers (stretching)	1000-1300	N-H, C=N	1560-1570
Alcohols	1049-1276, 3200-3640	Cyclic amides	646,1461,1546,1685
Phenolic groups		C-N aromatic ring	1000, 1250, 1355
–C-OH (stretching)	1000-1220	C-N	1190
O-H	1160-1200, 2500-3620	C=C=N	2070-2040
Carbonates; carboxyl-carbonates	1100-1500, 1590-1600	N-O-	1300-1000
–C-C aromatic (stretching)	1585-1600		
Quinones	1550-1680		
Carboxylic acids	1120-1200, 1665-1760, 2500-3300		
Lactones	1160-1370, 1675-1790		
Carboxylic anhydrides	980-1300, 1740-1880		
C-H (stretching)	2600-3000		

UNIVERSITY of the
WESTERN CAPE

The Figure 2.24 shows that the stretch of S-OH shift to lower wave number, stretch of S=O shift to higher wave number, and stretch of C-F shift to lower wave number during the formation. Also, the shift of S-OH stretching and S=O stretching are more seriously in faster formation **[201, 202].** The bonding strength strongly depends on wave number.

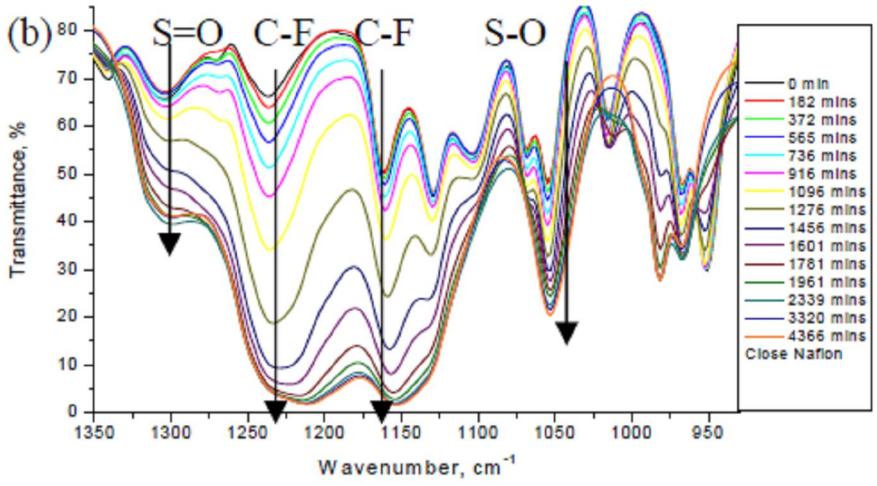

Figure 2. 24: FTIR representing Sulphur- oxygen stretching **[202].**

Also, in the faster formation process, the sulfonic groups are more easily aggregated; but in the slower one, the sulfonic groups are more easily to bond with water. A band of medium intensity centered near 940-960 cm^{-1} is attributed to Si-OH stretching vibrations. This band is, however, not univocally assigned because it can overlap or coincide with Si-O-, Si-O-C (from unhydrolyzed OEt groups), and several vibrations from residual CTAB **[202].**

UNIVERSITY of the WESTERN CAPE

2.20. ANALYTICAL METHODS FOR MERCURY DETERMINATION

A variety of methods exist to detect mercury sensitively and selectivity **[203].** Several review papers have been published for the determination of total mercury concentration in environmental and biological samples. These methods are listed as follows: Cold vapour atomic absorption spectrometry (CVAAS) [204] atomic fluorescence spectrometry (CVAFS) **[204]**, inductively coupled plasma atomic emission spectrometry (ICP-AES) **[205],** mass spectrometry (ICP-MS) **[206],** chromatography **[207]** and UV-Vis spectrophotometric determination [**209].**

UNIVERSITY of the
WESTERN CAPE

2.20.1. Atomic absorption spectrometry

The most popular method for determining mercury is cold vapour atomic absorption spectrometric measurement (CVAAS). This analytical technique is still widely used **[203,209].** Mercury is unique among the heavy metals in that it has a very high vapour pressure at low temperatures and can be introduced to the spectrometer as a vapour with ease. Absorption at 253.7nm in the UV region has been measured with the use of mercury vapour lamps and also hollow cathode lamps as the light source. The way of releasing mercury from digested or aqueous samples is reduction. This process is then followed by

volatilisation and introduction of the mercury by aid of a gas stream. Sn^{2+} ions have been used as reductants **[208, 210].**

Procedures to eliminate interference have been important in the determination of mercury in different matrices. Two approaches have been used to remove interferences by organic vapour. A gold amalgamation method to purify the mercury vapour and an optical background correction method for the spectrometry. The gold amalgamation is based on the selective absorption of mercury on a gold surface. The organic vapour is purged out and mercury is released from the gold fibre trap by heating and then introduced into the spectrometer. Optical background correction is used to eliminate molecular absorption by organic vapours. Earlier work used a continuum light source and later work used the Zeeman Effect. These methods are necessary for electrothermal atomization, or flameless atomic absorption spectrometry. Zeeman AAS is suitable for the direct analysis of solid samples or samples without prior acid digestion. Use of quartz lamps and the 184.9 nm resonance line in the UV region provided increased sensitivity over the commonly used employed 253.7 nm line. Improved accuracy for CVAAS was obtained by using the 184.9 nm resonance line. Detection limits for Hg using the 184.9 nm is 30 times lower than using the 253.7 nm line **[211- 214].**

UNIVERSITY of the
WESTERN CAPE

2.20.2. Atomic fluorescence spectrometry

Several articles have appeared on the determination of Hg using CVAFS **[215, 216].** Most of the early work used flame atomization. This technique was

later further developed by using an electrothermal atomization or cold vapour atomization **[217].** This technique makes use of Hg autofluorescence, the narrow band emission of UV radiation by Hg^0 atoms during relaxation to the ground state after absorption of radiation of wavelength 253.7 nm. The result is a sensitive and selective detection of mercury in the picogram range **[212, 217].** Mercury is liberated by aeration or reduction and trapped on an Au filament. The Au filament is then heated to 700 ºC to liberate Hg^0 which is then introduced to a flow type atomic fluorescence cell. The detection limit is 5 pg Hg with a relative standard deviation of 3%. Using an atomic fluorescence instrument that uses ICP as an atomization cell and a pulsed Hg hollow cathode lamp can lower the detection limits to 0.5 ng dm^{-3} **[212, 216].**

UNIVERSITY of the WESTERN CAPE

2.20.3. Gas chromatography (GC)

In gas chromatography (GC) species are separated on the basis of volatility and the interaction between the analytes and the stationary phase. There are both packed and open capillary columns for GC, the latter being used the most efficient. Capillary columns are between 10 and 100 meters long, having an internal diameter (i.d) of 0.2 – 0.7 mm and the inner wall coated with a 0.2 – 0.5 µm thick film of stationary phase. The mobile phase is a gas, typically helium that transports the vaporized analytes toward the detector. The GC column is placed in an oven and heated to required temperatures **[217- 220].**

For good performance in GC most mercury species need to be derivatised to become volatile and thermally stable. Butylation with Grignard reagent in an organic solvent is a common derivatisation method **[221].** However, if the excess Grignard is not deactivated, methyl butyl mercury can be transformed to dibutyl mercury and the same transformation has also been seen for dimethyl mercury **[219 - 221].** The presence of halogens such as iodine in a sample has shown to decompose alkyl mercury **[221].** In aqueous solution sodium tetraethyl borate $NaBEt_4$, is used for derivatization of mercury species and produce volatile ethyl mercury species **[223].** These species are purged out of solution with an inert gas onto a Tenax packed column. The mercury species are then desorbed from the Tenax by heating and with a gas stream the species are injected into the GC **[212, 219, 224].** A disadvantage of using this method is that inorganic mercury, mono ethyl mercury and diethyl mercury cannot be separated when using $NaBEt_4$. All these mercury species are derivatised to the same chemical form. Another drawback is that if the sample contains high concentrations of halides, methylmercury is reduced to Hg^0 during derivatization **[223, 224].** A major disadvantage of this method is the interactions of mercury compounds with the chromatographic support such as decomposition of mercury and adsorption onto tubing and pipes. This phenomenum can cause serious problems and influence experimental results. Studies have shown that after the injection of methylmercury chloride, substitution of the halide occurred with the formation of methylmercury iodide. The use of glass capillary columns can improve and solve these problems **[224, 225].**

UNIVERSITY of the WESTERN CAPE

2.20.4. Liquid chromatography

The use of High Performance Liquid Chromatography (HPLC) for mercury speciation has the advantage of simplified sample preparation **[226].** In GC analysis it is necessary to form volatile thermally stable derivates, whereas this is not necessary for HPLC. Another advantage of using HPLC is the relatively low cost of analysis. Aqueous buffers are used as mobile phase but in GC more expensive carrier gases are required. Combining HPLC with spectroscopic detection provides a simple and selective method for metal speciation **[212].**

UNIVERSITY of the
WESTERN CAPE

There are different types of columns for separation of analytes. Most columns are packed with silica based particles and to the silica surface a stationary phase is chemically attached. The most common stationary phase in HPLC is octadecylsilane, ODS, also called C_{18} **[127].** ODS is non polar and is used in combination with polar mobile phase. For each analyte injected into the column there will be an equilibrium between the stationary phase and the mobile phase. A polar compound has a short retention time as the equilibrium is shifted toward the polar mobile phase and for a non polar analyte the equilibrium is shifted towards the stationary phase and it has a longer retention time **[227, 228].**

For mercury speciation with HPLC mercury species are usually mixed with sulphur containing reagents to form a complex, which improves the

chromatographic separation properties of the species. Cysteine **[228]** and dithizone **[229]** were successfully used as complexing agents for mercury speciation. There is however also some disadvantages using HPLC for metal speciation. Some of these disadvantages are the poor retention reproducibility, tailing of peaks, the use of hazardous organic solvent, time consuming extractions to remove interfering compounds and decomposition of diphenylmercury **[212].** HPLC is less sensitive than GC and is better suited for polar species separation **[230, 231].**

2.20.5. Inductively coupled plasma mass spectroscopy (ICP-MS)

UNIVERSITY of the WESTERN CAPE

Recently mass spectrometers (MS) have become more commonly used as detectors in analytical chemistry. In the MS the sample introduced is ionised and components are separated on a mass to charge ratio in the mass analyser. Samples are introduced as liquids into an inductively coupled plasma (ICP). The liquid passes through a nebulizer to form an aerosol. The ICP is an ion source, which operates at high temperatures (5000 K – 10000 K) and at atmospheric pressure. The argon plasma is generated in a quartz torch under the conditions of a radio frequency electromagnetic field (27– 40 MHz) **[33].** The solvent evaporates and molecules are decomposed to single atomic ions in the plasma. As the ICP is operated at atmospheric pressure and high temperatures, the MS requires high vacuum and ambient temperatures.

The ability to distinguish between masses is dependent on the resolution of the mass analyser. The resolution R, is usually defined as R = m/M. where m

is the mean value of the two masses that are separated and M is the mass difference between them.

The main advantage of ICP-MS is that it can be used for detecting most elements at a low concentration. Detection limits are generally in the ng/l range or lower. By scanning the MS signals for many different elements or isotopes to charge ratios can be detected within a few seconds. The ICP-MS performance is affected by introduction of solutions containing high amount of salts or organic solvents, as these will cause deposits of salt and carbon in the interface and MS. Organic solvents give rise to a high organic vapour pressure that will cause a high carbon load of the plasma. High amounts of carbon and salt in the plasma absorbs energy and therefore decreases the ionisation efficiency of the plasma leading to deterioration in sensitivity **[212, 231].**

UNIVERSITY of the
WESTERN CAPE

2.20.6. UV-VIS Spectrophotometry

UV-Vis has become the most important analytical instruments for the last 40 years because of its simplicity, versatility, speed, accuracy and cost-effectiveness . Different molecules absorb radiation of different wavelengths. An absorption spectrum will show a number of absorption bands corresponding to structural groups within the molecule. For example, the absorption that is observed in the UV region for the carbonyl group in acetone is of the same wavelength as the absorption from the carbonyl group in diethyl ketone. UV-Vis has three types of electronic transition, (1) transitions involving

π, *σ*, and *n* electrons (2) charge-transfer electrons (3) and *d* and *f* electrons (not covered in this thesis). When an atom or molecule absorbs energy, electrons are promoted from their ground state to an excited state. In a molecule, the atoms can rotate and vibrate with respect to each other. These vibrations and rotations also have discrete energy levels, which can be considered as being packed on top of each electronic level. Figure 2.25 show the example of different electronic transitions.

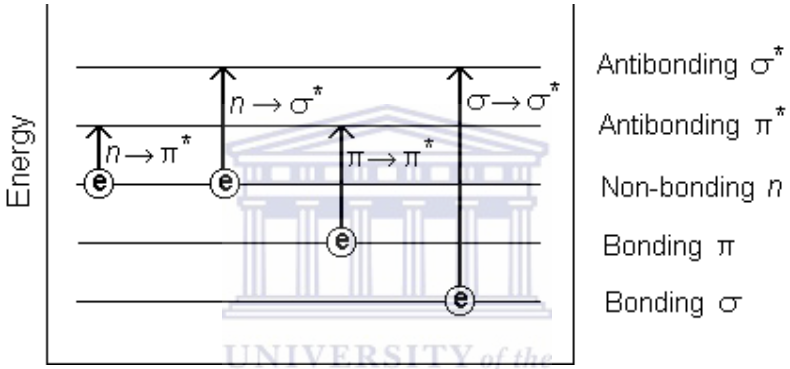

UNIVERSITY of the
WESTERN CAPE

Figure 2. 25: Possible electronic transitions of *π*, *σ*, and *n.*

From figure 2.25 it can be seen that when an electron *σ* bonding is excited to the anti-bonding (*σ* -*σ* * transitions) a large energy is required. Most of these transitions show a maximum wavelength which is less than 200nm. Saturated compounds containing atoms with lone pairs (non-bonding electrons) are capable of n - *σ** transitions. These transitions usually need less energy than *σ* -*σ* * transitions. They can be initiated by light whose wavelength is in the range 150 - 250 nm. The number of organic functional groups with n - *σ** peaks in the UV region is small. Most absorption spectroscopy of organic compounds is based on transitions of *n* or *π* electrons to the *π** excited state.

This is because the absorption peaks for these transitions fall in an experimentally convenient region of the spectrum (200 - 700 nm). These transitions need an unsaturated group in the molecule to provide the π electrons. The solvent in which the absorbing species is dissolved also has an effect on the spectrum of the species. With an increase in solvent polarity peaks resulting from n - π * transitions are shifted to shorter wavelengths (blue shift). This is due to increased solvation of the lone pair, which lowers the energy of the n orbital. Most of the time, the reverse (i.e. red shift) is seen for π -π * transitions. Many inorganic and some organic species show charge-transfer absorption and are called charge-transfer complexes. For a complex to demonstrate charge-transfer behaviour one of its components must have electron donating properties and another component must be able to accept electrons. Absorption of radiation then involves the transfer of an electron from the donor to an orbital associated with the acceptor.

UNIVERSITY of the
WESTERN CAPE

2.20.6.1. Instrumental set up of UV-vis Spectrophotometry

UV-Visible absorption spectroscopy involves passing a monochromatic beam of light through a sample and measuring the absorption of the material at this wavelength (Figure 2.25). This absorption is measured as a function of frequency over a frequency range from infrared to ultraviolet. The absorption is usually measured in reference to a blank sample in a double beam arrangement, to eliminate variations caused by the differences in lamp

intensities at different frequencies. Typically, measurement ranges here were 900 nm down to 200 nm.

As the photons pass through a material, it is possible that photons of a suitable energy can interact with the material, resulting in an electron being excited to a higher energy state, and the photon being absorbed. By measuring the amount of light absorbed for a particular wavelength, it is possible to deduce information about the electronic structure of the material. In conjugated polymers, UV-Visible absorption is primarily due to π-π^* transitions, as the energy gap between these levels ranges from near UV to infrared. Excitations from π electrons are in the near to far ultraviolet, so these are correspondingly left unaffected by the measurements in this study. As ultraviolet light affects these π bonds, it tends also to alter the polymer's structure, resulting in photo-degradation of the polymer. Different parts of the polymer are excited at different frequencies. This is useful as it allows us to use UV-Visible spectroscopy as a probe to determine how the polymer is affected by changes in its environment due to such factors as solvent interaction, concentration changes leading to aggregation and in this case the introduction of nanotubes to a polymer solution.

UNIVERSITY of the
WESTERN CAPE

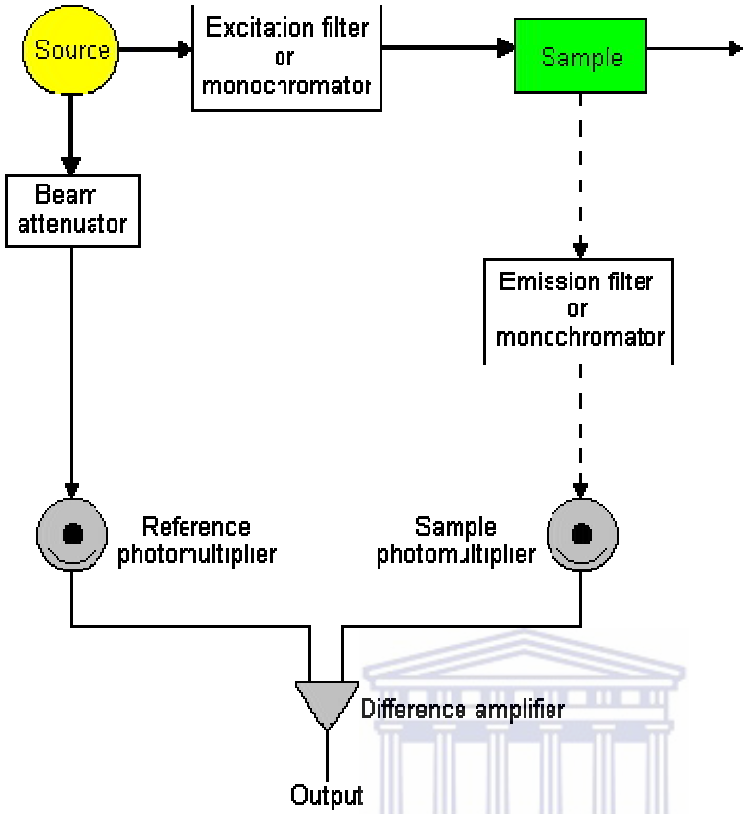

UNIVERSITY of the WESTERN CAPE

Figure 2. 26: Schematic diagram of a UV-Vis instrument showing the important parameters and the direction of light from the light source **[233].**

The UV-Vis spectrophotometry is an example of a direct detection mode; this refers to an analytical signal related directly to the chemical or physical properties of the metal ion itself (e.g. the energy of emitted X-rays). Measuring the UV-Vis absorption of the analyte directly provides some specificity, when the entire spectra are obtained. The optical pathlength through the separation capillary is very small and therefore, the direct measurement of absorption is limited to compounds which have relatively high molar absorptivities **[233].**

Attempts have been made to increase the optical path length by use of a z-cell, bubble capillary, rectangular capillary or extended light-path cell **[232].** Metal ions have weak absorption peaks in the UV-Vis wavelength range. Because of this draw back a complexing ligand must be added to the background mercury solution to give adequate separation.

Amongst complexing ligand methods proposed, the method of T.V. Ramakrishna et al **[232]** based on ternary complex formation for mercury (II) seem to provide the best alternative choice to the conventional method based on extraction with dithizone as it is associated with superior sensitivity and selectivity, in addition to high stability and reproducibility. By making use of UV-Vis Spectrophotometry, Ramakrishna and co-workers utilized a simple and reliable method of determining mercury (5 – 25 µg) in 25 ml by treating Rhodamine 6G with tetraiodomercurate(II). The reaction occurs immediately over the pH range of 1 -7 and, the absorbance remains unchanged at 575 nm for at least 24 hours. The method provides molar absorptivity of 7.0×10^4 $mole^{-1}cm^{-1}$ **[232].**

UNIVERSITY of the WESTERN CAPE

2.21. CONCLUSIONS

Mercury is one of the most toxic metals in the environment. Mercury is particularly dangerous once it gets into aquatic systems, because under certain conditions it is converted into methyl mercury a more toxic form. It is readily taken up by phytoplankton and then accumulates up the food chain,

with the result that people eating methyl mercury-contaminated fish on a regular basis soon experience the symptoms of mercury poisoning. Once it enters the food chain, accumulation of mercury compounds takes place in humans and animals. Mercury attacks the central nervous system, so dementia, memory loss and speech and gait problems are typical symptoms of mercury poisoning. The term as 'mad as a hatter' was coined because, in the old days, mercury was used in the manufacture of felt hats, so mercury poisoning was somewhat of an occupational hazard.

Coal-fired power stations are the primary source of mercury emissions globally, and given that most of South Africa's power stations are located in Mpumalanga - where 80% of the country's coal are produced especially the Olifants Water Management Area (WMA). Another major mercury emitter is the cement industry, which uses coal as a kiln fuel. Although the cement industry is more evenly distributed throughout South Africa, there is a concentration of facilities in the Crocodile (West) and Marico WMA.

UNIVERSITY of the
WESTERN CAPE

Adsorption on activated carbon is one of the cost effective and conventional methods for removal of Hg (II) from wastewater. Activated carbons (ACs) are utilized worldwide in many industries as adsorbents for waste water treatment. ACs have highly developed internal surface area and porosity. The development of micro and mesopores allows activated carbon to adsorb molecules of different sizes. The complexity of the carbon structure prevents the conventional activation process from preparing carbon materials with strictly controlled or uniform pore structure, although voluminous research has

been done and a great effort has been made towards the control of pore size and its distribution.

To discover chemically interesting phenomena specific to a particular pore size, ordered porous materials are needed which have a defined pore size and a well developed porous structure. The recent development of industrial technology requires that carbon should have desired pore structure for new application fields. For adsorption the carbon material should have mesoporosity and a high surface area. Mesoporous carbons with accessible pore sizes > 2 nm can be obtained as inverse replicas of mesoporous silica materials used as templates. However, the framework of these carbons contains some amorphous character. The research problem is that, it is not possible to modify OMC with nitric acid and later graft sulphur containing ligands on the OMC surface.

UNIVERSITY of the
WESTERN CAPE

The objective of this study is to develop novel adsorbents for effective removal of mercury from water. By utilisation of ordered mesoporous silica (OMSi) material as sacrificial templates for attainment of ordered mesoporous carbon (OMC) material. The goal is to obtain a negative replica of the initial OMSi as well as to ensure a high level of mesoporosity in the desired OMC product.
Surface properties of the OMCs will be investigated by probing the OMC product with acid and basic dyes. In this work, a novel and facile route to prepare ordered mesoporous carbon (OMC) from ordered mesoporous silica (SiO_2) based sacrificial templates is described by making use of hydrocarbon vapours. The optimum conditions to achieve OMC from OMSi will be

investigated. These ordered mesoporous carbon (OMC) nanostructured materials will be synthesized via a pyrolysis method using ordered mesoporous silica (OMSi) materials as solid templates. Chemical vapor deposition (CVD) with the use of liquefied petroleum gas (LPG) as the carbon precursor will be applied for the preparation of graphitic ordered mesoporous carbon analogues. The optimum conditions to achieve OMC from OMSi will be investigated. The approach applied in this study is presented schematically in the following diagram (Figure 2.27), where an end product is expected to be either 100% carbon material conversion or carbon-silica material with “silica islands”.

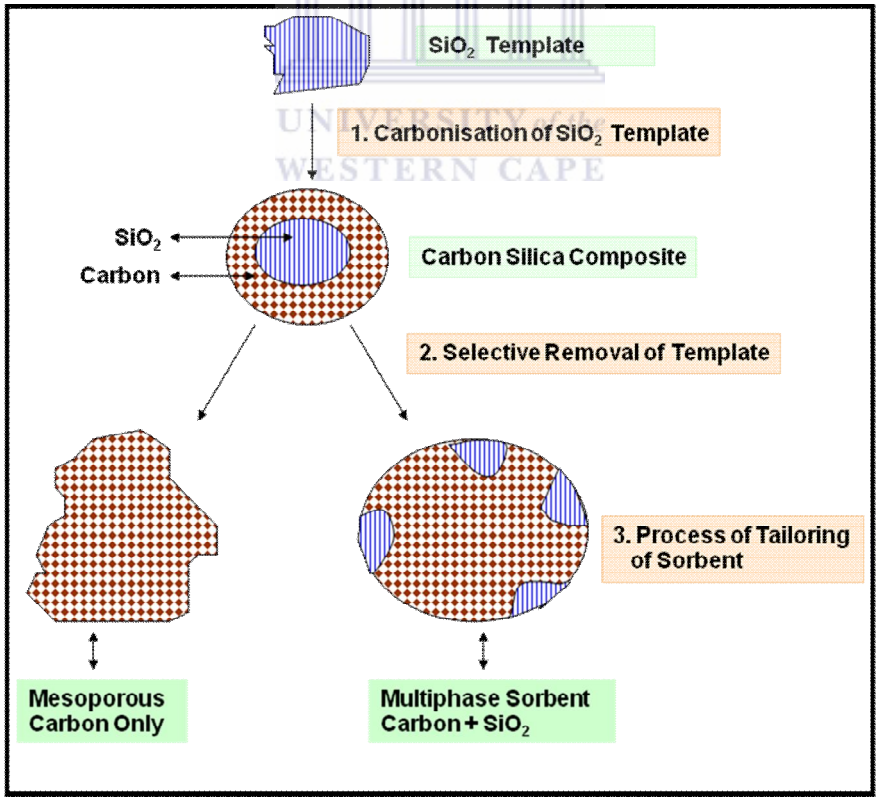

Figure 2. 27: Schematic diagram for synthesis of OMC from OMSi.

The method developed is based on the use of ordered mesoporous silica materials SBA-15, HMS and MCM-41 as templates. Liquefied Petroleum Gas (LPG) which will be used as carbon precursor is normally composed of 90 % propane (C_3H_8), 2.5 % butane (C_4H_{10}) and higher hydrocarbons, and the balance ethane and propylene. The transformation process of silica templates to OMC will be achieved through use of LPG as a carbon precursor by being infiltrated in the porous silica framework and then the precursor will be carbonised at high temperatures. The pores will be filled up to create a negative replica of the template's structural order in the desired carbon product. Infiltration of carbon into the silica pores and carbonization will be followed by the dissolution of the SBA-15, HMS and MCM-41 silica framework by chemical etching with NaOH. Etching will be performed to remove the silica skeleton / framework from the silica-carbon composite; so that the remaining framework is mostly made up of carbon. Thus a negative carbon replica or carbon analogue of the parent silica material will be formed.

UNIVERSITY of the
WESTERN CAPE

The synthesised mesoporous carbon with the desired structural properties will be modified with nitric acid (HNO_3) and sulphur containing ligands (3-mercaptopropyltriethoxysilane, MPTES) and these will be designated as modified ordered mesoporous carbon (MOMC). The MOMC will eventually be utilized as adsorbents for Hg(II) removal from water. The mercury (II) removal efficiency of the unmodified OMC as well as MOMC will be compared to that of commercialized activated carbon.

CHAPTER 3

METHODOLOGY

Chapter 3 presents the materials and methodology of the experimental approaches for the preparation and characterisation of mesoporous silica, mesoporous carbons and modified mesoporous carbon. All aspects of the preparation of sample material, characterisation, and treatment of data will be detailed. The chapter is initiated with an introduction to the detailed methodologies for the preparation of mesoporous silica, mesoporous carbons and modified mesoporous carbon, followed by instrumental parameters used in the study.

UNIVERSITY of the
WESTERN CAPE

3.1. CHEMICALS AND MATERIALS

3.1.1. Chemicals

The chemicals that were used in this study are presented in Table 3.1

Table 3. 1: Summary of chemicals used in the study.

Chemical name	Specification	Supplier
Mercury Chloride ($HgCl_2$)	AR	Kimix
Mercury nitrate standard solution ($HgNO_3$)	99 %	Merck
Acid Orange 8 (AO8)	65 %	Sigma Aldrich
Methylene Blue (MB)	99 %	Sigma Aldrich
Rhodamine B (RB)	96 %	Sigma Aldrich
Rhodamine 6G (R6G)	96 %	Sigma Aldrich
Citric acid monohydrate	AR	Kimix
di- Sodium Hydrogen Orthophosphate anhydrous	AR	Kimix
Potassium iodide	99 %	Sigma Aldrich
Potasium hydrogen phthalate	98%	Merck
1-Hexadecylamine, Tech,	90 %	Sigma Aldrich
Gelatine	CP	Kimix
Charcoal Activated Carbon (powder) (AC)	AR	Saarchem
Poly(ethylene glycol) – block – poly(propylene glycol) – block – polyethylene glycol (P123)	99.9 %	Sigma Aldrich
Tetraethoxysilane	99.9 %	Sigma Adlrich

UNIVERSITY of the WESTERN CAPE

Hexadecyl-trimethylammonium bromide	99 %	Sigma Adlrich
Tetraethyl orthosilicate	98 %	Sigma Aldrich
Hydrochloric acid	32 %	Sigma Aldrich
Nitric acid	55 %	Kimix
Toluene, anhydrous	99.8 %	Sigma Aldrich
Aluminium Chloride	99.7 %	Fluka
Sodium hydroxide pellets (NaOH)	99.8 %	Merck
1, 2, 4, Trimethyl benzene	> 98 %	Merck
3- Mercaptopropyltriethoxysilane	98%	Sigma Aldrich
Ethanol	99.8 %	Merck
Sodium hydrogen orthophosphate anhydrous (AR)	40 %	Kimix
Liquefied Petroleum Gas (LPG)	A mixture of 90 % propane (C_3H_8) and 2.5 % butane (C_4H_{10}) and higher hydrocarbons	Afrox

UNIVERSITY of the WESTERN CAPE

3.1.2. Materials

The materials that were used in this study are presented in Table 3.2

Table 3. 2: Summary of materials used in the study.

Material name	Model/Specification	Supplier
Microprocessor pH meter	HI 221	Hanna
Water bath	1 m x 0.5 m	Kimix
Quartz spectrophotometer cuvettes	10 mm	Hellma
Schott bottle	100 ml, 1000 ml	Simax (Czech republic)
Centrifuge tubes	50 ml	Kimix
Medical bottles	100 ml	Kimix
Filter papers	MN 615, 125 mm	Macherey - Nagel

UNIVERSITY of the WESTERN CAPE

3.2. PREPARATION OF ORDERED MESOPOROUS SILICA (OMSi)

The procedure for the preparation of ordered mesoporous silica (OMSi) is reviewed in Section 2.13.2 of the literature review; in this study ordered mesoporous silicas were used as sacrificial templates for the synthesis of

ordered mesoporous carbons (OMCs). Therefore, ordered mesoporous carbons were a negative replica of the parent ordered mesoporous silica materials. These sacrificial templates included SBA-15, hexagonal mesoporous silica (HMS) and MCM-41.

3.2.1 Preparation of SBA-15

In this study the parent mesoporous SiO_2 based SBA-15 used as sacrificial template was synthesised using a similar method to that reported by Lu and coworkers **[233].**

A homogeneous mixture was sequentially prepared in the following order comprising of 4.1g of Poly(ethylene glycol) – block –poly(propylene glycol) – block – polyethylene glycol (P123, a triblock copolymer (TCP), 20.0 g H_2O , 13.2 g of 37 % HCl and then 10 g TEOS (tetraethyl orthosilicate) was stirred at room temperature for 3 h in a (100 ml) beaker and thereafter was transferred to a capped polyethylene bottle. The resulting gel was subjected to further stirring at 25 ^{0}C for 3 days. As synthesised SBA-15 was subjected to aging at 90 ^{0}C for three days by being transferred to a sealed Schott bottle (1L) and placed in a hot air oven. When the aging process was finished, as synthesised SBA-15 was separated by filtration, followed by washing with distilled water and subsequently dried at room temperature for 24 h. In a post heat treatment or calcinations process, as-synthesised SBA-15 was heated at 1 ^{0}C/min to 550 ^{0}C and held at that temperature for 5 h to remove the template. The yield of SBA-15 obtained was 27.03 g. The final product was

UNIVERSITY of the WESTERN CAPE

stored in a desiccator under vacuum and characteristics of this material are presented in Sections 4.2 to 4.9.

3.2.2. Preparation of hexagonal mesoporous silica (HMS)

In this study the parent mesoporous SiO_2 based HMS used as sacrificial template was synthesized in a similar method to that reported by Pinnavaia and coworkers **[235]** by adding 4g of a primary amine surfactant 1-hexadecylamine (Aldrich) as structure directing agent under stirring to 100 mL ethanol and 250 mL water mixture (35/70, v/v). The mixture was subjected to stirring in an open vessel for 24 h. In a typical synthesis, 4.0 g of the silica source (Tetraethoxysilane, TEOS, Aldrich) was added dropwise under stirring to the solution containing the surfactant in an ethanol/water mixture (1/2.5, v/v) i.e.100 ml ethanol and 250 ml water. The mixture was once more subjected to stirring at 25 ^{0}C in an open vessel for 24 h.

UNIVERSITY of the WESTERN CAPE

The solid product was filtered and washed with distilled water. 150 ml of ethanol was added to the solid product and this mixture was heated at 100 ^{0}C under reflux with stirring for 2 h. The suspension was filtered and dried at 100 ^{0}C. The solid product was heated in a furnace to 550 ^{0}C at a heating rate of 1 ^{0}C/min and then calcined at 550 ^{0}C for 8 h. The high temperature calcination step was necessary for detemplation and efficient removal of the (primary amine surfactant) template molecule, in order to access the pores in the following step. The yield of HMS product was approximately 2 g when using

the specified amounts of starting materials **[235, 234].** Characteristics of this material are presented in Sections 4.2 – 4.6 and Section 4.9.

3.2.3. Preparation of MCM-41

In this study the parent mesoporous SiO_2 based MCM-41 used as sacrificial template was synthesized in a similar method to that reported by Beck and coworkers **[236].**

To a mixture of distilled water (80 g), ethanol (64 g), and cetyltrimethylammonium bromide (40 g) which had been adjusted to pH = 10 with tetramethylammonium hydroxide (25 wt.% aqueous solution) and then aged at (60°C) in a water bath for 1 h, tetraethoxysilane (25 g) was added. The mixture was stirred for 48 hours at (20°C). The resulting precipitate was separated by filtration under suction, washed with distilled water, evaporated to dryness at (70 ^{0}C), followed by calcinations in air at (600°C) for 4 h to remove the template **[236 - 240].**

UNIVERSITY of the WESTERN CAPE

3.3. PREPARATION OF MESOPOROUS CARBON MATERIAL

In this study mesoporous carbon was synthesized in a similar method to that reported by Ndungu and coworkers **[241].** The procedure for the preparation of ordered mesoporous carbons (OMCs) is reviewed in Section 2.13.2 of the literature review; in this study ordered mesoporous carbons were used as adsorbents for removal of organic dyes and mercury (II) from water. The OMCs were negative replicas of OMSi (i.e. SBA-15, HMS and MCM-41) and in this study were designated as carbon analogues (CA) of the parent OMSi;

i.e. CA_SBA-15, CA_HMS and CA_MCM-41. Table 3.3, lists all the OMCs materials made form OMSi materials and the actual conditions applied.

Table 3. 3: OMC materials made from OMSi.

Ordered Mesoporous Silica template (OMSi)	Carbon Infiltration Time (min)	Carbon Infiltration Temperature (^{0} C)	Product code
HMS	80	800	CA-HMS_LPG_80
	90		CA-HMS_LPG_90
	105		CA-HMS_LPG_105
	120		CA-HMS_LPG_120
MCM-41	80	800	CA-MCM-41_LPG_80
	90		CA- MCM-41_LPG_90
	105		CA- MCM-41_LPG_105
	120		CA- MCM-41_LPG_120
SBA-15	80	800	CA-SBA-15_LPG_80
	90		CA- SBA-15_LPG_90
	105		CA- SBA-15_LPG_105
	120		CA- SBA-15_LPG_120

UNIVERSITY of the WESTERN CAPE

3.3.1. Preparation of mesoporous carbon using SBA-15

The preparation of mesoporous carbon using SBA-15 as sacrificial template was as follows:

2 g of ordered mesoporous silica (SBA-15) was loaded into a ceramic sample boat; this was then placed inside a quartz tube located in a horizontally aligned tube furnace. Once appropriately sealed, an LPG flow was initiated at 50.0 ml/min, and the furnace was ramped to 800 °C using a heating rate of 1.67 °C/min. Four different samples were prepared in this fashion with different carbonization times, after 80, 90, 105 and 120 minutes at 800 ^{0}C, the LPG flow was terminated and the furnace was cooled to ambient. Depending on the time held at 800 ^{0}C, the resulting silica/carbon composite samples were designated as SBA-15_LPG_80, SBA-15_LPG_90, SBA-15_LPG_105 and SBA-15_LPG_120. The mesoporous silica/carbon composites were each refluxed with 50.0 ml of 1.0 M NaOH (Kimix, South Africa) at 75 °C for 3.0 h, and the mixture was continuously stirred to aid in dissolving the silica template. Each silica/carbon composite product, for example, SBA-15_LPG_105 was rinsed with ultra pure water over a nylon membrane filter (0.45μm pores, Whatman), until the pH was between 7 and 8 as determined by pH paper. Finally the CA_SBA-15_LPG_80, CA_SBA-15_LPG_90, CA_SBA-15_LPG_105 and CA_SBA-15_LPG_120 products were each dried at 90 °C in an oven for 60.0 minutes. Characteristics of these materials are presented in Sections 4.2 to 4.9.

UNIVERSITY of the WESTERN CAPE

3.3.2. Preparation of mesoporous carbon using HMS

The preparation of mesoporous carbon using HMS as sacrificial template was as follows:

2 g of hexagonal mesoporous silica (HMS) was loaded into a ceramic sample boat; this was then placed inside a quartz tube located in a horizontally aligned tube furnace. Once appropriately sealed, an LPG flow was initiated at 50.0 mL/min, and the furnace was ramped to 800 °C using a heating rate of 1.67 °C/min. Four different samples were prepared in this fashion with different carbonization times, after 80, 90, 105 and 120 minutes, the LPG flow was terminated and the furnace was cooled to ambient. Depending on the time held at 800 ^{0}C, the resulting silica/carbon composite samples were designated as HMS_LPG_80, HMS_LPG_90, HMS_LPG_105 and SBA-15_LPG_120. The mesoporous silica/carbon composites were each refluxed with 50.0 ml of 1.0 M NaOH (Kimix, South Africa) at 75°C for 3.0 h, and the mixture was continuously stirred to aid in dissolving the silica template. Each silica/carbon composite product for example, HMS_LPG_80, was rinsed with ultra pure water over a nylon membrane filter (0.45 μ m pores, Whatman), until the pH was between 7 and 8 as determined by pH paper. CA_HMS_LPG_80, CA_HMS _LPG_90, CA_HMS _LPG_105 and CA_ HMS_ LPG_120 products were each dried at 90 °C in an oven for 60.0 minutes. Characteristics of these material are presented in Sections 4.2 to 4.9.

UNIVERSITY of the WESTERN CAPE

3.3.3. Preparation of mesoporous carbon MCM – 41

The preparation of mesoporous carbon using MCM-41 as sacrificial template was as follows:

2 g ordered mesoporous silica (MCM-41) was loaded into a ceramic sample boat; this was then placed inside a quartz tube located in a horizontally aligned tube furnace. Once appropriately sealed, an LPG flow was initiated at 50.0 mL/min and the furnace was ramped to 800°C using a heating rate of 1.67° C/min. Four different samples were prepared in this fashion with different carbonization times, after 80, 90, 105 and 120 minutes, the LPG flow was terminated and the furnace was cooled to ambient. Depending on the time held at 800 ^{0}C, the resulting silica/carbon composite samples were designated as MCM-41_LPG_80, MCM-41_LPG_90, MCM-41_LPG_105 and MCM-41_LPG_120. The mesoporous silica/carbon composites were each refluxed with 50.0mL of 1.0 M NaOH (Kimix, South Africa) at 75°C for 3.0 h, and the mixture was continuously stirred to aid in dissolving the silica template. Each silica/carbon composite product for example, MCM-41_LPG_80 was rinsed with ultra pure water over a nylon membrane filter (0.45μ m pores, Whatman), until the pH was between 7 and 8 as determined by pH paper. Finally the CA_MCM-41_LPG_80, CA_MCM-41_LPG_90, CA_MCM-41_LPG_105 and CA_MCM-41_LPG_120 product were each dried at 90 °C in an oven for 60.0 minutes. Characteristics of these materials are presented in Sections 4.2 to 4.9.

UNIVERSITY of the
WESTERN CAPE

3.4. MODIFICATION OF ORDERED MESOPOROUS CARBON (CA_SBA-15_LPG_105)

Modification of ordered mesoporous carbon materials as adsorbents was described in Section 2.18. Modification was done in order to increase the binding efficiency i.e. to have high uptake capacity, quantitative uptake by all ligands and to obtain low levels of remaining mercury ions (II) in solution. Modification was also done to improve the selectivity of the binding process with respect to other metal ions in solution.

Ordered mesoporous carbon (OMC) i.e. CA_SBA-15_LPG_105 synthesized from SBA-15 as described in Section 3.3.1 was used as a starting material for synthesis of modified ordered mesoporous carbon (MOMC). This CA_SBA-15_LPG_105 sample was chosen because it displayed high surface area (1800 m^2/g) and an average pore size of about 3 nm, as will be discussed in Section 4.9; these parameters indicated that this material could be suitable for future adsorption studies. Modification was done via a two step process i.e. oxidation by treatment with nitric acid and functionalisation by a grafting agent, 3- mercaptopropyltriethoxysilane (MPTES) **[193].**

UNIVERSITY of the WESTERN CAPE

3.4.1. Treatment of OMC with nitric acid

In this study acid treatment was used to increase the percentage of surface oxides of OMC derived from SBA-15 (CA_SBA-15_LPG_105). Nitric acid enhanced acidic properties and improved the hydrophilicity of CA_SBA-15_LPG_105 surface **[194].** The oxidation of OMC derived from SBA-15 (CA_SBA-15_LPG_105) was performed using reflux apparatus as indicated in Figure 3.1. Thus, 6 g of OMC (CA_SBA-15_LPG_105) was weighed and added to 200 cm^3 of 5 M HNO_3 in a 250 cm^3 round bottom flask. The mixture was heated to boiling with a heating mantle. Reflux was performed under stirring for 3 h. The modified material MOMC was washed with distilled water to neutral pH, dried in an air convection oven at 90 ^{0}C for 24 h and stored in the desiccator for later use **[242].** This nitric acid modified sample (O_ CA_SBA-15_LPG_105) was used as a starting material for grafting with 3-mercaptopropyltriethoxysilane.

UNIVERSITY of the
WESTERN CAPE

3.4.2. Functionalisation by grafting agent

3- mercaptopropyltriethoxysilane.

In this study modified ordered mesoporous carbon (MOMC) was obtained by adding 6 ml of 3-mercaptopropyltriethoxysilane to a 50 ml stirred suspension containing 5 g of nitric acid treated OMC (O__ CA_SBA-15_LPG_105), in refluxing toluene. Reflux under stirring was maintained for 24 h and special attention (see Figure 3.1) was given to protect the reaction vessel from

ambient air by placement of bent distilling adapters with silica beads. This was performed to overcome significant oxidation of thiol groups into disulfide moieties during the reaction. The silica beads in the distilling adapter were flanked on both sides with cotton wool **[244].**

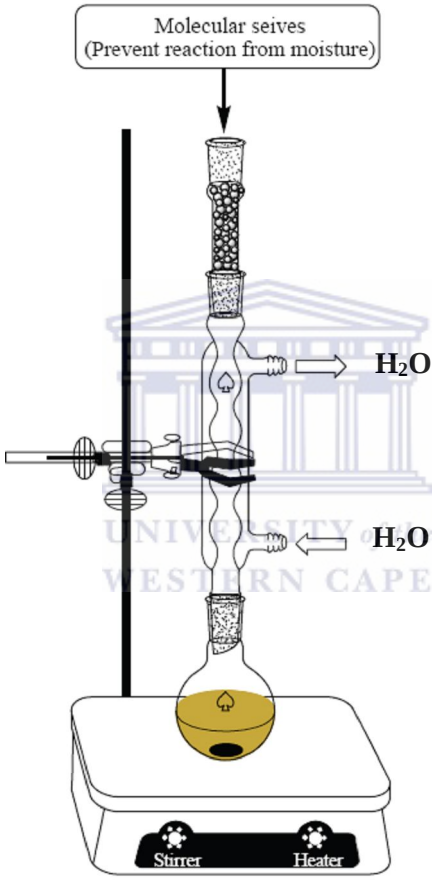

Figure 3. 1: Reflux apparatus for OMC modification **[191].**

After filtration and thorough washing with dry toluene, the grafted product (MOMC) was dried overnight under vacuum and stored in the desiccator for later use **[244].**

3.5. SPECTROPHOTOMETRIC DETERMINATION OF MERCURY (II) AS THE TERNARY COMPLEX WITH RHODAMINE 6G AND IODIDE

In this study UV-Vis spectrophotometry was used to directly measure the molar absorptivity of Hg (II) ions in solution. Complexing ligands in a form of Rhodamine 6G with tetraiodomercurate (II) were used as analyte solutions to give adequate separation and strong detection of Hg (II) ions in solution **[232].** The results using this measurement technique are given in Section 6.3 – 6.4.

The following apparatus, reagents and experimental procedure were employed for the determination of Mercury (II), as presented in adsorption experiments (see Section 3.4.1 to 3.5.4) **[232].**

UNIVERSITY of the
WESTERN CAPE

3.5.1. Apparatus and reagents

A GBC UV/Vis 920 spectrophotometer with 10 mm quartz cells was used for mercury (II) analysis. (GBC is an Australian company which was founded by Australian engineers in 1997 – Ron Grey, Ivan Barlett and Peter Charlton. They had all been previously employed by the Australian company Techtron, which was subsequently bought out by the American company, Varian Inc).

3.5.2. Preparation of Mercury (II) solution

0.3385 g of mercury(II) chloride was dissolved in deionised water and diluted to 250 ml to make a 1000 ppm solution. Appropriate volumes of this stock solution was diluted in water to provide a 5 ppm solution of mercury.

3.5.3. Preparation of buffered potassium iodide solution

5 g of potassium iodide and 5 g of potassium hydrogen phthalate were dissolved in deionised water; a few crystals of sodium thiosulphate were added. This solution was diluted to 250 ml with deionised water.

UNIVERSITY of the
WESTERN CAPE

3.5.5. Preparation Rhodamine 6G solution (0.005 %)

0.005 g of Rhodamine 6G was dissolved in deionised water and diluted to 1L with deionised water.

3.5.6. Preparation of gelatine solution

1g of gelatine was transferred to a 150 ml sealed schott bottle and 100 ml of deionised water was added. This mixture was subjected to microwave heating at 1400 Watts (three times) for 3 minutes. Within the three minutes of micro wave heating caution was taken to stop the heating when the solution boiled.

3.5.7. Procedure for the formation of rhodamine 6G with tetraiodomercurate (II) complex

Suitable aliquots (up to 11 ml) of sample solution containing not more than 25 µg of mercury were transferred to a 25 ml volumetric flask. With mixing 5 ml of buffered potassium iodide and 5 ml of the Rhodamine 6 G were added followed by 1 ml of 1 % (w/v) Gelatine solution prepared as in Section 3.5.6. The solution was diluted to the mark with deionised water and the absorbance was measured by UV-Vis in 10 mm cells at 575 nm against a reagent blank. A calibration curve 5-25 µg of mercury was prepared by the above procedure **[245].**

UNIVERSITY of the
WESTERN CAPE

3.6. ADSORPTION OF DYES AND MERCURY (II) BY ORDERD MESOPOROUS CARBON (CA_SBA-15_LPG_105) AND ACTIVATED CARBON (AC)

Three analyte dye solutions (Methylene Blue (MB), Acid Orange 8 (AO8), Rhodamine B (RB) as well as Mercury (II) were employed for adsorption studies. Dye adsorption studies were performed in order to determine the surface properties of ordered mesoporous carbon (CA_SBA-15_LPG_105). This CA_SBA-15_LPG_105 sample was chosen because it displayed high surface area (1800 m^2/g) and an average pore size of about 3 nm, as discussed in Section 4.9; these parameters indicated that this material could be suitable for future adsorption studies. The following experiments were performed for each analyte dye reagent.

UNIVERSITY of the WESTERN CAPE

3.6.1. Buffer solutions of various pH

Buffer solutions of various pH levels ranging from 2-8 were prepared by making use of 0.1 M citric acid and 0.2 M Na_2HPO_4 solutions. The citric acid solution was prepared by dissolving 21.014 g citric acid granules in a flask and diluting to the 1000 ml mark with distilled water. 0.2 M Na_2HPO_4 solution was prepared by dissolving 28.392 g Na_2HPO_4 in a beaker and diluting to the 1000 ml mark with deionized water.

Once the 0.1 M Citric acid and 0.2 M phosphate solutions were made buffer solutions of each analyte dye (MB; AO8; RB), adjusted to levels of pH between 2 – 8, were prepared as follows (see Table 3.4):

Table 3. 4: Preparation of buffer solutions of various pHs.

pH	*0.2 M Na_2HPO_4 (ml)*	*0.1 M Citric acid (ml)*
2	***2***	***98.00***
3	***20.55***	***79.45***
4	***38.55***	***61.45***
5	***51.50***	***48.50***
6	***63.15***	***36.85***
7	***82.35***	***17.65***
8	***97.25***	***2.75***

UNIVERSITY of the WESTERN CAPE

3.6.2. Preparation of 100 ppm AO8, MB and RB buffer solutions (pH 2-8).

To prepare a 100 ppm analyte using buffer solution, 50 ml of stock solution for each analyte dye was added to 1000 ml volumetric flask, then deionised water was added until the volumetric flask was ¾ full. Thereafter, the solution was transferred to a 2000 ml beaker with a magnetic stirrer. The (pH 2 citric acid – phosphate buffer solution for an example) buffer solution was added dropwise while the pH was monitored by a pH meter (Metrohm). When the desired pH was achieved, the solution was transferred back to the 1000 ml volumetric

flask and filled up to the mark with distilled water. The solution was transferred to 1000 ml plastic container and marked (pH 2 for example). The above steps were performed for all citric acid – phosphate buffer solutions (pHs 2-8) as specified in Table 3.3. Each solution after preparation was tilted 40 times to mix it thoroughly.

3.6.3. Preparation of 100 ppm Hg (II) buffer solutions (pH 2-8)

Stock mercury solution (1000 ppm) was prepared by dissolving 1.3535 g of $HgCl_2$, in about 700 ml of deionized double distilled water and 1.5 ml of concentration. HNO_3 (37 %) was added to prevent hydrolysis and made up to 1000 ml with deionized double distilled water. Working standards were prepared by progressive dilution of mercury stock solution. The initial concentration of mercury (II) stock solutions in the experiments were in the range of 20 to 100 ppm.

UNIVERSITY of the WESTERN CAPE

For mercury adsorption studies on OMC (CA_SBA-15_LPG_105), as well as preparation of 100 ppm mercury (II) buffer solutions (pH 2-8) a similar procedure as reported in Sections 3.6.1 to 3.6.2 were followed. Adsorption is a function of pH, hence at different pHs the OMC (CA_SBA-15_LPG_105) adsorbent would have different adsorption capacities for each stock solutions.

3.6.4. Batch adsorption experiments for acid orange 8 (AO8), methylene blue (MB), rhodamine B (RB) and Hg (II) solution on ordered mesoporous carbon (CA_SBA-15_LPG_105)

The adsorption capacity of ordered mesoporous carbon (CA_SBA-15_LPG_105) toward acid orange 8 (AO8), methylene blue (MB), rhodamine B (RB) and Hg (II) from solutions was evaluated by batch adsorption experiments and their performance was compared to activated carbon (AC). The batch experiments for the adsorption of each dye (AO8, MB, RB) and Hg (II)) was carried out in a 100 ml Erlenmeyer flask using a tray action shaker in a thermostated water bath to keep the temperature constant. Fixed amounts of the adsorbent (0.01 g) ordered mesoporous carbon (CA_SBA-15_LPG_105) or (0.01 g) activated carbon were respectively contacted for 24 h with 50 ml aliquots or solutions of variable initial concentrations and pH at 25 °C. The initial concentrations of (AO8, MB, RB) or Hg (II) stock solutions in the experiments were in the range of 20 to 100 ppm. Blank solutions were treated similarly without the adsorbent and the recorded concentrations at the end of each operation were taken as the initial concentration. The solutions were filtered using 1 mm Whatman filter papers. The residual dye (AO8, MB, RB) or Hg (II) concentration in solution after the desired treatment and time were measured by UV-Vis spectrophotometry according to their respective maximum wavelengths (λ max) stipulated in Table 3.6. The amount of dye (AO8, MB and RB) and Hg (II) retained (q, mg/g), and percent adsorption (% A) were calculated as shown by (Equations.3.1 to 3.4):

UNIVERSITY of the WESTERN CAPE

$$q(mg/g) = \frac{(C_o - C_f) \times V}{M} \quad (3.1)$$

$$q(meq/g) = \left[\frac{q(mg/g)}{Equavalent\ weight\ of\ M^{n+}} \right] \quad (3.2)$$

$$q(mmol/g) = \frac{(C_o - C_f) \times V}{Mr \times M} \quad (3.3)$$

$$Adsorption(\%) = \frac{(C_o - C_f)}{C_o} \times 100\% \quad (3.4)$$

where q is the amount adsorbed (mg/g) or (meq/g) or (mmol/g), C_o is the initial metal ion concentration, C_f is the final metal ion concentration (mg/L), V is the solution volume (L) M is the amount of adsorbent used (g), Equivalent weight of M^{n+} is the formulae weight divided by the charge on the metal ion, M^{n+} , and Mr is the atomic mass of the metal ion adsorbed **[246].**

UNIVERSITY of the
WESTERN CAPE

3.6.5. Effect of Adsorbent dose

Dye (AO8, MB, RB) or Hg (II) binding capacity was measured by the batch equilibration technique with varying adsorbent masses. Various dry adsorbent amounts (0.005-0.03g for OMC and AC) were contacted with 50 ml of 100 mg/L of each dye (AO8, MB, RB) and Hg (II) solution at 25 ºC for 24 h with continuous shaking. After equilibration was completed, the solution was

filtered and collected for concentration determination by UV-Vis spectrophotometry. This procedure was repeated for 100 mg/L of dye (AO8, MB, RB) or Hg (II) solution and all test samples were performed in duplicate.

3.6.6. Effect of Contact time

Contact time adsorption experiments were conducted at 25 °C in different Erlenmeyer flasks with covers. The same adsorbent amounts (0.01 g for OMC and AC) were contacted with 50 ml of 100 mg/L of each dye (AO8, MB, RB) and Hg (II) solution. The flasks were shaken for a different time intervals at constant temperature. After a prefixed time (30, 60, 90, 120 and 240 minutes) the phases were separated by filtration and the supernatant solution was filtered and collected. The residual dye (AO8, MB, RB) and Hg (II) concentrations were determined by UV-Vis spectrophotometry.

UNIVERSITY of the WESTERN CAPE

3.6.7. Effect of pH

Buffered solutions of each dye (AO8, MB, RB) or Hg (II) were prepared as described in Section 3.6.2 and 3.6.3. For the batch technique, duplicate masses of 0.01 g of the dry adsorbent (OMC or AC) were placed into a series of 100 ml Erlenmeyer flasks. The adsorbents were contacted for 24 h with 50 ml solution of each dye (AO8, MB, RB) or Hg (II) at varying pH (2 - 8) at 25 °C. The initial concentrations of (AO8, MB, RB) or Hg (II) stock solutions in the experiments were 100 mg/L. Blank solutions were treated similarly without the adsorbent and the recorded concentrations at the end of each operation were

taken as the initial concentration. The solutions were filtered using 1 mm Whatman filter papers. The residual dye (AO8, MB, RB) or Hg (II) concentration in solution after the desired treatment and time were measured by UV-Vis spectrophotometry according to their respective maximum wavelengths (λ max) stipulated in Table 3.6.

3.6.8. Equilibrium Adsorption Isotherms

Sorption isotherms were carried out in a series of 100 ml Erlenmeyer flasks. Each flask was filled with 50 ml of different concentrations of a specific analyte varying from 20 to 100 mg/L while maintaining the adsorbent dosage and temperature at constant level. After equilibration, the solution was separated and analysed. Blank solutions were treated similarly without the adsorbent and the recorded concentrations at the end of each operation were taken as the initial concentration. Each of the data sets was used to calculate the adsorption capacity, q_e, of the adsorbent. Finally the adsorption capacity was plotted against equilibrium concentration, C_e. Each experiment was carried out in duplicate under identical conditions.

UNIVERSITY of the
WESTERN CAPE

3.7. SAMPLE CHARACTERIZATION

Samples were characterized by various characterization techniques, Table 3.5 and the experimental conditions are specified in this section.

Table 3. 5: Characterization techniques used during adsorbent development.

Type	Purpose
Scanning electron microscope (SEM) & Energy dispersive X-ray (EDX)	Morphology & elemental composition
X-ray diffraction (XRD)	Crystallinity, particle size, phase identification, pore diameter
Transmission electron microscopy (TEM)	Morphology, particle size
Selective area electron diffraction (SAED)	Crystallinity and crystal symmetry
Raman spectrophotometry	Structural ordering
Thermo-gravimetric analysis (TGA)	Thermal stability
Brunauer-Emmet-Teller (N_2BET)	Surface area and pore diameter, Porosity
UV/Vis spectrophotometry	Concentration and functional groups

UNIVERSITY of the WESTERN CAPE

3.7.1. Scanning electron microscope (SEM)

Chemical composition of ordered mesopoprous silica template, ordered mesopoprous carbons and modified ordered mesopoprous carbon were obtained by electron dispersion spectroscopy (EDS) analysis which was coupled to a SEM Hitachi X650. OMSi samples were prepared by mounting some material on a double-sided conductive carbon tape. A thin (10 nm) coating of carbon was sputter coated onto the samples to reduce charging effects inside the microscope. The silica etched carbon analogue as well as silica-carbon composites material were not coated with carbon. Five analyses were conducted for each sample and an average was taken as a good representation of the elemental weight percentages of the sample.

UNIVERSITY of the
WESTERN CAPE

3.7.1.1 Sample preparation

A carbon tape was placed on top of a specimen holder and then the sample was mounted on top of the carbon tape, finally the specimen was introduced in the SEM instrument. The SEM was hyphenated with an EDS instrument coupled to a computer using GENESIS software for elemental analysis.

3.7.1.2 Instrumental setup conditions

Name of the instrument : Hitachi X 650 Scanning electron microscope

Applied voltage : 25 kV

Current : 100 µA

Illumination angle : 0.1 mrad

Magnification range : 0.35X to 1KX

Resolution : 50 µm

Working distance : 15 mm

3.7.1.3 EDS parameters

Counts per second (cps): 1500

Emission current of SEM : 100 µA

Collection time per spectrum: 100 seconds

Voltage of the SEM: 25 kV

Take off angle: 39.4 ^{0}

Dead time (DT) percent: 30 – 40 %

UNIVERSITY of the WESTERN CAPE

3.7.2. X-ray diffraction (XRD)

3.7.2.1 Sample preparation

The OMC adsorbents were each mounted in a sample holder leveled using a spatula and finally introduced in the x-ray diffractometer.

3.7.2.2 Instrumental setup conditions

Diffractometer	: Bruker AXS D8 Advance
Voltage	: 40 kV
Current	: 40 mA
Scanning range	: 2.5^{o}-90^{o} (2θ angle)
Time per step	: 29 seconds
Wavelength	: 1.54 Å (CuK_{α})
Step size	: 0.4 ^{o} (2θ angle)
Detector	: NaI

UNIVERSITY of the
WESTERN CAPE

3.7.3. High Resolution Transmission electron microscope (HRTEM)

3.7.3.1 Sample preparation

Two or three droplets of methanol were poured into sample holder, and a small amount of less than 5 mg of a sample was added and then the mixture was shaken for some time until all the nanoparticles were dispersed in the solution. One droplet of the solution was deposited on a holey carbon film supported on a copper grid and allowed to dry.

3.7.3.2 Instrumental setup conditions

Name of the instrument : Tecnai G2 F20 X-Twin MAT, 200 kV Field Emission Gun, Transmission Electron Microscope

Applied voltage : 200 kV

Emission current : 112.9 µA

Magnification : 620 K

Resolution : 5 nm

UNIVERSITY of the WESTERN CAPE

3.7.4 Selected-area electron diffraction (SAED)

Sample grids prepared for high resolution transmission electron microscopy (HRTEM) study were retained for SAED analysis. The SAED pattern was obtained using a spot analysis with a Tecnai G2 F20 HRTEM, and patterns were recorded electronically.

3.7.5. Raman spectroscopy

3.7.5.1 Experimental details.

The triple subtractive configuration of a Jobin-Yvon T64000 Raman spectrometer with a micro-Raman attachment and the 514.5 nm line of an argon ion laser were used to measure the Raman spectra of ordered mesoporous carbon (CA_SBA-15, CA_HMS and CA_MCM-41) samples synthesized from ordered mesoporous silica (SBA-15, HMS and MCM-41) parent materials. The laser diameter at the sample was approximately 1.5 micron, and the power at the sample was 1.22 mW. Spectra were

accumulated using a liquid nitrogen cooled CCD detector and the acquistion time was 240 seconds.

On sample carbon analogue (CA-HMS/LPG_90) three different spots were measured, and the laser spot was defocused by 35 micron vertically to minimize local heating.

3.7.6. Thermo-gravimetric analysis (TGA)

3.7.6.1 Sample preparation

A small amount of the sample powder was placed in quartz crucibles and introduced to the thermo-gravimatric (Rheometric scientific thermal analyzer, Q 800) furnace. The experiment was performed in an air atmosphere, whilst subjecting the sample to heating at a controlled rate.

UNIVERSITY of the WESTERN CAPE

3.7.6.2 Instrumental setup conditions

Name of the instrument	: Rheometric scientific thermal analyzer
Heating range	: 25 ^{o}C – 900 ^{o}C
Heating rate	: 5 ^{o}C/min
O_2 supply rate	: 50 ml/min

3.7.7. Brunauer-Emmett-Teller (N2BET)

Changes in the surface area, pore volume and pore size distribution of samples were determined by means of the Brunnauer-Emmet-Teller (N_2BET) technique using a Micromeritics Accelerated SA and Porosimetry (ASAP) 2010 system and nitrogen as probe gas.

3.7.7.1 Sample preparation

Approximately 20 mg of the sample was transferred and sealed in a sample tube. Samples were degassed and dried at 165 ^{0}C under vacuum. The experiment was conducted isothermally at –196 ^{0}C with a constant N_2 flow applied during analysis.

3.7.8. UV/Vis spectrophotometer

Absorbance measurements for analyte solutions were conducted in 10 mm quartz cells (Hellma) against a reagent blank. Measurements were applied at fixed wavelengths for different analyte solutions. The λ_{max} of absorbance for each analyte are represented in Table 3.6.

UNIVERSITY of the
WESTERN CAPE

Table 3. 6: Analyte solutions and corresponding maximum wavelengths.

Analyte solution	Corresponding $\lambda_{max\ (nm)}$
Ternary complex of Mercury (II) with Rhodamine 6G	575
Methylene blue	665
Acid Orange 8	490
Rhodamine B	552

3.7.9. Fourier Transform Infra Red Spectroscopy (FTIR).

Fourier Transform Infrared spectroscopy (FTIR) has been used to characterise ordered mesoporous (OMC) material and modified mesoporous materials (O_CA_SBA-15LPG_105, MOMC). This method of characterisation is very useful for identifying the different functional groups as well as to characterise acid sites. The spectral analysis from FTIR spectroscopy can be used to identify specific molecular groups that occur within the solid or crystal that has been formed e.g. Si-O bond stretching are found to be in the range 500 to 1100 cm^{-1}. About 0.05 g of this mixture was placed into an instrument disc.

3.8. CONCLUSIONS OF THE METHODOLOGY

UNIVERSITY of the
WESTERN CAPE

Characterization techniques used in this investigation included XRD, SEM, EDS, HRTEM, UV/VIS spectrophotometry, TGA, DSC and N_2BET and Raman spectrometry. The preparation methods were discussed; the selection of characterization techniques was justified in terms of a review of the properties of interest and analytical considerations; the fundamental principles of the selected characterization techniques were discussed and their operational parameters were given.

CHAPTER 4

PRODUCTION OF MESOPOROUS CARBON MATERIALS USING SBA-15, HMS AND MCM-41 MESOPOROUS SILICA TEMPLATES.

4.1. INTRODUCTION

Among the various methods used to prepare mesoporous carbons, the solid template approach is attractive because it allows control of the pore structure and morphology of the resulting carbon materials. Solid templating of mesoporous carbons is based on the pyrolysis of carbon precursors within the pore channels of mesoporous silica templates. There are two strategies by which carbon precursors may be introduced into the pore channels of mesoporous silica i.e. liquid impregnation (e.g. furfural alcohol) or chemical vapor deposition (CVD). Liquid impregnation, which is usually followed by polymerization and pyrolysis (carbonization) steps or cycles, has been extensively studied **[247].** Despite their excellent structural ordering and well-defined pore size distribution, mesoporous carbon materials obtained via sacrificial solid template approaches using liquid impregnation generally possess amorphous carbon pore walls. Mesoporous carbon materials have narrow pore size distribution and interconnected pore structures compared to mesoporous silica which have thick pore walls that are difficult to adjust **[248].**

UNIVERSITY of the WESTERN CAPE

It is therefore highly desirable to prepare mesoporous carbon materials, which have crystallinity (i.e., graphitic character) in their pore walls.

Various particle morphologies, including nanotube-like carbon and hollowsphere carbon, have been fabricated via chemical vapor deposition **[250].** Ryoo and co-workers **[251]** reported the fabrication of partially graphitic mesoporous carbon materials via an in-situ conversion of aromatic compounds into mesophase pitch within the pore channels of aluminosilicate mesoporous materials. Several heating and cooling cycles were required to obtain the graphitic mesoporous carbon materials. Pinnavaia and co-workers **[252]** employed a similar method to synthesize graphitic mesoporous carbon from aromatic hydrocarbon precursors at ambient pressures by the replication of mesostructured silica template in the presence of a catalyst. The methods reported by Ryoo and Pinnavaia required catalysts to convert the carbon precursor to mesoporous carbon. Fuertes and Alvarez **[253]** used liquid impregnation followed by carbonization of poly-vinyl chloride within the pore channels of mesoporous silica to prepare graphitic mesoporous carbons.

UNIVERSITY of the WESTERN CAPE

On the other hand, there are no reports on the synthesis of mesoporous carbon materials by gas-phase chemical vapor deposition (CVD). CVD is a well-established method for preparing porous carbon, carbon nanofibres, and carbon nanotubes **[249].** It has a number of advantages over the liquid phase impregnation method, such as high degree of pore filling and easy control over the amount of pyrolytic carbon deposited in the template pores, enabling the formation of graphitic pore walls and avoiding the formation of additional microporosity **[251].** In chemical vapor deposition, a carrier gas is used to

deliver the carbon precursors into the pore channels of the mesoporous silica template followed by thermal treatment at a target temperature to form the carbon framework by carbonization of the carbon precursor. Thermal treatment allows the polymerisation and carbonisation of the carbon precursor to occur simultaneously in the pore channels of the mesoporous silica template **[250].** In this study well-ordered mesoporous carbon materials with graphitic framework synthesised via a non catalytic CVD process using mesoporous silica materials as solid templates were the objective.

4.2. ELEMENTAL COMPOSITION BY EDS

UNIVERSITY of the WESTERN CAPE

Ordered mesoporous silica and their carbon analogues were prepared according to the synthesis routes described in Sections 3.2 and 3.3 respectively. Energy dispersive Spectroscopy (EDS) analysis was performed and provided elemental compositions in the typical OMSi as well as OMC materials of interest. The elemental compositions of ordered mesoporous silica SBA-15, HMS and MCM-41 used as templates as well as the formed carbon analogues CA_SBA-15_LPG_105, CA_HMS_LPG_80 and CA_MCM-41_LPG_80 are shown in Figure 4.1. The resultant carbon analogues were obtained by etching the silica carbon composite with NaOH as described in Section 3.3.

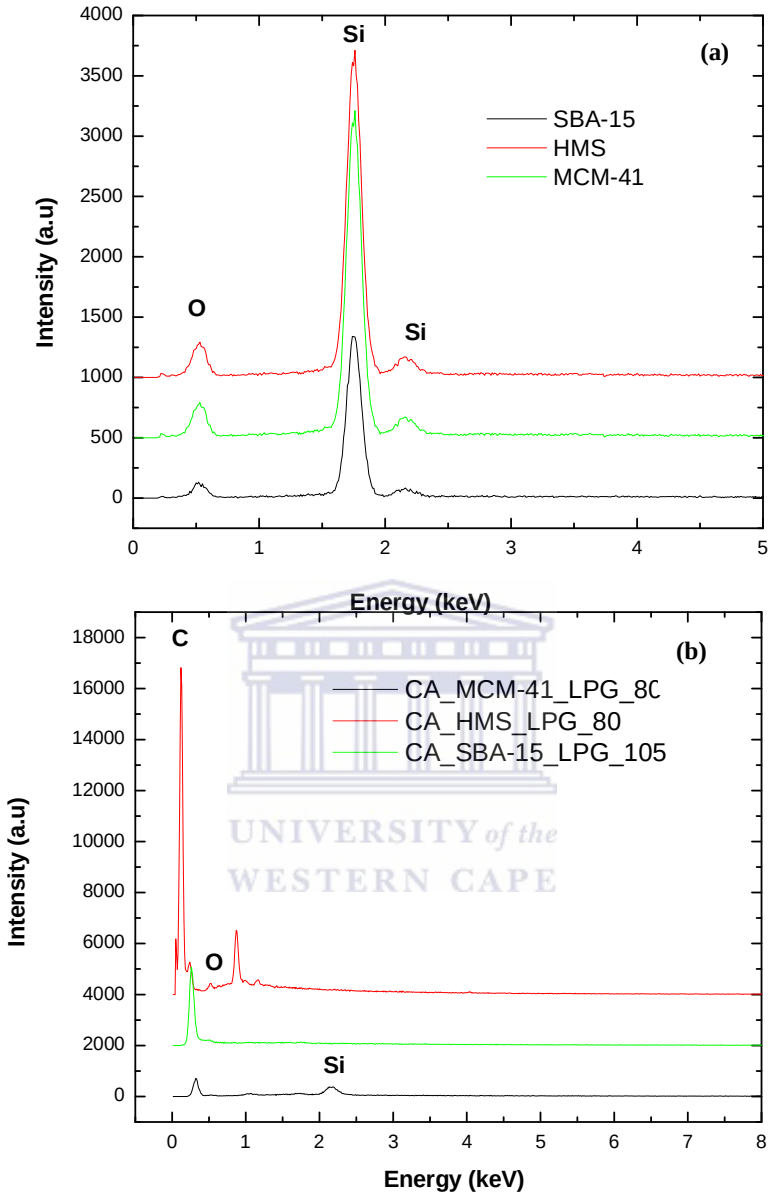

UNIVERSITY of the WESTERN CAPE

Figure 4. 1: EDS spectra of (a) Si templates SBA-15, HMS and MCM-41 and (b) CA_SBA-15_LPG_105, CA_HMS_LPG_80, CA_MCM-41_LPG_80, where 80 and 105 are optimum times of LPG pyrolysis.

Table 4. 1: Elemental composition of selected ordered mesoporous silica templates and ordered mesoporous carbon

Sample	Wt% Si	Wt% O	Wt% C
SBA-15	65.11	34.89	0.00
CA_SBA-15_LPG_105	0.69	17.13	82.18
HMS	63.54	36.46	0.00
CA_HMS_LPG_80	4.31	13.76	81.93
MCM-41	61.78	38.22	0.00
CA_MCM-41_LPG_80	5.35	26.20	68.45

UNIVERSITY of the
WESTERN CAPE

Quantitative analysis of the selected ordered mesoporous silica SBA-15, HMS, MCM-41 and the carbon analogues CA_SBA-15_LPG_105, CA_HMS_LPG_80, CA_MCM-41_LPG_80 were obtained using the GENESIS software and are presented in Table 4.1. The EDS analysis in Figure 4.1 and Table 4.1, reveal that SBA-15, HMS, MCM-41 are composed of Silicon (Si) and Oxygen (O). No carbon peaks were detected in the parent SiO_2 based detemplated SBA-15, HMS, MCM-41 used as sacrificial templates. After dissolution of the silica wall in the silica carbon composite when the carbon analogues are formed; there was a significant decrease in the silica weight percentage down to 0.69, 4.31 and 5.35 % for CA_SBA-15_LPG_105, CA_HMS_LPG_80, CA_MCM-41_LPG_80 respectively. A significant increase

in the weight percentage of carbon to 82.18, 81.93, and 68.45 % was respectively noted for CA_SBA-15_LPG_105, CA_HMS_LPG_80, CA_MCM-41_LPG_80. The EDS results represented in Figure 4.1 and Table 4.1 complimented the TGA data presented in Figure 4. 9 and clearly showed that the weight percentage of carbon in the resultant OMC materials ranged from 68 % to 82 %. The distinct peak at low energy which is due to the Kα fluorescence x-rays of carbon at 0.277 keV was observed for all the OMCs. Small peaks at Kα = 0.9 and 2.10 keV for CA_HMS_LPG_80, CA_M-41_LPG_80 respectively were observed and are due to Silicon. A peak due to Si (wt % 0.69) was not clearly visible in Figure 4.1 for the CA_SBA-15_LPG_105 but was observed during quantitative analysis (Table 4.1). This indicates that a small concentration of the silica template material is still present in the resultant carbon material, and was not completely dissolved during template etching with NaOH solution **[254].**

UNIVERSITY of the WESTERN CAPE

4.3. SCANNING ELECTRON MICROSCOPY (SEM)

This section presents morphological characterisation of ordered mesoporous silica (OMSi) templates as well as their respective carbon (OMC) analogues. Scanning electron microscopy was used to determine surface morphology of OMSi and their respective OMCs and the methodology for characterisation is described in Section 3.7.1. Ordered mesoporous silica and the carbon analogue were successfully prepared according to the synthesis routes

described in Sections 3.2 and 3.3 respectively. Amongst the series of carbon analogues of SBA-15, HMS and MCM-41 presented in Table 4.1, the products which had the highest surface area were chosen for characterisation by SEM. These selected carbon analogues are as follows: CA_SBA-15_LPG_105, CA_HMS_LPG_80 and CA_MCM-41_LPG_80.

Figures 4.2 shows the SEM micrographs of parent mesoporous silica templates used before carbon infiltration using CVD and carbon analogues after removal of the silica based templates. It can be seen in Figure 4.2 (a, b) that the HMS consisted of small crystallites < 1µm, whereas its carbon analogue was composed of agglomerated particles too small to resolve at the selected magnification. In Figure 4.2 (c, d) the SBA-15 template was composed of large globular particles as reported by Katiyar and co-workers **[255],** whereas its carbon analogue was composed of small particles smaller than 200 nm. In Figure 4.2 (e, f), the micrographs of MCM-41 silica and its carbon analogue (CA_MCM-41_LPG_80) composed of particles of about 5µm and its carbon analogue had a similar morphology as shown

UNIVERSITY of the
WESTERN CAPE

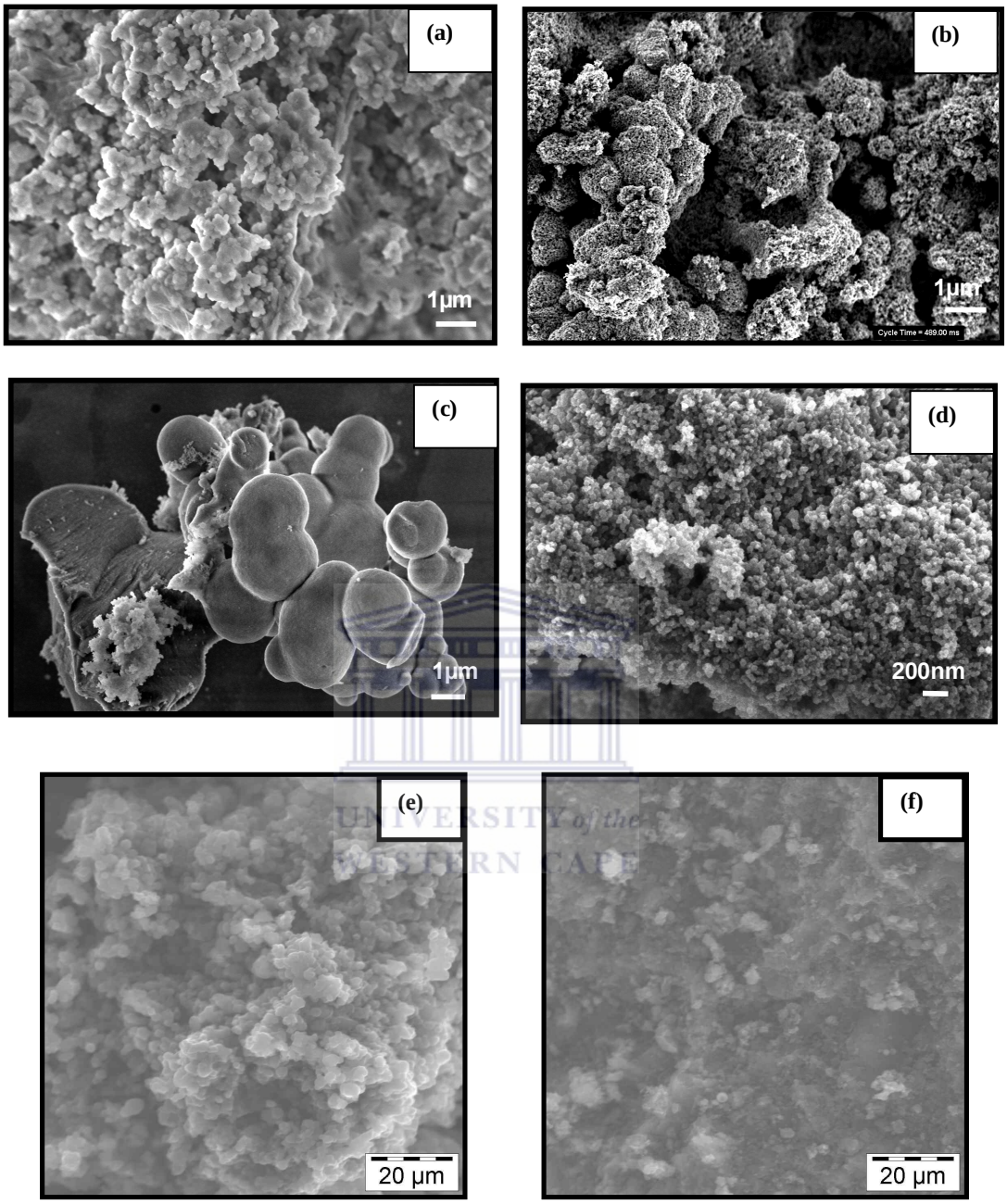

Figure 4. 2: SEM micrographs (a) HMS, (b) CA_HMS_LPG_80, (c) SBA-15, (d) CA_SBA-15_LPG_105, (e) MCM-41 and (f) CA_MCM-41_LPG_80.

UNIVERSITY of the WESTERN CAPE

Although a systematic transformation of structure occurred during the removal of silica framework as revealed by its change in the powder XRD patterns obtained during the framework removal as in Figure 4.6(a), the electron microscopy technique revealed that the template synthesis followed a replication process for the structure of the mesoporous silica. Nevertheless, the corresponding spherical particles are reduced due to the shrinkage of the silica template. Mbileni and coworkers **[254]** reported that the mesoporous carbons are smaller than their parent template (MCM-48) after dissolution of the silica template**.**

4.4. HIGH RESOLUTION TRANSMISSION ELECTRON MICROSCOPY (HR-TEM)

UNIVERSITY of the
WESTERN CAPE

This section presents characterisation of carbon (OMC) analogues by HRTEM. High resolution electron microscopy was used to determine morphology of OMCs and the methodology for characterisation is described in Section 2.19.3. Ordered mesoporous silicas and the carbon analogue were successfully prepared according to the synthesis routes described in Sections 3.2 and 3.3 respectively. Amongst the series of carbon analogues of SBA-15, HMS and MCM-41 presented in Table 4.1, the product which had the highest surface area were chosen for characterisation by HRTEM. These carbon analogues are as follows: CA_SBA-15_LPG_105, CA_HMS_LPG_80 and CA_MCM-41_LPG_80.

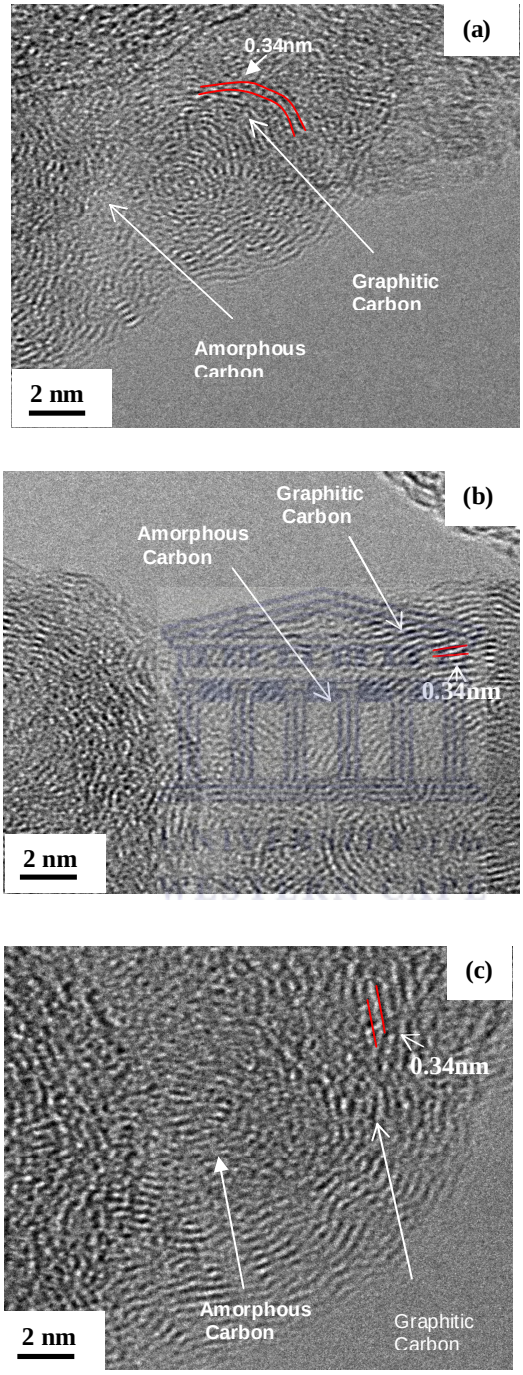

Figure 4. 3: HRTEM of (a) CA-SBA-15_LPG_105, (b) CA_HMS_LPG_80 and (c) CA_MCM-41_LPG_80

Figure 4.3 (a-c) displays HR-TEM images of CA_SBA-15_LPG_105, CA_HMS_LPG_80 and CA_MCM-41_LPG_80 obtained by LPG pyrolysis at 800 ^{0}C. The formation of ribbon-like structures identified in these materials (Figure 4.3) indicates the graphitic nature of the carbon. Small domains of graphitic carbon with lattice spacing of ~0.34 nm (Figure 4.3) are well observed as further confirmed by XRD results in Section 4.6 which shows that OMCs have lattice spacing of 0.38 nm. Thus, the OMCs prepared in this work display ordered porosity and partially graphitic structures. Some disordered structures of amorphous carbon have been identified. Su and co-workers **[256]** reported that the structural ordering of the resultant carbons produced from pyrolysis of the carbon precursors during high temperature carbonisation often lead to the emission of a large amount of small molecules such as water, which can deteriorate the pore structure of the templates hence resulting in amorphous carbon formation.

UNIVERSITY of the
WESTERN CAPE

4.5. SELECTED AREA ELECTRON DIFFRACTION (SAED)

This section presents characterisation of ordered mesoporous silica (OMSi) templates as well as their respective carbon (OMC) analogues. Selected area electron diffraction was used to determine crystallinity of OMCs and the methodology for characterisation is described in Section 3.7.4. Ordered mesoporous silicas and the carbon analogue were successfully prepared according to the synthesis routes described in Sections 3.2 and 3.3 respectively. Amongst the series of carbon analogues of SBA-15, HMS and MCM-41 presented in Table 4.1, the product which had the highest surface

area were chosen for characterisation by SAED. These carbon analogues are as follows: CA_SBA-15_LPG_105, CA_HMS_LPG_80 and CA_MCM-41_LPG_80.

The graphitic structural ordering of the carbon framework was evident in Figure 4.4 (a-f) which depicts the comparison of selected area electron diffraction (SAED) pattern of the silica parent versus the carbon analogue for each case. SBA-15, HMS, MCM-41 (mesoporous Si template) show only diffuse rings indicating a lack of crystalline pore walls ordering **[257],** whereas, CA_SBA-15LPG_105, CA_HMS/LPG_80 and CA_MCM-41_LPG_80 show graphitic structural ordering consistent with the XRD that is presented section 4.5 and in Figure 4.6. The SAED pattern of the mesoporous carbon depicts several diffraction rings that are characteristic of graphitic [000, 002 and 101] ordering.

UNIVERSITY of the
WESTERN CAPE

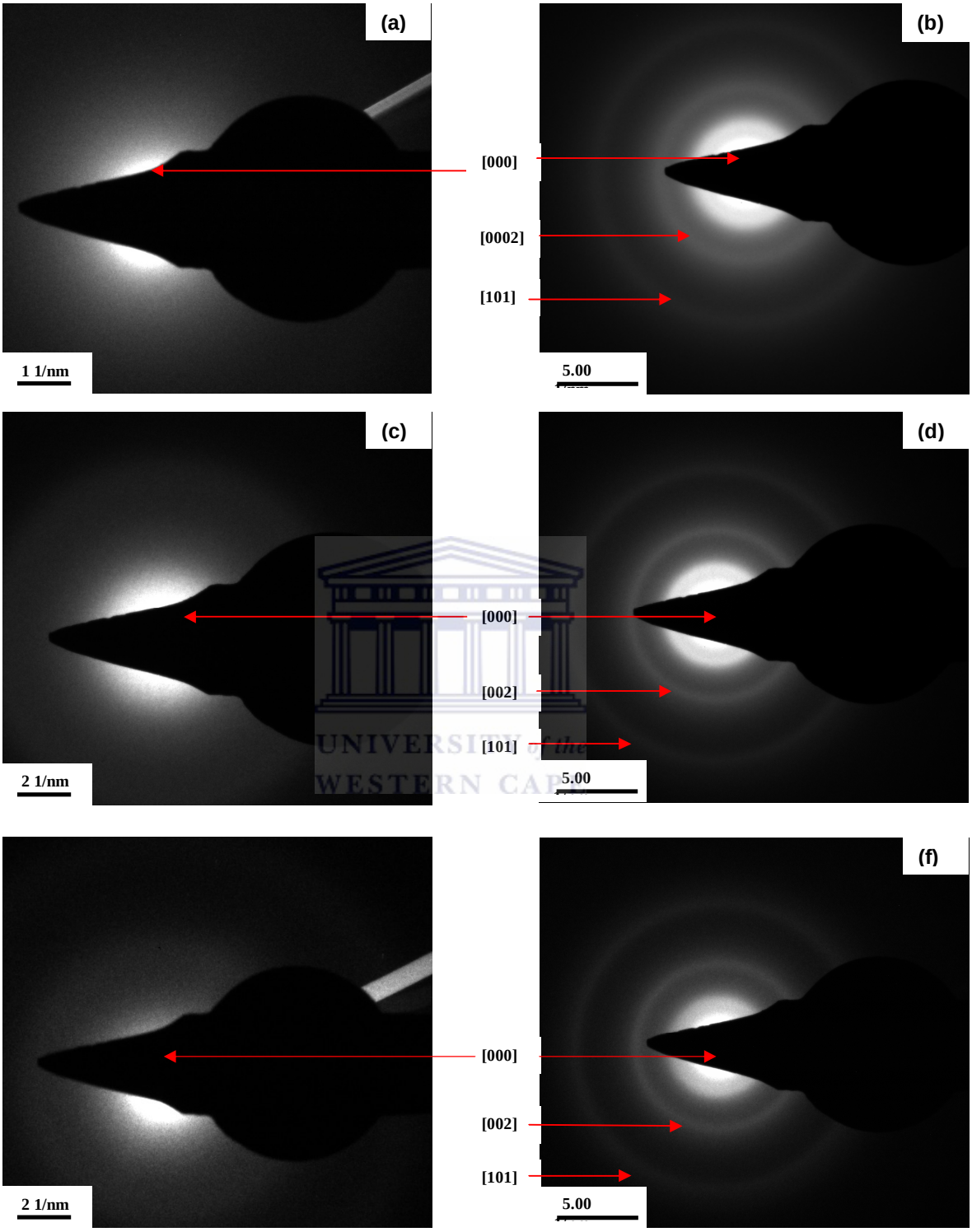

Figure 4. 4: Selective Area diffraction of (a) SBA-15, (b) CA_SBA-15_LPG_105 (c) HMS; (d) CA_HMS_LPG_80; (e) MCM-41 (f) CA_MCM-41_LPG_80

The SAED patterns confirm the graphitic crystallinity which is apparent in the XRD patterns (Figure 4.6(a-b)) and provide further evidence of the existence of some degree of graphitisation in the pore walls of the carbon analogues (CA_SBA-15_LPG_105, CA_HMS/LPG_80 and CA_MCM-41_LPG_80), obtained via a CVD process **[257].**

4.6. ELECTRON ENERGY LOSS SPECTROSCOPY (EELS)

This section presents characterisation of carbon (OMC) analogues. Electron energy loss spectroscopy was used to determine the graphitic nature of OMCs and the methodology for characterisation is described in Section 2.19.3. Ordered mesoporous silicas and the carbon analogue were successfully prepared according to the synthesis routes described in Sections 3.2 and 3.3 respectively. Amongst the series of carbon analogues of SBA-15, HMS and MCM-41 presented in Table 3.3 , the product which had the highest surface area were chosen for characterisation by EELS. These carbon analogues are as follows: CA_SBA-15_LPG_105, CA_HMS_LPG_80 and CA_MCM-41_LPG_80.

Figure 4.5 (a), (b) and (c) depict EELS spectra of OMCs synthesised from SBA-15, HMS and MCM-41 respectively. For each the carbon analogues, CA_SBA-15_LPG_105, CA_HMS_LPG_80 and CA_MCM-41_LPG_80.

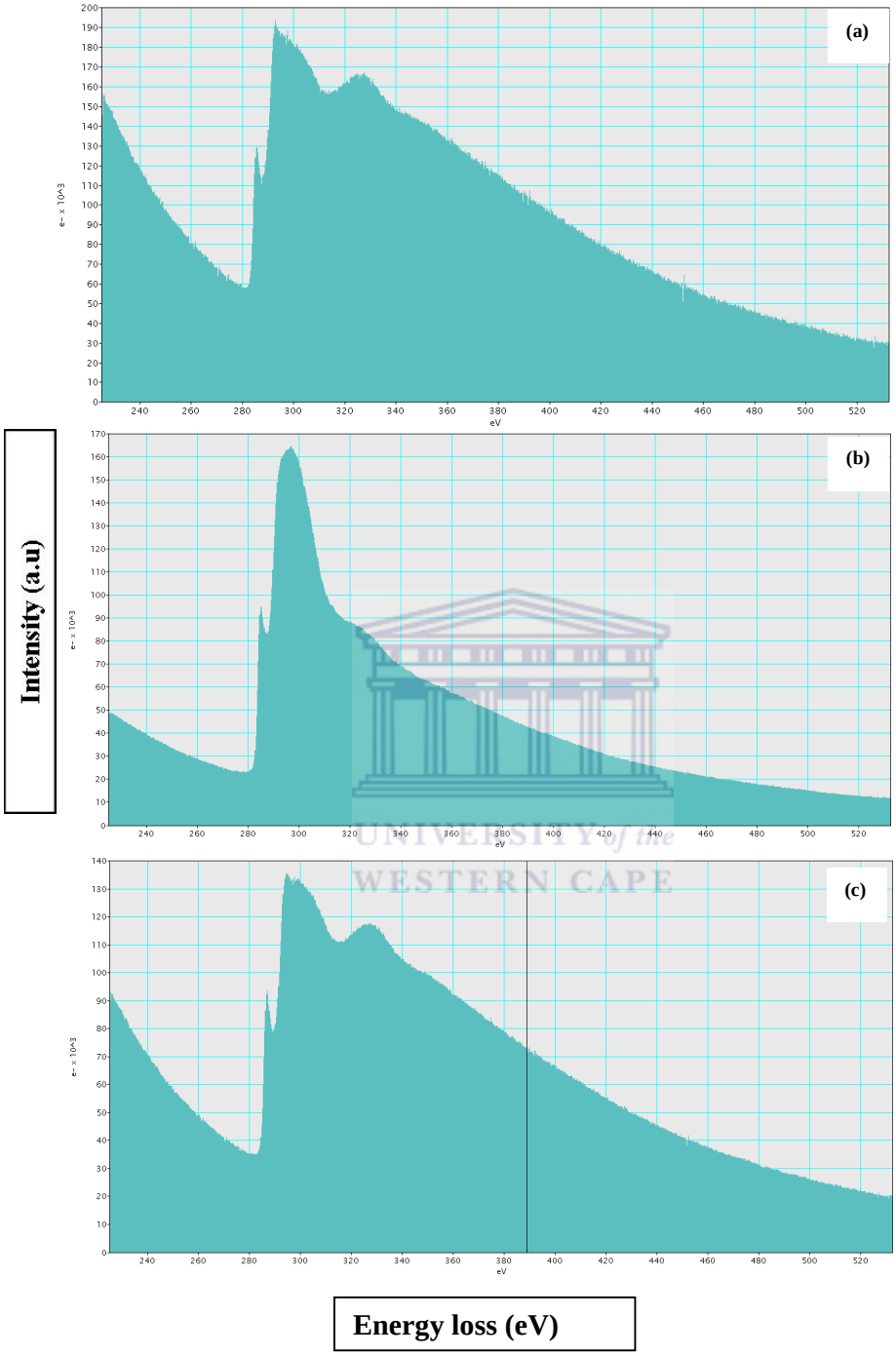

Figure 4. 5: EELS spectra of (a) CA_SBA-15_LPG_105, (b) CA_HMS_LPG_80 and (c) CA_MCM-41_LPG_80

UNIVERSITY of the WESTERN CAPE

The presence of a sharp peak at 285 eV in EELS studies of the pyrolysed OMCs in Figure 4.5 (a), (b) and (c) suggest that the carbon materials obtained as results are graphitic in nature.

The electron diffraction patterns showed reflections corresponding to the distance 0.34 nm as normally observed with graphite.

Thus comparing these results with those of literature **[258]**, it can be concluded that the detected peak in all the carbon analogues (CA_SBA-15_LPG_105, CA_HMS_LPG_80 and CA_MCM-41_LPG_80) originates from the graphitic nature of the carbon material.

4.7. STRUCTURAL CHARACTERIZATION BY XRD

UNIVERSITY of the

This section presents characterisation of ordered mesoporous silica (OMSi) templates as well as their respective ordered mesoporous carbon (OMC) analogues X-ray diffraction (XRD). X-ray diffraction was used to determine crystallinity and graphitic character of OMCs. Moreover, low angle XRD was used to determine mesoporosity of OMSi and OMCs. The methodology for XRD is described in Section 3.7.2. Ordered mesoporous silicas and the carbon analogue were successfully prepared according to the synthesis routes described in Sections 3.2 and 3.3 respectively. Amongst the series of carbon analogues of SBA-15, HMS and MCM-41 presented in Table 4.1, the products which had the highest surface area were chosen for characterization by XRD. These selected carbon analogues are as follows: CA_SBA-

15_LPG_105, CA_HMS_LPG_80 and CA_MCM-41_LPG_80. In Figure 4.6 (a) and (b) the XRD patterns of mesoporous silica templates (SBA-15, HMS, MCM-41) and carbon analogues (CA_SBA-15_LPG_105, CA_HMS_LPG_80 and CA_MCM-41_LPG_80) scanned at high angle between 10 – 120 ^{0} 2 θ are shown.

UNIVERSITY of the
WESTERN CAPE

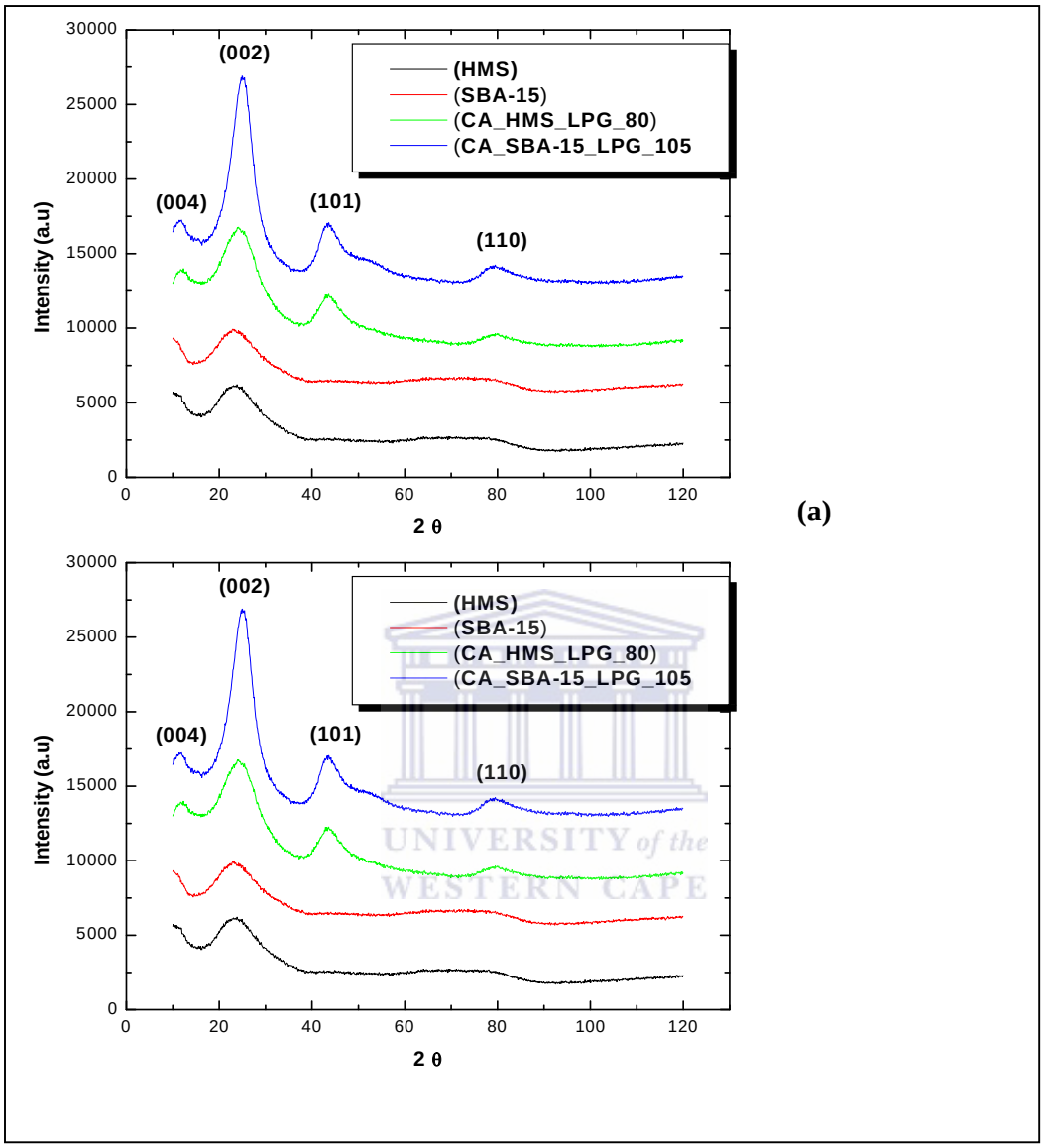

Figure 4. 6: (a) High angle XRD patterns for mesoporous silica SBA-15, HMS and its carbon analogue CA_SBA-15_LPG_105, CA_HMS_LPG_80

UNIVERSITY of the WESTERN CAPE

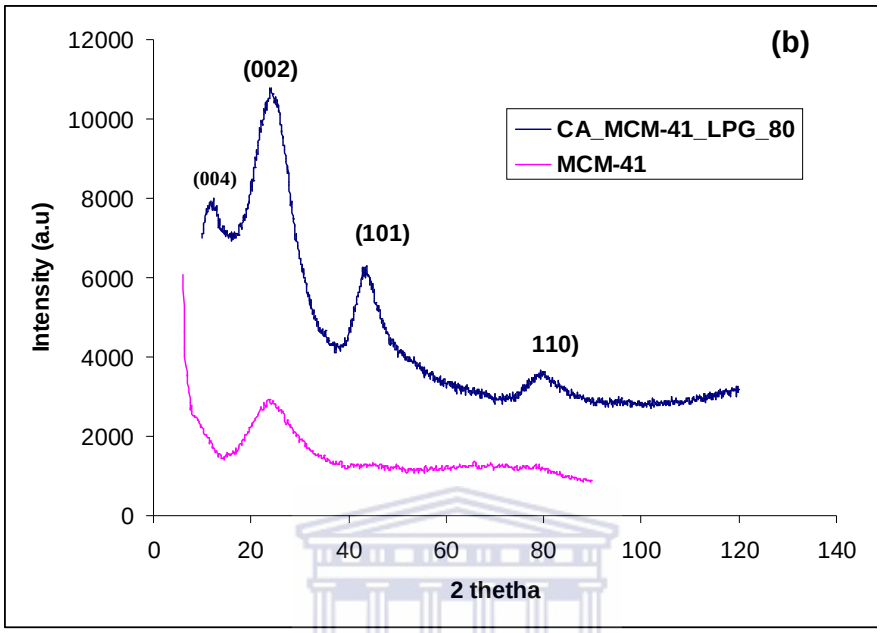

Figure 4. 7: (b) High angle XRD patterns for mesoporous silica MCM-41 compared with its carbon analogue CA_MCM-41_LPG_80 .

The wide angle XRD of the mesoporous silica templates (SBA-15, HMS, and MCM-41) as well as corresponding carbon analogues, show broad peaks at about 23^0 2θ (Figure 4.6 (a) and (b)) but are devoid of any other characteristic sharp peaks at relatively high angles, which is typical for these materials as described by L.F. Petrik. Z.G. Godongwana and P. Ndungu **[259-270].** OMC also had well defined XRD peaks at 2θ values of 7.39^0 2θ, 25.3^0 2θ and 43.5^0 2θ. The 2θ values of peaks appearing at 25.3^0 and 43.5^0 are ascribed to the (002) and (101) diffraction peaks of graphitic carbon in the OMC pore walls. The d002 spacing obtained from the (002) peak is 3.38 Å, which is very close

to the d spacing of ideal graphite (with d002 = 3.35 Å). The peak d spacing of 11.6 which corresponds to the 2θ value of 7.39 ^{0} has been observed previously by L. Petrik. Z. G. Godongwana and P.Ndungu for the periodic structure of OMC from HMS template **[257].** Similar results have been observed for OMC's samples synthesised by LPG pyrolysis from SBA-15 and MCM-41 templates. This is a novel finding and had not been reported elsewhere. The 7.39 ^{0} 2θ peak is attributed to C (004). The peak at an angle of 7.39 ^{0} is a further indication of an ordered graphitic carbon framework appearing at periodic intervals. Hence, the OMC materials have XRD definable periodic pores and pore walls containing graphitic carbon. These peaks indicate that the OMC pore walls formed by carbon deposition in the pores of the parent Si templates during infiltration of LPG in the CVD treatment at 800 ^{0}C, were mostly converted thermally to graphitic carbon.

UNIVERSITY of the
WESTERN CAPE

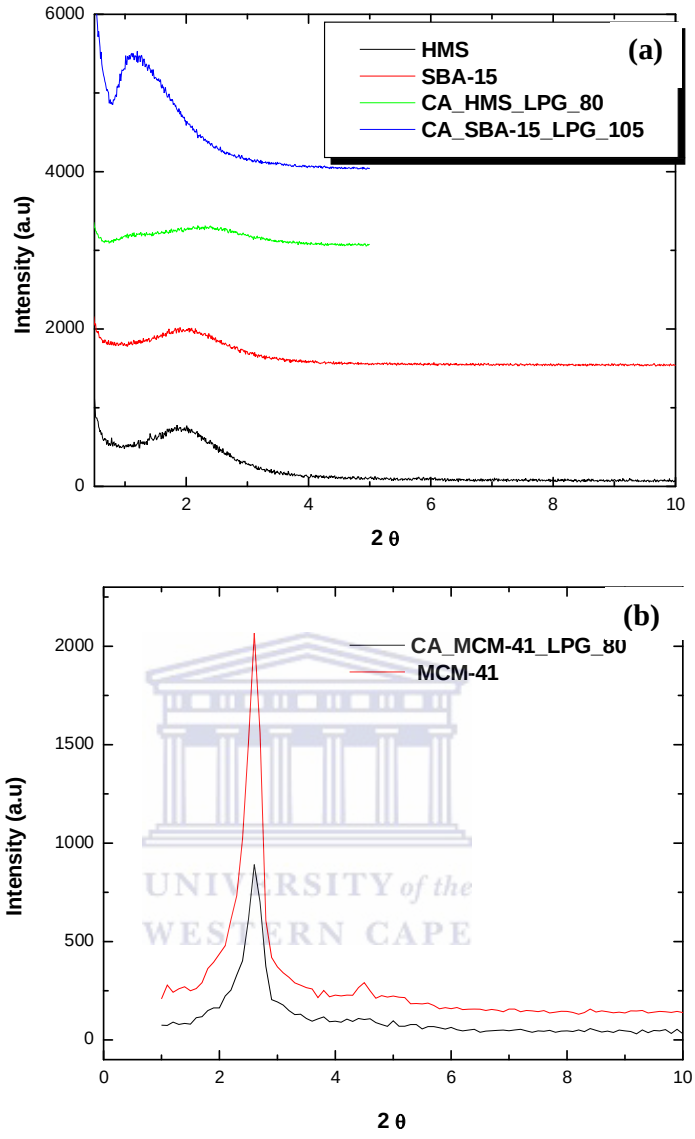

Figure 4. 8: a) Low angle XRD patterns for mesopoures silica SBA-15, HMS and its carbon analogue CA_SBA- 15_LPG_105, CA_HMS_LPG_80; (b) XRD for MCM-41 and its carbon analogue CA_MCM-41_LPG_80

Peaks between 0 ^{0} and 5 ^{0} 2θ were observed for parent silica templates as well as carbon analogues during low angle XRD scans done between 2θ

values of 0.50^0 and 9.9^0 2θ. Generally, all samples exhibited a prominent low angle peak in the diffraction pattern at approximately 2θ = 2 ^{0}, which indicates the presence of uniformly sized pores for ordered materials **[271].** The most intense peak was arbitrarily assigned as the d_{100} peak. The low angle XRD peaks, Figure 4.6 (a-b) for the silica template (1.57 ^{0} 2θ) and the OMC (1.83 ^{0} 2θ), are a typical feature of mesoporous materials with pores in the nanometre region. The low angle XRD patterns with peaks at 2.0 ^{0} 2θ for both SBA-15 and HMS but 2.4^0 2θ for MCM-41 is indicative of an average pore–pore correlation distance with d spacing of 0.27 Å for both SBA-15 and HMS but 0.32 Å for MCM-41. The low angle XRD peaks at 1.83 ^{0} 2θ for CA_SBA-15_LPG_105 and 2.4 ^{0} 2θ for both CA_HMS_LPG_80 and CA_MCM-41_LPG_80 are indicative of average pore–pore correlation distances with d spacing of 0.24 Å for CA_SBA-15_LPG_105 and 0.32 Å for both HMS_LPG_80 and CA_MCM-41_LPG_80. The OMCs pore organization is suggested to be an inverse analogue of OMSi materials **[259 - 270].** Because the pore walls of OMCs were created by carbon deposition in the pores of OMSi materials, the pore–pore distances of OMCs reflect similar dimensions as the OMSi template pore wall. Similar results were obtained by Ryoo et al **[145]** when they synthesized OMCs, CMK-1 from MCM-41 and MCM-48 templates by employing sucrose and furfuryl alcohol as carbon precursors **[145, 147].**

UNIVERSITY of the WESTERN CAPE

4.8. STRUCTURAL CHARACTERISATION BY RAMAN SPECTROSCOPY

This section presents characterisation of ordered mesoporous carbon (OMC) materials synthesized from ordered mesoporous silica (OMSi) as sacrificial templates. Raman spectroscopy was used to determine the graphitic nature of OMCs and the methodology for characterisation is described in Section 3.7.5. Ordered mesoporous silicas and the carbon analogue were prepared according to the synthesis routes described in Sections 3.2 and 3.3 respectively.

UNIVERSITY of the
WESTERN CAPE

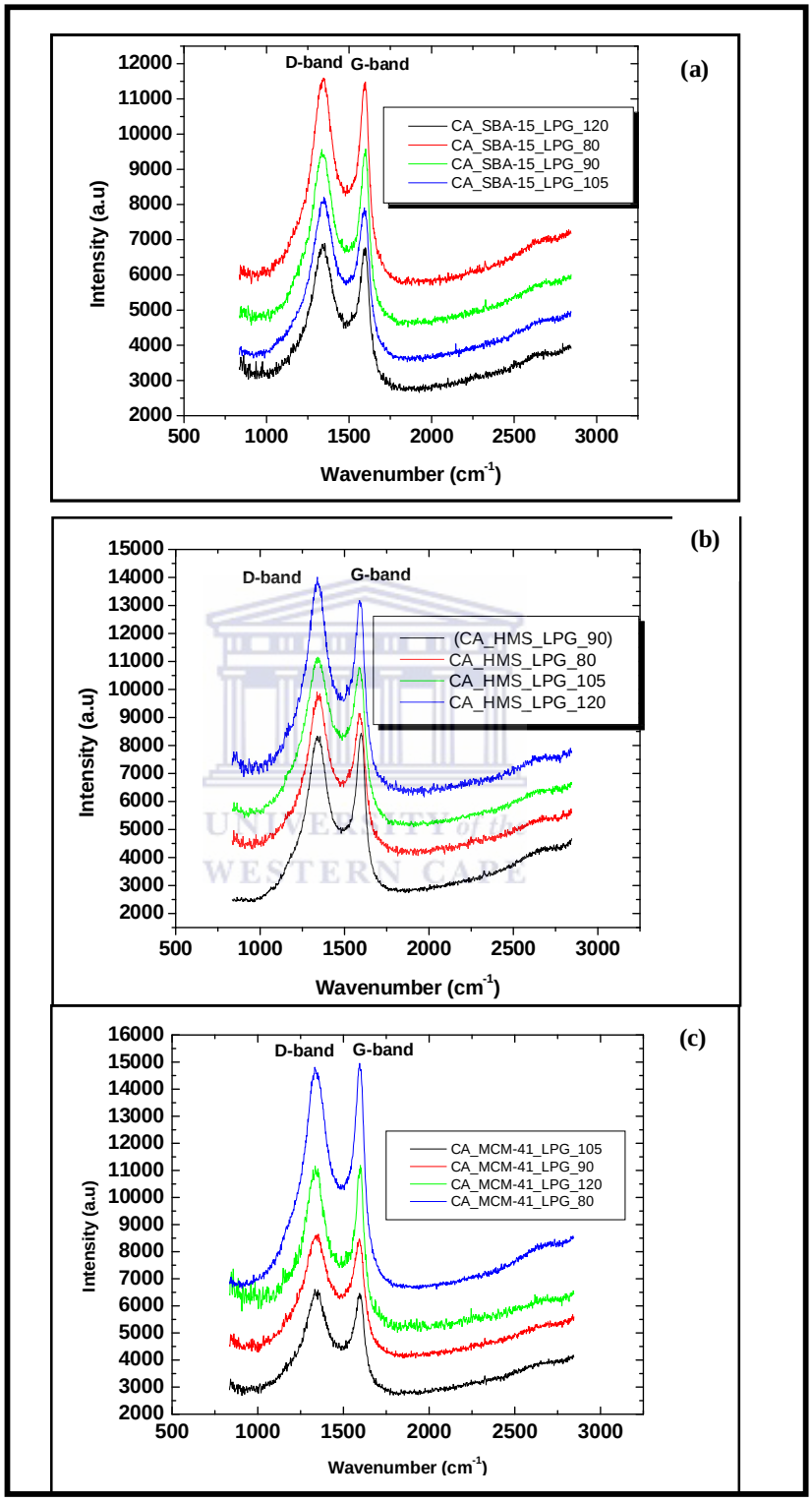

Figure 4. 9: Raman spectra of the carbon analogues (a) CA_SBA-15_LPG_105, (b) CA_HMS_LPG_80, (c) CA_MCM-41_LPG_80

Amongst the series of carbon analogues of SBA-15, HMS and MCM-41 presented in Table 4.1, the products which had the highest surface area were chosen for Raman spectroscopy characterization. These selected carbon analogues are as follows: CA_SBA-15_LPG_105, CA_HMS_LPG_80 and CA_MCM-41_LPG_80.

The Raman spectra shown in Figures 4.8 (a), (b) and (c) were fitted using a pseudo-Voigt function to extract the peak parameters of the G- and D-bands. Four peaks were fitted to each spectrum as this yielded the best fit of the experimental data. In addition to the G-band (around 1595 cm^{-1}) and the D-band (around 1342cm^{-1}), there is a broad band with centre ranging from 1200 cm^{-1} to 1240 cm^{-1} for the different samples, as well as a broad band centered around 1530 cm^{-1}. The G-band is indicative of sp^2-hybridised carbon and it corresponds to the graphitic lattice vibration mode with E2g symmetry (vibration of sp^2-bonded carbon atoms in a 2-D hexagonal lattice, i.e. the stretching modes of C=C bonds in typical graphite). The band around 1350 cm^{-1} (D-band) originates from disorder and defects present in the carbon structure. The disorder and defects are associated with vibrations of carbon atoms with dangling bonds in plane terminations, as well as other defects. As mentioned above, it is possible to estimate the degree of crystallinity (or degree of graphitization) from the peak position of the G-band, the ID/IG intensity ratio and the Full Width at Half Maximum (FWHM) of the G-band. The parameters for graphite are e.g. 1585 cm^{-1}, ID/IG = 0.1 to 0.3 and FWHM = 20 cm^{-1} **[275].** In poorly ordered carbon-based materials these values are ~1535 cm^{-1}, ID/IG ~ 1 to 2.6 and FWHM > 100 cm^{-1}. In some cases the G-

UNIVERSITY of the WESTERN CAPE

band position moves to values larger than 1585 cm^{-1}, which also indicates imperfections in the graphitic sheets **[276].** Since the absolute values of the intensities of the fitted peaks depend on parameters such as the smoothness of the sample surface and the instrument that was used to obtain the spectra, the ratio of the intensities of the G- and D-bands is used to overcome this problem.

In the literature there is still some debate as to the origins of some of the Raman peaks of carbon, but the broad band around 1530 cm^{-1} is often attributed to amorphous carbon, and the band around 1215 cm^{-1} is attributed to sp^3 bonds or C-C and C=C stretching vibrations of polyene-like structures. The latter band has also been attributed to the C-O stretch of C-O-H surface groups **[272].**

UNIVERSITY of the
WESTERN CAPE

The Raman spectra of the carbon analogues synthesised using MCM-41, HMS and SBA-15 templates are similar. The ID/IG ratio for CA_MCM-41 series ranges from 1.05 to 1.35, the G-band position varies from 1593 cm^{-1} to 1597 cm^{-1}, and the G-band FWHM ranges from 55 cm^{-1} to 64 cm^{-1}. The ID/IG ratio for CA_HMS series ranges from 1.39 to 1.60, the G-band position varies from 1593 cm^{-1} to 1598 cm^{-1}, and the G-band FWHM ranges from 55 cm^{-1} to 61 cm^{-1}. The ID/IG ratio for CA_SBA-15 series ranges from 1.22 to 1.37, the G-band position varies from 1594 cm^{-1} to 1597 cm^{-1} and the G-band FWHM varies from 55 cm^{-1} to 61 cm^{-1}.

In terms of the pyrolysis time, there is no clear trend in terms of the parameters given above. It is observed that the ID/IG ratio is largest for 105 minutes for CA_MCM41 and CA_HMS series, while for CA_SBA-15 series the ratio value is 1.37 for 80, 90 and 105 minutes, decreasing to 1.22 for 120 minutes.

Ferrari et al **[277]** describes a so-called amorphisation trajectory, which combines the value of the ID/IG ratio and the G-band position to indicate the predominant structure of the carbon-based material being analysed. Comparing the above data with Ferrari et. al, shows that all the samples are equivalent to nano-crystalline graphite in structure. This is consistent with the FWHM values quoted, as the peak width values are larger than for pure graphite, but much less than the >100 cm^{-1} values associated with poorly ordered carbon-based materials.

UNIVERSITY of the
WESTERN CAPE

Although there is no clear trend in the peak parameter values linked with pyrolysis time, the trend indicates the least ordered structure is obtained for a pyrolysis time of 105 minutes for CA_MCM41 and CA_HMS series, while for CA_SBA-15 series the pyrolysis time has little influence, with a slightly more ordered structure obtained for 120 minutes pyrolysis time.

The ID/IG ratio values and the G-band position values can be used to rank the structural order or crystallinity of the carbon analogues synthesised with the different templates. The HMS template yielded the least ordered structure

(largest ID/IG values), while SBA-15 yielded a more ordered structure, with MCM-41 giving the most ordered structure (smallest ID/IG values).

The D band might be due to the presence of a new mesostructural ordering of the pore walls as is shown by the low angle peaks visible in the XRD spectrum in Sections 4.6, Figure 4.7(a–b) which are consistent with the presence of graphene sheets within the pore walls of the carbon analogues **[278].**

4.9. STRUCTURAL CHARACTERIZATION BY THERMOGRAVIMETRIC ANALYSIS

UNIVERSITY of the
WESTERN CAPE

This section presents characterisation of ordered mesoporous silica (OMSi) templates as well as their respective carbon (OMC) analogues. Thermogravimetric analysis was used to determine thermal stability and graphitic nature of OMCs and the methodology for characterization is described in Section 3.7.6. Carbon analogue of OMSi templates were prepared according to the synthesis routes described in Sections 3.2 and 3.3 respectively. Amongst the series of carbon analogues of SBA-15, HMS and MCM-41 presented in Table 3.3, the product which had the highest surface area were chosen for characterisation by thermogravimetric analysis. These selected carbon analogues are as follows: CA_SBA-15_LPG_105, CA_HMS_LPG_80 and CA_MCM-41_LPG_80. The presence of a degree of graphitic carbon within the pore walls is further supported by

thermogravimetric analysis, when the sample was slowly heated in air as specified in Section 3.7.6. The weight loss curves thus obtained are represented in Figure 4.9 for carbon analogues. Thermogravimetric weight changes were recorded under a nitrogen atmosphere and were used to determine the carbon and the silica contents in the mesoporous carbon materials. The weight loss at temperatures below 100 ^{o}C amounted to 2 – 5 % and can be related primarily to the thermo-desorption of physisorbed water for all samples. A further weight loss was not observed with all the OMC materials indicating that more than 90 % carbon was formed in the material. A weight loss of approximately 15 % was centered at 400 ^{o}C for the CA_SBA-15LPG_105 and CA_HMS_LPG_80, which can be attributed to the decomposition of SiO_2 content in the material. A major weight loss of approximately 95 % occurred at 550 ^{0}C for the carbon material. These results provide additional confirmation of the graphitised nature for both CA_SBA-15LPG_105 and CA_HMS_LPG_80 carbon frameworks, which is responsible for the much improved thermal stability.

UNIVERSITY of the
WESTERN CAPE

The analysis of a CA_MCM-41_LPG_80 sample gave no mass loss at T < 550 ^{o}C. Above 550 ^{o}C, 60 % of the carbon was combusted indicating that the partially graphitised more stable form of carbon constituted about 40 % of the carbon formed after a pyrolysis step at 600 ^{o}C, which plays the crucial role of forming the polymerised mesoporous carbon material. These results provide additional confirmation of the graphitised nature of the mesoporous carbon frameworks, which is responsible for the much improved thermal stability.

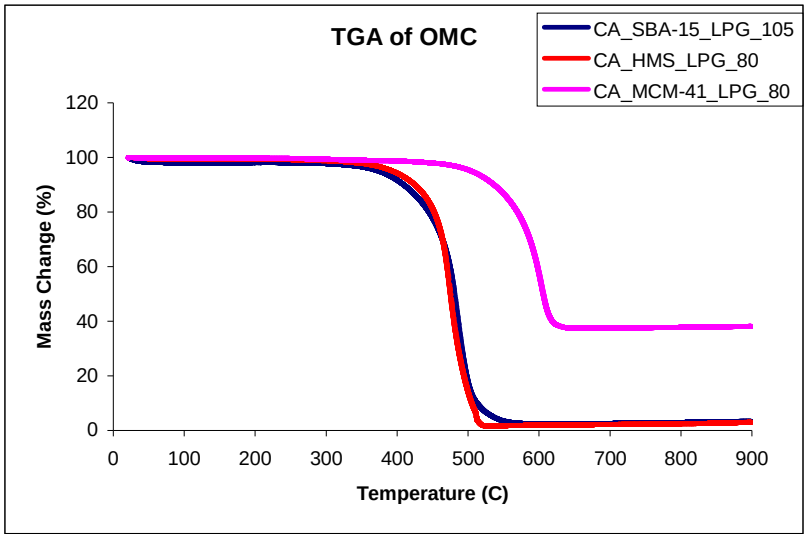

Figure 4. 10: TGA of CA_SBA-15_LPG_105, CA_HMS_LPG_80 and CA_MCM-41_LPG_80

UNIVERSITY of the
WESTERN CAPE

4.10. PORE SIZE DISTRIBUTION AND SURFACE AREA

This section presents characterisation of ordered mesoporous silica (OMSi) templates as well as their respective carbon (OMC) analogues. Brunauer-Emmet-Teller Nitrogen physisorption (N_2BET) technique was used to determine surface area and pore size distribution of OMSi and their respective OMCs and the methodology for characterisation is described in Section 3.7.7. Moreover, the technique also discloses to what extent the measured surface area is associated with micro-, meso- or macropores. Through BET it was possible to determine structural properties (BET surface area, pore volume

and average pore size diameter) of OMSi and OMCs. Ordered mesoporous silica and the carbon analogue were prepared according to the synthesis routes described in Sections 3.2 and 3.3 respectively. Amongst the series of carbon analogues of SBA-15, HMS and MCM-41 presented in Table 3.3, the product which had the highest surface area were chosen and characterised by BET analysis. These selected carbon analogues are as follows: CA_SBA-15_LPG_105, CA_HMS_LPG_80 and CA_MCM-41_LPG_80. Figures 4.10 (a) and 4.10 (b) display the nitrogen isotherms and pore size distribution obtained by N_2 BET of OMSi (SBA-15, HMS and MCM-41) and Figures 4.10(c) and 4.10(d) depict nitrogen isotherms and pore size distribution of the corresponding carbon analogues (CA_SBA-15_LPG_105, CA_HMS_LPG_80 and CA_MCM-41_LPG_80).

UNIVERSITY of the
WESTERN CAPE

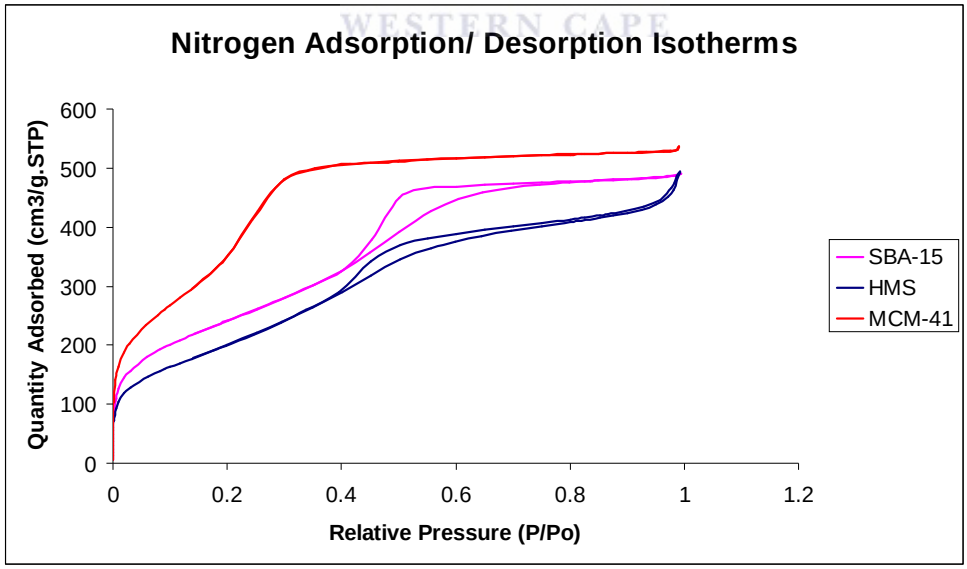

7

Figure 4. 11(a): N_2 BET of SBA-15, HMS and MCM-41

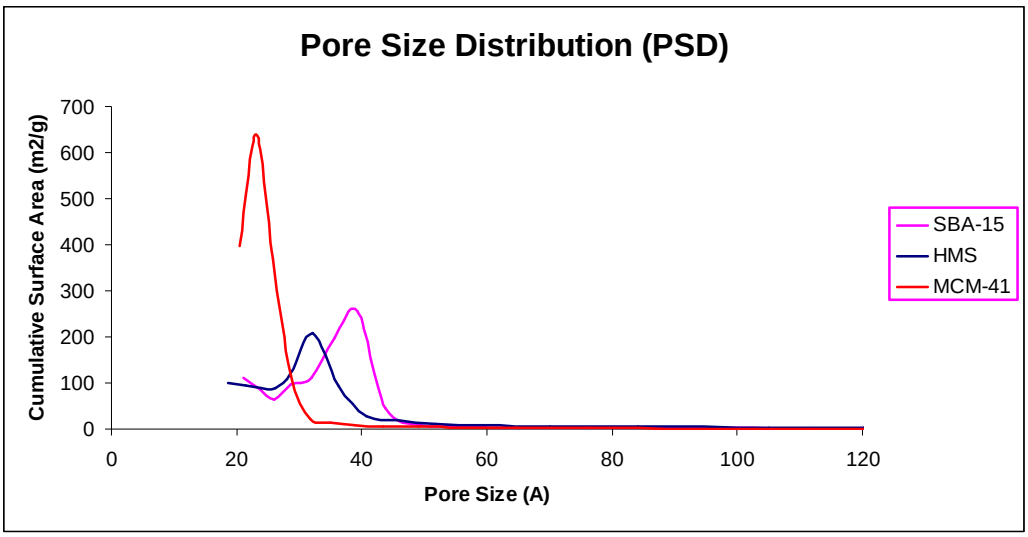

Figure 4. 120(b): Pore size distribution by N_2 BET of SBA-15, HMS and MCM-41

In Figure 4.10 (a-b), both the adsorption and desorption isotherms and the corresponding BJH pore size distributions derived from SBA-15, HMS and MCM-41 are shown. The structural properties of these materials are listed in Table 4.2.

UNIVERSITY of the WESTERN CAPE

Table 4. 2: Textural properties of SBA-15, HMS and MCM-41, and CA_SBA-15_LPG_105, CA_HMS_LPG_80 and CA_MCM-41_LPG_80 materials

Sample	**Surface area (m^2/g)**	**Pore diameter (nm)**
SBA-15	878	4.41
CA_SBA-15_LPG_105	1867	2-3
HMS	725	3
CA_ HMS/LPG_80	874	2-3
MCM-41	897	2.4
CA- MCM-41_LPG_80	910	2-3

UNIVERSITY of the
WESTERN CAPE

SBA-15 and HMS exhibit Type IV isotherm according to the IUPAC classification, which is typical of ordered mesoporous materials with accessible pores **[185, 187].** However, MCM-41 exhibits Type I isotherm which is typical of mesoporous materials with pore sizes close to the micropore range. Intermediate adsorption-desorption hysteresis loops between Types H2 and H1 are observed for SBA-15 and HMS. These intermediate hysteresis loops exhibit isotherms with broad loops but without any significant differences in steepness of adsorption and desorption branches. These are attributed to materials with uniform cagelike pores and thus suitable as model solids with ink bottle pores **[186].**

The pore size distribution (PSD), Figure 4.10(b) derived from the adsorption isotherms of SBA-15, HMS and MCM-41 unimodal with pore sizes of 4, 3 and 2.4 nm respectively as depicted in Table 4.2. It can be noted that SBA-15 has the largest PSD and MCM-41 has the least with pores close to the microporous region as confirmed by Type 1 isotherm in Figure 4.10(a).

Figure 4.10 (c-d) display the adsorption and desorption isotherms and the corresponding BJH pore size distributions derived from carbon analogues of OMSi, i.e. CA_SBA-15_LPG_105, CA_HMS_LPG_80 and CA_MCM-41_LPG_80. The structural properties of these materials are listed in Table 4.2. All the OMCs exhibited Type IV isotherm according to the IUPAC classification, which is typical of ordered mesoporous materials with accessible pores **[184, 185].** Type H3 loops were observed for all OMCs, i.e. CA_SBA-15_LPG_105, CA_HMS_LPG_80 and CA_MCM-41_LPG_80 which is attributed to materials comprised of aggregates of platelike particles forming slitlike pores **[186].**

The OMC's pore size distribution reveal that CA_SBA-15_LPG_105, CA_HMS_LPG_80 and CA_MCM-41_LPG_80 had three pore types (i.e. a trimodal pore size distribution). These pore types could have originated from dissolution or etching of SiO_2 from the silica – carbon composite resulting in OMCs with micropores, primary mesopores and secondary mesopores. The pore diameters obtained were approximately 1.7 nm, 2.3 nm and 3 nm for CA_SBA-15_LPG_105. Whereas for CA_HMS_LPG_80 diameters for the trimodal pore size distribution were approximately 1.8 nm, 2.4 nm and 2.7 nm

and for CA_MCM-41_LPG_80 sample the diameters were 2 nm, 2.5 nm and 3nm. Yuan and Su **[273]** reported that the introduction of larger secondary pores in mesoporous materials, to form hierarchical porous materials with bimodal or multimodal pore-size distributions (PSDs), improves the activity of mesoporous materials **[273].** Similar results regarding multimodal distribution on OMCs were obtained in studies by Chmiola et al **[274]**, when these coworkers synthesized nanoporous carbons obtained by selective leaching of Ti and Al from Ti_2AlC**.** Hence the OMC materials produced with trimodal pore size distribution could serve as potential adsorbents for dye and mercury adsorption.

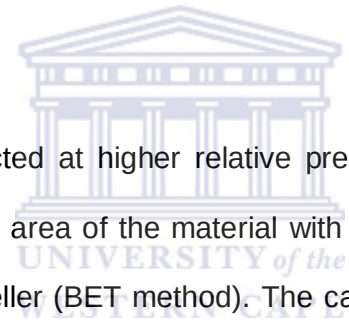
UNIVERSITY of the
WESTERN CAPE

The isotherm data collected at higher relative pressures were used for the calculation of the surface area of the material with the method developed by Brunauer, Emmet and Teller (BET method). The calculated surface areas for OMSi as well as OMCs used in this study are stipulated in Table 4.2. N_2BET analysis shows that SBA-15, HMS and MCM-41 and the carbon analogues CA_SBA-15_LPG_105, CA_HMS_LPG_80 and CA_MCM-41_LPG_80 have considerable nanoporosity in the size range 2 – 4 nm.

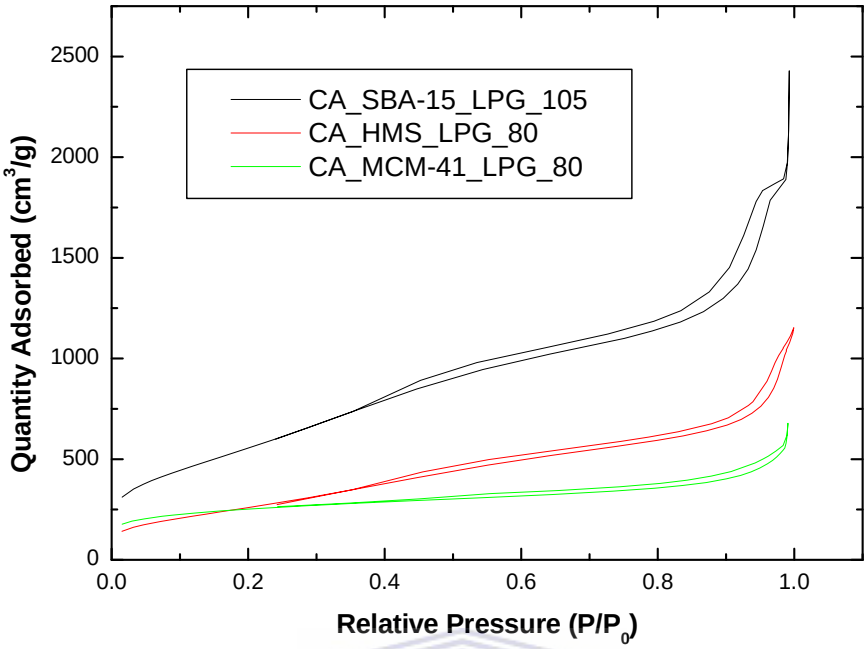

Figure 4. 130(c): N_2 BET of CA_SBA-15_LPG_105, CA_HMS_LPG_80 and CA_MCM-41_LPG_80

UNIVERSITY of the WESTERN CAPE

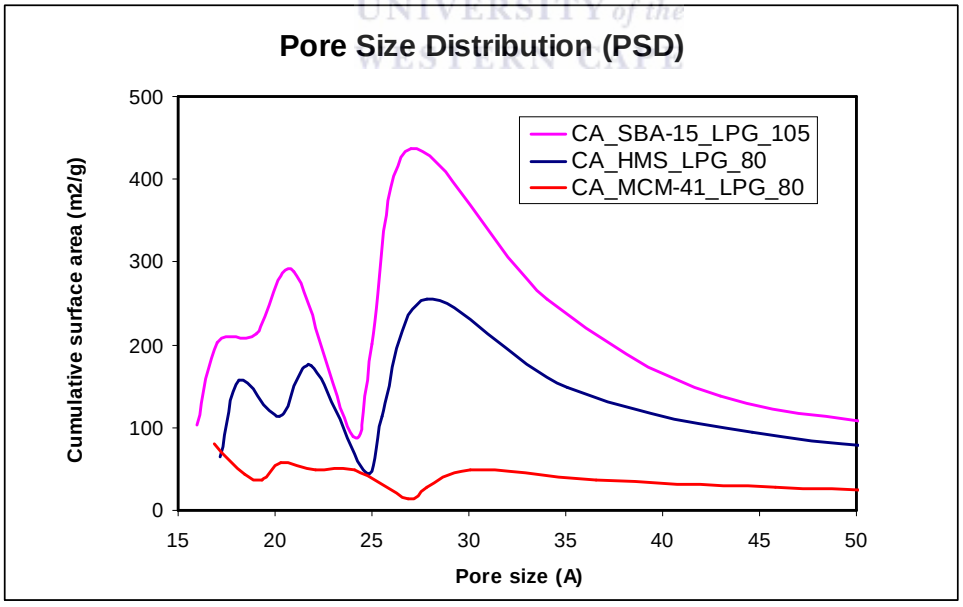

Figure 4. 140(d): Pore size distribution by N_2 BET of CA_SBA-15_LPG_105, CA_HMS_LPG_80 and CA_MCM-41_LPG_80

Table 4.2 compares the surface area of the parent silica materials SBA-15, HMS and MCM-41 and the carbon analogues CA_SBA-15_LPG_105, CA_HMS_LPG_80 and CA_MCM-41_LPG_80. The results show that the carbon analogues obtained after etching away the parent silica template had surface areas of 1867, 874 and 910 m2/g for CA_SBA-15_LPG_105, CA_HMS_LPG_80 and CA_MCM-41_LPG_80 respectively. These surface areas exceeded those of the parent mesoporous silica sacrificial templates that had surface areas of 878, 725 and 897 m^2/g. The carbon analogues (CA_SBA-15_LPG_105, CA_HMS_LPG_80 and CA_MCM-41_LPG_80) had pores in the similar range as that of SiO_2 templates. The data shows that negative carbon mesoporous replicates or analogues of SiO_2 based templates were successfully achieved. Amongst the porous carbon analogues, CA_SBA-15_LPG_105 had the highest surface area (Table 4.2) with largest volume of mesoporous framework and was therefore considered in this study as an adsorbent for dye as well as Hg(II) adsorption.

UNIVERSITY of the
WESTERN CAPE

4.10.1. Pore Size Distribution and Surface Area of Modified Ordered Mesoporous Carbon (MOMC).

This sections presents structural properties (surface areas and pore size distribution) of modified CA_SBA-15_LPG_105 referred to as Modified Ordered Mesoporous Carbon (MOMC). MOMC was prepared according to the synthesis routes described in Sections 3.2. In this study MOMC, OMC and AC are employed as adsorbents for Hg (II) adsorption in Chapter 6. Whereas OMC (CA_SBA-15_LPG_105) and AC are used as adsorbents for dye

adsorption in Chapter 5. The structural properties of both MOMC and AC are presented in Figures 4.11 (a-b) as well as Table 4.3 for AC. Figure 4.11(a) display BET isotherm of MOMC, which clearly demonstrate a type IV hysteresis and type H3 adsorption desorption loop which is similar to that obtained for OMC (CA_SBA-15_LPG_105) in Section 4.9.

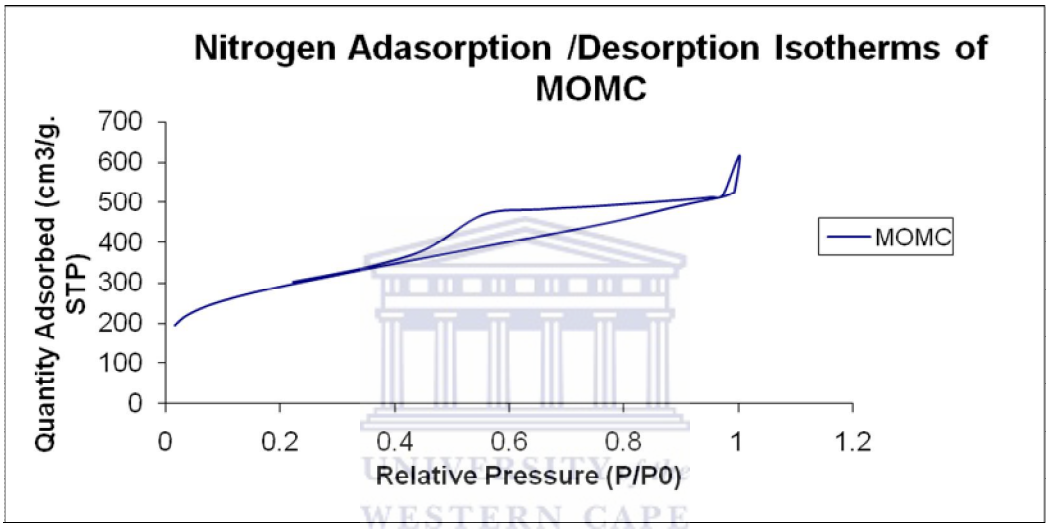

Figure 4. 11a: Characterization of modified ordered mesoporous carbon (MOMC) by N_2 BET

This simply implies that the CA_SBA-15_LPG_105 structural properties remained intact during the modification process. Regarding the pore size distribution, MOMC also exhibits a multimodal or trimodal pore size distribution as obtained previously by the OMC (CA_SBA-15_LPG_105), Figure 4.10(d). According to Yuan and Su **[271]** multimodal pore size distribution is a good indication that the activity of mesoporous materials could

improve. MOMC displays pore size distribution between 2nm - 3.5 nm, Figure 4.11(b).

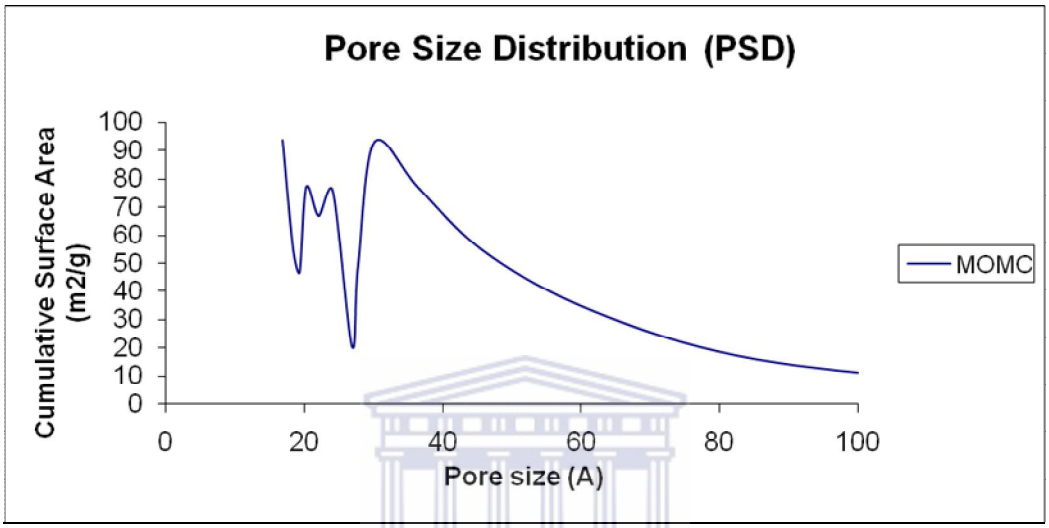

UNIVERSITY of the WESTERN CAPE

Figure 4. 11(b): Pore size distribution by N_2 BET of modified CA_SBA-15_LPG_105 (MOMC).

Table 4. 3: Textural Properties of SBA-15, OMC and AC

Sample	d^a (nm)	S_{BET} (m^2/g)	$S_{micro}{}^a$ (m^2/g)	$S_{meso}{}^b$ (m^2/g)	$S_{lm}{}^c$ (cm^3/g)
SBA-15	4.41	878.3	206.6	671.7	8.0
OMC	3.53	1782.5	0	2122.1	238.3
AC	2	551.2	167.4	383.8	46.7

4.10.2 Pore Size Distribution and Surface Area of Activated Carbon (AC)

This section presents structural properties (surface areas and pore size distribution) of Activated Carbon. In this study the activated carbon was used as a base line material for the adsorption studies presented in Chapters 5 and Chapter 6 for both Dye adsorption and Mercury adsorption studies respectively. The structural properties of AC are presented in Figure 4.10 (c-d) as well as Table 4.3. Figure 4.11(c) display BET isotherm of AC, which demonstrates a type IV hysteresis and type H3 adsorption desorption loop similarly obtained by OMC as well as MOMC. OMC has better structural properties than AC as can be seen in Table 4.3. The AC has a unimodal pore size distribution, Figure 4.11(d) contrary to OMC and MOMC, Figure 4.10(d).

UNIVERSITY of the WESTERN CAPE

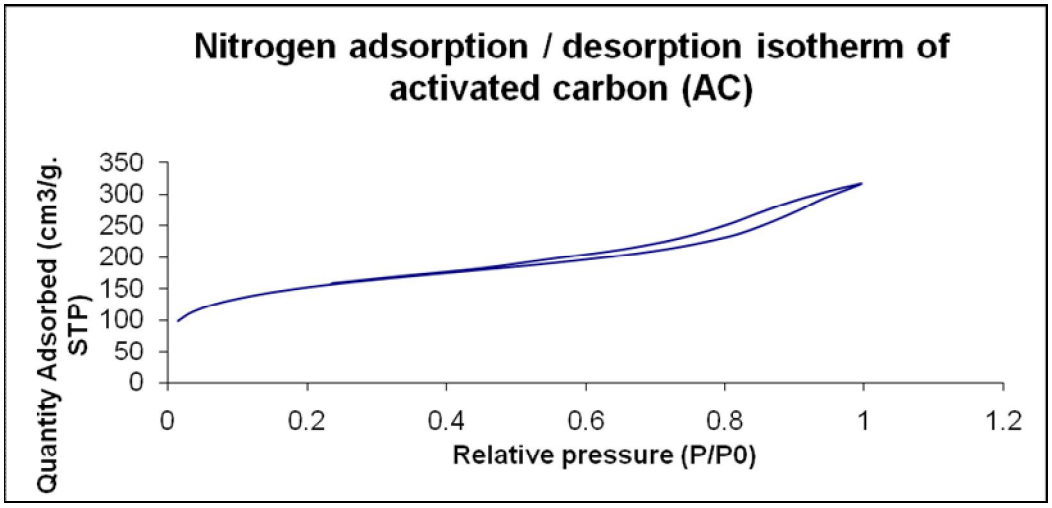

Figure 4. 11(c): Characterisation of modified ordered mesoporous carbon (MOMC) by N_2 BET

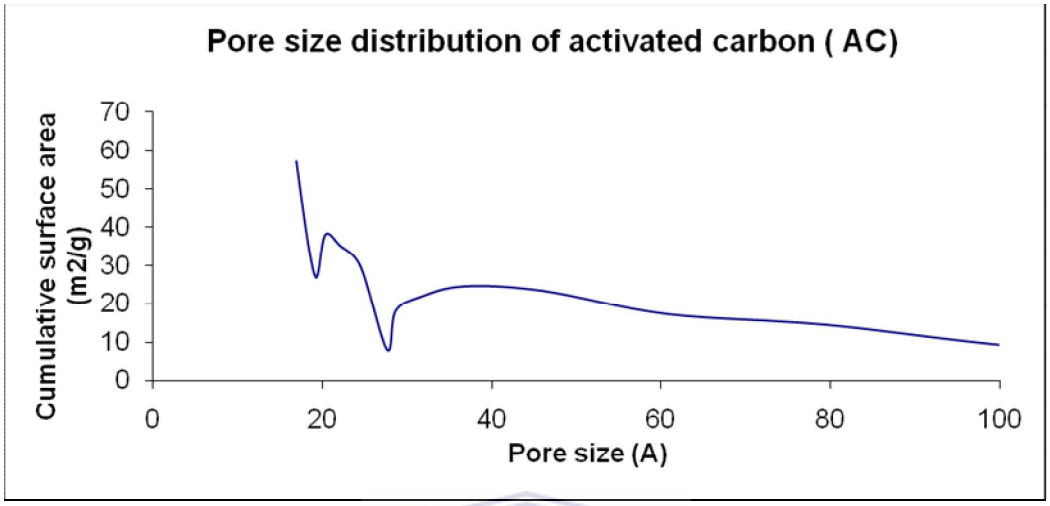

Figure 4. 11(d): Pore size distribution by N_2 BET of Activated Carbon (AC).

UNIVERSITY of the
WESTERN CAPE

4.11. CHARACTERISATION BY FOURIER TRANSFORM INFRA RED SPECTROSCOPY (FTIR).

This section presents characterisation of ordered mesoporous carbon (CA_SBA-15_LPG_105), oxidised CA_SBA-15_LPG_105 (O_ CA_SBA-15_LPG_105) and modified CA_SBA-15_LPG_105 (MOMC) by Fourier Transform Infra Red (FTIR). FTIR was used to determine qualitative structural analysis of CA_SBA-15_LPG_105, O_ CA_SBA-15_LPG_105 and MOMC and the methodology for characterisation is described in Section 3.7.6. Modified ordered mesoporous carbon was prepared according to the synthesis routes described in Sections 3.4.

The FTIR spectrum presented in Figure 4.12 showed several bands for OMC(CA_SBA-15_LPG_105) at vibration frequencies between 500 - 900 cm^{-1}, 1450 cm^{-1}, 1700 -2200 cm^{-1}, 2300 cm^{-1} which are identified as (Si-OH, Si-O-Si), C=C, C=O and C-C stretching vibrational modes respectively **[279, 280].** In comparison with OMC spectrum, (on oxidation OMC with HNO_3) there were several new additional bands that appeared on the Oxidised OMC (O_ CA_SBA-15_LPG_105) spectrum at 1620 cm^{-1} which are identified as COOH stretching vibrational modes. Regarding the MOMC, additional vibrational modes to those observed from OMC and Oxidised OMC were identified at 980 cm^{-1} and 1210cm^{-1} which are identified as Si-O-C and S-O stretching **[280, 281].**

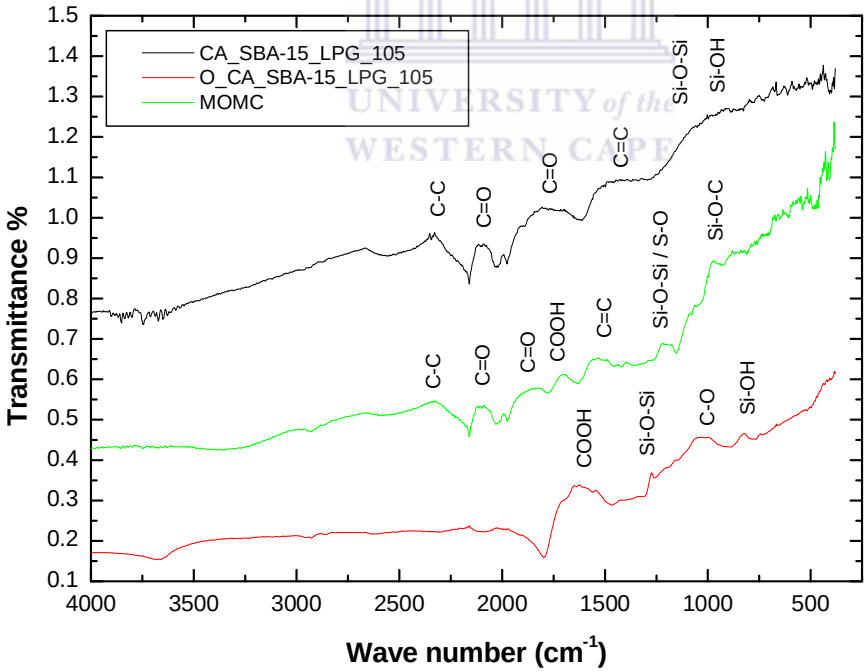

Figure 4. 12: FTIR spectra of CA_SBA-15_LPG_105, Oxidised CA_SBA-15_LPG_105 (O_CA_SBA-15_LPG_105) and modified CA_SBA-15_LPG_105 (MOMC).

The presence of sulphur-oxygen stretching modes and silica-carbon stretching modes observed in the MOMC suggest that the silica groups of MPTES had been successfully introduced to the silica islands as well as on carbonyl groups of the OMC surface during modification process, which would generate new sites for Hg(II) adsorption. This is a novel finding and has never been reported before.

4.12. CONCLUSIONS

A well defined synthesis route to mesoporous graphitic carbon is reported in this work. The use of different templates with distinguished mesopore frameworks is essential in the synthesis of mesoporous carbon framework. These carbon analogues were found to have higher surface areas than their silica precursor templates, and well defined pore structures. The non catalytic LPG carbonisation procedure used was of advantage, as uniform infiltration of the carbon precursor can be easily accomplished inside the silica mesopores so that the resultant carbon materials retain the mesostructural order of the silica templates. In principle, from the experimental observation in this study, the ordered mesoporous silica (SBA-15 HMS and MCM-41) materials and ordered mesoporous carbons (CA_SBA-15_LPG_105, CA_HMS_LPG_80 and CA_MCM-41_LPG_80) show similar crystal morphology, which indicates the following two important points:

(i) SBA-15 HMS and MCM-41 play a role as a templates or “skeleton”, as carbons are formed inside the pore system of the crystal without serious

UNIVERSITY of the WESTERN CAPE

damage to the mesoporous material due to precipitation on the external surface and

(ii) The mesoporous carbons can keep the same structural order/organization after dissolution of the silica template.

Furthermore, it has been shown that by varying pyrolysis time, mesoporous carbons with different pore sizes and surface areas can be obtained, with the pores formed within the parent SBA-15, HMS and MCM-41 framework dependent on the Temperature (800 ^{0}C) applied during pyrolysis. The Raman, XRD, TGA, HRTEM, EELS, and SAED techniques illustrate that the LPG successfully infiltrated the template, and was thermally decomposed to a crystalline, graphitic form of carbon, which formed an independent and structurally robust mesoporous material after removal of the silica template.

UNIVERSITY of the
WESTERN CAPE

The XRD pattern as well as the BET adsorption indicates a high degree of mesostructural ordering in the parent silica templates synthesized hydrothermally. The nitrogen sorption data confirms that the silica templates possessed good mesostructural ordering and was therefore suitable for use as a solid template for mesoporous carbon synthesis. BET data also showed that the carbon analogues were highly porous and exhibited larger surface areas exceeding that of the parent silica sacrificial templates. The apparently regular mesostructure of the carbons could be further supported by the appearance of the new XRD peaks at 7.39 and 12.64 ^{0} 2 θ that may indicate that there is a regular carbon framework at 11.6 and 6.8 Å d spaced distances. This is a novel finding and has not been previously reported for carbon analogues synthesized from SBA-15 and MCM-41 as sacrificial

templates. Moreover, the large mass loss obtained by TGA at 550 ^{0}C may indicate that most of the carbon analogue comprise of the graphitic carbon. This is further supported by clear graphite XRD peaks in the region 26.11^0 2 θ and 43.54^0 2 θ and also by Raman spectroscopy. This degree of graphitisation in a mesoporous analogue has also not previously been reported for carbon analogues synthesized from SBA-15 and MCM-41 as sacrificial templates.

The EDS data indicated that a small concentration of the silica template or "silica islands" material are still present in the resultant carbon materials, and was not completely dissolved during template etching with NaOH solution. These "silica islands" were used as ligating groups during the modification steps of OMC with an organic ligand, 3-mercaptopropyltriethoxysilane (MPTES) as a grafting agent. This is further confirmed by FTIR data which indicated that the silica groups of MPTES had been successfully introduced to the silica islands as well as on carbonyl groups of the OMC surface during modification process, which would generate new sites for Hg(II) adsorption.

UNIVERSITY of the WESTERN CAPE

CHAPTER 5

DYE ADSORPTION

5.1. Introduction

It is well known that silicate materials, such as SBA-15, HMS and MCM-41, have a negative charge density due to the presence of Si—O and Si—OH groups, which should adsorb positive charged dyes and do not permit the adsorption of the negative ones **[282].** However, it is found from the literature **[283]** that the adsorption capacity of both acid and basic dyes on pure silica materials is very low, indicating that other factors (such as structure stability of silica framework during the adsorption process) must be considered for dyes adsorption on SiO_2 in addition to the factor of negative charge density. Carbon materials just like silicate material are considered to have an overall negative charge density on their surfaces however they are found to have better structural stability compared to silicate materials. In this study their adsorption capacities as well as surface properties were investigated for adsorption of acid and basic dyes. Acid orange 8 (AO8), an acidic dye containing one sulfo group, Methylene Blue (MB), a cationic basic dye containing two alkyl amino groups and Rhodamine B (RB), a non polar basic dye **[284].** Activated carbon was employed as a base line material in all the adsorption studies.

UNIVERSITY of the WESTERN CAPE

Surface properties of activated carbon have been determined in literature via the use of Acid dyes which are anionic and basic dyes which are either cationic or neutral. Adsorption of cationic and anionic dyes from dilute solutions have been used to characterise the polarity of carbon materials. Graham **[285]** studied the adsorption of two dyes from dilute aqueous solutions; methylene blue and metanil yellow, of opposite character but approximately the same molecular dimensions from aqueous solutions on a number of activated carbons, measuring separately the effect of pore size and the surface acidic groups. Graham **[285]** concluded that adsorption towards these dyes by activated carbon is influenced by the number of carbon-oxygen surface groups. Similar studies were obtained by Goyal **[286]** when he studied the effect of MB adsorption on oxidation of carbon with nitric acid. The results indicated that the adsorption of methylene blue on activated carbon depends upon the amount of acidic surface groups. Methylene Blue, a cationic dye has large interactions containing two alkyl amino groups with carbons that have negatively charged-sites when placed in aqueous solution. As oxidised carbon have carboxylic or lactonic acidic groups which ionize in water producing COO^- sites. Hence the larger adsorption of MB on oxidized carbon with nitric acid was visualized. As these carbons were degassed there was less negative sites on the carbon surface, due to the removal of acidic surface groups, hence the adsorption of methylene blue decreased.

Since a novel ordered mesoporous material has been synthesised, its surface properties had to be determined using AO8, RB and MB and thereafter, compare its surface properties with those of known AC for AO8,

UNIVERSITY of the WESTERN CAPE

RB and MB adsorption capability. The experimental results were fitted to Langmuir and Freundlich adsorption models and accuracy of the experimental data was examined by using correlations coefficients of the models and then separation factor calculations. This concept relates very well to the research question in terms of proving whether surface properties of an ordered mesoporous material can be determine by probing the surface with acidic and basic dyes. The **CA_SBA-15_LPG_105** sample, ***often referred to as Ordered Mesoporous Carbon (OMC)*** in this chapter was chosen to perform the adsorption studies; since it displayed the highest surface area compared to other carbon analogues synthesized as stipulated in Table 4.2. Yuan and Su **[273]** in their studies on synthesis of hierarchical porous materials with bimodal or multimodal pore-size distributions (PSDs) reported that multimodal pore size distribution increases the activity of materials. As stipulated in Section 4.9 the OMC displayed a multimodal (trimodal) pore size distribution (PSD) with micropores, primary mesopores and secondary mesopores. Since adsorption capacity depends mainly on pore characteristics such as specific surface area, pore size and its distribution **[287]**; it was therefore anticipated that adsorbates with similar molecular dimensions as the adsorbing species would diffuse rapidly easily into the associated pore size distribution (PSD) or pore volume. Hence the higher the specific surface area (e.g. mesopores) in the adsorbent the more adsorption sites could be available for adsorption. On the other hand larger molecules are denied access to the pore volume or pore size distribution as a result of sterical hindrance.

UNIVERSITY of the WESTERN CAPE

The results presented in Section 5.5 to Section 5.7 include adsorption by OMC and AC of the following: (a) Acid Orange (AO8), (b) Methylene Blue (MB) and (c) Rhodamine B (RB). In each of the cases mentioned above (a - c) the following sequence will be employed in presenting the results: Effect of pH, Effect of Adsorbent Dosage and Adsorption Equilibrium.

5.2. The adsorption capacity and the adsorption models

OMC (CA_SBA-15_LPG_105) and activated carbon (AC) were examined for their adsorption capability of acid dye, i.e. acid orange 8 (AO8); basic dyes i.e. Methylene Blue (MB) and Rhodamine B (RB). The experimental procedures for effect of adsorbent dosage, effect of pH and adsorption equilibrium isotherms are described in Sections 3.6.4 - 3.6.8. The two basic dyes were chosen as a result of their overall charge; methylene blue (MB) being cationic and rhodamine B (RB) being neutral.

UNIVERSITY of the WESTERN CAPE

5.3. Acid Orange 8 (AO8) Adsorption by OMC and AC

Acid Orange 8 (MW 364.4 $g.mol^{-1}$) was obtained from Sigma Aldrich and was used without further purification. Acid orange, an acid dye was utilized in this study as a probe molecule to investigate its adsorption behavior by OMC (i.e. CA_SBA-15_LPG_105) and Activated Carbon (AC). The adsorption behavior was investigated by performing a series of tests on OMC and AC adsorbents

with AO8 as an adsorbate material. These tests include the following: Effect of pH, effect of adsorbent dosage and adsorption equilibrium.

5.3.1. Effect of pH

It is well known that pH, besides various physicochemical effects, is an important variable in adsorption processes, by which surface charges may be changed or modified **[34].** The pH studies presented in this section were carried out according to the procedure given in Section 3.6.1 and 3.6.2, to show the effect of pH on the adsorption of AO8 solutions containing 100 mg/L with a fixed quantity of OMC and AC. The pH of the AO8 solution was adjusted by adding few drops using a pipette bulb to the desired pH values with 0.1 M Citric acid and 0.2M phosphate solutions (Table 3.3 and Section 3.6.1). The pH range that was explored was from pH 2 to pH 8. The experiments were conducted as described in Section 3.6.7 by shaking 0.01 g of OMC (CA_SBA-15_LPG_105) and AC adsorbents with 50 ml of 100 mg/L of pH adjusted AO8 for 24 h at 25 ºC.

UNIVERSITY of the WESTERN CAPE

The determination of the uptake and percentage removal of AO8 in aqueous solution by OMC and AC was performed using the procedure set out in Section 3.6.7 and the results shown in Figure 5.1; indicate that pH plays a significant role in the uptake of AO8 by OMC and AC.

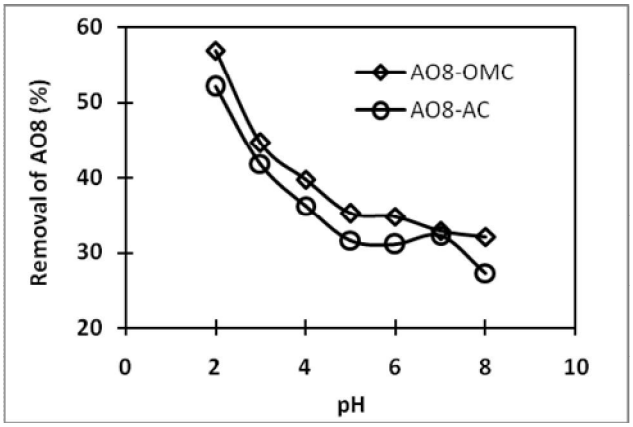

Figure 5. 1: Effect of pH on AO8 adsorption by OMC and AC. Initial concentration of AO8, 100 mg/L; adsorbent dosage, 10 mg/50 mL, temperature, 25±2 ^{o}C; pH, 2. Where OMC = CA_SBA-15_LPG_105 and AC = Charcoal Activated Carbon supplied by Saarchem (see Table 3.1).

UNIVERSITY of the
WESTERN CAPE

Figure 5.1 shows that the AO8 adsorption by OMC and AC is at a maximum pH of 2. Depending on this result the equilibrium adsorption experiments were carried out at pH 2. Adsorption is affected by pH change of the solution, which primarily affects the degree of ionization of the AO8 dye adsorbate and the surface properties of the OMC and AC adsorbents. Two possible mechanisms of adsorption of AO8 on OMC and AC may be considered: (a) electrostatic interaction between the protonated groups of carbon and acid dye and (b) chemical reaction between the adsorbate and the adsorbent **[287].** At pH 2 a significant high electrostatic attraction exists between the positively charged surface of the adsorbent and anionic AO8 dye. As the pH of the system increases, the number of negatively charged sites increases and the number of positively charged sites decreases. A negatively charged surface site on

the OMC and AC adsorbents does not favour the adsorption of AO8 dye anions due to the electrostatic repulsion. Also, lower adsorption of AO8 dye anions at alkaline pH is due to the presence of excess OH^- ions competing with the AO8 dye anions for the adsorption sites. At alkaline pH significant adsorption of the anionic AO8 dye on the OMC and AC adsorbents still occurred. This suggests that the second mechanism, i.e. chemisorption might be operative **[284, 287].**

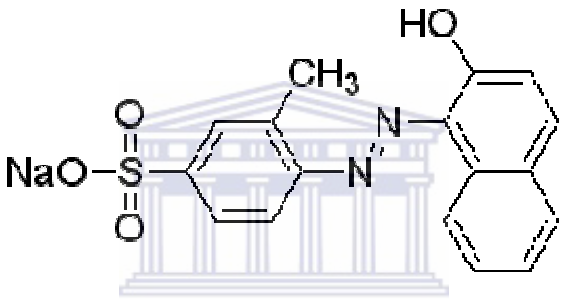

Figure 5. 2: Structural representation of Acid Orange 8 **[287].**

UNIVERSITY of the
WESTERN CAPE

OMC has a higher adsorption capacity AO8 than AC due to its specific surface area, pore size and its distribution (figure 4.9 and Table 4.3). Depending on these pH experimental results, further dosage and equilibrium studies were made at pH 2.

5.3.2. Effect of Adsorbent Dosage

Adsorbent dosage is an important parameter in adsorption studies because it determines the capacity of an adsorbent to adsorb a given initial concentration of analyte in solution **[287].** Figure 5.3 shows the removal of AO8 as a function of adsorbent (OMC or AC) dosage.

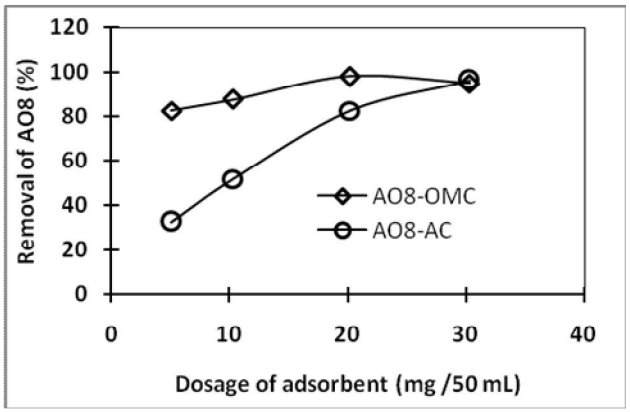

Figure 5. 3: Effect of carbon dosage on AO8 adsorption by OMC and AC. Initial concentration of AO8, 100 mg/L; temperature, 25±2 ^{o}C; pH, 2.

UNIVERSITY of the WESTERN CAPE

Increase of carbon dosage increased percent removal of AO8 which is due to the increase in absorbent surface area of the adsorbent **[288].** An OMC dosage of 10 mg/50mL has 87 % removal capacity for AO8 whereas for an AC dosage of 10 mg/50mL, 57 % percentage removal capacity of AO8 is achieved. For quantitative removal of AO8 from 50 mL of 100 mg/L, a maximum dosage of 20 mg/L for OMC and 30 mg/L for AC is required. OMC has a higher percentage removal capacity of AO8 compared to AC due to its higher surface. However, in this study the optimum adsorbent dosage was chosen as 10 mg/50 mL for both OMC and AC in all the AO8 adsorption experiments. This was performed in order to work within the mass dosage limit instead of the maximum dosage to see the adsorption response.

5.4. The adsorption capacity

The adsorption capacity (Q_e) was obtained by using a mass equilibrium equation as follows **[216].**

$$Q_e = \frac{(C_o - C_e) * V}{m} \qquad (5.1)$$

where C_o and C_e being the initial and the equilibrium concentrations of the contaminant in the liquid phase (mg/L), respectively. In this equation V is the experimental volume of the adsorption solution (L), and m is the mass of the adsorbent (g).

UNIVERSITY of the
WESTERN CAPE

5.4.1. The Langmuir isotherm model

Adsorption is usually described through isotherms, that is, the amount of adsorbate on the adsorbent as a function of concentration of the liquid we want to purify at constant temperature. The adsorption isotherms of dyes both in ordered mesoporous carbon (OMC) and activated carbon (AC) were fitted to both Langmuir and Freundlich models, in order to establish the model that was most appropriate.

The Langmuir isotherm assumes monolayer adsorption onto a surface containing a finite number of adsorption sites of uniform energies of adsorption with no transmigration of adsorbate in the plane of surface **[38, 219].** The isotherms assumes that adsorption takes place at specific homogenous sites within the adsorbent, which implies that all adsorption sites

are identical and enegertically equivalent. Langmuir isotherm equation has several linear forms. The following forms (Equation 5.2) and (Equation 5.3) were used in modeling of the adsorption in this study. The form giving the higher correlation coefficient (compared to the other form) was used in the calculation of capacity of the adsorbent

$$\frac{1}{Q_e} = \frac{1}{Q_o} + \frac{1}{bQ_oC_e} \tag{5.2}$$

$$\frac{C_e}{Q_e} = \frac{1}{bQ_o} + \frac{C_e}{Q_o} \tag{5.3}$$

UNIVERSITY of the
WESTERN CAPE

where, C_e is the equilibrium concentration (mg/L) and Q_e is the amount of dye adsorbed (mg/g) at equilibrium time. Q_o and b are Langmuir constants related to adsorption capacity and rate of adsorption, respectively. The plots of 1/ Q_e versus 1/ C_e or C_e/Q_e versus C_e give straight lines; the intercept and slope of these lines are used to calculate the Langmuir constants.

5.4.2. The Freundlich isotherm model

The Freundlich equation is an empirical equation employed to describe a heterogeneous system. The linear form of Freundlich adsorption isotherm model was also applied to describe the adsorption of dyes by OMC and AC **[45].** The Freundlich equation is an empirical equation employed to describe a

heterogeneous system, in which it is characterized by the heterogeneity factor 1/n, as follows $q_e = K_F C_e^{1/n}$.

The equation can be linearized by taking natural logarithms:

$$\ln Q_e = \ln K_F + (\frac{1}{n}) \ln C_e \qquad (5.4)$$

where C_e (mg*L^{-1}) and Q_e (mg/g) are equilibrium liquid and solid dye concentrations, K_F and n are Freundlich constants, n showing if the adsorption was favourable or not and K_F [(mg*g^{-1})*(L/mg)^n] showing the adsorption capacity of the adsorbent. The values of n and K_F are calculated from the slope and intercept of the plots of ln Q_e vs. ln C_e. According to Traybal **[289]**, n values between 1 and 10 is an indication of favourable adsorption of adsorbate onto the adsorbent.

UNIVERSITY of the
WESTERN CAPE

5.5. Acid Orange 8 Adsorption Isotherms

After contacting the AO8 containing liquid and solid OMC or AC for 24 h equilibrium time, the concentration of AO8 in the liquid was measured by UV/VIS spectrophotometer (C_e). The equilibrium concentration of AO8 in the solid phase was found from the difference between the initial and equilibrium liquid concentration of AO8 (Table 5.1). Table 5.1 gives initial concentrations of AO8, equilibrium concentrations of AO8 in solution and equilibrium

concentrations of AO8 in the solid OMC or AC. The adsorption equilibrium curves or adsorption isotherms of AO8 adsorption by OMC and AC were plotted as shown in Figure. 5.4.

Table 5. 1: Adsorption of AO8 by OMC and AC

	Adsorption of AO8 by OMC		**Adsorption of AO8 by AC**	
Prepared initial concentration of AO8 (mg/g)	Equilibrium concentration of AO8 in the solution (mg/L)	Equilibrium concentrati-on of AO8 in the solid (mg/g)	Equilibrium concentration of AO8 in the solution (mg/L)	Equilibrium concentration of AO8 in the solid (mg/g)
0	0	0	0	0
50	7.7586	215.2918	8.8183	203.3527
75	19.7334	278.7401	26.1697	240.4387
100	43.1087	289.4856	45.9438	262.7819
125	62.3038	321.0257	68.6396	284.1070

UNIVERSITY of the WESTERN CAPE

Table 5.1 compiles the adsorption capacities for AO8 over OMC and AC. AO8 maximum adsorption amounts were 321.0257 mg/g for OMC and 284.1070 mg/g for AC. Suggesting a higher AO8 adsorption capacity for OMC than that of AC. Further investigation on the equilibrium concentrations of AO8 in the solution, it was found that AO8 adsorption amounts were 62.3038 mg/L for OMC and 68.6396 mg/L for AC. This also further suggests that OMC has a higher adsorption capacity for AO8 than AC. N_2BET results (Table 4.3, Figure 4.10(d)) show that OMC mainly consists of specific surface area with

mesopores in the most probable pore diameter of 3.0 nm, which are fully accessible for AO8. Therefore, the maximum adsorption amount is only dependent on adsorption thermodynamics. However, Table 4.3 depicts that AC consists of specific areas of micropores (551.2 m^2/g) and mesopores specific surface area (383.8 m^2/g) indicating that AC has higher pore volume of micropores. Considering that molecular size of AO8 is 1.50x0.88x0.46 nm^3, it is therefore rationally expected that AO8 adsorption in the micropores with pore diameters below 0.88 nm is sterically prohibited owing to size exclusion **[290, 291].** Hence, the markedly higher maximum adsorption capacity of OMC for AO8 can be attributed to its higher accessible pore volume compared to that of AC (Table 4.3). It is interesting to note (see Table 5.2) that Langmuir adsorption constants b are 0.2098 and 0.1774 L/mg for AO8 adsorption over OMC and AC, respectively. In principle the Langmuir adsorption constant is characteristic of the affinity of AO8 to the adsorbent. The substantially larger Langmuir adsorption constant reflects a stronger adsorption of AO8 on OMC compared to that of AC. Long et al **[292]**, studied the adsorption of reaction dyes on polymeric adsorbents and concluded that the optimum ratio of the pore diameter to sorbate molecular diameter is about 2 to 6 for effective adsorption. For OMC the most probable pore diameter is about 3.75 nm, which is about five times larger than that of AO8 molecule. In addition OMC pore structure is constructed via an ordered array of long carbon rods to form mesoporous channels with $p6\,mm$ hexagonal symmetry, which is especially suitable for hosting sorbate molecules with a large aspect ratio. In contrast, AC are characteristic of a broad pore size distribution.

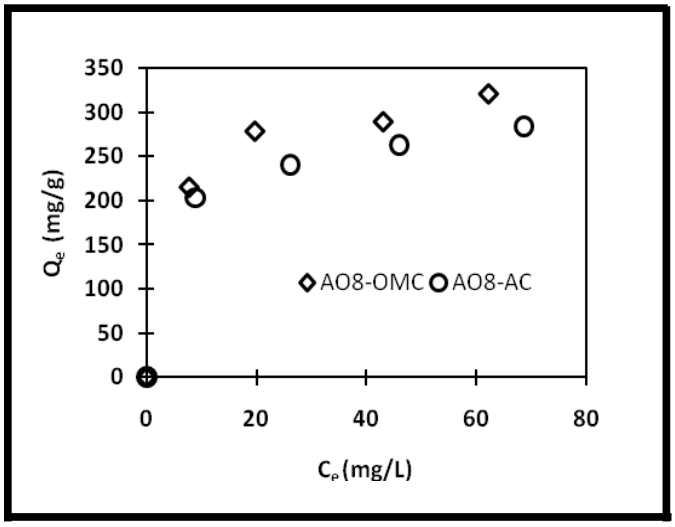

Figure 5. 4: The experimental adsorption isotherms of AO8. Temperature, 25±2 ^{o}C; pH, 2. Where OMC = CA_SBA-15_LPG_105 and AC = Charcoal Activated Carbon supplied by Saarchem (see Table 3.1).

UNIVERSITY of the
WESTERN CAPE

Figure 5.4 shows the equilibrium adsorption isotherms of AO8 on OMC and AC adsorbents. The isotherms belong to Type I curve, characteristic of Langmuir isotherms. The amount of adsorbed AO8 dramatically increases at a lower solution concentration, suggesting a high affinity between the dye molecule and the carbonaceous adsorbent surface, the adsorbed amount reaches a plateau at a higher equilibrium solution concentration, reflecting the saturated adsorption. Hence, an order for the adsorption capacity of AO8 with a small molecular size on the two adsorbents is as follows: OMC > AC.

The second step was to fit the results obtained in Figure 5.4 to a model. For this purpose the data was fitted to the Langmuir and Freundlich models. The

Langmuir and Freundlich isotherms of AO8 adsorption by OMC and AC can be seen in Figure 5.5.

The linear forms of Langmuir and Freundlich models as illustrated in equations 5.3 and 5.4 are applied to the results presented in Figure 5.5. The linear plot of $\frac{C_e}{Q_e}$ vs. C_e shows that adsorption follows Langmuir isotherm model, Figure 5.5(a). The Langmuir isotherm model seems to fit on AC better than OMC since AC had high correlation coefficients (0.9969) compared to that of OMC (0.9951). This implies that there was monolayer coverage of AO8 on the surface of AC and OMC but this coverage was more pronounced in AC.

UNIVERSITY of the WESTERN CAPE

The Freundlich isotherm was also applied for the adsorption of AO8 by AC and OMC. Linear plots of $\ln Q_e$ vs. $\ln C_e$ show that the adsorption also follows Freundlich isotherm. The correlation constant for AO8 on AC and OMC were 0.9981 and 0.9275 respectively; (Figure 5.5(b)). Showing that the coverage of AO8 adsorption was more pronounced on AC compared to OMC. Values of K_F and n which are constants incorporating all factors affecting (adsorption capacity and intensity of adsorption) the adsorption process are presented in Table 5.2. In general as the K_F values increase the adsorption capacity for a given dye increases. Table 5.2 shows that the K_F value for OMC (154.12) is higher compared to that of AC (142.77) as a result the adsorption capacity of AO8 by OMC is higher compared to that of AC (Figure 5.4).

Both models seem to fit AC better for AO8 adsorption with high correlation constants, R^2 (Langmuir, 0.9969 and Freundlich, 0.9981). However, AC tends to favour the Freundlich model for AO8 adsorption more than the Langmuir. This is also is confirmed by a higher value of n (6.2112) compared to that of OMC (5.6433). On the other hand OMC seem to favour the Langmuir model with a correlation constant of 0.9951 compared to the Freundlich with a correlation constant of 0.9275 (Table 5.2). It is generally accepted that any carbon having an adsorption capacity of at least 200 mg/g can be named as a good decolorizing carbon **[293].** The present AC showed an adsorption capacity of 303.03 mg/g. The high adsorption capacity of AC can be correlated with its mesoporous structure.

UNIVERSITY of the
WESTERN CAPE

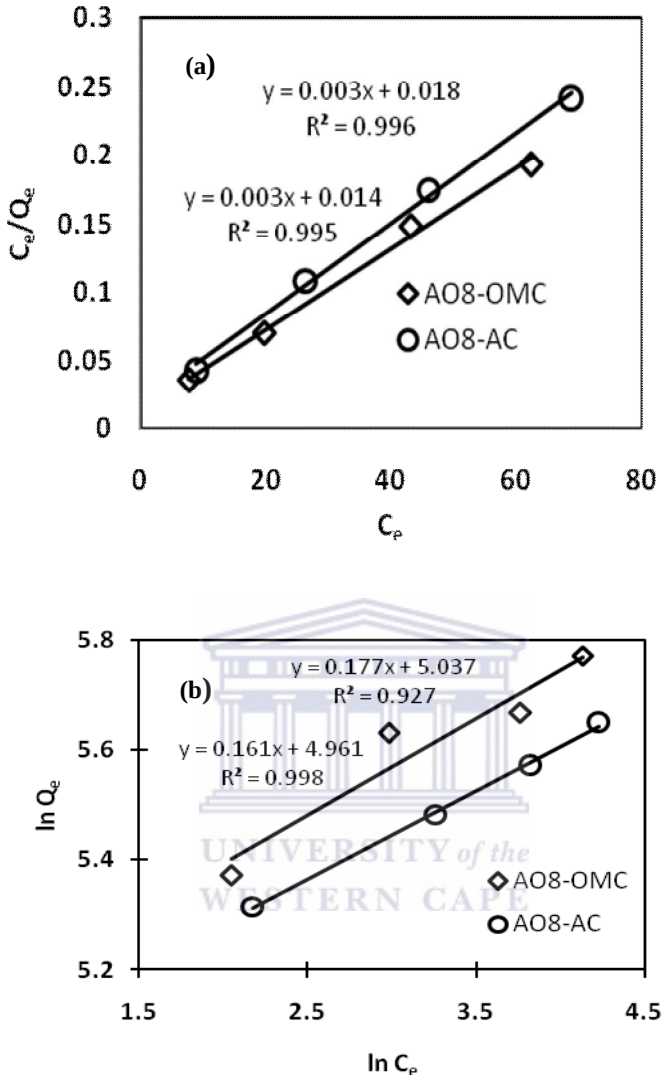

UNIVERSITY of the WESTERN CAPE

Figure 5. 5: Adsorption of AO8 by OMC and AC. (a) The Langmuir (b) Freundlich isotherms. Temperature, 25±2 ^{o}C; pH, 2.

The Langmuir monolayer capacities Q_0 for AO8-OMC and AO8-AC system, correlation coefficient, R^2, and b Langmuir constant related to rate of adsorption are represented in Table 5.2. Q_0 represents the saturation capacity of AO8.

Table 5. 2: The Langmuir and Freundlich constants for AO8 adsorption by OMC and AC

Adsorbent	Langmuir model			Freundlich model		
	Q_o (mg/g)	b (L/mg)	R^2	K_F [(mg/g)X(mg/L)^n]	n	R^2
OMC	333.33	0.2098	0.9951	154.12	5.6433	0.9275
AC	303.03	0.1774	0.9969	142.77	6.2112	0.9981

The saturation capacity of AO8 for OMC (333.33 mg/g) is higher compared to that of AC (303.03 mg/g). This could be due to the specific mesopore surface area of OMC compared to AC (see Table 4.3).

UNIVERSITY of the
WESTERN CAPE

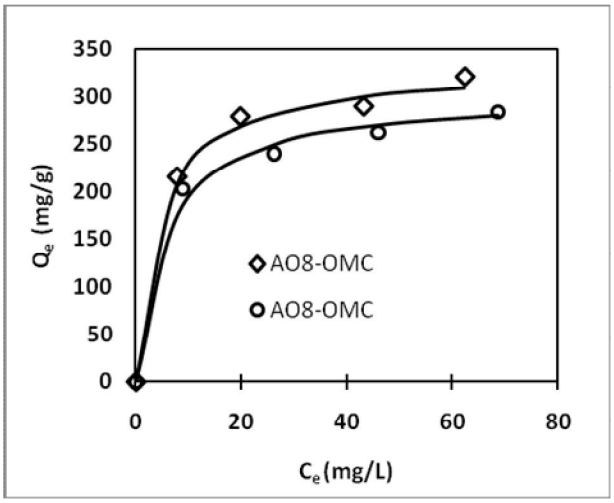

(a)

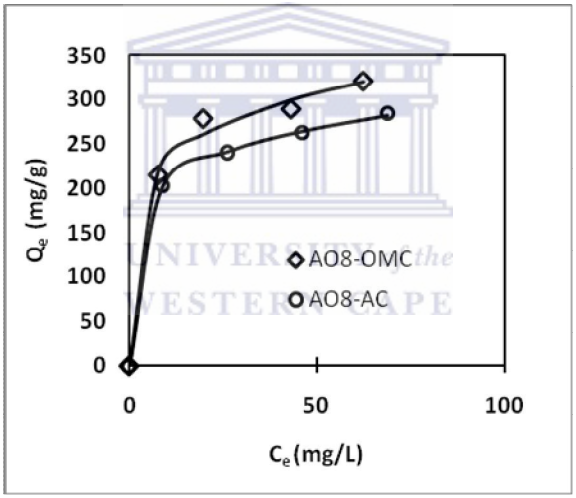

(b)

Figure 5. 6: Model and experimental equilibrium isotherms of AO8 adsorption by OMC and AC. Solid lines present the models. (a) The Langmuir (b) Freundlich plots. Temperature, 25±2 ^{o}C; pH 2.

Adsorption isotherms describe the mechanism by which adsorbates interact with the adsorbents and therefore are critical in optimizing the use of adsorbents **[294].** The plots in Figure 5.6 (a) are typical and demonstrate that the Langmuir equation provides an accurate description of the experimental data which is further confirmed by the extremely high values of the correlation coefficients for the AO8-OMC and AO8-AC systems (see Table 5.2). The high degree of correlation for the linearized Langmuir relationship suggests a single surface reaction for both AO8-OMC and AO8-AC systems with constant activation energy and is deemed to be the predominant adsorption step. Sharp curvature close to saturation indicates a high degree of irreversibility **[34].** The Freundlich equation predicts that the dye concentration on the adsorbent will increase as long there is an increase in the dye concentration in the liquid. The experimental data in the present AO8-OMC and AO8-AC systems (Figure 5.6(b)) indicate that there is a limiting value of the solid phase concentration. The correlation coefficients in the table are well correlated to the Langmuir correlation coefficients.

UNIVERSITY of the

However, the correlation coefficients for AO8-AC system for both Freundlich (0.9981) and Langmuir (0.9969) isotherms were higher compared to those of the AO8-OMC system (see Table 5.2). The high correlation coefficient for the Langmuir model indicates that in the AO8-AC there is the higher existence of monolayer coverage of the adsorbate at the outer surface of the AC compared to OMC. The high correlation coefficient for the Freundlich model indicates that the AO8-AC system is a more heterogeneous system compared to AO8-OMC system.

The essential characteristics of the Langmuir isotherm can be expressed by dimensionless constant separation factor, R_L, given by Hall, et al (1966). R_L is a dimensionless constant called equilibrium parameter defined by

$$R_L = 1/(1 + bC_0) \quad (5.5)$$

where b is the Langmuir constant and C_0 is the initial dye concentration (mg/l), R_L values indicate the type of isotherm. An R_L value between 0 and 1 indicates favorable adsorption **[293, 294, 295].**

Table 5. 3: R_L and types of isotherms.

R_L	Type of isotherm
RL>1	Unfavourable adsorption
R_L=1	Linear adsorption
0<R_L<1	Favorable adsorption
R_L=0	Irreversible adsorption

R_L values were calculated at different AO8 initial concentrations and plotted as R_L vs. initial concentration in Figure 5.7. It can be seen from Figure 5.7 that all the R_L values are between 0 to 1, which indicates favourable AO8 adsorption by OMC and AC.

OMC with abundant mesoporosities and high surface area as well as AC were shown to be effective in removing AO8 from aqueous solutions.

The Langmuir and Freundlich model were applied to the adsorption data of OMC and AC. The Langmuir data was more fitted than Freundlich for OMC adsorbent. Whereas the Freundlich data was more fitted than Langmuir for AC. The maximum adsorption capacities of AO8 onto OMC and AC were 333.33 and 303.03 mg/g at 25±2^{0}C, pH 2.

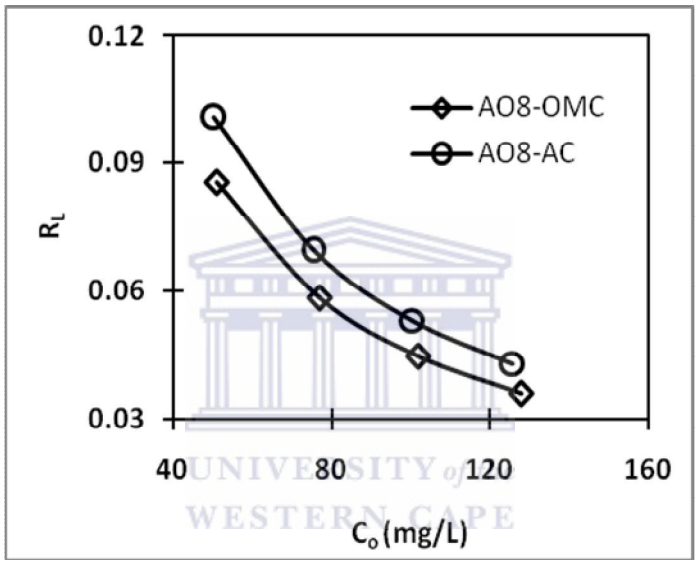

Figure 5. 7: Separation factor for AO8 adsorption by OMC and AC based on Langmuir.

Fig 5.6 was plotted using experimental and model data points. Again as it can be seen from Fig. 5.6, adsorption of AO8 by OMC and AC followed both the Langmuir and Freundlich isotherms. In Figure 5.7 the R_L values for AC and OMC towards AO8 adsorption are found to be favourable, between 0 and 1. The R_L values seem to decrease with an increase in initial concentration (C_0).

At low concentration (45 mg/L) the R_L values for OMC and AC are 0.087 and 0.015 respectively. Whereas at high concentrations (125 mg/L) the R_L values for OMC and AC are 0.0335 and 0.045 respectively. Hence, AC has higher R_L values compared to OMC indicating that monolayer adsorption of AO8 is more favourable on OMC compared to AC. Low values of R_L indicate a high and favourable solute/adsorbent adsorption process **[293, 296, 297].** This could be attributed to the specific surface area of mesopores or pore volume which is higher in OMC compared to AC (see Table 4.3).

5.6. Methylene Blue (MB) Adsorption by OMC and AC

Methylene Blue (MB) with molecular weight of 319.85 g.mol^{-1} was obtained from Sigma Aldrich and was used without further purification. Methylene Blue, a cationic basic dye containing two alkyl amino groups was utilized in this study as a probe molecule to investigate its adsorption behavior over OMC and Activated Carbon (AC). The adsorption behavior was investigated by performing a series of tests on OMC and AC adsorbents with MB as an adsorbate material. These tests include the following: Effect of pH, effect of adsorbent dosage and adsorption equilibrium.

UNIVERSITY of the WESTERN CAPE

5.6.1. MB Adsorption Isotherms

After contacting the MB containing liquid and solid OMC or AC for 24 h equilibrium time, the concentration of MB in the liquid was measured by UV/VIS spectrophotometer (C_e) as stipulated in Section 3.7.8.

5.6.2. Effect of pH

The pH of an aqueous medium is an important factor that may affect the uptake of the adsorbate. The chemical characteristics of both adsorbate and adsorbent vary with pH **[298].** The pH studies presented in this section were carried out according to the procedure given in Section 3.6.1 and 3.6.2, to see the effect of varying pH on the degree of adsorption of MB solutions (containing 100 mg/L MB) with a fixed quantity of OMC or AC. The pH of the MB solution was adjusted to the desired values which was between 2 and 14 with 0.1 M Citric acid and 0.2 M phosphate solutions (Table: 3.3 and section 3.6.1). The experiments were conducted as described in Section 3.6.7 by shaking 0.01 g of OMC (CA_SBA-15_LPG_105) and AC adsorbents with 50 ml of 100 mg/L MB for 24 h at 25 ºC. The determination of the uptake and percentage removal of MB in aqueous solution by OMC and AC was performed using the procedure set out in Section 3.6.7 and the results are shown in Figure 5.8.

UNIVERSITY of the WESTERN CAPE

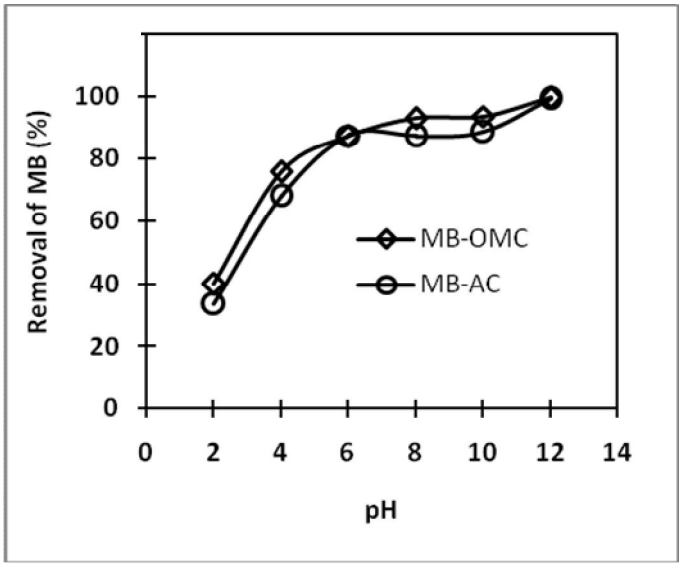

Figure 5. 8: Effect of pH on MB adsorption by OMC and AC. Initial concentration of MB, 100 mg/L; temperature, 25±2; pH, 2-12; contact time, 24h.

UNIVERSITY of the
WESTERN CAPE

It can be seen from Figure 5.8 that the adsorption of MB on OMC and AC increases with an increase in pH. MB adsorption by OMC and AC is almost the same at pH values between 6 and 10. As previously stated in Section 5.3.1 adsorption is affected by the hydrogen ion concentration or pH change of the solution, which primarily affects the degree of ionization of the dye (MB) and the surface properties of OMC and AC adsorbents.

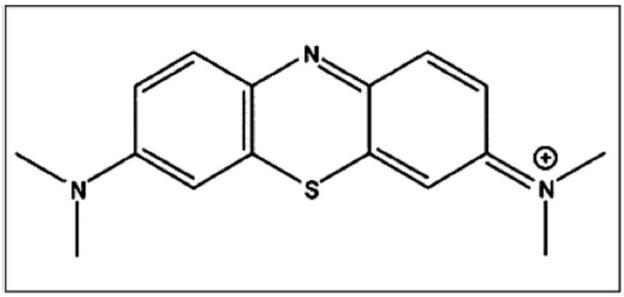

Figure 5. 9: Chemical structure of Methylene Blue **[293].**

This is due to the fact that MB is a cationic dye (see figure 5.9). Adsorption is affected by pH change of the solution, which primarily affects the degree of ionization of MB and the surface properties of the OMC and AC adsorbents. Two possible mechanisms of adsorption of MB on OMC and AC may be considered: (a) electrostatic interaction between the protonated groups of carbon (OMC or AC) and MB; (b) chemical reaction between the adsorbate and the adsorbent. At pH 2 a significant high electrostatic repulsion exists between the positively charged surface of the adsorbent and cationic MB basic dye. As the pH of the system increases, the number of negatively charged sites increases and the number of positively charged sites decreases. A negatively charged surface site on the OMC and AC adsorbents favours the adsorption of MB dye cations due to the electrostatic attraction. Also, higher adsorption of MB dye cations at alkaline pH is due to the presence of excess OH^- ions attraction with the MB dye cations to the adsorption sites on the carbon surface. At alkaline pH significant adsorption of the cationic MB dye on the OMC and AC adsorbents still occurred. This suggests that the second mechanism, i.e. chemisorption might be operative.

UNIVERSITY of the
WESTERN CAPE

Similar results were obtained by Yasin et al **[299]**, Hameed et al **[298]** and Graham Et al **[285]** in their studies on adsorption of cationic and anionic dyes from dilute aqueous solutions. OMC has a higher percentage removal adsorption capacity than AC due to its higher surface area compared to AC (see Table 4.3). Because of these results as presented in Figure 5.8, dosage and equilibrium studies were done at the natural pH of MB aqueous solutions. The natural pH of 100 mg/L MB solution was pH 6.

5.6.3. Effect of Adsorbent Dosage

Adsorbent dosage is an important parameter in adsorption studies because it determines the capacity of the adsorbent for adsorbing a given initial concentration of metal or analyte in solution.

UNIVERSITY of the
WESTERN CAPE

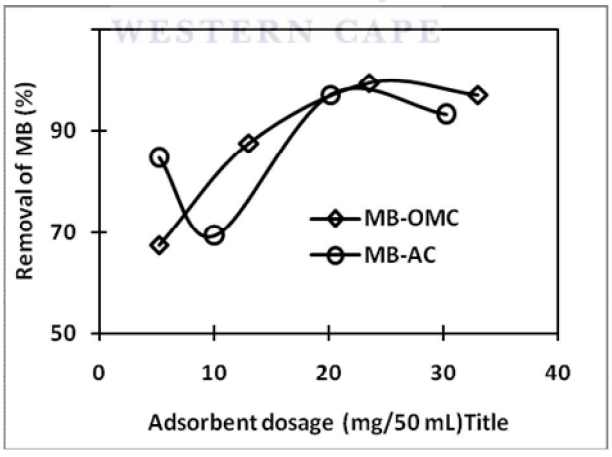

Figure 5. 10: Effect of carbon dosage on MB adsorption by OMC and AC. Initial concentration of MB, 100 mg/L; temperature, 25±2 ^{o}C; pH 6; 24 h contact time.

Figure 5.10 shows the effect of carbon dosage on MB adsorption by OMC and AC adsorbents. The percent removal of MB increased with the increased adsorbent dose due to the increase in the total available surface area of the adsorbent particles. It was observed that the adsorption capacity reached an equilibrium value beyond which there was a decrease in the residual MB concentration. The optimum dosage was found to be 20 mg/50mL and 25 mg/50 mL for OMC and AC respectively. Hence at optimum dosage for an initial concentration of 100 mg/mL, the uptake of MB reached 100 % or saturation for an adsorbent dose of 20 mg/50mL and 25 mg/50 mL for OMC and AC respectively. Similar results were obtained by Yasin et al **[299]**, in their study on adsorption of MB onto treated AC. However, in this study the optimum adsorbent dosage was chosen as 10 mg/50 mL for both OMC and AC in all the AO8 adsorption experiments. This was performed in order to work within the mass dosage limit instead of the maximum dosage to see the adsorption response.

UNIVERSITY of the
WESTERN CAPE

5.6.4. Adsorption Equilibrium

Langmuir and Freundlich models were examined for their applicability to the experimental data obtained for MB adsorption. Using model and experimental data Fig. 5.11 was formed, showing model/experiment fitting.

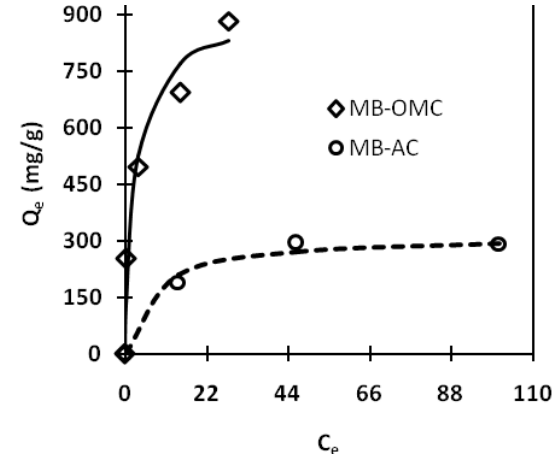

(a)

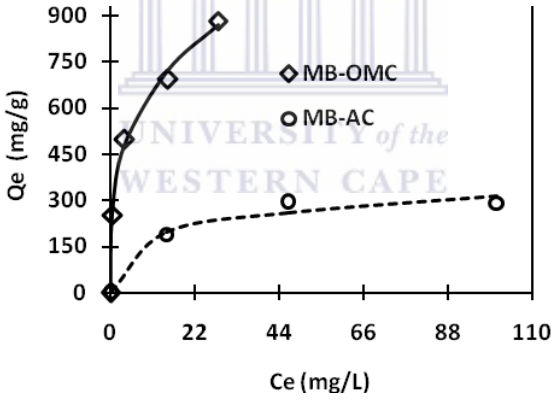

(b)

Figure 5. 11: Model and experimental equilibrium isotherms of MB adsorption by OMC and AC. Solid lines present the models. (a) The Langmuir (b) Freundlich plots). Temperature, 25±2 ^{o}C.

UNIVERSITY of the WESTERN CAPE

Figure 5.11 shows model and experimental equilibrium isotherms of MB adsorption by OMC and AC. Conformation of the experimental data with the Langmuir isotherm (Figure 5.11(a)) model for AC adsorbent indicates the homogeneous nature of the AC surface, i.e. each MB dye molecule adsorption has equal adsorption activation energy the results also demonstrate the formation of monolayer coverage of MB dye molecule at the outer surface of AC. Contrary to MB-AC adsorption, conformation of the experimental data with the Freundlich isotherm (Figure 5.11(b)) model for OMC adsorbent indicates a non-ideal sorption that involves heterogeneous sorption of MB dye on the OMC surface.

Moreover, the experimental adsorption isotherms are generally Type I and their linear plots (Figure 5.11) as stipulated in equation 5.3 and 5.4 were used to calculate the monolayer capacity, Q_0; the Langmuir adsorption constant, b; Freundlich adsorption or distribution coefficient, K_F; Freundlich constant incorporating the intensity of adsorption, n; and correlation coefficients, R^2; for both Langmuir and Freundlich isotherms and the actual values are specified in Table 5.3.

UNIVERSITY of the WESTERN CAPE

Figure 5.12 shows straight lines representing MB-OMC and MB-AC systems each with slope of 1/n and intercept of ln K_F when $\ln Q_e$ is plotted against $\ln C_e$. The slope 1/n ranging from 0 to 1, is a measure of adsorption intensity or surface heterogeneity, becoming more heterogeneous as its values get closer to zero. A value of 1/n below one indicates a normal Langmuir isotherm while 1/n above one is indicative of cooperative adsorption **[293, 295].** The

Freundlich constants (K_F and n) as specified in Table 5.3 suggest that MB is favourably adsorbed by OMC. The Freundlich isotherm fits quite well with the experimental data (correlation coefficient R^2 = 0.9956), whereas the low correlation coefficient (R^2 = 0.9792) show poor agreement of Freundlich isotherm with the experimental data. On the other hand Table 5.3 also suggests that MB is favourably adsorbed by AC. The Langmuir isotherm fits quite well with the experimental data (correlation coefficient R^2 = 0.9943), whereas the low correlation coefficient (R^2 = 0.8289) show poor agreement of Langmuir isotherm with the experimental data.

Table 5.4 also lists a comparison of maximum monolayer adsorption capacity of MB dye with OMC and AC adsorbents. Table 4.3 shows that the OMC adsorbent studied in this work has very large adsorption capacity (909.09 mg/g) compared to a small adsorption capacity of AC (312.50). This is due to the fact that OMC has a high surface area (1782.5 $m^2.g^{-1}$) and a larger average pore size diameter (2-4nm) which were larger than the size of MB dye (1.43 × 0.61 × 0.4nm^3) **[292].** Therefore, it is rationally expected that MB adsorption in the mesopores with pore diameters above 0.61 nm is feasible or sterically uninhibited as evident from the pore size distribution of OMC with pore diameters above 2 nm (see Table 4.3). This could be attributed to the specific surface area of mesopores or pore volume which is higher in OMC compared to AC.

UNIVERSITY of the
WESTERN CAPE

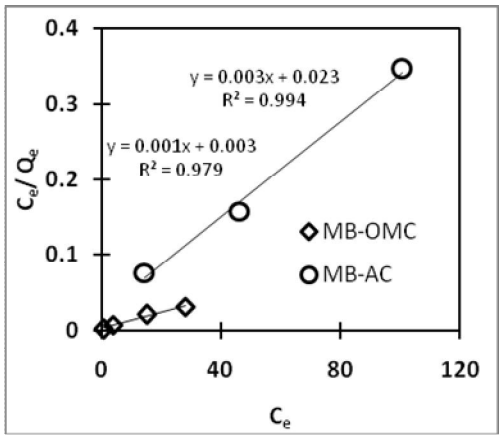

(a)

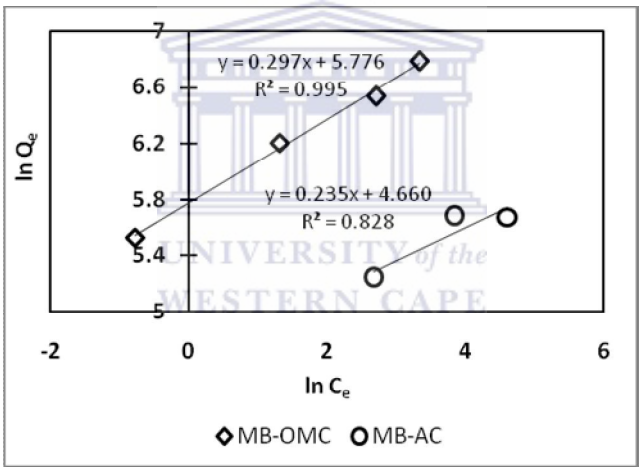

(b)

Figure 5. 12: Adsorption of MB by OMC and AC. (a) The Langmuir (b) Freundlich plots. Temperature, 25±2 ^{o}C

Table 5. 4: The Langmuir and Freundlich constants for MB adsorption by OMC and AC

Adsorbent	Langmuir model			Freundlich model		
	Q_o (mg/g)	b (L/mg)	R^2	K_F [(mg/g)X(mg/L)^n]	n	R^2
OMC	909.09	0.3667	0.9792	322.56	3.3613	0.9956
AC	312.50	0.1373	0.9943	105.69	4.2535	0.8289

UNIVERSITY of the
WESTERN CAPE

The dimensionless separation factor, R_L; defined in equation 5.5 confirm the applicability of the Langmuir model (Figure. 5.13). Figure 5.12 (a) and Figure 5.12 (b) shows that the Langmuir model is better to represent the system than Freundlich model. The fact that Langmuir isotherm fits the experimental data very well may be due to the homogenous distribution of active sites on the OMC and AC adsorbent surfaces; since the Langmuir equation assumes that the surface is homogeneous. The value of the adsorption coefficient K_F and the monolayer capacity V_m calculated from Langmuir equation are given in Table 5.4. The value K_F is related to the degree of adsorption. The greater the value of K_F , the greater the affinity of the MB towards adsorbent. The lower the K_F , the lower the affinity **[293].** In this case there is a significant difference between the K_F values of the OMC and AC implying that there is greater affinity for adsorption of MB on OMC surface compared to AC. The value of

1/n < 1 is an indication that the amount of MB adsorbed increases less rapidly than the concentration **[293, 295].**

The essential characteristics of the Langmuir equation can be expressed in terms of a dimensionless separation factor, RL, as defined in equation 5.5 **[298].** Separation factor, R_L, values were calculated at different MB initial concentrations and the results were presented in Figure 5.13.

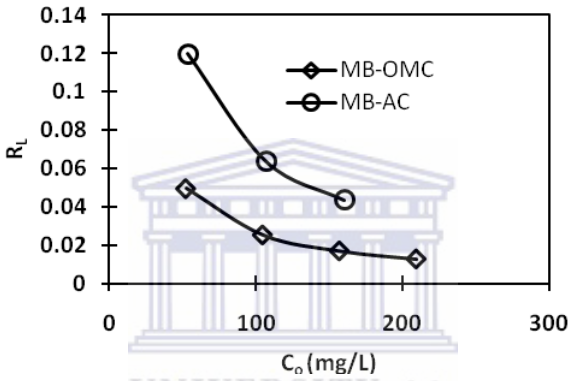

UNIVERSITY of the
WESTERN CAPE

Figure 5. 13: Separation factor for MB adsorption by MB and AC at 25±2 ^{o}C; pH 7.5; contact time, 24h.

Table 5.3 defines the type of isotherm associated with a specified value of R_L. R_L values of MB adsorption by OMC and AC are between 0 and 1, indicating favorable adsorption of MB by OMC and AC. Values of R_L were found to be 0.12 and 0.005 for AC and OMC respectively. Low values of R_L indicate a high and favourable solute/adsorbent adsorption process **[293, 296, 297].** This further confirms that OMC is more favourable for adsorption of MB dye than AC under conditions used in this study. This could be attributed to the specific surface area of mesopores or pore volume which is higher in OMC compared to AC (see Table 4.3).

5.7. Rhodamine B (RB) Adsorption by OMC and AC

Rhodamine B (RB) is a basic dye which is non-polar with molecular formula $C_{28}H_{31}ClN_2O_3$, molecular size 1.59X1.18X0.56 nm^3 and molecular weight of 479.01 $g.mol^{-1}$ was obtained from Sigma Aldrich and was used without further purification. Rhodamine B was utilized in this study as a probe molecule to investigate its adsorption behavior over OMC and Activated Carbon (AC). The adsorption behavior was investigated by performing a series of tests on OMC and AC adsorbents with RB as an adsorbate material. These tests include the following: Effect of pH, effect of adsorbent dosage and adsorption equilibrium. These tests were conducted in order to ascertain the surface properties of the novel OMC material, AC carbon was utilized as a base line material. Comparison of the adsorption capacities of OMC and AC for removing RB dye from solution was also investigated.

UNIVERSITY of the WESTERN CAPE

5.7.1. Effect of pH

The pH studies presented in this section were carried out according to the procedure given in Section 3.6.1 and 3.6.2, to show the effect of pH on the adsorption of RB solutions containing 100 mg/L RB with a fixed quantity of OMC and AC. pH is one of the important parameters controlling the adsorption process. The pH of the RB solution was controlled by additions of 0.1 M Citric acid and 0.2 M phosphate solutions (Table: 3.3 and section 3.6.1). The experiments were conducted as described in Section 3.6.7 by shaking 0.01 g of OMC and AC adsorbents with 50 ml of 100 mg/L RB dye for 24 h at

25 ºC. The determination of the uptake and percentage removal of RB in aqueous solution by OMC and AC was performed using the procedure set out in Section 3.6.7 and the results are shown Figure 5.14.

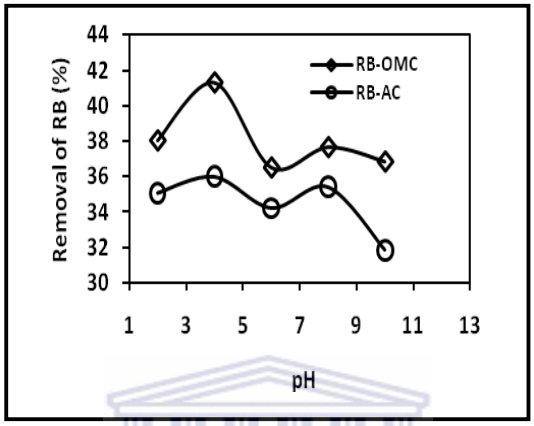

Figure 5. 14: Effect of pH on RB adsorption by OMC and AC. Initial concentration of RB, 100 mg/L; temperature, 25±2 ^{o}C; contact time, 24 h; pH, 7.5.

UNIVERSITY of the
WESTERN CAPE

Fig. 5.14 shows that the RB adsorption by OMC and AC showed no significant difference with the change in pH from 2 to 12. Hence adsorption of RB on OMC and AC was pH independent. Similar results were obtained by Guo et al **[300]**, when they investigated the adsorption of RB by rice husk-based porous carbon. Based on pH experimental results, dosage and equilibrium studies were made at neutral pH of RB which was 7.5. As previously stated, adsorption is affected by the hydrogen ion concentration (pH) change of the solution, which primarily affects the degree of ionization of the dye (RB) and the surface properties of the OMC and AC adsorbents. It is apparent that RB

exists in two molecular forms depending on the pH of the solution. These molecular forms of RB are stipulated in Figure 5.15, (a) representing the monomeric cationic form whereas (b) represents the Zwitterionic form.

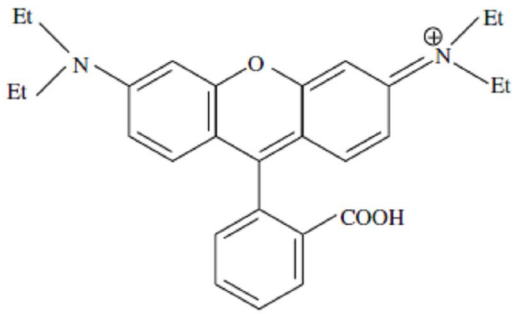

(a) Cationic form

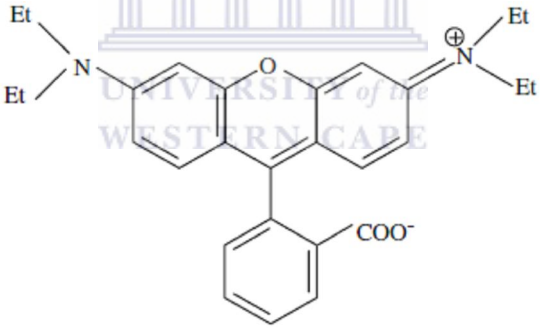

(b) Zwitterionic form

Figure 5. 15: Molecular forms of Rhodamine B **[301].**

Figure 5.15 shows that the adsorption of RB on OMC and AC is not affected by a change in pH. It appears that a change in pH of the solution results in the formation of different ionic species, and different carbon surface charge. At pH

values lower than 4, the RB ion is cationic and in a monomeric molecular form **[301]**. Thus RB ions can enter into the pore structure of OMC and AC because of the mesopores specific surface area 2122.1 m^2/g for OMC and 383.8 m^2/g for AC (see Table 4.3). The pore size distribution of OMC is between 2-3 nm and molecular size of RB is 1.59X1.18X0.56 nm^3. It is rationally expected that RB adsorption in the mesopores with pore diameters above 1.18 nm is feasible. Hence 4% increase in percentage removal of RB by OMC between in pH 2-4. Considering adsorption of RB on AC, it is expected that adsorption in micropores of AC with pore diameters below 1.18 is sterically prohibited owing to size exclusion. Adsorption only takes place in the mesopores of AC with a surface area of 383.8 m^2/g, hence a 1% increase in percentage removal, which is almost insignificant. At a pH value higher than 4, the zwitterionic form of RB in water may increase the aggregation of RB to form a bigger molecular form (dimer) and become unable to enter into the pores of OMC and AC, Ghanadzadeh et al **[301]** have studied the aggregation of RB in the microporous solid hosts. Lopez Arbeloa and Ruiz Ojeda **[303]** determined the equilibrium constant for the dimer ↔ monomer transition of RB in aqueous solution. The greater aggregation of the zwitterionic form is due to the attractive electrostatic interactions between the carboxyl and xanthene groups of the monomers **[304].** Therefore, the effect of the charge on the carbon surface and the electrostatic force of attraction and repulsion between the carbon surface and the RB ions cannot explain the result.

UNIVERSITY of the WESTERN CAPE

The percent removal of RB by OMC and AC is almost the same in a wide pH range (Figure 5.14). Depending on the results from Figure 5.14 dosage and

equilibrium studies were performed at natural pH of RB. (The pH of 100 mg/L RB solution was measured as 7.5).

5.7.2. Effect of Adsorbent Dosage

In order to investigate the effect of adsorbent mass on the adsorption of Rhodamine B dye, a series of adsorption experiment was carried out with different adsorbent dosages at initial dye concentration of 100 mg/L. Figure 5.16 shows the effect of adsorbent dosage on the removal of RB using OMC and AC. The results follow the expected pattern, in which the percentage sorption increased with the increase in adsorbent dosage.

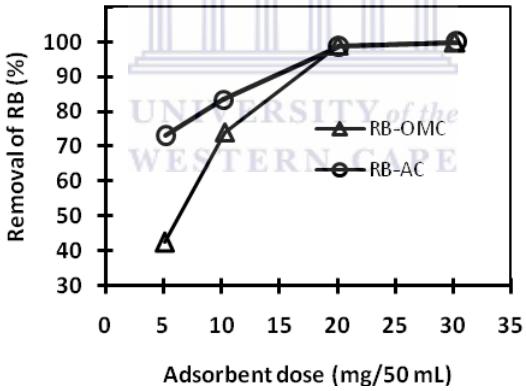

Figure 5. 16: Effect of carbon dosage on RB adsorption by OMC and AC. Initial concentration of RB, 100 mg/L; temperature, 25±2 ^{o}C; pH, 7.5; contact time, 24h.

As shown in the Figure 5.16, the percentage uptake of RB increased very fast at low dosage up to a point, after which the increase in the dosage did not increase the uptake of RB significantly. The saturation occurred at 20

mg/50mL for both OMC and AC. Similar results were obtained by Arivoli et al **[305]**, in their studies of RB adsorption by acid activated low cost carbon. The observed trend in carbon dosage might be due to a larger external surface area available for the adsorption. It can also be seen that the RB uptake by AC was higher at low dosage of adsorbent in contrast to OMC. For example, at 5 mg dosage, the RB uptake by AC was about 30 % higher than OMC, indicating that AC is a better adsorbent than OMC at low dosage. The higher external micropore surface area (167.4 m^2/g) of AC contributed to this factor compared to OMC which had no significant external micropore surface area (0 m^2/g), as stipulated in Table 4.3. However, in this study the optimum adsorbent dosage was chosen as 10 mg/50 mL for both OMC and AC in all the RB adsorption experiments. This was performed in order to work within the mass dosage limit instead of the maximum dosage to see the adsorption response.

UNIVERSITY of the
WESTERN CAPE

5.7.3. Adsorption Equilibrium Isotherms

The Langmuir and Freundlich models were examined for their applicability to the experimental data. Model and experimental data were plotted in Figure 5.17 to form the model and experimental isotherms. It can be seen from Figure 5.18 that model and experimental points are close to each other.

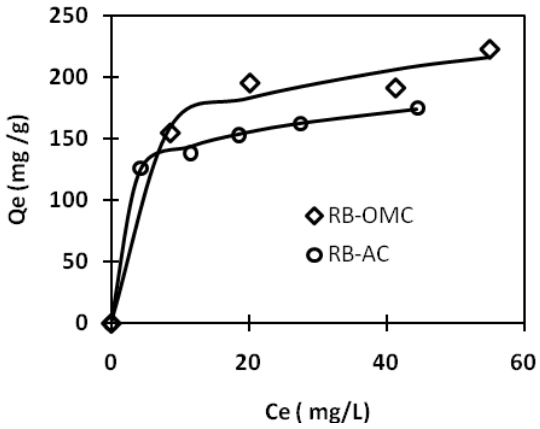

(a)

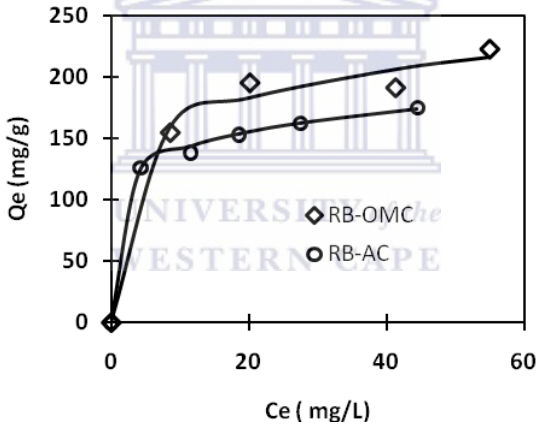

(b)

Figure 5. 17: Model and experimental equilibrium isotherms of RB adsorption by OMC and AC. Solid lines present the models (a) The Langmuir (b) Freundlich plots. Temperature, 25±2 ^{o}C; pH, 7.5; contact time, 24h.

Figure 5.17 shows model and experimental equilibrium isotherms of RB adsorption by OMC and AC. Conformation of the experimental data with the Langmuir isotherm (Figure 5.17(a)) model for AC adsorbent indicates the homogeneous nature of the AC surface, i.e. each RB dye molecule adsorption has equal adsorption activation energy the results also demonstrate the formation of monolayer coverage of RB dye molecule at the outer surface of AC. Contrary to RB adsorption on AC, conformation of the experimental data with the Freundlich isotherm (Figure 5.17(b)) model for OMC adsorbent indicates a non-ideal sorption that involves heterogeneous sorption of RB dye on the OMC surface. This results show that OMC and AC effectively uptake RB with Q_0 about 232.56 mg/g and 185.19 mg/g respectively. The experimental adsorption isotherms (Figure 5.17) are generally Type I **[306]** and their linear plots (Figure 5.18) as stipulated in equation 5.4 were used to calculate the monolayer capacity, Q_0, the Langmuir adsorption constant related to adsorption capacity; b; Freundlich constant related to the rate of adsorption; K_F, Freundlich constant incorporating the intensity of adsorption; n, and correlation coefficients; R^2, for both Langmuir and Freundlich isotherms and the actual values are specified in Table 5.6 **[293, 294, 295].**

UNIVERSITY of the WESTERN CAPE

Table 5. 5: The Langmuir and Freundlich constants for RB adsorption by OMC and AC

Adsorbent	Langmuir model			Freundlich model		
	Q_o (mg/g)	b (L/mg)	R^2	K_F [(mg/g)X(mg/L)^n]	n	R^2
OMC	232.56	0.2129	0.9824	111.14	6.0314	0.8333
AC	185.19	0.3140	0.9968	100.89	6.9881	0.9803

UNIVERSITY of the
WESTERN CAPE

The Langmuir constants can be calculated from the Langmuir equation (5.3) and the calculated constants are given in Table 5.6. As can be seen in the Table, the resulting Q_0 values for OMC and AC are 232.56 mg/g and 185.19 mg/g respectively. The results indicate that OMC shows higher adsorption capacity of RB compared to AC. OMC has a higher mesopores specific surface area (2122.1 m^2/g) compared to AC (383.8 m^2/g). Therefore, it is rationally expected that RB adsorption capacity will be higher on the OMC adsorbent with higher mesopores specific surface area and a higher pore size distribution (PSD).

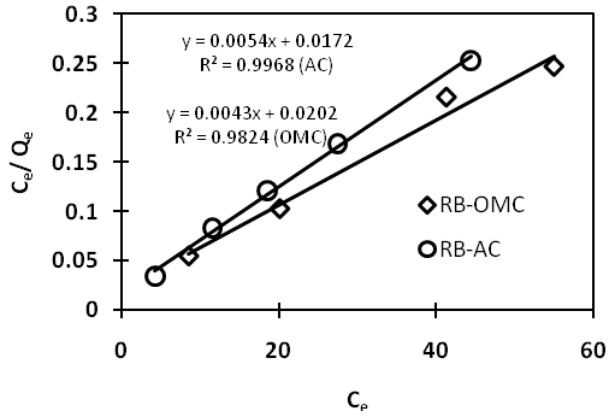

(a)

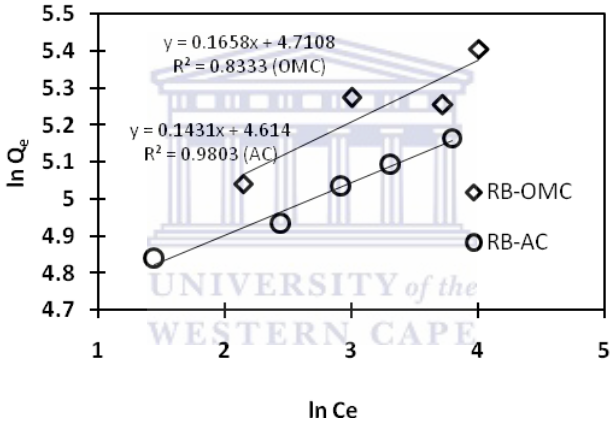

UNIVERSITY of the
WESTERN CAPE

(b)

Figure 5. 18: Adsorption of RB by OMC and AC. (a) The Langmuir (b) Freundlich plots. Temperature, 25±2 ^{o}C; pH, 7.5; contact time, 24h.

The plot of $\frac{C_e}{q_e}$ against C_e in Figure 5.18(a) gave straight lines for all the concentrations; this implies that the adsorption for both adsorbents well fitted to Langmuir isotherm. The correlation coefficients, R^2, was found to be 0.9968

for AC and 0.9824 for OMC. Moreover, b , the Freundlich constant related to the rate of adsorption was found to be 0.3140 L/mg for AC and for OMC it was 0.2129 L/mg. Higher correlation coefficients and higher rate constants of adsorption for AC compared to OMC suggest that RB is favourably adsorbed by AC and that the adsorption isotherm of RB using AC gives a good fit to the Langmuir model compared to OMC **[294].** Conformation of the experimental data with the Langmuir isotherm (Figure 5.18(a)) model for AC adsorbent indicates the homogeneous nature of the AC surface, i.e. each RB dye molecule adsorption has equal adsorption activation energy the results also demonstrate the formation of monolayer coverage of RB dye molecule at the outer surface of AC.

UNIVERSITY of the
WESTERN CAPE

The plot of $\ln Q_e$ against $\ln C_e$ in Figure 5.16(b) gave straight lines for all the concentrations; this implies that the adsorption for both adsorbents (OMC and AC) fitted well to Freundlich isotherm. Freundlich constants (K_F and n) were calculated and recorded, which are listed in Table 5.6. The greater the value of K_F , the greater the affinity of the RB towards adsorbent **[293, 295].** In this case there is no significant difference between the K_F values of the OMC and AC implying that the degree of adsorption is almost the same. The lower the K_F , the lower the affinity. The value of 1/n < 1 is an indication that the amount of RB adsorbed increases less rapidly than the concentration. The low correlation coefficient, R^2, for OMC (R^2= 0.8333) and for AC (R^2= 0.9803) show poor agreement of Freundlich isotherm with experimental data.

The essential characteristics of the Langmuir equation can be expressed in terms of a dimensionless separation factor, RL, as defined in Equation 5.5. Separation factor, R_L, values were calculated at different RB initial concentrations and the results were presented in Figure 5.19.

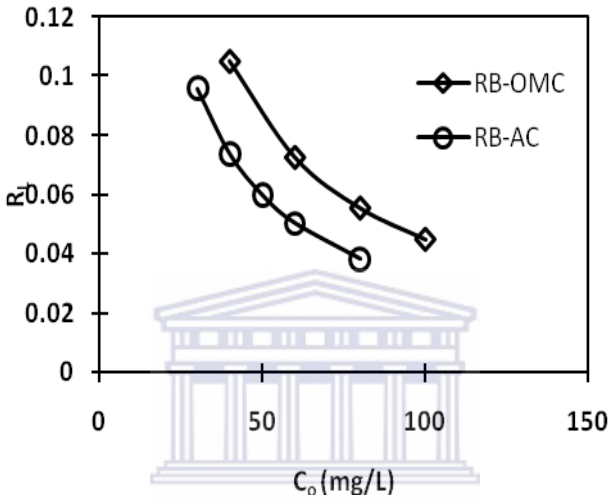

UNIVERSITY of the
WESTERN CAPE

Figure 5. 19: Separation factor for RB adsorption by OMC and AC.

Table 5.3 defines the types of isotherms associated with a specified value of R_L. R_L values of RB adsorption by OMC and AC are between 0 and 1, indicating favorable adsorption of RB by OMC and AC. Values of R_L were found to be between 0.04 and 0.097 for AC, whereas for OMC were between 0.045 and 0.15. Low values of R_L indicate a high and favourable solute/adsorbent adsorption process **[293, 296,297].** This further confirms that AC is more favourable for adsorption of RB dye than OMC under conditions used in this study. This could be attributed to the specific surface area of mesopores or pore volume which is higher in OMC compared to AC (see

Table 4.3). This confirms that OMC is more favourable for adsorption of RB dye than AC under conditions used in this study. This is contrary to the results obtained in Table 5.6 where adsorption of RB on AC seem to favour the Langmuir model. The larger pore size distribution of OMC compared to AC plays as significant role.

5.8. Conclusions

In order to ascertain surface properties of novel ordered mesoporous carbon (OMC), ordered mesoporous materials were probed with acid and basic dyes with the use of activated carbon (AC) as a base line material. Acid Orange 8 (AO8) as an anionic acidic dye, Methylene Blue (MB) as cationic basic dye, as well as Rhodamine B as a non-polar basic dye. Effect of pH, effect of dosage and adsorption equilibrium isotherms were investigated for all 3 dyes on both OMC and AC as mechanisms to obtain the surface properties of novel material OMC. Activated carbon (AC) and ordered mesoporous carbon (OMC) were successfully employed as adsorbents for quantitative removal of methylene blue, Acid Orange 8(AO8) and Rhodamine B from aqueous solution. OMC and AC were both found to be at a maximum pH of 2 , 6, and 7.5 for AO8, MB, and RB respectively. The maximum adsorbent dosage for RB adsorption for both OMC and AC was found to be similar (20 mg). Whereas, the maximum dosage for AO8 and MB adsorption for OMC was found to be 20mg. For AC the maximum dosage was found to be 30 mg and 25 mg for AO8 and RB respectively. The larger mass requirement by AC for adsorption of AO8 and MB compared to OMC is a result of lower specific

UNIVERSITY of the WESTERN CAPE

mesopore surface area of AC compared to OMC. OMC was found to have a trimodal pore size distribution with a larger pore volume of mesopores compared to AC. For AO8 OMC obeyed the Langmuir adsorption model and AC obeyed Freundlich adsorption model. For MB the OMC obeyed Freundlich adsorption model whereas AC obeyed the Langmuir adsorption model. However, for RB both OMC and AC followed only Langmuir adsorption model. The R_L values for AO8, MB and RB were found to be between 0 and 1 indicating that adsorption was favorable for the OMC and AC adsorbents. Hence, the novel OMC material exhibited similar surface properties to those of the well studied base line material (AC).

UNIVERSITY of the
WESTERN CAPE

CHAPTER 6

MERCURY ADSORPTION

6.1. INTRODUCTION

Mercury adsorption experiments were conducted on three different types of adsorbents namely; activated carbon (AC) ordered mesoporous carbon (OMC) and modified ordered mesoporous carbon (MOMC) in this chapter. Modification of ordered mesoporous carbon materials as adsorbents is described in Section 3.4.2. Modification was performed by adding 6 ml of 3-mercaptopropyltrithoxysilane to 50 mL stirred suspension containing nitric acid treated (see Section 3.4.1) OMC in reflux toluene and reflux under stirring was maintained for 24h. Modification was done in order to increase the binding efficiency i.e. to have high uptake capacity, quantitative uptake by all ligands and to obtain low levels of remaining Hg(II) in solution. Modification was also done to improve the selectivity of the binding process with respect to other metal ions in solution. On each adsorbent a series of experimental tests were done, monitoring the effect of the following key parameters on mercury adsorption; effect of pH, effect of adsorbent dosage, equilibrium adsorption isotherms and desorption studies. These experimental details are stipulated in Sections 3.6.7, 3.6.5 and 3.6.8. Results of these sets of tests are presented and discussed in Sections 6.2.1 to 6.2.5.

UNIVERSITY of the WESTERN CAPE

6.2. Mercury (II) Adsorption by MOMC, OMC and AC

6.2.1. Effect of pH

The pH studies presented in this section were carried out according to the procedure given in Section 3.6.1 and 3.6.2, to see the effect of pH on the adsorption of Hg(II) solutions containing 100 mg/L with a fixed quantity of modified ordered mesoporous carbon (MOMC), OMC (CA_SBA-15_LPG_105) and AC. The pH of the Hg (II) solution was adjusted to the desired values with 0.1 M Citric acid and 0.2 M phosphate solutions (Table: 3.3 and section 3.6.1). The experiments were conducted as described in Section 3.6.7 by shaking 0.01 g of MOMC, OMC and AC adsorbents with 50 ml of 100 mg/L Hg (II) solution for 24 h at 25 ºC. The determination of the uptake and percentage removal of Hg (II) in aqueous solution by MOMC, OMC and AC was performed using the procedure set out in Section 3.6.7 and the results shown in Figure 5.7; indicate that pH plays a significant role in the uptake of MOMC by OMC and AC.

UNIVERSITY of the WESTERN CAPE

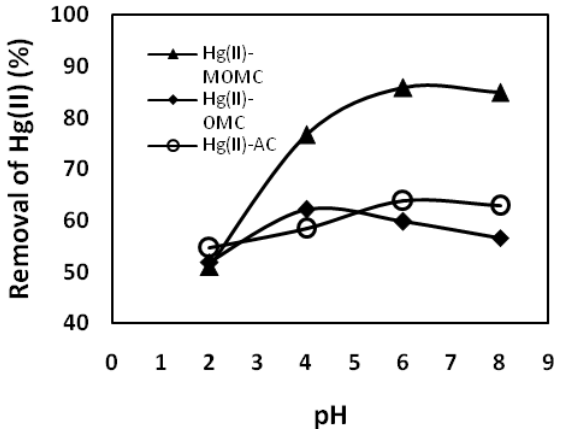

Figure 6. 1: Effect of pH on Hg(II) adsorption by MOMC,OMC and AC. Initial concentration of Hg(II), 100 mg/L; adsorbent dosage, 10 mg/50 mL, temperature, 25±2 ^{o}C; pH, 5.5; contact time, 24 h.

UNIVERSITY of the
WESTERN CAPE

Figure 6.1 shows the effect of pH on Hg (II) removal by adsorption. The adsorption of Hg (II) depends upon the nature of the adsorbent surface and the species distribution of Hg (II) in solution, which mainly depends on the pH of the system. The Hg (II) removal by carbon was observed over a range of initial pH values between 2 and 8. The percent of mercury removal by AC, OMC and MOMC adsorbents increases with increasing initial solution pH. The influence of initial pH on Hg (II) removal may be explained as follows: in the acidic condition, all adsorbents and the adsorbate are positively charged (M^{2+} and H^{+}) and therefore, the net interaction is that of electrostatic repulsion **[307]**. Besides, the higher concentration of H^{+} ions present in the reaction mixture competes with the positively charged Hg (II) ions for the surface adsorbing sites, resulting in a decrease in the removal of Hg (II). Kadirvelu et al **[308]**, reported similar results for the adsorption of Hg (II) from aqueous

solution by coir pith carbon. It is apparent from Figure 6.1 that the removal efficiencies of metal ions are affected by the initial metal ion concentration, with the removal efficiency decreasing as the metal ion concentration increases at constant pH. This can be explained as follows: at low metal/carbon ratio, the metal ion adsorption involves the high-energy sites. As the metal/carbon ratio increases **[308]**, the higher energy sites are saturated and adsorption begins on the lower energy sites, resulting in a decrease in adsorption efficiencies, as the pH curves are shifted to alkaline regions, as has been previously reported by several authors **[309, 310].** At a pH value of 6 maximum removal was observed, which might be due to partial hydrolysis of Hg (OH) and Hg $(OH)_2$. A pure carbon surface is considered to be non-polar, but in actual practice some carbon–oxygen complexes CxO, CO_x and CxO_2 are usually present. Since there is no satisfactory method for determining the polar characteristics of the surface quantitatively, the above statement is relative **[310].** As the initial metal ion concentration increases, the resultant equilibrium pH decreases. It can be concluded from these trends that as more metal ions are adsorbed onto the carbon, more hydrogen ions are released from the carbon into solution. The hydrogen ion sources are most likely the carboxylic, phenolic and lactonic groups in AC and OMC adsorbents. An additional sulfonic group to the carboxylic, phenolic and lactonic in the case of MOMC adsorbent is present. These groups are generally considered responsible for cation exchange capacity of carbon **[308].** On increasing the pH from 4, the percentage removal increased and became quantitative over the pH range 5.0–8.0. This implies that Hg(OH) species may be retained in

UNIVERSITY of the WESTERN CAPE

the micropores of carbon particles by chemisorption involving surface complexes **[310].**

As can be seen from Fig. 6.1 removal of Hg(II) by the adsorbents is the lowest at pH 2. Adsorption did not change significantly between pH 4 and 8. It was decided from the pH curve presented in Fig 6.1 that the optimum pH for adsorption of Hg(II) by the carbon adsorbents is 5.5. Namasivayan et al **[310]** and Kardiveli et al **[308]** also observed optimum pH in a similar range between pH 5 and pH 6. Hence, in this study dosage, equilibrium and desorption studies were performed at pH 5.5. OMC does not show a higher percentage Hg(II) removal adsorption capacity than AC due to its lower specific micropore surface area compared to AC. Whereas MOMC has the highest Hg(II) removal adsorption capacity due to the presence of the engrafted sulphur containing ligands which bind strongly to Hg(II) on the surface sites of MOMC.

UNIVERSITY of the WESTERN CAPE

6.2.2. Effect of Adsorbent Dosage

Adsorbent dosage is an important parameter in adsorption studies because it determines the capacity of adsorbent for a given initial concentration of metal or analyte in solution. In the adsorption of Hg(II) by MOMC, OMC and AC the optimum carbon dosage was chosen as 10 mg/50 mL.

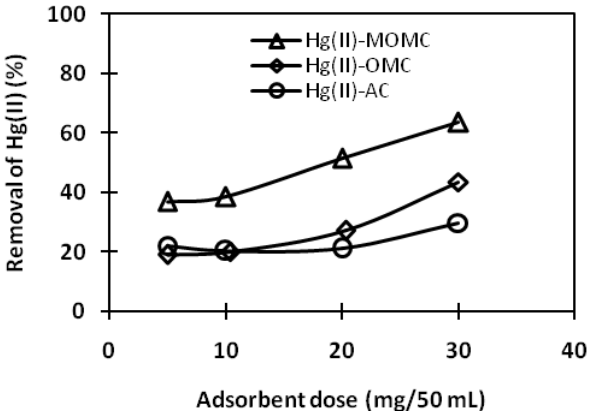

Figure 6. 2: Effect of carbon adsorbent dosage on Hg(II) adsorption by MOMC, OMC and AC. Initial concentration of Hg(II), 100 mg/L; adsorbent dosage, 10 mg/50 mL, temperature, 25±2 ^{o}C; pH, 5.5.

Figure 6.2 shows the removal of Hg(II) as a function of carbon dosage. Increasing carbon dosage increased the percent removal of Hg(II). For quantitative removal of Hg(II) from 50 ml of 100ml a maximum dosage of 30 mg is required. Namasivaya et al **[310]**, reported similar results with maximum dosage ranging between 25 mg to 30 mg in their study on uptake of Hg(II) from wastewater by activated carbon. MOMC show the highest percentage Hg(II) removal adsorption capacity than OMC and AC due to its specific mesopore surface area compared to AC. The highest Hg(II) removal adsorption capacity for MOMC is due to the presence of the engrafted sulphur containing ligands which bind strongly to Hg(II) on the surface sites of MOMC. The removal adsorption capacity of OMC is higher than AC due its higher specific surface area (see Table 4.3) of mesopores.

6.2.3. Adsorption Equilibrium Isotherms

Isotherms for Hg(II) adsorption by MOMC, OMC and AC were presented in Figure 6.3. Langmuir and Freundlich models were examined for their applicability to the experimental data.

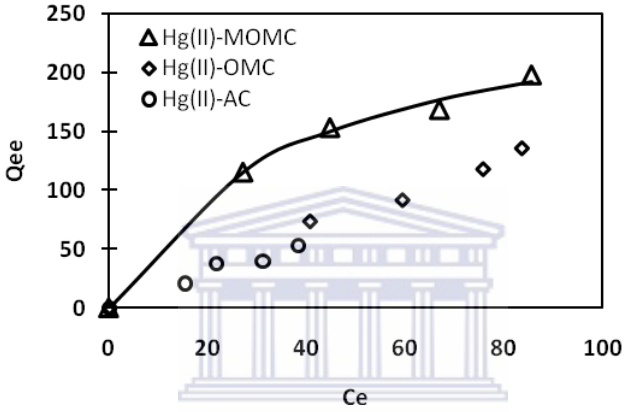

(a)

UNIVERSITY of the
WESTERN CAPE

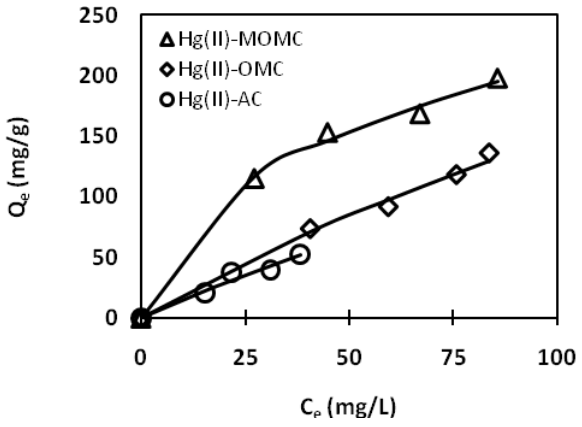

(b)

Figure 6. 3: Model and experimental equilibrium isotherms of Hg(II) adsorption by MOMC, OMC and AC. (a) The Langmuir (b) Freundlich plots (25±2 ^{o}C). Solid lines present the models.

Figure 6.3 shows model and experimental equilibrium isotherms of Hg(II) adsorption by MOMC, OMC and AC. Conformation of the experimental data with the Langmuir isotherm (Figure 6.3a) model for MOMC adsorbent indicates the homogeneous nature of the MOMC surface, i.e. each Hg(II) ion adsorption has equal adsorption activation energy, the results also demonstrate the formation of monolayer coverage of Hg(II) ion at the outer surface of MOMC. On the contrary to Hg(II) ion adsorption on OMC and AC adsorbents, conformation of the experimental data with the Langmuir isotherm (Figure 6.3a) model for OMC and AC adsorbent indicates a non-ideal sorption of Hg(II) ions on the OMC and AC surface.

UNIVERSITY of the
WESTERN CAPE

Figure 6.3(b) shows conformation of the experimental data with the Freundlich isotherm model for MOMC, OMC and AC adsorbents indicating an ideal sorption that involves heterogeneous sorption of Hg(II) ions on the MOMC, OMC and AC adsorbent surfaces. These results show that MOMC, OMC and AC adsorbents effectively uptake Hg(II) ions with Q_0 about 285.71 mg/g, 666,67 mg/g and 400.00 mg/g respectively. The experimental adsorption isotherms are generally Type I **[311]** and their linear plots (Figure 6.4) as stipulated in Equation 5.4 were used to calculate the monolayer capacity, Q_0, the Langmuir adsorption constant related to adsorption capacity; b; Freundlich constant related to the rate of adsorption; K_F, Freundlich constant incorporating the intensity of adsorption; n, and correlation coefficients; R^2, for both Langmuir and Freundlich isotherms and the actual values are specified in Table 6.1.

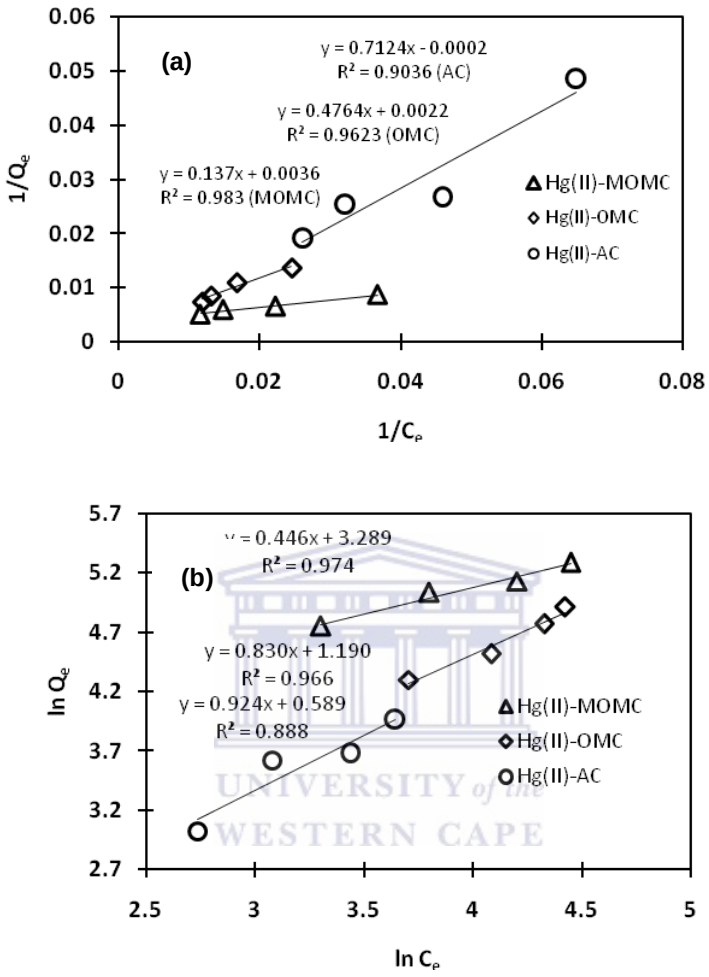

Figure 6. 4: Adsorption of Hg(II) by MOMC, OMC and AC. (a) The Langmuir on top (b) Freundlich plots at 25±2 ^{o}C and pH,5.5; contact time, 24h at bottom.

The model constants were calculated from Figure 6.4. The plot of $\frac{C_e}{q_e}$ against C_e in Figure 6.4(a) gave straight lines for all the concentrations; this implies that the adsorption for all adsorbents (MOMC, OMC, and AC) well fitted to Langmuir isotherm. The correlation coefficients, R^2, were found to be 0.9830

for MOMC and 0.9623 for OMC and 0.9036 for AC. Moreover, b , the Langmuir constant related to the rate of adsorption was found to be 0.0263, 0.0046 and 0.0039 L/mg for MOMC, OMC and AC respectively. Higher correlation coefficients (R^2) and higher rate constant (b) of adsorption for MOMC compared to OMC and AC (Table 6.1b) suggest that Hg(II) is favourably adsorbed by MOMC than OMC and AC. This suggest that adsorption isotherm of Hg(II) using AC gives a good fit to the Freundlich model compared to OMC And AC. Conformation of the experimental data with the Langmuir isotherm (Figure 6.3 (a)) model for MOMC adsorbent indicates the homogeneous nature of the MOMC surface, i.e. each Hg(II) ion adsorption has equal adsorption activation energy, the results also demonstrate the formation of monolayer coverage of Hg(II) ion at the outer surface of MOMC. However, OMC and AC showed non conformity to Langmuir model. This anomaly is further confirmed by lower values of b, the Langmuir constant related to the rate of adsorption for OMC and AC compared to that of MOMC (Table 6.1). According to Table 6.1 (a), OMC and AC have higher adsorption capacities compared to MOMC however OMC and AC have lower rates of adsorption (b) constants as previously stated. Indicating that the ligating MPTES group was highly effective in selectively adsorbing Hg(II) ions from solution. The mechanism of adsorption anticipated for OMC and AC could be chemisorption within the specific mesopores surface area.

UNIVERSITY of the WESTERN CAPE

The plot of $\ln Q_e$ against $\ln C_e$ in Figure 6.4 (b) gave straight lines for all the concentrations; this implies that the adsorption for all adsorbents (MOMC,

OMC and AC) fitted well to Freundlich isotherm. Freundlich constants (K_F and n) were calculated and recorded, which are listed in Table 6.1 (b). The greater the value of K_F the greater the affinity of the Hg(II) towards the adsorbent. MOMC has a significantly high K_F value compared to OMC and AC. This confirms that MOMC has high adsorption affinity for Hg(II). Whereas the degree of adsorption is almost the same in OMC and AC. The lower values of K_F for OMC and AC are indicative of the lower adsorption affinity for Hg(II). The value of $1/n < 1$ is an indication that the amount of Hg(II) adsorbed increases less rapidly than the concentration. The n values were found to be 2.2396, 1.2044 and 1.0819 respectively for MOMC, OMC and AC. According to Treybal **[312]**, the n values between 1 and 10 represent beneficial adsorption.

UNIVERSITY of the
WESTERN CAPE

Table 6. 1: The model constants for Hg(II) adsorption by MOMC, OMC and AC (a) Langmuir model (b) Freundlich model

(a)

Adsorbent	Langmuir model $\frac{1}{Q_e} = \frac{1}{Q_o} + \frac{1}{bQ_oC_e}$		
	Q_o (mg/g)	b (L/mg)	R^2
MOMC	277.78	0.0263	0.9830
OMC	454.55	0.0046	0.9623
AC	400	0.0039	0.9036

UNIVERSITY of the WESTERN CAPE

(b)

Adsorbent	Freundlich model		
	K_F [(mg/g)*(mg/L)^n]	n	R^2
MOMC	26.82	2.2396	0.9747
OMC	3.29	1.2044	0.9669
AC	1.80	1.0819	0.8886

The high correlation coefficient, R^2 for MOMC (R^2 = 0.9747), indicate a strong agreement to Freundlich isotherm as further confirmed by a significantly high K_F values. Whereas low correlation coefficient for and OMC (R^2 = 0.9669) and AC (R^2 = 0.8886) indicate poor agreement of Freundlich isotherm with experimental data as further confirmed by K_F values. The Langmuir model constants and correlation coefficients were given in Table 6.1. The above results show that MOMC obeys both Langmuir and Freundlich isotherm whereas OMC and AC obey only the Freundlich isotherm for Hg(II) adsorption.

The essential characteristics of the Langmuir equation can be expressed in terms of a dimensionless separation factor, RL, as defined in equation 5.5.

UNIVERSITY of the
WESTERN CAPE

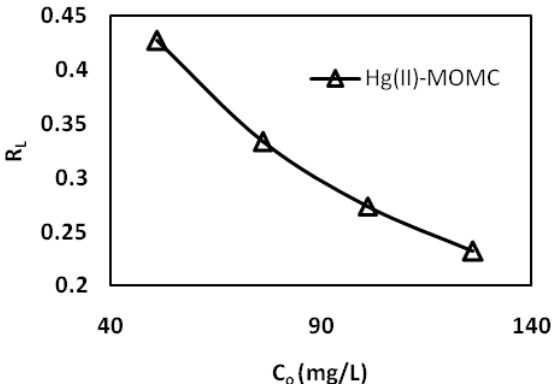

Figure 6. 5: Separation factor for Hg(II) adsorption by MOMC.

Separation factor R_L values were calculated at different Hg(II) initial concentrations and the results were presented in Figure 6.5 for adsorption of Hg(II) by MOMC. R_L values are between 0 and 1, suggesting favorable Hg(II) adsorption by MOMC **[310].**

6.2.4. Desorption of Hg(II)

Desorption studies help elucidate the mechanism of adsorption and recover precious metals from wastewater and adsorbent as to well as recover Hg (II) from the spent adsorbent apart from protecting the environment from solid waste disposal problems. Attempts were made to desorb Hg (II) from the metal loaded MOMC, OMC and AC using various ionic strengths adjusted with 2 % KI. Desorption of Hg(II) from carbon samples was made by shaking Hg(II) adsorbed samples in KI solutions for 1 h.

UNIVERSITY of the
WESTERN CAPE

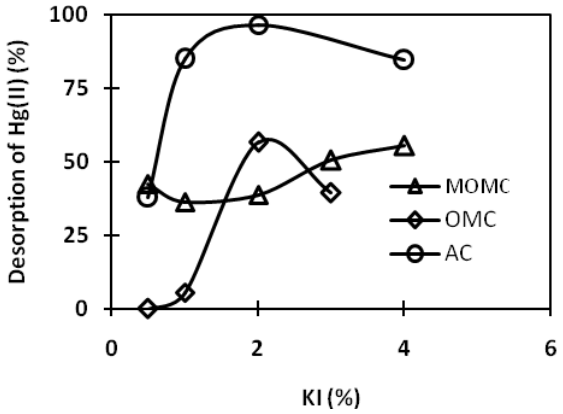

Figure 6. 6: Desorption of Hg (II) by MOMC, OMC and AC.

As shown in Figure 6.6 the maximum desorption obtained with KI was 97%, 57% and 39% for AC, OMC and MOMC respectively using 2% KI solution. The higher desorption of Hg (II) by iodide is due to the formation of relatively more soluble iodide complexes **[313].** The fact that only partial or incomplete Hg (II) desorption was achieved shows that ion exchange is not the only mechanism involved in this study. Other mechanisms, such as hydrolysis/precipitation or chemisorptions might also be responsible for the adsorption of Hg (II) on the adsorbents **[308, 310].** It could be deduced that the lowest Hg(II) desorption observed for MOMC is attributed to MPTES ligating groups which are strongly bonded to Hg(II) on the MOMC surface.

6.3. Conclusion

UNIVERSITY of the
WESTERN CAPE

Removal of Hg(II) from aqueous solution by MOMC, OMC and AC is influenced by effect of pH, effect of dosage, adsorption equilibrium isotherms. The role of sulphur containing ligands (MPTES) for both Hg (II) adsorption and desorption studies was investigated. The optimum pH conditions for the removal of Hg(II) were discovered at pH 5.5 which was substantially supported by literature. Increasing carbon dosage increased the percentage removal of Hg(II) from solution. For quantitative removal of Hg(II) adsorbate solution a maximum dosage of 30 mg was achieved in this study. MOMC obeyed both Langmuir and Freundlich isotherm whereas OMC and AC followed only the Freundlich isotherm for Hg(II) adsorption. MOMC had a significantly high K_F value compared to OMC and AC. This confirmed that

MOMC has high adsorption affinity for Hg(II). OMC and AC have higher adsorption capacities compared to MOMC however OMC and AC were found to have lower Langmuir rates of adsorption (b) constants indicating that the ligating MPTES group was highly effective in selectively adsorbing Hg(II) ions from solution. Desorption studies revealed that maximum desorption of Hg(II) ions obtained were 97%, 57% and 39% for AC, OMC and MOMC adsorbents respectively using 2% KI solution. The lowest Hg(II) desorption observed for MOMC was attributed to MPTES ligating groups which could be strongly bonded to Hg(II) on the MOMC surface thereby resisting detachment of the Hg (II) ions. Hence a novel adsorbent for removal of Hg(II) from water was effectively developed by modification of OMC with MPTES.

UNIVERSITY of the
WESTERN CAPE

CHAPTER 7

CONCLUSIONS AND RECOMMENDATIONS

7.1. General Conclusions

Highly selective novel mesoporous adsorbents for effective removal of Hg(II) ions from wastewater were successfully synthesised. By utilisation of ordered mesoporous silica (OMSi) material as sacrificial templates ordered mesoporous carbon (OMC) material were obtained. These OMC products were of multiphase character consisting of islands of SiO_2 and were not composed of 100% carbon content. The following schematic diagram (Figure 7.1) represent a summary of the synthetic route taken for OMC synthesis from OMSi. These carbon analogues were found to have higher surface areas than their silica precursor templates, and well defined pore structures. The non catalytic LPG carbonization procedure used was of advantage, as uniform infiltration of the carbon precursor can be easily accomplished inside the silica mesopores so that the resultant carbon materials retain the mesostructural order of the silica templates.

UNIVERSITY of the
WESTERN CAPE

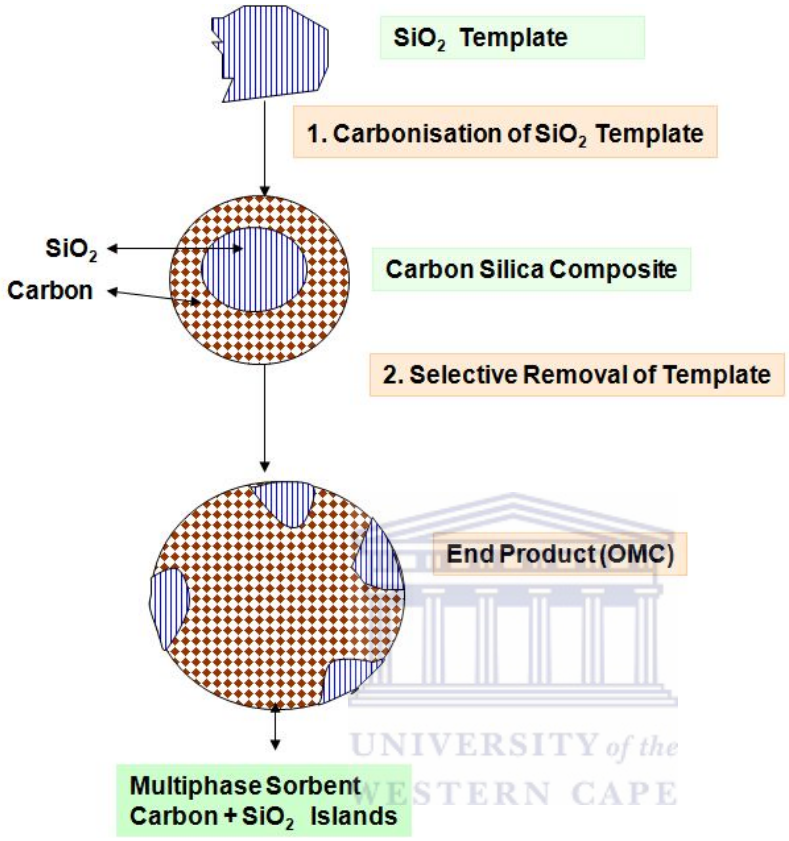

UNIVERSITY of the WESTERN CAPE

Figure 7. 28: Schematic diagram for synthesis of OMC from OMSi.

In principle the ordered mesoporous silica (SBA-15 HMS and MCM-41) materials and ordered mesoporous carbons (CA_SBA-15_LPG_105, CA_HMS_LPG_80 and CA_MCM-41_LPG_80) show similar crystal morphology, which indicates the following two important points:

(i) SBA-15 HMS and MCM-41 play a role as a templates or “skeleton”, as carbons are formed inside the pore system of the crystal without serious

damage to the mesoporous material due to precipitation on the external surface and

(ii) The mesoporous carbons can keep the same structural order/organization after dissolution of the silica template.

Furthermore, it has been shown that by varying pyrolysis time, mesoporous carbons with different pore sizes and surface areas can be obtained, with the pores formed within the parent SBA-15 HMS and MCM-41 framework dependent on the Temperature (800 ^{0}C) applied during pyrolysis. The Raman, XRD, TGA, HRTEM, EELS, and SAED techniques illustrate that the LPG successfully infiltrated the template, and was thermally decomposed to a crystalline, graphitic form of carbon, which formed an independent and structurally robust mesoporous material after removal of the silica template.

UNIVERSITY of the
WESTERN CAPE

The XRD pattern as well as the BET adsorption indicates a high degree of mesostructural ordering in the parent silica templates synthesized hydrothermally. The nitrogen sorption data confirms that the silica templates possessed good mesostructural ordering and was therefore suitable for use as a solid template for mesoporous carbon synthesis. BET data also showed that the carbon analogues were highly porous and exhibited larger surface areas exceeding that of the parent silica sacrificial templates. The apparently regular mesostructure of the carbons could be further supported by the appearance of the new XRD peaks at 7.39 and 12.64 ^{0} 2 θ that may indicate that there is a regular carbon framework at 11.6 and 6.8 Å d spaced distances. This is a novel finding and has not been previously reported for carbon analogues synthesized from SBA-15 and MCM-41 as sacrificial

templates. Moreover the large mass loss obtained by TGA at 550 ^{0}C may indicate that most of the carbon analogue comprise of the graphitic carbon. This is further supported by clear graphite XRD peaks in the region 26.11^0 2 θ and 43.54^0 2 θ and also by Raman spectroscopy. This degree of graphitization in a mesoporous analogue has also not previously been reported for carbon analogues synthesized from SBA-15 and MCM-41 as sacrificial templates.

The EDS data indicated that a small concentration of the silica template or "silica islands" material are still present in the resultant carbon materials, and was not completely dissolved during template etching with NaOH solution. These "silica islands" were used as ligating groups during the modification steps of OMC with an organic ligand, 3-mercaptopropyltriethoxysilane as a grafting agent. This is further confirmed by FTIR data which indicated that the silica groups of MPTES had been successfully introduced to the silica islands as well as on carbonyl groups of the OMC surface during modification process, which generated new sites for Hg(II) adsorption.

UNIVERSITY of the
WESTERN CAPE

In order to ascertain surface properties of novel ordered mesoporous carbon (OMC), ordered mesoporous materials were probed with acid and basic dyes with the use of activated carbon (AC) as a base line material. Acid Orange 8 (AO8) as an anionic acidic dye, Methylene Blue (MB) as cationic basic dye, as well as Rhodamine B as a non-polar basic dye. Effect of pH, effect of dosage and adsorption equilibrium isotherms were investigated for all 3 dyes on both OMC and AC as mechanisms to obtain the surface properties of novel

material OMC. Activated carbon (AC) and ordered mesoporous carbon (OMC) were successfully employed as adsorbents for quantitative removal of methylene blue, Acid Orange 8 (AO8) and Rhodamine B from aqueous solution. OMC and AC were both found to be at a maximum pH of 2 , 6, and 7.5 for AO8, MB, and RB respectively. The maximum adsorbent dosage for RB adsorption for both OMC and AC was found to be similar (20 mg). Whereas the maximum dosage for AO8 and MB adsorption for OMC was found to be 20mg. For AC the maximum dosage was found to be 30 mg and 25 mg for AO8 and RB respectively. The larger mass requirement by AC for adsorption of AO8 and MB compared to OMC is a result of lower specific mesopore surface area of AC compared to OMC. OMC was found to have a trimodal pore size distribution with a larger pore volume of mesopores compared to AC. For AO8 OMC obeyed the Langmuir adsorption model and AC obeyed Freundlich adsorption model. For MB the OMC obeyed Freundlich adsorption model whereas AC obeyed the Langmuir adsorption model. However, for RB both OMC and AC followed only Langmuir adsorption model. The R_L values for AO8, MB and RB were found to be between 0 and 1 indicating that adsorption was favorable for the OMC and AC adsorbents. Hence, the novel OMC material exhibited similar surface properties to those of the well studied base line material (AC).

UNIVERSITY of the
WESTERN CAPE

Removal of Hg(II) from aqueous solution by MOMC, OMC and AC is influenced by effect of pH, effect of dosage, adsorption equilibrium isotherms. The role of sulphur containing ligands (MPTES) for both Hg (II) adsorption and desorption studies was investigated. The optimum pH conditions for the removal of Hg(II) were discovered at pH 5.5 which was substantially

supported by literature. Increasing carbon dosage increased the percentage removal of Hg(II) from solution. For quantitative removal of Hg(II) adsorbate solution a maximum dosage of 30 mg was achieved in this study. MOMC obeyed both Langmuir and Freundlich isotherm whereas OMC and AC followed only the Freundlich isotherm for Hg(II) adsorption. MOMC had a significantly high K_F value compared to OMC and AC. This confirmed that MOMC has high adsorption affinity for Hg(II). OMC and AC have higher adsorption capacities compared to MOMC however OMC and AC were found to have lower Langmuir rates of adsorption (b) constants indicating that the ligating MPTES group was highly effective in selectively adsorbing Hg(II) ions from solution. Desorption studies revealed that maximum desorption of Hg(II) ions obtained were 97%, 57% and 39% for AC, OMC and MOMC adsorbents respectively using 2% KI solution. The lowest Hg(II) desorption observed for MOMC was attributed to MPTES ligating groups which could be strongly bonded to Hg(II) on the MOMC surface thereby resisting detachment of the Hg (II) ions. Hence a novel adsorbent for removal of Hg(II) from water was effectively developed by modification of OMC with MPTES.

UNIVERSITY of the
WESTERN CAPE

7.2. Recommendation and future work

Modified and unmodified ordered mesoporous carbon and activated carbon could be applied for removal of mercury from water. In this study, greater mercury adsorption efficiency was achieved by modified mesoporous carbon (OMC). In future, MOMC and OMC should be used to treat mercury contaminated industrial wastewater or real brine solutions with the view of analyzing their performance on adsorption of other heavy metals or major elements. Column studies should also be pursued. Most industrial applications of adsorption processes are usually implemented in the continuous column operation with the capacity of treatment and the recovery factors in mind. These parameters are normally determined by the type of adsorbent, the equilibration time (kinetics), the size of the column and the break through curves.

UNIVERSITY of the
WESTERN CAPE

CHAPTER 8

REFERENCES

[1] Fyte, C.A., Gies, H., Kokotailo, G.T., Marler, B., and Cox, D.E., *J. Phys. Chem.*, **94** (1990) 3718.

[2] Zhang, W., Pauly, T.R., Pinnavaia, T.J., Tailoring the Framework and Textural Mesopores of HMS Molecular Sieves through an Electrically Neutral (S°I°) Assembly Pathway. *Chem. Mater.,* **9** (1997) 2491-2498

[3] An-Hui Lu, Wen-Cui Li, Wolfgang Schmidt, Ferdi Schuh., Template synthesis of large pore ordered mesoporous carbon. *Microporous and Mesoporous Materials* **80** (2005) 117–128.

[4] Hansen, E.W., Courivard. F., Karlsson, A., Kolboe, S., Stocker, M., Effect of pore dimension and pore surface hydrophobicity on the diffusion of n-hexane confined in mesoporous MCM-41 probed by NMR – a preliminary investigation. *Microporous and Mesoporous Materials* **22** (1998) 309–320.

[5] Pereira L.S., Cordery, I., and Iacovides, I., 2002. *Coping with water scarcity.* No. 58. Paris: UNESCO.

[6] Rijsberman, F.R., 2006. Water scarcity: Fact or fiction? *Agricultural Water Management,* **80**(1-3), 5-22.

UNIVERSITY of the WESTERN CAPE

[7] Bell, F.G., Bullock, S.E.T., Halbich, T.F.J. and Lindsay, P., Environmental impacts associated with an abandoned mine in the Witbank Coalfield, South Africa. *International Journal of Coal Geology,* **45** (2001) 195-216.

[8] Schoeman, J.J. and Steyn, A.,. Investigation into alternative water treatment technologies for the treatment of underground mine water discharged by Grootvlei Proprietary Mines Ltd into the Blesbokspruit in South Africa. *Desalination,* **133** (2001) 13-30.

[9] Basson, M.S., Van Niekerk, P.H., and Van Rooyen, J.A., 1997. Overview of Water Resources Availability and Utilisation in South Africa. Department of Water Affairs and Forestry, Pretoria. 72.

[10] Zamxaka. M., and Riley. J.,(2010). Nanotechnology's campainge for safe drinking water. Nanotechnology public engagement.

[11] Water sewage and effluent, water management solutions for Africa. 2011, vol 31, no1.

[12] Oehmen, A., Viegas, R., Velizarov, S., M.A. M. Reis, M.A. M., Crespo, J.G., Removal of heavy metals from drinking water supplies through the ion exchange membrane bioreactor. *Desalination*, **199** (2006) 405–407.

[13] Baeyens, R., Ebinghous, R., Vasilev, O., 1996. Global and Regional Mercury Cycles: Sources, Fluxes and Mass Balances. Kluwer Academic Publishers.

UNIVERSITY of the WESTERN CAPE

[14] Morimoto, T., Wu, S., Azhar Uddin, Md., Sasaoka, E.,. Characteristics of the mercury vapor removal from coal combustion flue gas by activated carbon using H_2S. *Fuel* **84** (2005) 1968 - 1974.

[15] Yardim, M.F., Budinova, T., Ekinci, E., Petrov, N., Razvigorova, M., Minkova, V., 2003. Removal of mercury(II) from aqueous solution by activated carbon obtained from furfural. *Chemosphere* **52**, 835 - 841.

[16] Namasivayam, C., Kadirvelu, K., 1999. Uptake of mercury (II) from wastewater by activated carbon from an unwanted agricultural solid by-product:coirpith. *Carbon* **37**, 79 - 84.

[17] Mohan, D., Gupta, V.K., Srivastva, S.K., Chander, S., 2001. Kinetics of mercury adsorption from wastewater using activated carbon derived from fertilizer waste. *Colloid. Surface. Physicochem. Eng. Aspect.* **117 (**2001) 169 -181.

[18] Krishnan, K.A., Anirudhan, T.S.,. Removal of cadmium(II) from aqueous solutions by steam activated sulphurised carbon prepared from sugar-cane bagasse pith: kinetics and equilibrium studies. *Water SA*., **29** (2003) 147.

[19] Kannan, N., Malar, S.J.S., Removal mercury (II) ions by adsorption onto dates nut and commercial activated carbons: a comparative study. *Indian J. Chem. Technol*. **12** (2005) 522 - 527.

[20] Spiro, T.G., Stagliani, T.G., *Chemistry of the Environment,* Prentice Hall, NewYork, 1996.

[21] Hutchison, A.R., Atwood, D.A. J. Chem. Crystallogr. **33** (2003) 631.

[22] Morita, M., Yoshinga, J., Edmonds, J.S. *Pure Appl. Chem*. **70** (1998) 1585.

UNIVERSITY of the
WESTERN CAPE

[23] Timerbaev, A.R. Talanta **52**, (2000), 573-606.

[24] Kuban, P., Hauser, P.C., Kuban, V. *Electrophoresis* **28**, (2007), 58-68.

[25] Hutchison, A.R., Atwood, D.A. *Journal of Chemical Crystallography* **33** (2003), 631-645.

[26] UNEP Global Mercury Assessmant Revised Draft July 2002, Geneva Switzerland

[27] Leermakers, M., Baeyens, W., Horvat, M. Trends in Analytical Chemistry **24**, (2005), 353- 360.

[28] Choi, S.C., Chase, T., Bartha, R. *Applied Environmental Microbiology*., **60**, (1994), 1342.

[29] Clarkson, T.W., Environmental Health Perspectives **100**, (1992), 31-38.

[30] Rabenstein, D.L., *Journal of Chemical Education* **55**, (1978), 292-296.

[31] Pycyna, J.M., Pacyna, E.G., Steenhuisen, F., Wilson, S. *Atmospheric Environmental* **37**, (2003), 109-117.

[32] Morita, M., Yoshinga, J., Edmonds, *J. Pure & Appl. Chem*., **70**, 1998, 1585-1615.

[33] Bailey, S.E. Olin, T.J., Bricka, R.M., Adrian, D.D. A review of potentially low-cost sorbents for heavy metals., *Wat. Res*. **33** (1999) 2469 – 2479.

[34] Bansal, R.C., Goyal, M., (2005), Activated carbon adsorption. 67-123

UNIVERSITY of the
WESTERN CAPE

[35] Fryxell, G.E., Cao, G., (2007), Environmental applications of nanomaterials. 241 -274

[36] Sing, K.S.W., Everett, D.H., Haul, R.H.W., Moscou, L., Pierotti, R.A., Rouquerol, J., and Siemieniewska, T., *Pure Appl. Chem.*, **57** (1985) 603.

[37] Bansal, R.C., Vastola, F.J., Walker, P.L., *Jr., Colloid and interface, colloid and interface Sci*., **32** (1970) 187.

[38] Bansal, R.C., Vastola, F.J., Walker, P.L., *Jr., Carbon*, **8** (1970) 113.

[39] Bansal, R.C., Vastola, F.J., Walker, P.L., *Jr., Carbon*, **9** (1971) 185.

[40] Langmuir, I., *J. Am. Chem. Soc*., **40** (1361) 1918.

[41] Brunauer, S., in The Adsoprtion of Gases and Vapors, Princeton Unv. Press, Princeton, 1943.

[42] Young, D.M., Crowell, A.D., in physical Adsorption of Gases, Butterworth, London, 1962.

[43] Dacey, J.R., Thomas, D.G., *Trans. Faraday Soc*., **50** (1954) 740,

[44] Culver, R.E., Heath, N.S., *Trans. Faraday Soc*., **51** (1955) 1569,1575,

[45] Tittof, A., Z*. Phys. Chem*., **74**, 650, 1910

[46] Langmuir, I., *J. Am. Chem. Soc*., **40** (1918)1361,

[47] Freundlich, H., Adsorption. *Journal of Physical Chemistry,* **7** (1926), 57-64.

[48] Leppert D. (1990) Heavy metal sorption with clinoptilolite zeolite: alternatives for treating contaminated soil and water. Mining Eng. **42** (6), 604 - 608.

UNIVERSITY of the
WESTERN CAPE

[49] Ming D. W. and Dixon J. B. Quantitative determination of clinoptilolite in soils by a cation-exchange capacity method. *Clays Clay Miner*. **35** (1987) 463-468.

[50] Grover M. and Narayanaswamy M. S. (1982) Removal of hexavalent chromium by adsorption on Flyash. J. Inst.Eng. (India) Environ. Eng. Div. EN 1 63, 36-39.

[51] Kapoor A. and Viraraghavan T. Treatment of metal industrial wastewater by fly ash and cement fixation. *J. Environ. Eng. ASCE* **122** (1996) 243.

[52] Banerjee K., Cheromisino P. N. and Cheng S. L. Adsorption kinetics of o-xylene by fly ash. Water Res **31** (1997) 249-261.

[53] Srivastava S. K., Singh A. K. and Sharma A. Studies on the uptake of lead and zinc by lignin obtained from black liquor a paper industry waste material. *Environ. Technol*., **15** (1994), 353-361.

[54] Masri M. S. and Friedman M. Effect of chemical modification of wool on metal ion binding. *J. Appl.Polymer Sci*. **18** (1974) 2367-2377.

[55] Berkeley R. C. W. (1979) Chitin, Chitosan and Their Degradative Enzymes. In Microbial Polysaccharides,eds. R. C. W. Berkeley, C. W. Gooday and D. C.Elwood, pp. 205-236. Academic Press. New York.

[56] Chang, K.; Tsai, G.; Lee, J.; Fu, W. Heterogeneous *N*Deacetylation Of Chitin In Alkaline Solution; *Carbohydrate Research;* **303** (1997) 328.

[57] No, H.; Meyers, S.; Muzzarelli, R. (Editors); 1997; Preparation Of Chitin and Chitosan; Chitin Handbook; European Chitin Society; 485

UNIVERSITY of the
WESTERN CAPE

[58] Yang T. C. and Zall R. R. (1984) Absorption of metals by natural polymers generated from seafood processing wastes. Ind. Eng. Chem. Prod. Res. Dev. **23**, 168-172.

[59] Hsien T.Y. and Rorrer G. L. Efects of acylationand crosslinking on the material properties and cadmium ion adsorption capacity of porous chitosan beads. Separ. Sci. Technol. **30** (1995) 2455-2475.

[60] Babel, S., Kurniawan, T.A., Low cost adsorbents for heavy metals uptake from contaminated water: Review, *Journal of hazardous Materials*, **97** (2003) 219-243.

[61] Kwon J.H., (2007), M.Sc thesis Sorption studies of the surface modified activated carbon with β- Cyclodextrin. University of Saskatchewan.

[62] Izotova T.I, Dubini M.M., Zh. *Fiz. Khim*., **39** (1965) 2796.

[63] Dubinin M.M., Nikolaev K.M., Petukhova G.A., and Polyakov N.S., Izv.Akad., Nauk SSSR., *Ser Khim*., **1** (1991) 35.

[64] Garten V.A and Weiss D.E., *Revs. Pure Appl. Chem*., **7** (1957) 69

[65] Watt J.D., Franklin R.E., Industrial carbon and graphite, Soc. Chem. Ind., London 1958, p-32

[66] Harker H., Marsh H., and Wynne-Jones W.F.K., Chemisorption, Proceeding of a symposium held at Kele in 1956, Butterworths, London p-25

[67] Juza R., Luble H. and Heinlein, Z. *Anorg. Chem*., **258** (1949) 105.

[68] Khan M.A., Kemp W., *J.Chem. Soc. Pak*., **5** (1983) 35 .

[69] Kerner T.C., and Zhou D., Environ.Prog. **9** (1990) 40.

UNIVERSITY of the WESTERN CAPE

[70] Bedgar G., Orbach H.K., and Riesenfeld, *Ind. Eng. Chem*., **50** (1958)1165

[71] Tonge B.L., Proceeding of 4th conference on Carbon, Pergamon Press Inc., London 1960, p-87

[72] Mochida I. and Kawano, *Ind. Eng. Chem. Res*. **30** (1991) 2322.

[73] Glass A.S., and M.D.J. Low, *Spectrosc. Lett.*, **19** (1986) 397.

[74] Morterra C., and Low M.D.J., Spectrosc. Lett., **15** (1982) 689.

[75] Crawford V.A., Quart. Rev., **14** (1960) 378.

[76] Little L.H., Infra-red Spectra of adsorbed species" Academic Press, London, New York, 1966

[77] O'Reilly D.E., Advances in Catalysis XII, Academic Press, New York, 1960,p-31

[78] Thompson J.K., Krebs J.J., and Resing H.A., *L. Chem. Phys*. **43** (1965) 3853.

[79] Mattson J.S., Mark jr H.B., Malbin M.D., Weber Jr. W.J., and Crittennden J.C*., J. Colloid Interface Sci*., **31** (1969) 116.

[80] Youssef A.M., ElShobaky G.A., and El-Nabarawy T., Surf. Technol., **7** (1978) 451.

[81] Radeke K.H., and Neffe S., *Chem. Tech*. *Liepzig*, **41** (1989) 32.

[82] Opplod. W.A., 44th Water Pollution Control Fed. Conf. San Fransisco CA, Oct 5 (1971).

[83] Thiem. L., Badoreck. D., O' Conner. J.T.,. *J. Am. Water Works Assoc*., **68** (1997) 447

[84] Homerick, M.J., Jnr and Schoor J.L., *J. Am. Soc. Environ. Eng. Div*., **100** (1974) 1249

UNIVERSITY of the WESTERN CAPE

[85] Lopez- Gonzalez J.D., Moreno-Castilla C., Guerrero Ruiz A, Rodriguez-Reinoso F, *J. Chem. Technol. Biotechnol*. **32** (1982) 575,

[88] Jayson GG, Lowless TA, Farihurst D, *J. Coll. Interface. Sci*. **86** (1982) 397.

[89] Periasamy K., and Namasivayam C., *Chemosphere* **32** (1996) 769.

[90] Zhang, W., Pauly, T.R., Pinnavaia, T.J., Tailoring the Framework and Textural Mesopores of HMS Molecular Sieves through an Electrically Neutral (S°I°) Assembly Pathway. *Chem. Mater.* **9** (1997) 2491-2498.

[91] An-Hui Lu, Wen-Cui Li, Wolfgang Schmidt, Ferdi Schuth., Template synthesis of large pore ordered mesoporous carbon. *Microporous and Mesoporous Materials* **80** (2005) 117–128.

[92] Hansen, E.W., Courivard. F., Karlsson, A., Kolboe, S., Stocker, M., Effect of pore dimension and pore surface hydrophobicity on the diffusion of n-hexane confined in mesoporous MCM-41 probed by NMR – a preliminary investigation. *Microporous and Mesoporous Materials* **22** (1998) 309–320.

[93] Godongwana, Z.G., 2006 M.Sc thesis, Homogeneity of nanophase electrocatalysts supported on mesoporous materials, University of the Western Cape.

[94] Ndungu, P., Godongwana, Z.G., Petrik, L.F., Nechaev, A., Liao, S., Linkov, V., Synthesis of carbon nanostructured materials using LPG *Microporous and Mesoporous Materials* **116** (2008) 593–600.

UNIVERSITY of the
WESTERN CAPE

[95] Petrik L.F., Godongwana, Z.G., Iwuoha, E.I., Platinum nanophase electro catalysts and composite electrodes for hydrogen production, *Journal of Power Sources*. **185** (2008) 838–845.

[96] Petrik, L.F., 2002 M.Sc thesis, Nanophase composite catalysts for electrosynthesis, University of the Western Cape.

[97] Al-Othman, Z. A., 2006 PhD thesis, King Saud University (KSU) Synthesis, Modification, and Application of mesoporous materials based on MCM-41. King Saud University (KSU)

[98] Ciesla, U., Schuth, F., *Microporous and Mesoporous Mater*. **27** (1999) 131.

[99] Ying, J.Y., Mehnert, C.P., Wong M.S., *Angew. Chem. Int*. Ed. **38** (1999) 56.

[100] Huo, Q., Margolese, D.I., Ciesla, U., Feng, P., Gier T.E., Sieger, P., Leon, P., Petroff, P.M., Schuth, F., and Stucky, G.D., *Nature* **368** (1994) 317.

[101] Van Bekkum, H., Flanigen, E.M., Jacobs, P.A., Jansen (eds), J.C., Introduction to Zeolite Science and practice (Elsevier, Amsterdam, 2001).

[102] Kinoshita, K., Carbon (Wiley interscience publication, New York, 1988)

[103] Breck, D.W., "*Zeolites Molecular Sieves*" Wiley, New York (1974).

[104] Szostak, R., "*Molecular Sieves: Principles of Synthesis and Identification*" Van Nostrand Reinfold, New York (1989).

[105] Wilson, S.T., Lok, B.M., and Flanigen, E.M., *U.S. Pat*., 4, 310, 440 (1982)

UNIVERSITY of the
WESTERN CAPE

[106] Davis, M.E., Saldarriaga, C., Montes, C., Garces, J.M., and Crowder, *J.A., Nature*, **331** (1988) 698.

[107] Estermann, M., McCusker, L.B., Baerlocher, C., Merrouche, A., and Kessler, H., *Nature*, **352** (1991) 320.

[108] Jones, R.H., Thomas, J.M., Chen, J., Xu, R., Huo, Q., Li, S., Ma, Z., and Chippindale A.M., *J. Solid State Chem.*, **102** (1993) 204.

[109] Freyhardt, C.C., Tsapatsis, M., Lobo, R.F., Balkus Jr., K.J., and Davis, M.E., *Nature,* **381** (1995) 369.

[110] Zhao, X.S., (Max) Lu, G.Q., and Miller, G.J., *Ind. Eng. Chem. Res.*, **35** (1996) 2075.

[111] Meier, W.E., and Olson, D.H., *Atlas of Zeolite structure Types;* Butterworth-Heinemann, London, (1987).

[112] Lok, B.M., Messina, C.A., Lyle Patton, R., Gajek, R.T., Cannon T.R., Wilson, S.T., and Flanigen, E.M., *J. Am. Chem. Soc.*, **106** (1984) 6092.

[113] Schlenker, J.L., Rohrbaugh, W.J., Chu, P., Valyocsik, E.W., and Kokotailo, G.T., *Zeolite*, **5** (1985) 355.

[114] Van Koningsveid, H., Jansen, J.C., and van Bakkum, H., *Zeolite*, **10** (1990) 235.

[115] Olson, D.H., *J. Phys. Chem.*, **74** (1970) 2758.

[116] Bialek, R., Meier, W.M., and Davis, M.E., *Zeolite*, **11** (1991) 438.

[117] Fyte, C.A., Gies, H., Kokotailo, G.T., Marler, B., and Cox, D.E., *J. Phys. Chem.*, **94** (1990) 3718.

[118] Dessau, R.M., Schlenkar, J.L., and Higgins, J.B., *Zeolite*, **10** (1990) 522.

UNIVERSITY of the
WESTERN CAPE

[119] Iler, R.K., *The Chemistry of Silica*; J. Wilwy & Sons, Inc., 1979.

[120] Wefers, K., and Misra, C., *Oxides and Hydroxides of Aluminium*; Alcoa Technical Paper No. 19, Revised, Alcoa Laboratories, 1987.

[121] Pinnavaia, T.J., *Science*, **220** (1983) 365.

[122] Yanagisawa, T., Schimizu, T., Kuroda, K., Kato, C., *Bull. Chem. Soc. Japan*., **63** (1990) 988.

[123] Corma, A., Pérez-Pariente, J., Fornés, V., Rey, F., and Rawlence, D., *Appl. Catal.*, **63** (1990) 145.

[124] Kresge, C.T., Leonowicz, M.E., Roth, W.J., and Vartuli, J.C., *U.S. Patent*, 5,098,684 (1992).

[125] Kresge, C.T., Leonowicz, M.E., Roth, W.J., Vartuli, J.C., and Beck, J.S., *Nature*, **359** (1992) 710.

[126] Beck, J.S., Chu, C.T., Johnson, I.D., Kresge, C.T., Leonowicz, M.E., Roth, W.J., and Vartuli, J.C., *U.S. Patent*, **5** (1992) 108, 725.

[127] Beck, J.S., Calabro, D.C., McCullen, S.B., Pelrine, B.P., Schmitt, K.D., and Vartuli, J.C., *U.S. Patent,* 5, 145, 816 (1992).

[128] Beck, J.S., Kresge, C.T., Leonowicz, M.E., Roth, W.J., and Vartuli, J.C., *U.S. Patent*, 5, 264, 203 (1993).

[129] Beck, J.S., Vartuli, J.C., Roth, W.J., Leonowicz, M.E., Kresge, C.T., Schmitt, K.D., Chu, C.T-W., Olson, D.H., Sheppard, E.W., McCullen, S.B., Higgins, J.B., and Schlenker, J.L., *J. Am. Chem. Soc.*, **114** (1992) 10834.

[130] Vartuli, J.C., Kresge, C.T., Leonowicz, M.E., Chu, A.S., McCullen, S.B., Johnson, I.D., and Sheppard, E.W., *Chem. Mater*., **6** (1994) 2070.

UNIVERSITY of the
WESTERN CAPE

[131] Vartuli, J.C., Roth, W.J., Beck, J.S., McCullen, S.B., and Kresge, C.T., *"Molecular Sieves, Science and Technology",* Eds: Karge, H.G., Weitkamp, J., **1** (1998) 97.

[132] Huo, Q., Margolese, D.I., Ciesla, U., Demuth, D.G., Feng, P., Gier, T.E., Sieger, P., Firouzi, A., Chmelka, B.F., Schüth, F., and Stucky, G.D., *Chem. Mater*., **6** (1994)1176.

[133] Cheng, C.F., He, H., Zhou, W., and Klinowski, J., *Chem. Phys. Lett.*, **244** (1995) 117.

[134] Chen, C.Y., Burkett, S.L., Li, H.Y., and Davis, M.E., *Microporous Mater.*, **2** (1993)

[135] Xia, Y., and Mokaya, R., *Chem. Materials* **17** (2005) 1553-1560

[136] S. Jun, S. H. Jo, R. Ryoo, M. Kruk, M. Jaroniec, Z. Liu, T. Oshuna and O. Terasaki, *J. Am. Chem. Soc*., **122** (2000) 10712

[137] Fulvio P. F., 2009 Ph.D Thesis. Synthesis and characterization of ordered mesoporous inorganic nanocomposite materials, Kent State University.

[138] L.M. Knijff, 1993 Ph.D. Thesis, Utrecht University, The Netherlands, Chapters 2 and 3.

[139] Prabhuram. J; Zhao. T.S; Wong. C.W; Guo. J.W; (2004) *Journal of Power Sources*, **134** (1): 1-6.

[140] Chenite, A., Page, Y.L., and Sayari, *Chem. Mater.*, **7** (1995) 1015.

[141] Bell, A.T., *Science* **299** (2003) 1688.

[142] Jinwoo Lee, Sangjin Han and Taeghwan Hyeon, Synthesis of new nanoporous Carbon materials using nanostructured silica materials as templates. *J. Mater. Chem.*, **14 (**2004) 478-486.

UNIVERSITY of the WESTERN CAPE

[143] Fuertes, A.B., Nevskaia, D.M., Control of mesoporous structure of carbons synthesised using a mesostructured silica as template. Microporous and Mesoporous Materials **62** (2003) 177–190.

[144] Gierszal, K., (2008) Ph.D dissertation, Synthesis, adsorption and structural properties of carbons with uniform and ordered mesopores. Kent State University.

[145] Ryoo, R., Joo, S.H., Jun, S., J. Phys. Chem. B **103** (1999) 7743.

[146] Kim, T.W; Park, I.S; Ryoo, R. *Angew. Chem., Int. Ed*. **42** (2003) 4375.

[147 Ryoo, R., Joo, S.H., Kruk, M., Jaroniec, M., *Adv. Mater*. **13** (2001) 677.

[148] Jun, S., Jo, S.H., Ryoo, R., Kruk, M., Jaroniec, M., Liu, Z., Oshuna, T., Terasaki, O., *J. Am. Chem. Soc*. **122** (2000) 10712.

[149] Parmentier, J., Patarin, J., Dentzer, J., Vix-Guterl, C., *Ceram. Int*. **28** (2002) 1–7.

[150] Kim, S.S., Pinnavaia, T.J., Chem. *Commun*. (2001) 2418.

[151] Lee, J., Joo, S.H., Ryoo, R., *J. Am. Chem. Soc*. **124** (2002)1156.

[152] Kim, S.S., Pauly, T.R., Pinnavaia, T.*J., Chem*. Commun. (2000) 835.

[153] Lee, J., Sohn, K., Hyeon, T., *J. Am. Chem. Soc.* **123** (2001) 5146.

[154] Joo, S.H., Choi, S.J., Oh, I., Kwak, J., Liu, Z., Terasaki, O., Ryoo, R., *Nature* **412** (2001) 169.

[155] Ndungu, P., Godongwana, Z.G., Petrik, L.F., Nechaev, A., Liao, S., Linkov, V., Synthesis of carbon nanostructured materials using LPG Microporous and Mesoporous Materials **116** (2008) 593–600.

UNIVERSITY of the
WESTERN CAPE

[156] Jal, P. K, Patel, S, Mishra, B. K. Chemical modification of silica surface by immobilization of functional groups for extractive concentration of metal ions, *Talanta*, **62** (2004) 1005-1028.

[157] Walcarius, A., Etienne, M., Delacote, C., Uptake of inorganic Hg^{II} by organically modified silicates: influence of pH and chloride concentration on the binding pathway and electrochemical monitoring of the process. *Analytica Chimica Acta*, **508** (2004) 87–98.

[158] Shen ,W., Li, Z., and Liu, Y., Surface Chemical Functional Groups Modification of Porous Carbon. *Recent Patents on Chemical Engineering* 2008, *1,* 27-40

[159] Izquierdo M.T., Rubio, B., Mayoral, C., Andres, J.M., Modifications to the surface chemistry of low-rank coal-based carbon catalysts to improve flue gas nitric oxide removal. *Appl Catal B Environ* **33** (2001) 315-324.

[160] Shim, J.W., Park, S.J., Ryu. S.K., Effect of modification with HNO3 and NaOH on metal adsorption by pitch-based activated carbon fibers. *Carbon* **39** (2001) 1635-1642.

[161] Yin, C.Y., Aroua. M.K., Daud WMAW. Review of modifications of activated carbon for enhancing contaminant uptakes from aqueous solutions. *Sep Purif Technol* **52** (2007) 403-415.

[162] Radovic, L.R., Moreno-Castilla, C., Rivera-Utrilla J. Carbon materials as adsorbents in aqueous solution in “Chemistry and Physics of Carbon”, radovic lr, Ed. Marcel Dekker: New York, 2001; 27: 227-405.

UNIVERSITY of the
WESTERN CAPE

[163] El-Sayed, Y., Bandosz, T.J., Adsorption of valeric acid from aqueous solution onto activated carbons: role of surface basic Sites. *J Colloid Interf Sci* **273 (**2004) 64-72.

[164] Lukaszewicz, J.P., Carbon-film-based humidity sensor containing sodium or potassium. recovery effect. *Sens Actuators B Chem*., **60** (1999) 184-190.

[165] Conway, B.E., Electrochemical supercapacitors. New York: Kluwer-Plenum Pub. Co.; 1999. Frackowiak E, Beguin F. Carbon materials for the electrochemical storage of energy in capacitors. *Carbon,* **39** (2001) 937-950.

[166] Rodriguez-Reinoso, F., The role of carbon materials in heterogeneous catalysis. *Carbon* **36** (1998) 159-171.

[167] Feron, P.H.M., Jansen, A.E., The production of carbon dioxide from flue gas by membrane gas absorption. Energy Convers Manage

[168] Figueiredo, J.L., Pereira, M.F.R., Freitas, M.M.A., Orfao, J.J.M., Modification of the surface chemistry of activated carbons. *Carbon* **37** (1999) 1379-1389.

[169] Yang, R.T., Adsorption, John Wiley & Sons Inc., Hoboken, New Jersey 2003.

[170] Abe, M., Kawashima, K., Kozawa, K., Sakai, H., Kaneko, K., Amination of activated carbon and adsorption characteristics of its aminated surface. *Langmuir* **16** (2000) 5059 -5063.

[171] Perez-Cadenas, A.F., Maldonado-Hodar, F.J., Moreno-Castilla, C., On the nature of surface acid sites of chlorinated activated carbons. *Carbon* **41** (2003) 473-478.

UNIVERSITY of the
WESTERN CAPE

[172] Liu, S.X., Chen, X., Chen, X.Y., Liu, Z.F., Wang ,H.L.. Activated carbon with excellent Chromium (VI) adsorption performance prepared by acid-base surface modification. *J Hazard Mater* **141** (2007) 315-319.

[173] Manuel Fernando, F. Pereira, Samanta F. Soares, Jose´ J.M. Orfao, Jose, L., Figueiredo., A dsorption of dyes on activated carbons: influence of surface chemical groups. *Carbon* **41** (2003) 811–821

[174] Sanchez Uria. J.E., Sanz-Medel. A., *Talanta*. **47** (1998) 509.

[175] Walcarius. A., Etienne. M., Sayen. S., Lebeau. B., *Electroanalysis*. **15** (2003) 414.

[176] Stumm. W., (Ed). (1987). Aquatic surface chemistry: Chemical Process at the particle-water interface. Wiley, New York.

[177] Chen. J.P., Wu S.N., Chong, K.H., Surface modification of a granular activated carbon by citric acid for enhancement of copper adsorption. *Carbon* **41** (2003) 1979-1986.

[178] Elwing. H., Lunderstroem. I., Structure of 3-aminopropyltriethoxysilane on silicon oxides. *J Colloid interface* Sci. **147** (1991) 103-111.

[179] Homerick, M.J., Jnr and Schoor J.L., *J. Am. Soc. Environ. Eng. Div*., **100** (1974) 1249

[180] Bejbouji, H.; Vignau, L.; Miane, J. L.; Dang, M.-T.; Oualim, E.M.; Harmouchi, M.; Mouhsen, A., Polyaniline as a hole injection layer on organic photovoltaic cells. *Solar Energy Materials and Solar Cells* **94** (2010) 176-181.

UNIVERSITY of the WESTERN CAPE

[181] Mavundla, S.; Malgas, G.; Motaung, D.; Iwuoha, E., Physicochemical and morphological properties of poly(aniline-pyrrole). *Journal of Materials Science.,* **45** (2010) 3325-3330.

[182] Shimura, F. *Semiconductor silican crystal technology*, Academic Academic Press Inc, San Diego (1989).

[183] Brunauer, S., Emmett P.H., and Teller E., *J.Am. Chem Soc.*, **60** (1938) 309.

[184] Sing, K. S. W.; Everett, D. H.; Haul, R. A. W.; Moscou, L.; Pierotti, R. A.; Rouquerol, J.; Siemieniewska, T. *Pure Appl. Chem.* **57** *(*1985) 603.

[185] Rouquerol, F.; Rouquerol, J.; Sing, K. *Adsorption by Powders and Porous Solids*; Academic Press: San Diego, 1999.

[186] Kruk M., and Janiec M., Gas Adsorption Characterization of Ordered Organic−Inorganic Nanocomposite Materials*Chem. Mater.*, **13** (2001) 3169-3183

[187] Kresge, C.T., Leonowicz, M.E., Roth, W.J., and Vartuli, J.C., *U.S. Patent*, 5,098,684 (1992).

[188] Beck, J.S., Kresge, C.T., Leonowicz, M.E., Roth, W.J., and Vartuli, J.C., *U.S. Patent*, 5, 264, 203 (1993).

[189] Xia, Y and Mokaya, R. *Chem. Materials* **17** (2005) 1553-1560.

[190] Jun, S., Jo, S. H., Ryoo, R., Kruk, M., Jaroniec, M., Liu, Z., Oshuna T., Terasaki, O. *J. Am. Chem. Soc*., **122** (2000) 10712.

[191] Al-Othman, Z.A., 1997 Ph.D Thesis. Synthesis, modification and application of mesoporous materials based on MCM-41. King Saud University.

UNIVERSITY of the WESTERN CAPE

[192] Liao, L., Zheng, M., Zhang, Z., Yan, B., Chang, X., Ji, G., Shen, Z., Wu, T., Cao, J., Zhang, J., Gong, H., Cao, J., Yu, T. The characterization and application of p-type semiconducting mesoporous carbon nanofibers *Carbon* **4 7** (2009) 1841 –1845.

[193] Peng S, Cho KJ, Qi PF, Dai HJ. Ab initio study of CNT NO2 gas sensor. *Chem Phys Lett* 2004; **387**(4–6): 271–6.

[194] Transmission Electron Microscopy L. Reimer, Spriner , 1997 Microscopy" Spriner

[195] Egerton, R.F. Electron Energy Loss Spectroscopy in the Electron Microscope, second edition (Plenum Press, New York, 1996). Egerton, Energy.

[196] Energy Filtering Transmission Electron Microscopy, L. Reimer, Springer, 1994 Energy.

[197] Chenite, A., Page, Y.L., and Sayari, *Chem. Mater.*, **7** (1995) 1015.

[198] Kim, T.W; Park, I.S; Ryoo, R. *Angew. Chem., Int. Ed***. 42** (2003) 4375.

[199] Electronic references, Bath university, Cyclic Voltammetry, [ONLINE]. Available: http://www.cartage.org.lb/en/themes/Sciences/Chemistry/Electrochemis/Electrochemical/CyclicVoltammetry/CyclicVoltammetry.htm

[200] Thermo Nicolet (2001), Introduction to fourier transform infrared spectroscopy.

[201] Hwang B.J., Zheng Y.Z., Lin Y.C., Lee Y.C., Chen C.I., investigation of membrane formation by FTIR.14A1 BM-IR Microscopy.

UNIVERSITY of the
WESTERN CAPE

[202] Innocenzi P. and Falcaro P., Order-Disorder Transitions and Evolution of Silica Structure in Self-Assembled Mesostructured Silica Films Studied through FTIR Spectroscopy. *J. Phys. Chem. B* **107** (2003) 4711-4717

[203] Kuban, P., Hauser, P.C., Kuban, V., *Electrophoresis* **28** (2007) 58-68.

[204] Browner, F., West, T.S., *Talanta* **16** (1969), 75-80.

[205] Hymer, B, C., Wrobel, K., Caruso, J.A., *Journal of Chromatography*, **975**, (2002), 245-266.

[206] Barshick, C., Britt, P., Lake, A., Vance, A., *International Journal of Mass Spectrometry* **178** (1998) 31-41.

[207] Hempel , M., Hintelmann, H., Wilken, R.D., *Analyst*, **117**, (1992), 669-672.

[208] Yin, X., Scholer, H.F., *Frensius Journal of Analytical Chemistry*, **361** (1998) 761-766.

[209] Ombaba, J.M., *Microchemical Journal*, **53** (1996) 424-428.

[210] Morita, M., Yoshinga, J., Edmonds, J., *Pure & Appl. Chem*., **70** (1998) 1585-1615.

[211] Emeteborg, H., Hadgu, N., Baxter, D., *Journal of Analytical Atomic Spectrometry* **9** (1994) 297-302.

[212] Lindest, G., *Analyst*., **95** (1970) 264.

[213] Bloom, N., *Journal of Fisheries and Aquatic Sciences.,* **46** (1989) 1131-1140.

[214] Vickers, T. J., Vaught, R.M., *Analytical Chemistry.,* **41** (1969) 1470-1476.

UNIVERSITY of the
WESTERN CAPE

[215] Wiaeferder, J.D., Stab, R.A., Analytical Chemistry., **36** (1964) 1367-1372.

[216] Chai, Y., Jaffe, R., Alli, A., Jones, R., *Anal. Chim. Acta*., **334** (1996) 251-256.

[217] Demuth, N., Heumann, K.G., Analytical Chemistry., **73** (2001) 4020-4027.

[218] Lambertsson, L., Lundberg, E., Journal of Analytical Atomic Spectrometry., **16** (2001) 1296-1301.

[219] Tu, Q., Quin, J., Frech, W., Journal of Analytical Atomic Spectrometry., **15** (2000) 1583-1588.

[220] Quimby, B.D., Sullivan, J.J., Analytical Chemistry., **62** (1990) 1027-1034.

[221] Jimenez, M., Sturgeon, R.E., *Journal of Analytical Atomic Spectrometry* **12** (1997) 597-601.

UNIVERSITY of the
WESTERN CAPE

[222] Liang, L., Horvat, M., Bloom, N., Talanta 41, (1994), 371-379.

[223] Clarkson, T.W., *Environmental Health Perspectives* ., **100** (1992) 31-38.

[224] Hight, S.C., Cheng, J*., Anal. Chim. Acta*., **567** (2006) 160-172.

[225] Wang, Y.C., Wang, C.W., *Journal of Chromatography A*., **628** (1993) 133-137.

[226] Sarzanni, C., Aceto, M., Mentasti, E., *Journal of Chromatography A* **626** (1992) 151-157.

[227] Eiden, R., Falter, R., Scholer, H., *Frensius Journal of Analytical Chemistry.,* **359** (1997), 439-441.

[228] Liang, L., Horvat, M., Gelein, B., Balogh S., *Talanta.,* **43** (1996) 1883-1888.

[229] Liu, W., Lee, K., *Journal of Chromatography A*., **796** (1998) 385-395.

[230] Vogt, C., Klunder, G.L., *Frensenius Journal of Analytical Chemistry* **370** (2001) 316-331.

[231] Timerbaev, A.R., Shpigun, O.A., *Electrophoresis*., **21** (2000) 4179-4191.

[232] Ramakrishna T.V., Aravamudhan G., Vijayakumar M., Spectrophotometric determination of mercury (II) on ternanary complex with Rhodamine 6G and iodide*. Anal. Chem*. Acta. **85** (1976) 205.

[233] Lu A.H, Li,W.C., Schmidt,W., Schu¨th, F., Template synthesis of large pore ordered mesoporous carbon. *Microporous and Mesoporous Materials.,* **80** (2005) 117–128.

[234] Zhang, W., Pauly, T.R., Pinnavaia, T.J., Tailoring the Framework and Textural Mesopores of HMS Molecular Sieves through an Electrically Neutral (S°I°) Assembly Pathway. *Chem. Mater.* **9** (1997) 2491-2498.

[235] Pinnavaia, T.J., *Science*, **220** (1983) 365.

[236] Beck, J.S., Calabro, D.C., McCullen, S.B., Pelrine, B.P., Schmitt, K.D., and Vartuli, J.C., *U.S. Patent,* 5, 145, 816 (1992).

[237] Beck, J.S., Kresge, C.T., Leonowicz, M.E., Roth, W.J., and Vartuli, J.C., *U.S. Patent*, 5, 264, 203 (1993).

[238] Beck, J.S., Vartuli, J.C., Roth, W.J., Leonowicz, M.E., Kresge, C.T., Schmitt, K.D., Chu, C.T-W., Olson, D.H., Sheppard, E.W., McCullen,

UNIVERSITY of the
WESTERN CAPE

S.B., Higgins, J.B., and Schlenker, J.L., *J. Am. Chem. Soc.*, **114** (1992) 10834.

[239] Vartuli, J.C., Kresge, C.T., Leonowicz, M.E., Chu, A.S., McCullen, S.B., Johnson, I.D., and Sheppard, E.W., *Chem. Mater*., **6** (1994) 2070.

[240] Vartuli, J.C., Roth, W.J., Beck, J.S., McCullen, S.B., and Kresge, C.T., *"Molecular Sieves, Science and Technology",* Eds: Karge, H.G., Weitkamp, J., (1998) 97.

[241] Ndungu, P., Godongwana, Z.G., Petrik, L.F., Nechaev, A., Liao, S., Linkov, V., Synthesis of carbon nanostructured materials using LPG *Microporous and Mesoporous Materials*., **116** (2008) 593–600

[242] Fernando, M., Pereira*, F., Soares, S.F., Jose´ J.M. O´ rfa˜o ., Figueiredo, L., Adsorption of dyes on activated carbons: influence of surface chemical groups. *Carbon* **41** (2003) 811–821

[243] Feron, P.H.M., Jansen, A.E., The production of carbon dioxide from flue gas by membrane gas absorption. Energy Convers Manage

[244] Walcarius A., Etienne, M., Delacote, C., Uptake of inorganic HgII by organically modified silicates: influence of pH and chloride concentration on the binding pathways and electrochemical monitoring of the processes. *Analytica Chimica Acta* **508** (2004) 87–98.

[245] Ramakrishna, T.V, Aravamudan, G., Yakumar, M.V. Spectrophotometric determination of Mercury (II) as the ternary complex with Rhodamine 6G and Iodide. *Anal. Chem*. Acta. **84** (1976) 369.

UNIVERSITY of the
WESTERN CAPE

[246] Tang, W., and Ng, H.Y., Concentration of brine by forward osmosis: Performance and influence of membrane structure. *Desalination,* **224** (2008) 143-153.

[247] Smirtniotis in Studies in Surface Science and Catalysis **135** 13th Meeting of IZA, 2001.

[248] Zhibin Lei, Yi Xiao, Liqin Dang, Shiying Bai, Lizhen An Graphitized carbon with hierarchical mesoporous structure templated from colloidal silica particles Microporous and Mesoporous Materials **109** (2008) 109–117

[249] Zhang, W. H.; Liang, C.; Sun, H.; Shen, Z.; Guan, Y.; Ying, P.; Li,C. *Adv. Mater.* **14** (2002) 17.

[250] Vix-Guterl, C.; Boulard, S.; Parmentier, J.; Werckmann, J.; Patarin, J. *Chem. Lett.* (2002) 1062.

[251] Kim, T.W; Park, I.S; Ryoo, R. *Angew. Chem., Int. Ed*. **42** (2003) 4375.

[252] Kim, C. H.; Lee, D.K.; Pinnavaia, T. J. *Langmuir* **20** **(**2004) 5157.

[253] Fuertes, A. B.; Alvarez, S. *Carbon* **42** *(*2004) 3049.

[254] Mbileni C.M, PhD Thesis, 2007, Application of Mesoporous Carbonaceous Materials as supports for Fischer-Tropsch Metal Catalysts. Wits University.

[255] Katiyar A., Santosh Yadav, Panagiotis G. Smirniotis, Neville G. Pinto et al Synthesis of ordered large pore SBA-15 spherical particles for adsorption of biomolecules. *Journal of Chromatography A*, **1122** (2006) 13–20.

UNIVERSITY of the
WESTERN CAPE

[256] Su, F., Zeng, J., Bao, X., Yu, Y., Lee, J,Y., Zhao, X,S., Chem. Mater., **17**, (2005) 3960.

[257] Ndungu, P., Godongwana, Z.G., Petrik, L.F., Nechaev, A., Liao, S., Linkov, V., Synthesis of carbon nanostructured materials using LPG *Microporous and Mesoporous Materials* **116** (2008) 593–600.

[258] Neil J. Coville1 Alufelwi M. Tshavhungwe1,2 Mesoporous ethanesilica materials with bimodal and trimodal pore-size distributions synthesised in the presence of cobalt ions. *South African Journal of Science*, **106** (2010) 1– 5.

[259] Fuertes, A. B., and Centeno, T. A., *Journal of Materials Chemistry*, **15** (2003) 5.

[260] Tanev, P.T. Pinnavaia, T. *J. Science* **267** (1995) 865.

[270] Zhang, W. Pauli, T.R. Pinnavaia, T.*J. Chem. Mater*. **9** (1997) 2491.

[271] Beck JS, Vartuli JC, Roth WJ, et al. A new family of mesoporous molecular sieves prepared with liquid crystal templates. *J Am Chem Soc*. **114** (1992)10834–10843.

[272] Armandi et al, *Microporous and Mesoporous Materials*, **103** (2007) 150-157.

[273] Yuan Z, Su B. Insights into hierachically meso-macroporous structured materials. J Mater Chem. **16** (2006) 663–67.

[274] J. Chmiola J., G. Yushin,a R. K. Dash,a E. N. Hoffman,a J. E. Fischer, W. Barsoum,a and Y. Gogotsia, (2004) Double-Layer Capacitance of Carbide Derived Carbons in Sulfuric Acid *Electrochemical and Solid-State Letters,* 8,7

UNIVERSITY of the
WESTERN CAPE

[275] Beyssac et al, *Contrib Miner Petrol*, **143** (2002) 19-31.

[275] Bourlinos et al, *Carbon*, **45** (2007) 852-857 and Su et al, *J. Phys. Chem. B*, **109** (2005) 20200-20206.

[277] Ferrari et al, *Phys Rev B* **61** (2000) 14095-14107,

[278] Kao et al, *Materials Letters*, **62** (2008) and *J Phys Chem B paper* from 2005.

[279] Zhu J., Yang J. and Deng B., Enhanced mercury ion adsorption by amine- modified activated carbon. *Journal of Hazardous Materials*, **166** (2009) 866-872.

[280] Innocenzi P. and Falcaro P., Order-Disorder Transitions and Evolution of Silica Structure in Self-Assembled Mesostructured Silica Films Studied through FTIR Spectroscopy. *J. Phys. Chem. B*, **107** (2003) 4711-4717.

[281] Hwang B.J., Zheng Y.Z., Lin Y.C., Lee Y.C., Chen C.I., investigation of membrane formation by FTIR.14A1 BM-IR Microscopy

[282] K.Y. Ho, G. McKay, K.L. Yeung, Selective adsorbents from ordered mesoporous silica, *Langmuir* **19** (2003) 3019–3024.

[283] Muto, S., Imai, H., Relationship between mesostructures and pH conditions for the formation of silica–cationic surfactant complexes, Micropor. Mesopor. Mater. **95** (2006) 200–205.

[284] Khoklova T.D., Hien Le T., Adsorption of dyes on activated carbon and graphitic carbon black. *Moscow University chemistry Bulletin*, 62(3), (2007) 128-131.

[285] Graham, D., *J. Phys. Chem*., **59** (1955) 896.

[286] Goyal, M., Ph.D. dissrttation, Panjab Univ., Chandigarh, India, 1998.

UNIVERSITY of the
WESTERN CAPE

[287] Namasivyam C., Kavitha D., Removal of Congo Red from water by adsorption onto activated carbon prepared from coir pith, an agricultural solid waste. *Dyes and Pigments* **54** (2002) 47-58.

Namasivayam, D. Kavitha, *Dyes Pigments* **54** (2002) 47.

[288] Tamai H., Yoshida T., Sasaki M., Yasuda H., Dye adsorption on mesoporous activated carbon fibre obtained from pitch containing yttrium complex. *Carbon* **37** (1999) 983-989.

[289] Traybal, R.E., Mass Transfer Operations, 1980, 3rd ed. New York, McGraw Hill.

[290] Liu F., Wang J., Li L., Shao Y., Xu Z., Zheng S., Adsorption of direct yellow 12 onto ordered mesoporous carbon and activated carbon. *J. Chem. Eng. Data,* **54** (2009) 3043-3050.

[291] Zhuang X., Wan Y., Feng C., Shen Y.,Zhao D., Highly efficient adsorption of bulky dye molecules in wastewater on ordered mesoporous carbons. *Chem. Mater*. **21** (2009) 706 – 716.

[292] Long. C., Lu, Z. Y., Li, A.M., Liu, W., Jiang, Z.M., Chen, J.L., Zhang, Q.X., adsorption of reactive dyes onto polymeric adsorbents: Effect of pore structure and surface chemistry group of adsorbent on adsorptive properties. *Sep. Purif. Technol*. **44** (2005) 91-96.

[293] Yan C., Wang C., Yao J., Zhang L., Liu X., Adsorption of mythylene blue on mesoporous carbons prepared using acid- and alkaline-treated zeolite X as the template. *Cololoids and Surface A: Physicochem. Eng. Aspects* **333** (2009) 115-119.

UNIVERSITY of the
WESTERN CAPE

[294] Kadirvelu K., Kavipriya M., Karthika C., Vennilamani N., Pattabhi S., Mercury (II) adsorption by activated carbon made from sago waste. *Carbon*, **42** (2004) 745-752.

[295] McKay G, Blair H, Gardiner JR. The adsorption of dyes onto chitin in fixed bed column and batch adsorbers. *J Appl Polym Sci,* **28** (1989) 1499–544.

[296] Attia, A.A., Girgis, B.S., Fathy, N.A., Removal of methylene blue by carbons derived from peach stones by H_3PO4 activation: batch and column studies, *Dyes Pigments* **76** (2008) 282–289.

[297] Al-Degs, Y.S., El-Barghouthi, M.I., El-Sheikh, A.H., Walker, G.M., Effect of solution pH, ionic strength, and temperature on adsorption behavior of reactive dyes on activated carbon, *Dyes Pigments* **77** (2008) 16.

[298] Hameed B.H., Ahmad A.L., Latiff K.N.A., Adsorption of basic dye (methylene blue) onto activated carbon prepared from rattan sawdust. *Dyes and Pigments* **75** (2007) 143-149.

[299] Yasin Y., Hussein M.Z., and Hj Ahmad F.,Adsorption of Methylene Blue onto treated Activated Carbon. *The* Malaysian Journal of Analytical Sciences, **11**(11), (2007) 400 - 406

[300] Guo Y., Zhao J., Zhang H., Yang S., Qi J., Wang Z., Xu H., Use of rice husk-based porous carbon for adsorption of Rhodamine B from aqueous solutions. *Dyes and Pigments* **66** (2005) 123-128.

[301] Deshpande AV, Kumar U. Effect of method of preparation on photophysical properties of Rh-B impregnated sol-gel hosts. *J Non-Cryst Solids* **306** (2002) 149 -159.

UNIVERSITY of the
WESTERN CAPE

[302] Ghanadzadeh A, Zanjanchi MA, Tirbandpay R. The role of host environment on the aggregative properties of some ionic dye materials. *J Mol Struct* **616** (2002) 167-74.

[303] Lopez Arbeloa I, Ruiz Ojeda P. Dimeric states of rhodamine B. *Chem Phys* Lett, **87** (1982) 556-60.

[304] Lin C., James A.R., Branko N.P., Correlation of double-layer capacitance with the pore structure of sol-gel derived carbon xerogels. *J Electrochem Soc* **146** (1999) 363-943.

[305] Arivolo. S., Thenkuzhali. M., Kinetic, Mechanistic, Thermodynamic and equilibrium studies on the adsorption of Rhodamine B by Acid Activated low cost carbon. *E-Journal of chemistry*, **5** (2008) 187-200.

[306] Nagy, L.G., and Schay, G., *Mag. Kem. Foly*, **66** (1960) 31.

[307] Langmuir I., Adsorption of gases on plane surfaces of class. Mica and Platinum*, J Am Chem Sci* **40** (1918) 361-403.

[308] Kadirvelu K., Kavipriya M., Karthika C., Vennilamani N., Pattabhi S., Mercury (II) adsorption by activated carbon made from sago waste. Carbon **42** (2004) 745-752.

[309] Ramakrishna T.V., Aravamudhan G., Vijayakumar M., Spectrophotometric determination of mercury (II) on ternanary complex with Rhodamine 6G and iodide*. Anal. Chem*. Acta. **86** (1978) 300.

[310] Namasivayam C., Kardivelu K., Uptake of mercury (II) from waste water by activated carbon from an unwanted agricultural solid by-product: coipith*. Carbon* **37** (1999) 79-84.

[311] Nagy, L.G., and Schay, G., *Mag. Kem. Foly*, **66** (1960) 31.

UNIVERSITY of the
WESTERN CAPE

[312] Treybal R.E., (1980), Mass transfer operations. 3rd edn. New York, McGraw Hill.

[313] Periasamy K., and Namasivayam C., *Chemosphere* **32** (1996) 769.

UNIVERSITY of the
WESTERN CAPE